Leaching of concrete : experiments and modelling

Ekström, Tomas

2001

LUND INSTITUTE OF TECHNOLOGY
Division of Building Materials

LEACHING OF CONCRETE

Experiments and Modelling

Tomas Ekström

LUND UNIVERSITY

Report TVBM-3090 2001

PREFACE

This work has been carried out at the Division of Building Materials at the Lund Institute of Technology and has been financed by Swedish National Board for Industrial and Technical Development (NUTEK), Elforsk AB and Sydkraft AB, Miljö och Utveckling. The research project was initiated by NUTEK and professor Kyösti Tuutti, Skanska Teknik.

My supervisor has been Göran Fagerlund, whom I wish to thank for his support and inspiration.

I would also to thank my colleagues at the Div.of Building Materials for their help and support. A special thanks to Björn Johannesson for discussion about modelling, Mårten Janz for helping me with the experimental determination of the water retention curves, Sture Lindmark for a decisive idea concerning the water pressure equipment, Stefan Backe for his quick and effective help with computers and finally Bo Johansson and Ingemar Larsson for help in the laboratory.

I would also express my gratitude to my company Sycon Energikonsult AB with staff for having such patience with my studies.

The work presented in this report is almost identical with the licentiate thesis report TVBM-7153 (Ekström 2000), but the results have been further developed and analysed.

Contents

ABSTRACT

The report contains a literature survey of concrete leaching, and presents the results of an experimental determination of leaching. Deionized water was pressed through a number of defect-free concrete specimens in order to study lime leaching. The result showed low and uniform water flow during the first time. After a certain period, however, most specimens obtained a rapidly increased flow. This was probably due to breakthrough in some distinct percolation paths. Around these paths of "flow pipes" the solid material was leached and the concrete became disintegrated with almost no continuos cementitious material left to maintain strength and tightness. The main results of the experimental study are presented. A model for how to model the leaching process and its effects, is theoretically outlined and applied to the experimental data.

Key words: concrete dams, leaching, water permeability.

SUMMARY

Many concrete dams, and other concrete structures within the hydropower industry in Sweden and other western countries, are old and in a more or less severe state of degradation. The economical value of these structures is very high. Besides, they are urgently needed for production of electricity. *Leaching* is, together with freeze-thaw, the most common degradation problem in Swedish hydraulic concrete structures. In mountainous terrain, river water is often relatively free from dissolved ions (soft water). Such water is aggressive to concrete structures because of its high dissolving ability. In leaching of concrete, hydration products are dissolved from the pore system of the concrete and transported away by ion diffusion or by the water flow. When solid material is leached, porosity and permeability will increase and strength will decrease. Influencing factors that increase leaching are; (i) high permeability of the concrete and any increase of permeability due to leaching, (ii) high amount of calcium in the concrete, especially calcium hydroxide, (iii) high content of carbon dioxide in the water (iv) low hardness of the water (soft water).

Published literature before 1970 mainly deals with percolation of concrete, i.e. concrete exposed to water pressure with resulting water and ionic flow through the concrete. Also extraction studies of concrete i.e. concrete that lays in stagnant aggressive water with a resulting diffusion of ions to the water, are reported.

Literature after 1970 deals also with extraction studies with careful analysis and modelling of the ionic diffusion from cement paste or mortar to the outside water. Self-healing phenomena where the permeability decreases are also treated both in cracks and in homogenous concrete.

A leaching process starts when water dissolves compounds in pore walls inside the concrete. A dissolution can be looked upon as a diffusion process where, (i) water molecules diffuses to the reaction place in the pore walls, (ii) water molecules dissolve solid compounds, (iii) the dissolved compounds are transported away from the reaction place to the pore solution. The dissolution rate of different compounds in concrete depends on the solubility of the actual compound and on how close the compound is to pure water. Except for potassium hydroxide and sodium hydroxide, which are always in the pore solution, calcium hydroxide is the most soluble compound in concrete. Calcium silicate hydrates and aluminium ferrite phases are less soluble, but the more calcium that is incorporated in these phases, the more soluble they are. When the pore walls become poor of soluble compounds, dissolution to the pore solution will decrease and the concentration of dissolved ions in the drainage water, flowing through the structure, will decrease.

The purpose with the experimental work and the modelling was to investigate the flow of de-ionised water through homogenous concrete and the leaching process. Changes in permeability, leaching rate and strength were therefore studied.

In the leaching model, water is assumed to flow through a number of tortuous *flow pipes* of different average diameter, within a saturated continuous concrete body. The water flow is calculated by a reduced Hagen-Poiseuilles law, regarding the deviation between flow in a real tortuous flow pipe and flow in a perfect cylinder. In the model, solid material is supposed to be dissolved from the pipe walls and transported downstream, and out of the body. No diffusion of ions in upstream direction is regarded. When solid material is leached, the pipe becomes wider and the water permeability increases. Due to a gradually reduced amount of dissolvable material in the pipe walls, the dissolving rate decreases. Another effect is that the porosity increases and the strength decreases. The concrete body is divided into one element, so any effect of gradients

of leaching effects throughout the body is not regarded. The model does not consider any self-healing effect, e.g. re-crystallisation of $CaCO_3$. Strength changes is modelled by involving an assumed fictitious strength of the solid phase of the cement paste together with calculated porosity changes due to leaching. The leaching model gives interesting results despite its simplicity and the many assumptions made. The leaching model can easily be connected to ordinary static calculations for estimations of the safety margin for concrete structures over time.

To imitate a concrete dam subjected to soft water under pressure, de-ionised water was pressed through a number of concrete specimens. The experiment was *accelerated* regarding (i) the pressure gradient, (ii) the water to cement ratio and (iii) the water aggressiveness. The test equipment consisted of a de-ionising aggregate, a storage tank for the de-ionised water, a pump, a pressure tank and a steel pipe system that carried the water to a number of stainless steel test cells in which cylindrical "pressure" specimens of concrete were placed. "Reference" specimens of the same size were cast, hardened and cured in the same way as the pressure specimens were. All specimens were made of ordinary Portland cement of type CEM I 42.5, without any admixtures or additives. Aggregate was of quartzite and had a maximum size of 16 mm. The specimens were made with three different w/c ratios, w/c 0.6, 0.8 and 1.3. The specimens were cured in three different ways; (i) *virgin* specimens were water cured for 2 months, (ii) *late-dried* specimens were dried one week in oven +55°C after 6 months of water curing, (iii) *early-heated* specimens were wrapped in plastic bags and then heated immediately in an oven in a cycle from +20° to +55-60°C and then down again to +20°C during a week. They were then placed in laboratory air at +20°C for 2 months.

The w/c ratios 0.8 and 1.3 were used for virgin and late-dried specimens and the w/c ratios 0.6 and 0.8 for early-heated specimens. All specimens had a height of 50 mm. The diameters was 155 mm and 45 mm. The pressure specimens were cast in conical steel cylinders in which they were later placed during the leaching test. The conical shape, together with silicon grease and a latex tube around the circumference, made the joint between the specimen and the steel cylinder tight. Percolated water, *drainage water,* was collected in measuring glasses and measured by volume. Flow of dissolved ions in the drainage water was measured by ion selective electrodes and to some extent by ICP-AES technique (Inductive Coupled Plasma Atom Emission Spectroscopy). Unleached components in one, leached specimens was measured by dissolving the specimen in HNO_3 and then analysing the solution by ICP-AES. Compressive strength of some leached specimens and of some reference specimens was measured by a strength test machine.

The experimental results shows that pure water percolating the concrete specimens has an ability to dissolve hydration products, probably mainly $Ca(OH)_2$, and also to carry the dissolved ions out of the specimen by diffusion and convection. Depending on the w/c ratio and the curing history, the extent of leaching was different. A high water to cemetn ratio made the specimens more porous, resulting in higher water permeability. *Virgin specimens* had a low and constant permeability with small deviations between the specimens. However, one specimens with w/c 0.8 and one with w/c 1.3 had a rapidly increased permeability after a certain period. *Late-dried specimens* became 100 times more permeable than in the virgin state. This was probably caused by micro-cracks appearing during drying. Because of the high hydration ratio almost all cement was hydrated and there was not much cement left for any self-healing. The permeability of these specimens often increased rapidly, after some time. *Early-heated specimens*, had about 100 times higher initial water permeability than the virgin specimens. However, immediately after the test started, the permeability began to decrease in the specimens. After about eight month it

was close to the permeability at the virgin state. The reduced permeability was probably caused by re-started hydration and resulting self-healing. If the test time had been long enough, probably all specimens had sooner or later been so leached that the permeability had increased once again.

Observations of the specimens indicated that water had flown in a rather few, distinct flow pipes. Also other authors have suggested that the main water flow through concrete, exposed to water pressure, occurs in certain main flow channels, or *flow pipes*, that are continuous throughout the concrete. Such main flow paths can be large-sized capillaries, inter-facial contact zones between paste and aggregate, cracks or construction joints in real structures.

In the tested concrete, water dissolved solids from the walls of such flow pipes and when the pipes grew wider, the water flow increased further and even more solid material was leached. Finally, the pipe walls became so exhausted in lime that the lime leaching rate and the water flow increased only slowly. The dissolution of the pipe walls was governed by a diffusion process from the interior of the solid towards the pipe wall. Around these pipes the concrete became very disintegrated with almost no continuos cementitious material left to maintain strength and tightness. Between the flow pipes, or in less permeable concrete, more of the leaching seems to have been governed by diffusion to the inlet water at the upstream face of the specimens. A detailed analysis of the residual elements of one specimen also showed that the most important element in concrete, calcium, mostly was leached from the upstream part of the specimen. This was probably due to diffusion in the upstream direction. Another possibility is that permeating water became saturated with lime already at the upstream part due to dissolution of lime. Therefore, its dissolving ability was very much reduced when it reached the deeper parts of the specimen.

Another part of the specimen, which lost quite a lot of calcium, was where the aggregate content was high. The cause of the leaching in this part was probably water percolation in porous and easily soluble areas between the aggregate and the cement paste. Because of leaching, porosity was increased in these parts of the specimen.

The measured residual content of substances in the leached specimens corresponded fairly well to the measured ionic flow in the drainage water flow. The results also show that when solid material is leached, the porosity will increase. The strength reduction, was to a high degree a local phenomenon. In parts of the specimen, where much solid material had been leached, the strength was very much reduced. But if these parts were small compared to the whole specimen, the average strength of the whole specimen was not much influenced. The number of specimens used for strength testing were however too few for any more detailed analysis of relations between leaching and strength.

The work shows that there is need of more research of leaching. Examples of research areas are; (i) a more precise study of the diffusion of ions upstreams combined with measurements of ions in the drainage water, (ii) experiments of leaching in cracks or other defects and inhomogenities, (iii) studies of porosity changes due to leaching, (iv) studies of strength changes in leached concrete.

List of symbols and abbreviations

All symbols are explained where they first appear in the text. Most of the symbols are also presented here. All dimensions are in SI units

Symbol	Definition	SI unit
a	Approximation matrix of a state variable in the Finite Element Method	(-)
A	Area	(m^2)
A	Aggregate content	(kg)
A_i	Area of pipes with size i at time t	(m^2)
A_{solid}	Ion releasing area in flow pipe walls	(m^2)
A_{tot}	Total area	(m^2)
B	Permeability coefficient	(s)
c	Ionic concentration	(mole/m^3), (mole/l), (kg/l), (g/l)
c_i	Ionic concentration for specie i	(mole/m^3)
$c_{i(s)}$	Ionic concentration for specie i in a solid phase	(mole/m^3)
c_{sat}	Saturation concentration	(mole/m^3)
C	Cement content	(kg)
dm_i	Mass of leached material for pipes with size i	(kg)
D	Constitutive matrix	(-)
D	Diffusion coefficient	(m^2/s)
D_a	Apparent diffusion coefficient , regarding tortuosity, constrictivity and chemical reactions with the pore walls.	(m^2/s)
D_f	Free water diffusion coefficient	(m^2/s)
dt	Time increments	(s)
E	Electrical potential	(V)
E	Energy	(J)
E	Modulus of elasticity	(Pa)
F	Faraday constant ($9.65 \cdot 10^4$)	J/(V ·mole)
$\mathbf{F}_i$	Total ionic flux	(mole/(m^2·s))
$\mathbf{F}_{iu}$	Ionic flux due to diffusion	(mole/(m^2·s))
$\mathbf{F}_{iv}$	Ionic flux due to convection	(mol/(m^2·s))
f_0	Fictitious strength of the solid phase without pores	(Pa)
f_0'	Fictitious strength of the cement gel with gel pores included	(Pa)
f_{pc}	Compressive strength of cement paste	(Pa)
g	Acceleration of gravity	(m/s^2)
$g(f_{cck})$	Model of compressive strength for concrete	(Pa)
I	Ion strength	(mole/l)
K	Empirical parameter in strength model	(-)
K	Resistance matrix in the Finite Element Method	(-)
K_H	Henry's constant	(mole/l·atm)
K_{sp}	Solubility product	(-)
k_w	Water permeability	(m/s)
$k_w^i(t)$	Water permeability for pipes with size i at time t	(m/s)
k_{ion}	Ion diffusivity coefficient	(m^2/s)
$k_{ion(s)}$	Diffusion coefficient in solid diffusion layers	(m^2/s)

$k_{ion(aq)}$	Diffusion coefficient in pipe solutions	(m^2/s)
L	Length of flow pipes	(m)
L	Length of strength tested cylinders	(m)
m	Molarity	($mole/m^3$) (mole/l)
M	Molar weight	(kg/mole)
m_{paste}	Weight of cement paste	(kg)
$m_{wet,air}$	Weight of saturated slices in air	(kg)
$m_{wet,water}$	Weight of saturated slices beneath water	(kg)
$m_{,dry,air}$	Weight of dried (+105°C) slices in air	(kg)
$M_{flushed}$	Flushed-out mass of ions from the inlet of the test cells	(g)
N	Number of different pipe sizes in a body	(nos.)
n_i	Number of flow pipes with size i	(nos.)
P	Pressure	(Pa)
P	Partial pressure	(atm)
P_w	Water pressure head	(m)
P	Wet perimeter	(m)
P	Porosity	(m^3/m^3)
P_c	Total porosity of concrete	(m^3/m^3)
P_p	Total porosity of cement paste	(m^3/m^3)
$(P_{cap})_p$	Capillary porosity in paste before leaching	(m^3/m^3)
$(P_{cap})_{pL}$	Capillary porosity of paste after leaching	(m^3/m^3)
Q	source term	(mole/s) (kg/s)
Q_{pipe}	Source term for one dimensional flow pipe	(mole/(ms)
Q	Heat energy	(J)
Q	Reaction matrix	(-)
q_{ion}	Flow of ions	(mole/(s))
$q_{ion\ diff}$	Ionic diffusion	(mole/s)
$q_{ion\ conv}$	Convection flow of ions	(mole/s)
q_w	Flow of water	(m^3/s) (kg/s)
q_{w0}	Initial flow of water	(m^3/s)
$q_w^i(t)$	Total water flow for pipes with pipe size i at time t	(m^3/s)
r_h	Hydraulic radius	(m)
RH	Relative humidity	(%)
r_i	Circular pore radius	(m)
R	Gas constant	(J/(K·mole))
R	Reaction quotient	(-)
r_w	Reduction coefficient due to deviation between flow in a real tortuous flow pipe and a perfect cylinder	(-)
S	Solubility	(kg/m^3)
S_0	Solubility at time zero	(kg/m^3)
share	Share of total pore volume that can percolate water	(-)
t	Diffusion layer thickness	(m)
$t_{(s)}$	Thickness of diffusion layers in solids	(m)
$t_{(aq)}$	Thickness of diffusion layers in solutions	(m)
T	Temperature	(K)
$V^i_{pipe,leached}$	Volume of leached material for all pipe sizes	(m^3)
$\sum V^i_{pipe}(t_0)$	Total pipe volume for pipe size i at time zero	(m^3)
$V^i_{one\ pipe}$	Volume of one pipe with pipe size i at time zero	(m^3)

$V^i_{p/m}$	Total pore volume per kg paste for pipe size *i* at time zero	(m^3/kg)
$V^i_{pipe,leached}$	Volume of leached material during a time step Δt	(m^3)
$V_{p/m}$	Total volume of cement paste per kg paste	(m^3/kg)
V_{gel}	Volume of cement gel	(m^3)
$(V_0)_a$	Compact volume of aggregate	(m^3)
$(V_0)_p$	Compact volume of cement paste	(m^3)
V_p	Volume of cement paste	(m^3)
$(V_p)_a$	Pore volume of aggregate	(m^3)
$(V_{cap})_p$	Volume of capillary pores in cement paste	(m^3)
$(V_p)_{gel}$	Volume of gel pores in cement paste	(m^3)
$(V_p)_p$	Total pore volume of cement paste	(m^3)
V_a	Volume of aggregate	(m^3)
V_{air}	Volume of air due to compaction or air additives	(m^3)
V_c	Volume of concrete	(m^3)
$V_{flushed}$	Flushed-out volume of ions from the inlet of the test cells	(litre)
v_w	Velocity of water	(m/s)
w	Crack width	(m)
w	Work	(J)
W_n	Chemical bonded water	(kg)
W	Free (or unbound) water fraction	(m^3/m^3)
W	Mixing water content	(kg)
w/c	Water to cement ratio	(kg/kg)
X	Gel space ratio	(m^3/m^3)
z_i	Valence of the ionic specie *i*	(-)
α	Degree of hydration	(-)
ΔP_w	Water pressure differences	(m)
Δt	Time step	(s)
ε	Dielectric constant	($F/m=J/(V^2 \cdot m)$)
ϕ	Diameter	(m)
ϕ^i_0	Diameter of pipes with size *i* at time zero	(m)
ϕ^i_t	Diameter of pipes with size *i* at time *t*	(m)
γ	Activity coefficient	(l/mole)
φ	contact angle between the liquid and the solid tube walls	(rad)
μ	Mean value	(-)
μ	Dynamic viscosity	(Ns/m^2)
μ_i	Electrochemical potential of specie *i*	(J/mole)
μ_{i0}	Standard chemical potential of specie *i*	(J/mole)
ν	Coefficient of variation	(-)
∇	Nabla operator $\left(\nabla^T = \left[\frac{\partial}{\partial x} \quad \frac{\partial}{\partial y} \quad \frac{\partial}{\partial z}\right]\right)$	
ρ	Electrical charge density	($J/(V \cdot m^3)$)
ρ	Bulk density	(kg/m^3)
ρ_a	Density of the aggregate	(kg/m^3)
ρ_c	Density of cement	(kg/m^3)
ρ_M	Density of leached material	(kg/m^3)
ρ_w	Density of water	(kg/m^3)

σ	Surface tension between liquid and air	(N/m)
σ	Compressive stress	(Pa)
σ	Standard deviation	(-)
τ	Reduction tensor regarding the tortuosity of a pore system	(-)

1 INTRODUCTION

1.1 General about leaching and its effects

Background

Many concrete dams, or other concrete structures in the hydropower industry in Sweden and other western countries, are old and in a state of degradation. These structures are very valuable because they represent a large amount of money invested and they are needed for production of electricity.

Leaching is, together with freeze-thaw, the most common degradation problem in Swedish concrete dams. In northern Sweden, river water is often relatively free from dissolved ions (soft water). Such water is aggressive to concrete structures because of the dissolving ability. It is mostly older dams, with often very porous concrete with high water permeability that has leaching problems. But even though they are erected by better methods and made of better concrete, also more recently built dams may be subjected to leaching damages in a near future. So, the knowledge how to predict leaching damages is needed now and even more in the future. This work is about lime leaching in concrete specimens subjected to soft water.

Concrete structures

To be a little witty one might say that there are two types of rocks; natural rocks (sedimentary, magmatic, and metamorphic) and man-made rocks as *concrete structures*. Concrete is made of approximately the same material as the natural rocks. However, because we do not have the supply of pressure or heat as the other rocks had when formed, the concrete rocks must be made in a chemical way. *Cement* is used to create cement paste that fix incorporated aggregates in a rigid structure. Cement reacts strongly with mixing water and forms hydration products. During the continuous hydration that can last for long time, a supply of water is needed. If there is no water available, hydration will cease.

Concrete structures are built with the shape and geometry needed to resist loads and to meet other requirements.

Leaching

If concrete is used for a dam in a river, water will penetrate the concrete due to the water pressure and due to the porosity of the concrete. Now, water is not only good for the continuous hydration. On the contrary, water can start to dissolve hydration products in the concrete. Concrete dams are subjected to exactly the same environmental impacts as the naturally built rocks; water will dissolve substances, water will together with low or high temperatures break up parts of the concrete and wind will erode the surfaces. When material dissolves from the rocks, wind and water will carry away the loose parts and the rock will become smaller and weaker.

If percolating water is soft, the leaching effect on the concrete will be strong. The water diffuses into the concrete and dissolve hydration products (and aggregate if it is easy soluble). Dissolved material will diffuse out of the concrete to the bulk of pure water in the reservoir. This is a slow leaching process.

If water also percolates through the concrete due to pressure gradients, the water will reach much more internal area of soluble products. Now, dissolved material will also be carried away by the flow of water downstream and out of the concrete. This can be a rapid leaching process, depending on how fast the water is percolated through the concrete and how much internal area the water will meet on its way.

Leaching is the name of the whole process of dissolving and transporting substances out of the concrete.

Leaching effects

When solid material is leached, the **porosity** will increase and the amount of **OH^- -ions** will decrease in the pore solution and in the pore walls. When the porosity increases, the water **permeability** will increase and the leaching process will accelerate. When the porosity increases, the **strength** will also decrease. When the permeability in different parts of a concrete dam changes, **internal pore pressure** will also change in the same way. The decreasing strength but also a changed pore pressure may lower the stability for parts of or for the whole dam.

Figure 1-1shows a old stone-faced concrete dam subjected to lime leaching. Water has percolated the dam and transported dissolved lime to the downstream face of the dam, where the lime have react with atmospheric carbondioxide and formed curtains of calcite. The calcite curtains has probably slowed down the water flow and the lime leaching due to a tightening effect, but the curtains can also change the internal pore pressure so the pushing force of water become worse.

There are also **synergy effects** between leaching and other degradation mechanisms. An example is showed in Figure 1-2, where a changed pore structure has changed (decreased) the resistance to freeze-thaw. The figure shows a concrete block supporting a steel tube, which conveys water down to a hydropower station. Rainwater has penetrated from the top of the block and through this. Water has penetrated especially through the slit between the concrete and the tube. The block lay in a slope in the terrain, so the water flows inside the block while dissolving lime and finally both water and the dissolved lime flows out through the downstream face. When coming out from the surface, the leached $Ca(OH)_2$ reacts with CO_2 in the air and a hard calcite-layer is formed. This layer has increased the water content in this part of the block. This increased water content, together with a possibly coarsened pore system, has in this case lead to substantially freezing damages. These damages open up the concrete for even more flow of water and this circle is running towards a total destruction of the load-bearing capacity of the block.

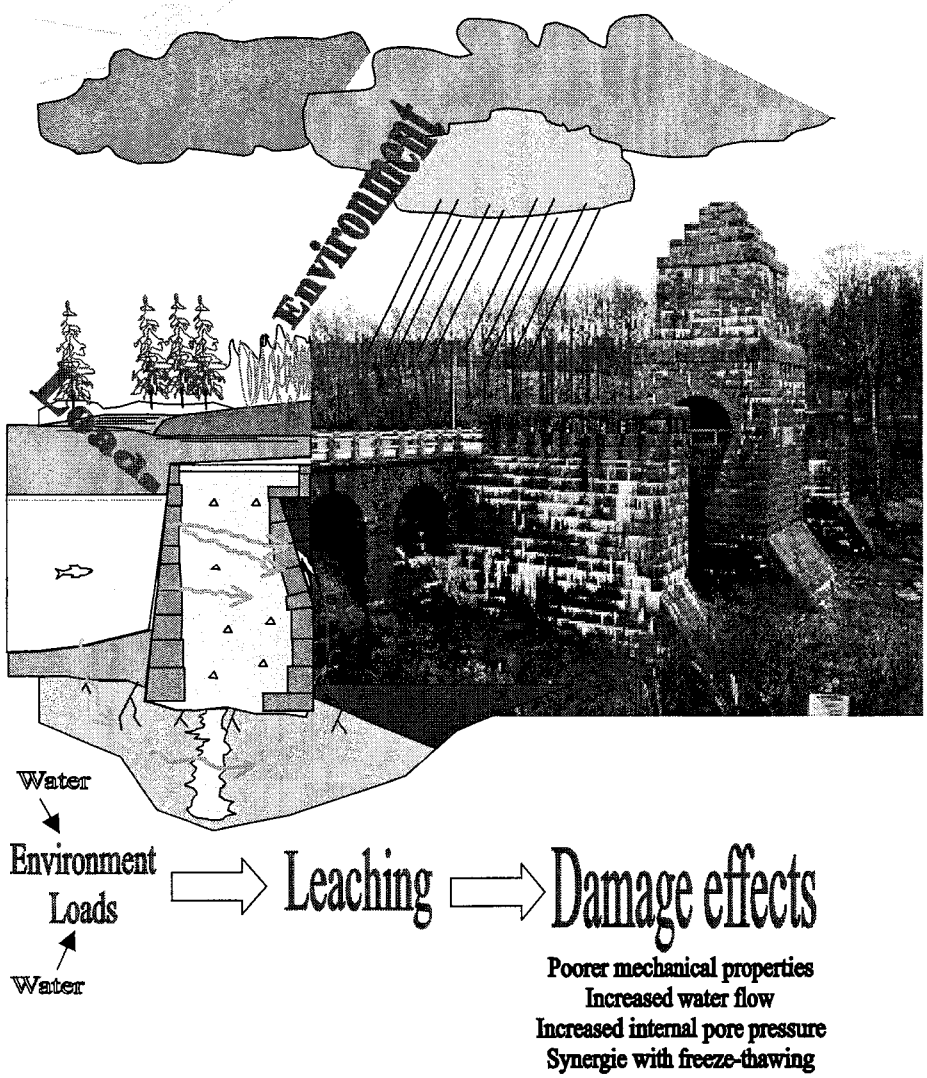

Figure 1-1 An old stone-faced concrete dam subjected to lime leaching. Pure water penetrates the cement paste inside the dam or under the dam and dissolve lime and other soluble substances. The white curtains on the downstream face is calcium carbonate formed by atmospheric CO_2 and $Ca(OH)_2$ transported by water coming out of the dam.

Figure 1-2 Synergy effects between lime leaching and freeze-thaw in a fix-block of concrete, supporting a water tube.

Another synergy effect could be between leaching and reinforcement corrosion. The pH value inside the concrete may decrease due to leaching, and this can finally open up for reinforcement corrosion.

Structures for which leaching is a problem

Most modern concrete structures can withstand leaching very well. For old dams, badly designed dams, badly cast dams, badly cured dams, dams in rivers with very pure or acid water and for joints or gate abutments in dams, leaching can be a problem. In the worst case, the leaching may in such structures decrease the strength, increase the internal forces, decrease the resistance against freeze-thaw and decrease the protection against corrosion on the reinforcement.

1.2 Literature survey

1.2.1 Introduction

Halvorsen (1966) performed a large study of lime leaching on water retaining concrete structures. The study is still rather up to date, in part because lime leaching in such structures have not been studied so much the last 30 years. The study also contains a large literature survey. Halvorsen divides leaching into three types:

1) Leaching through very porous concrete.
2) Leaching from free concrete surfaces.
3) Leaching through cracks in concrete.

Due to Halvorsen, leaching studies have only been performed on homogenous, very porous concrete (with percolation and extraction tests) and at concrete surfaces (with extraction tests). By *percolation* is meant flows of water that trickle through a homogenous body. An *extraction test* is to place a homogenous body in stagnant, aggressive water and letting the water dissolve material from the surfaces of the body.

Until 1966, not a single leaching test was carried out for cracked concrete! On the other hand, Halvorsen claims that the literature does not show any case where the concrete has been destroyed due to leaching in cracks.

Studies after 1966 regards mostly extraction tests with leaching from mortar or cement paste specimens in pure water without pressure gradients. Some percolation tests have been performed with homogenous or cracked concrete subjected to water pressure, but only self-healing effects have been regarded. By self-healing means that the main flow-paths in the concrete are filled with material during time, for example with calcium carbonates coming from reactions between Ca^{2+} in the pore solution and atmospheric CO_2 coming in from surroundings.

Below, some literature regarding the leaching process, influencing parameters on leaching and leaching effects on permeability, porosity and strength is given.

1.2.2 The leaching process

The leaching process is when solid compounds in the concrete are dissolved by water and then transported away, either due to concentration gradients (diffusion) or by the flow of water (convection). External or capillary pressures may for example cause water to flow. For future estimations of leaching degradation in concrete, it is important to have a knowledge about the kinetics and influencing variables on the process, i.e. from the dissolution of solids to the diffusion and the convection of dissolved ions.

Unsworth, Lota and Hubbard (unknown) exposed OPC mortar specimens with de-ionised water under a pressure of 2 Mpa, see Figure 1-3. The results shows a rapid rise of Na in the drainage water up to a maximum content of about 280 (µg/l) when a water volume corresponding to two pore volumes (PV) had percolated the specimens. The rise of K was almost as rapid as for Na and rise to about 1200 (µg/l), when three PV of water had percolated. At the same time, the pH value rise rapidly up to about 13.1 because of the rise in Na and K. After the maximum values was reached for Na and K, the concentration of these components rapidly decreased again down to very low values at about eight PV. As the content of Na and K started to decline, the pH value declined to about 12.5 and the content of Ca started to rise. After about ten PV had been flowed, the content of Ca reached its maximum value of about 530 (µg/l) and then only slowly (in a logarithmic time scale) decreased to about 460 (µg/l) after about 80 PV when the test stops. The pH value also decreased slowly as the content of Ca decreased. The

water permeability followed a slowly decreasing curve from about $7 \cdot 10^{-12}$ down to $6 \cdot 10^{-12}$ (m/s). The result shows that Na and K was quickly washed out of the pore system, followed by a dissolving of Ca to the pore solution. Because of the much larger amount of Ca, than Na and K in the mortar, the leaching rate of Ca was rather constantly high for the whole studied time. However, as Moskvin (1980) observes, the leaching rate usually decreases when the pore walls in the main flow paths become exhausted in lime. Main flow paths can be large-size capillaries, inter-facial contact between paste and aggregate, cracks or construction joints.

In Figure 1-4, generalised data from several studies presented in Moskvin (1980) is showed of the rate of lime (CaO) leaching from cement mortar and concrete as depended on the volume of percolated water. Moskvin observed that the leaching rate of lime per volume of percolated water decrease after removal of about 10-20 (g) of lime per kg of the initial cement. In other words, the leaching rate decrease after a certain volume of water has percolated.

Moskvin emphasis that when the seepage flow out of a surface is larger then the evaporation, the leaching process can continue undisturbed. If the evaporation is larger than the water flow, the concrete surface has a possibility to seal due to reaction with atmospheric CO_2.

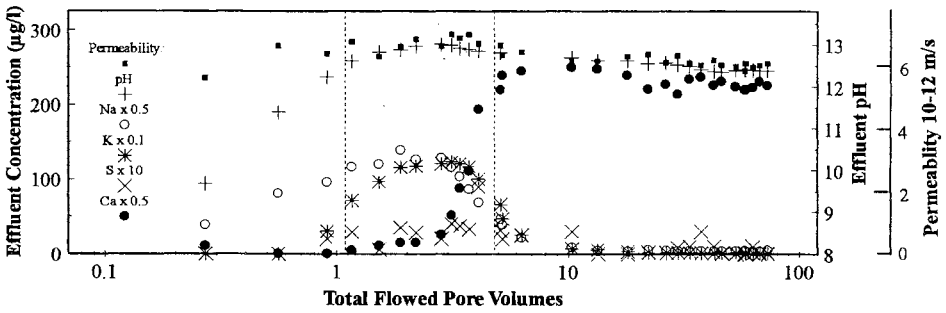

Figure 1-3 The permeability of OPC mortar subjected to 2 MPa water pressure and the ion concentrations and pH values in the drainage water. The x-axis is a function of collected drainage water in relation to measured capillary porosity. Unsworth et al (unknown)

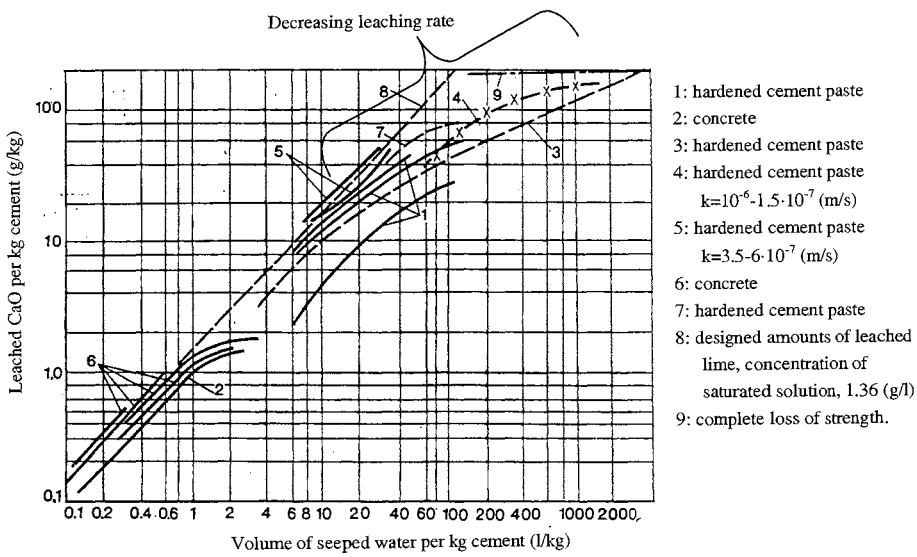

Figure 1-4 Quantity of lime leached from cement mortar or concrete vs volume of percolated water. Based on data from several authors and presented in Moskvin (1980). k = permeability (m/s)

Faucon et al (1996) and Faucon et al (1998) describes the leaching process in cement paste subjected to demineralised water without any water pressure gradient as a leaching process that creates calcium concentration gradients in a layer between the surface and the core of the specimens. Those gradients change the chemical equilibrium in the layer and the hydration products calcium hydroxide (CH), calcium aluminium hydrates (C_3A) and calcium aluminium iron hydrate (C_4AF) will start to dissolves. When the calcium content in the pore solution decrease, the calcium silicate hydrate (C-S-H) will also loose calcium. At a concentration of Ca^{2+} in the pore solution of about 1.8 (mmol/l), the residual silica matrix in the C-S-H will start to dissolve completely. However, at this moment the residual C-S-H gel have a large ion-exchange capability and iron and aluminium, released from crystallised hydrates, are partially incorporated into the residual C-S-H gel. Iron and aluminium incorporation enhances the stability of the C-S-H gel and slow down the dissolution by an significant degree.

Dissolving reaction

The kinetics of dissolution of inorganic material is usually very fast Atkins and Jones (1997). In Hedin (1962) some information is available about the reaction rate for crystals of $Ca(OH)_2$ in pure water, see Figure 1-5. It can be seen that the lower the concentration of dissolved CaO and the higher rates of stirring, the more rapid becomes the reaction. The increasing solution rate when stirring is probably caused of a decreasing diffusion layer nearest the solid particles. When the water is stirred, or moves of other causes, the thin diffusion layer is washed away and the pure water can move much closer to the solid. Pure water molecules in direct contact with solid $Ca(OH)_2$ dissolves the solid almost instantly. This behaviour leads to the conclusion that an ordinary dissolving reaction in cement paste is probably very much a diffusion-controlled

process. The time for pure water to diffuse to the solid and for the dissolved ions to diffuse away is much larger than the pure dissolving reaction.

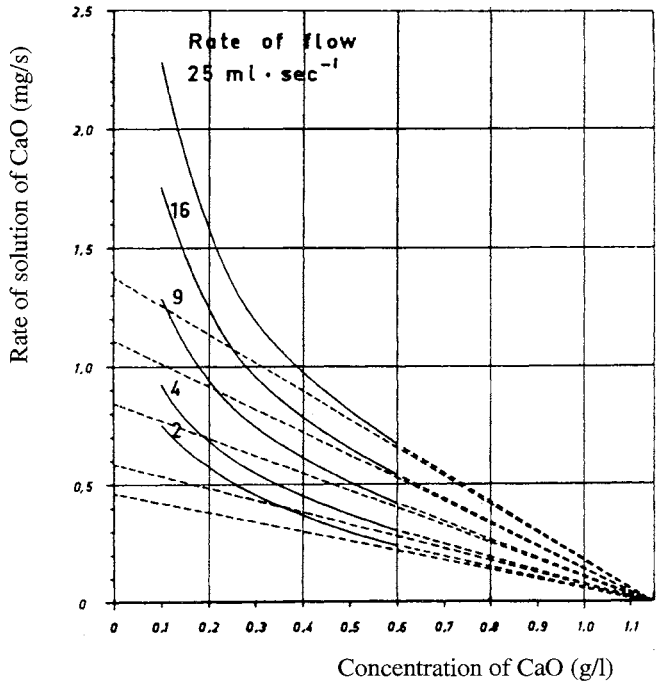

Figure 1-5 Rate of solution as a function of the concentration at various rates of flow (stirring). Hedin (1962).

In such a strong electrolyte as the pore solution in a cement paste, it is not easy to predict to which content the different ions are dissolved. Pitzer (1991) has developed an ion interaction model for electrolyte activity coefficients. With data of Ca-K-Cl-OH-H_2O systems from the literature and own experimental data of Ca-K-Na systems, Dushesne and Reardon (1995) has refined the parameters in the Pitzer model for $Ca(OH)_2$(aq) systems and obtain "excellent agreement" (the authors expression) with experimental data of $Ca(OH)_2$ in solutions with $CaCl_2$, $CaSO_4$, NaCl, NaOH, KCl, Na_2SO_4 and K_2SO_4. They used a solubility product of $K_{sp} = 10^{-5.2}$ for $Ca(OH)_2$.

Diffusion

When water has dissolved ions from the solid phases, the ions will flow away by convection and diffusion. The smaller the flow paths are, the less is the flow of water (Table 1-1) and the more of the ions will flow by diffusion.

Table 1-1 Related pore radius to permeability coefficients. Moskvin (1980)

Pore radius (m)	Permeability coefficient (m/s)	Transfer
$< 10^{-7}$	$< 10^{-10}$	Molecular diffusion
10^{-7} - 10^{-5}	10^{-10} - 10^{-9}	Molecular flow
$> 10^{-5}$	$> 10^{-9}$	Viscous flow

Some authors have tried to model the dissolving and diffusion part of the leaching process. Marchand, Samson and Maltais (1999) have modelled ionic diffusion mechanisms in saturated cement based material. They start by an equation that describes the time change in the solid phase, the time change in the pore solution and the balancing ionic flow:

$$(1-P)\frac{\partial c_{i(s)}}{\partial t}+\frac{\partial (W\, c_i)}{\partial t}=-div(W\,\mathbf{F}_i) \tag{1-1}$$

$$\mathbf{F}_i=\mathbf{F}_{iu}+\mathbf{F}_{iv} \tag{1-2}$$

where

	c_i	Ionic concentration in the free water solution (pore solution) (mole/m^3)
	$c_{i(s)}$	Ionic concentration in the solid phase (mole/m^3)
	$\mathbf{F}_i$	Total ionic flux (mole/(m^{2}s))
	$\mathbf{F}_{iu}$	Ionic flux due to diffusion (mole/(m^{2}s))
	$\mathbf{F}_{iv}$	Ionic flux due to convection (mole/(m^{2}s))
	P	Total porosity (m^3/m^3)
	W	"Free" (or unbound) water fraction (m^3/m^3)

Neglecting ion flow due to convection and neglecting interaction between the dissolved ions in the pore solution and bounded ions in the solid phase (no dissolving reaction), the authors uses a model, called STADIUM, by which they do numerical calculations of diffusion. So, neglecting the first term in equation (1-1), the diffusion is described by the equation:

$$\frac{\partial (W\, c_i)}{\partial t}=-div(W\,\mathbf{F}_{iu}) \tag{1-3}$$

The diffusion is assumed to be caused of local gradients of the electrochemical potential (μ_i).

$$\mathbf{F}_{iu}=-\frac{D_i}{RT}\,grad(\mu_i) \tag{1-4}$$

$$\mu_i=\mu_{i0}+R\cdot T\cdot ln(\gamma_i\cdot c_i)+z_i\cdot F\cdot E \tag{1-5}$$

where

	D_i	Diffusion coefficient for specie i (m^2/s)
	E	Local electrical potential (V)
	grad(μ_i)	Local gradient of μ
	F	Faraday constant ($9.65\cdot 10^4$ J/(V·mole))
	R	Gas constant (J/(K·mole))
	T	Temperature (K)
	$R\cdot T\cdot ln(\gamma_i\cdot c_i)$	Difference between any condition for specie i and the standard condition (at 1 atm, 20°C).
	z_i	Valence of the ionic specie i
	γ_i	Activity coefficient of specie i

μ_i	Electrochemical potential of specie *i* (J/mole)
μ_{i0}	Standard chemical potential of specie *i* (J/mole)

The local electrical field *E* between different ions is given as:

$$\nabla^2 E + \frac{\rho}{\varepsilon} = 0 \tag{1-6}$$

$$\rho = F\sum_{i=1}^{n} z_i c_i \tag{1-7}$$

where ε Dielectric field of the medium (F/m=J/(V^2·m))
ρ Electrical charge density (J/(V·m^3))

(1-4) is rewritten as an equation which the authors called an *extended Nernst-Planck* equation:

$$\mathbf{F_{iu}} = -D_i\left(grad\, c_i + c_i\, grad \ln\gamma_i + \frac{F z_i}{RT} c_i\, grad\, E \right) \tag{1-8}$$

By this equation, it is claimed that both viscous-drag on the ions and various electrical forces between different ions, are regarded. The ionic solution establishes an electroneutrality that slows down faster ions and speeds up slower ions. The authors said the equations are simply implemented in computer programs.

For the above equations, the activity coefficient $\gamma$is used. Many theories have been developed for calculation of the activity coefficient γ, e.g. the Debye-Hückel equation, the Pitzer equation (Pitzer (1991)), the Güntelberg equation (Stumm (1996)), etc. Marchand et al relates a equation proposed in Samson et al (1999), said to be suitable for calculations of activity effects in ionic solutions of high concentrations:

$$\ln\gamma_i = \frac{A z_i^2 \sqrt{I}}{1 + a_i B\sqrt{I}} + \frac{\left[4.7\cdot 10^{-5}\cdot I + 0.2\right] A z_i^2 I}{\sqrt{1000}} \tag{1-9}$$

$$I = \frac{1}{2}\sum_{1}^{N} z_i^2 \cdot c_i\,; \qquad A = \frac{\sqrt{2}F^2 e_0}{8\pi(\varepsilon RT)^{3/2}}\,; \qquad B = \sqrt{\frac{2F^2}{\varepsilon RT}}$$

where I Ion strength (mole/l)
a_i Adjustable parameter corresponding to the size of the ion, e.g. 3 (Å) for K^+, OH^-, 4 (Å) for Na^+ and 6 (Å) for Ca^{2+}, (Stumm 1996).

In a later work, Samson, Marchand and Beaudoin (1999), uses the same equations as (1-8), but they neglect the diffusion caused by gradients in chemical activity, $-D_i c_i$**grad** ln (γ_i). The variables of interest are also averaged on a representative elementary volume (REV). The averaging method is said to not require any detailed knowledge of the material inner structure and the included variables is measured easily in practice. The equations (1-3) and (1-8) are rewritten as:

$$\frac{\partial(\overline{c}_i^{\,L})}{\partial t} = div\left(-\mathrm{D_i\, grad}\,(\overline{c}_i^{\,L}) - D_i \frac{F z_i}{RT}\overline{c}_i^{\,L}\mathrm{grad}\,(\overline{E}^{\,L}) \right) \tag{1-10}$$

The electric field in (1-6) is rewritten as:

$$div\left(W\,\tau\,\mathrm{grad}\,(\overline{E}^{L})\right)+W\frac{F}{\varepsilon}\sum_{1}^{N}z_i\,\overline{c}_i^{L}=0 \tag{1-11}$$

Where $\overline{c}_i^{L}$ Average concentration of specie *i* in the liquid phase in a whole representative elementary volume (REV) (mole/m^3)

$\overline{E}^{L}$ Average electric potential in the liquid phase in a whole representative elementary volume (REV) (V)

τ Reduction tensor regarding the tortuosity of the pore system

Delagrave, Gérard and Marchand (1997) have modelled the calcium leaching mechanisms in hydrated cement pastes. The modelling starts with the same equation (1-1) as in Marchand et al(1999). However, they neglect the second term $\partial c_{i(s)}/\partial t$ on the left side by saying, "the amount of calcium ion initially in solution is very small in comparison with the amount dissolved by the calcium-bearing hydrates during the leaching process" and rewrite (1-1) to:

$$\frac{\partial c_{Ca(s)}}{\partial c_{Ca^{2+}}}\cdot\frac{\partial c_{Ca^{2+}}}{\partial t}=div\left(D_{Ca^{2+}}\,grad\,c_{Ca^{2+}}\right) \tag{1-12}$$

The first part of the first term on left side, $\partial c_{Ca(s)}/\partial c_{Ca}$ is the equilibrium curve between Ca^{2+} in pore solution and the Ca/Si ratio in the solid phase as showed in Figure 1-6. It is calculated with a complicated relation which is not easy to see through:

$$c_{Ca(s)}=a-b\cdot x^2+c\cdot x-\left[\frac{e}{1+\left(\frac{c_{Ca^{2+}}}{x_2}\right)^{N}}+\frac{f}{1+\left(\frac{c_{Ca_{2+}}}{x_1}\right)^{M}}\right] \tag{1-13}$$

$e = S_{por}$; $f = 0.565(S_{tot}-S_{por})$; $b = (S_{tot}-S_{por}-f)/400$; $c = (S_{tot}-S_{por}-f)/20 + 20b$; $a = S_{por}+b$

where $c_{Ca^{2+}}$ Concentration of Ca in the pore solution (mmole/l)

$c_{Ca(s)}$ Concentration of Ca in the solid phase (mmole/l)

S_{por} Molar fraction of portlandite (mmole/l)

S_{tot} Molar fraction of total calcium in the hydrated cement paste (mmole/l)

x_1 Average position of the dissolution front of portlandite (at a calcium concentration of 20 mmole/l).

x_2 average position of the dissolution front of C-S-H (at a calcium concentration of 2 mmole/l).

N Constant (70 to 100)

M Constant (5)

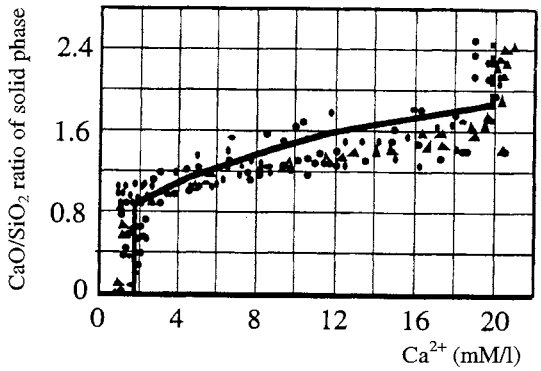

Figure 1-6 The ratio CaO/SiO_2 of the hydrated cement paste as a function of calcium concentration in solution. Data from Berner (1988), represented in Delagrave, Gerard and Marchand (1997)

Like in Samson et al (1999), and Delagrave et al (1997), the authors only considers the diffusivity due to concentration gradients and neglect gradients in local chemical activities and local electrical potentials.

The pore system is assumed to become more open when solid material is leached away and the authors assume the diffusivity to increase by the equation:

$$D = D_0 \left(\frac{D_L}{D_0} \right)^{\frac{\beta V^d_{por} + \alpha V^d}{V^e_{por} + V^i}} \tag{1-14}$$

$$\alpha = 1+(1-\beta)\cdot V^i_{por}/V^i \tag{1-15}$$

where
- D — Diffusion coefficient of the solid at a given time (m^2/s)
- D_0 — Initial diffusion coefficient (m^2/s)
- D_L — Diffusion coefficient of the totally degraded solid at the end of the calcium leaching process (m^2/s)
- V^d_{por} — Volume fraction of the portlandite (m^3/m^3)
- V^d — volume fraction of the hydrates other than portlandite (m^3/m^3)
- V^i — volume fraction of the hydrates calculated by subtracting the volume occupied by the portlandite and SiO_2 fraction to the total volume of hydrates in a fully hydrated system. (m^3/m^3)
- β — Empirical coefficient which mainly accounts for the effect of the dissolution of calcium hydrates on the diffusion properties of the material. A higher β gives a more open pore network, which make it easier for ions to move. (-)

The authors claim good agreement with test results and that the only parameter to be determined in the test was β.

Another example on modelling of the diffusion coefficient is given in Seveque, Cayeux, Elert and Nouguier (1992). The authors introduce the *apparent diffusion coefficient*, D_a, used in Fick's second law:

$$\frac{dc}{dt} = D_a \frac{d^2c}{dx^2} \tag{1-16}$$

Where c Ionic concentration in the pore solution (mole/m^3)
D_a apparent diffusion coefficient , regarding tortuosity, constrictivity and chemical reactions with the pore walls. (m^2/s)

$$D_a = \frac{D_f}{P\left(1+\frac{1-P}{P}\rho K_d\right)} \tag{1-17}$$

Where D_f Free water diffusion coefficient (m^2/s)
P Bulk porosity (m^3/m^3)
ρ Solid bulk density (kg/m^3)
K_d Sorption coefficient (m^3/kg)

Adenot and Richet (1997) have developed a Finite Difference model of chemical degradation of cement paste, DIFFUZON. The modelling starts with equation (1-1). However, like Samson et al (1999), and Delagrave et al (1997), they regard only diffusivity due to concentration gradients and neglect gradients in local chemical activities and local electrical potentials. In Figure 1-7, the authors show a calculation of the residual Ca and Si content in an OPC paste with w/c=0.4 after 3 months degradation in essentially deionized water at pH 7. They claim good agreement with experimental results. In the part of the paste nearest to pure water only silica gel remains. The other compounds have leached away by diffusion. The deeper into the specimen, the more original hydration compounds are still left and the more Ca remains in the hydration products.

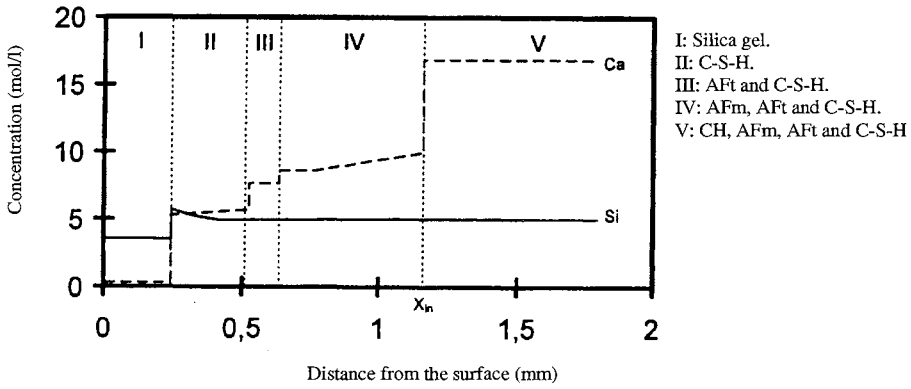

Figure 1-7 Calculated solid phase profiles of calcium, silicon, aluminium and sulphate in an OPC paste with w/c 0.4 after 3 months degradation in essentially deionized water at pH 7. Adenot and Richet (1997).

Bentz and Garboczi (1991a) and Garboczi and Bentz (1992) uses a somewhat different modelling approach to the leaching process. They use a computer model, laying cement particles of C_3S randomly in a 3-dimension space. The particles hydrates randomly and grow by the

volume effect $1.0C_3S \rightarrow 1.7(C\text{-}S\text{-}H) + 0.61CH$, where C-S-H is calcium silicate hydrate (cement gel) and CH is calcium hydroxide (volume ratios) into a 3D micro-structural model. By this, the porosity and the permeability decreases. The pixels can be solid phases or pore space. In the leaching process, the computer does the reverse, taking away hydration products (pixels) randomly and the porosity and the permeability increases again. The computer test at each hydration ratio or leaching ratio, how connected the pore-pixels are through the specimen and the results are the percolation (or diffusion) ability.

They have performed a large amount of simulations with this computer model on fictive cement pastes. They have modelled such properties as porosity, fraction of connected pores, percolation in capillary pores, ionic diffusivity for both the hydration phase and for any possibly leaching phase. The early hydration phase have also been simulated regarding interfacial zone percolation, strength development, thermal development and self-desiccation, see Bentz and Garboczi (1991b), (1992), Garboczi and Bentz (1992), (1998), (1998) and Bentz (1999).

Eijk and Brouwers (1998), referring to the same modelling method as that was used by Bentz and Garboczi, give other volume fractions for the hydration products by considering also chemical shrinkage; $C_sS \rightarrow 1.52(C\text{-}S\text{-}H)+0.61CH$.

Garboczi and Bentz (1996) have modelled the diffusivity of ions in a pore system of cement paste for different porosity based on degree of hydration and compared it to free water diffusivity, se Figure 1-8 . They denote the porosity as capillary porosity, but when looking at the porosity values of 0.34 for w/c ratio 0.45 and 0.45 for w/c 0.60, one must assume they mean total porosity.

$$D/D_0 = 0.001+0.07*Pp^2 + H(Pp-0.18)*1.8*(Pp-0.18)^2 \qquad (1\text{-}18)$$

Where
- D — Measured diffusivity (m^2/s)
- D_f — Free water diffusivity (m^2/s)
- Pp — Total porosity in the paste before leaching = $(w/c-0.39\alpha)/(0.32+w/c)$ (m^3/m^3)
- $H(Pp-0.18)$ = 0 for $Pp<0.18$ and
  = 1 for $Pp>0.18$, where 0.18 is a percolation threshold, due to Bentz and Garboczi (1992), where a unbroken path from one side of the system to the other for the first time appear.

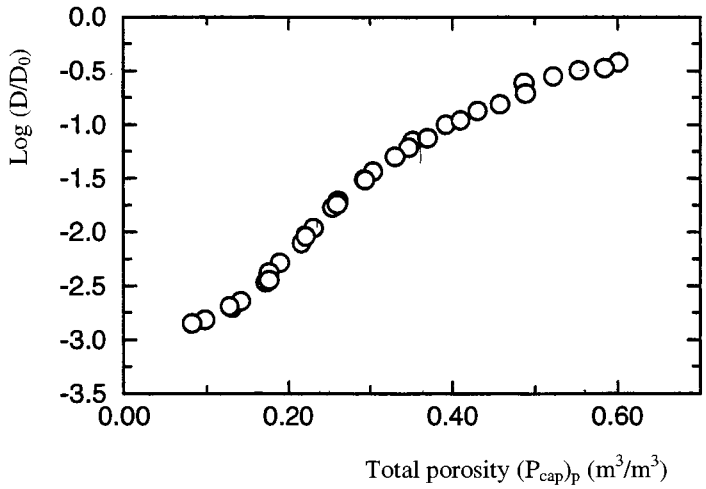

Figure 1-8 Calculated data for the diffusivity in cement pastes, normalized by the free water diffusivity, as a function of the total porosity. Data from Garboczi and Bentz (1996) but the porosity is here denoted as total porosity instead for capillary porosity in the reference.

Eijk, Brouwers (1998) instead use the leached capillary porosity:

$$D/D_f = 0.0025-0.07*Pp^2 - H(Pp-0.18)*1.8*(Pp-0.18)^2 + 0.14Pp_L^2 +$$

$$+ H(Pp_L-0.16)*3.6*(Pp_L-0.16)^2 \qquad (1\text{-}19)$$

Where Pp_L Capillary porosity of the paste after leaching (m^3/m^3)

In Table 1-2, values from literature of the diffusivity of different ions in free water are presented.

Table 1-2 The mass diffusivity D_f of ions in dilute, free water.

Ion	D_f (m^2/s)	Literature reference
Ca^{2+}	$1 \cdot 10^{-9}$	Moskvin (1980)
	$0.79 \cdot 10^{-9}$	Wallin (1988)
K^+	$1.96 \cdot 10^{-9}$	Johannesson (1998)
Na^+	$1.33 \cdot 10^{-9}$	Johannesson (1998)
OH^-	$5.27 \cdot 10^{-9}$	Wallin (1998)
	$5.30 \cdot 10^{-9}$	Johannesson (1998)
H^+	$9.30 \cdot 10^{-9}$	Wallin (1998)
CO_2	$2.00 \cdot 10^{-9}$	Wallin (1998)
HCO_3^-	$1.20 \cdot 10^{-9}$	Wallin (1998)
CO_3^{2-}	$0.70 \cdot 10^{-9}$	Wallin (1998)

Convection

In water retaining structures with water percolating through the concrete, ions in the pore water will move by the water flow (convection). Literature references on permeability is given in section 1.2.3.

1.2.3 Factors influencing leaching

Influencing factors on leaching in concrete is Halvorsen (1966):

- ✓ The water permeability
- ✓ The amount of total Ca in the concrete and the amount of $Ca(OH)_2(s)$.
- ✓ Any additives that can bind lime.
- ✓ Carbonation of $Ca(OH)_2$
- ✓ The hardness of the water
- ✓ The amount of carbonic acid which is free to attack the concrete.

The most important influencing factor is the water permeability of the concrete. The permeability is a measure how easy the water can flow in the three dimensional pore system of the concrete. The concrete consist of the three main phases paste, aggregate and the interfacial zone between the paste and the aggregate. The permeability can be divided in (Lawrence 1982):

1) The permeability of the paste
2) The permeability of the aggregate
3) The permeability of the interfacial zone
   a) Pore size distribution of the zone
   b) Crystals in the zone (mainly $Ca(OH)_2$)

In reference to Darcy's law, Halvorsen (1966) gives examples of permeability values for concrete from as highest 10^{-7} (m/s) to as lowest 10^{-13} (m/s) (pressure gradient in piezometric head/m). The most important factors due to the author are: (i) w/c ratio, (ii) maximum aggregate size, (iii) the curing conditions. He emphasis that permeability for real structures is often higher than measured in laboratory.

An attempt to relate the permeability of cement paste to the porosity, specific area and hydraulic radii, have been done by Nyame and Illstone (1981). They conclude that these factors are not uniquely related to permeability. However, the hydraulic radius of the pore system describes rather well the permeability except for pore sizes near to molecular dimension, see Figure 1-9 and Figure 1-10. The permeability is not a unique function of the porosity as can be seen in Figure 1-9. The authors suppose that continued hydration subdivided the pore system in many, not connected pores. They suggest that the water flow occur in distinct flow channels. The relationship between permeability and pore structure in hardened cement paste is summarised in Figure 1-11 as:

$$\text{Log } k_w = 38.45 + 4.08 \log (P \cdot r_h^2) \qquad (1\text{-}20)$$

Where	k_w	Water permeability (m/s)
	P	Porosity (unclear unit in reference, should probably be m^3/m^3)
	r_h	Hydraulic radius of the pore system (m)

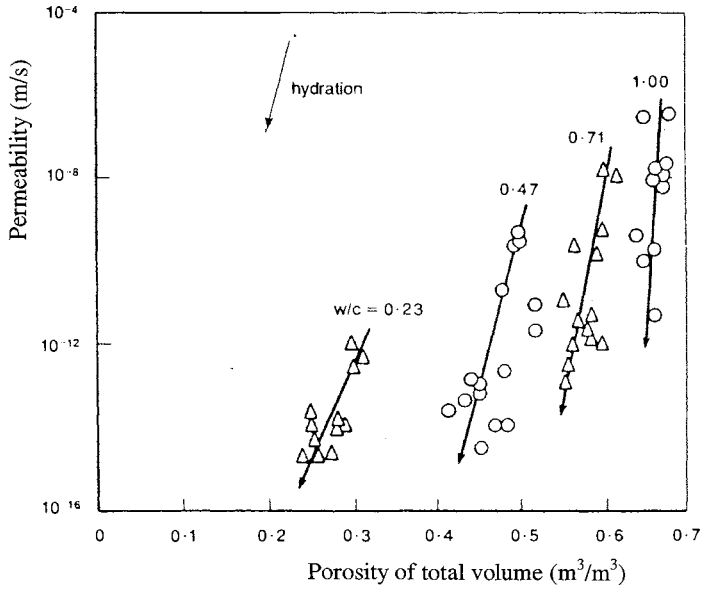

Figure 1-9 Permeability for cement paste as function of total porosity Nyame and Illston (1981)

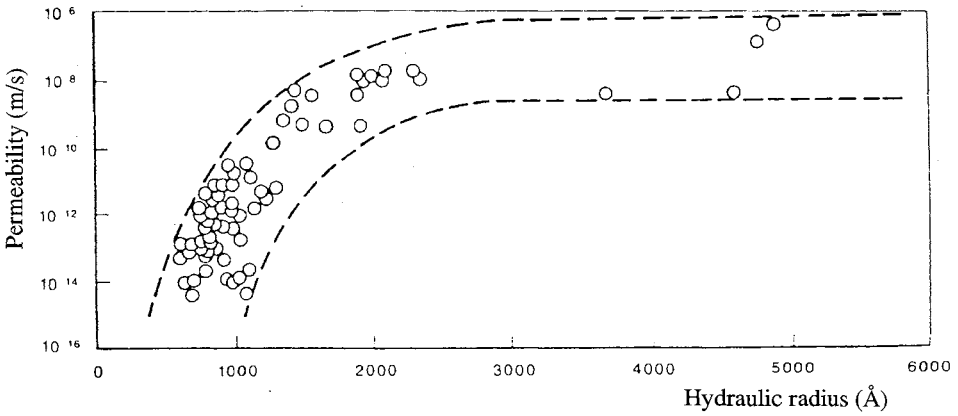

Figure 1-10 Relationship between permeability and hydraulic radius of the pore system Nyame and Illston (1981)

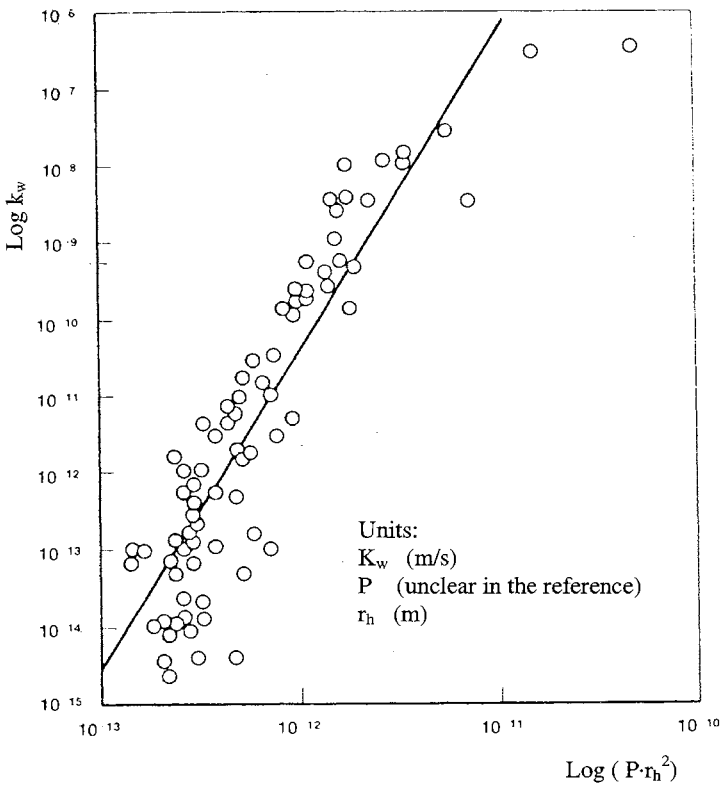

Figure 1-11 A comparison of permeability data for hardened cement paste with hydraulic radius theory. Nyame and Illston (1981)

Figure 1-12, Figure 1-13 and Figure 1-14 show early studies of permeability for cement paste and homogenous concrete. The relation between k and B is k = 10*B. It can be seen that the higher the w/c ratio, the higher the permeability for both cement paste and concrete. Concrete has higher permeability than cement paste. The larger the maximum aggregate size is in concrete, the higher the permeability. Of course, the influences from w/c ratio, aggregate or not and the size of aggregate on the permeability, all arise from the fact that they cause larger flow paths and that the water flow approximately is proportional to the radius raised to 4. Therefor, the larger the flow paths, the higher the water permeability.

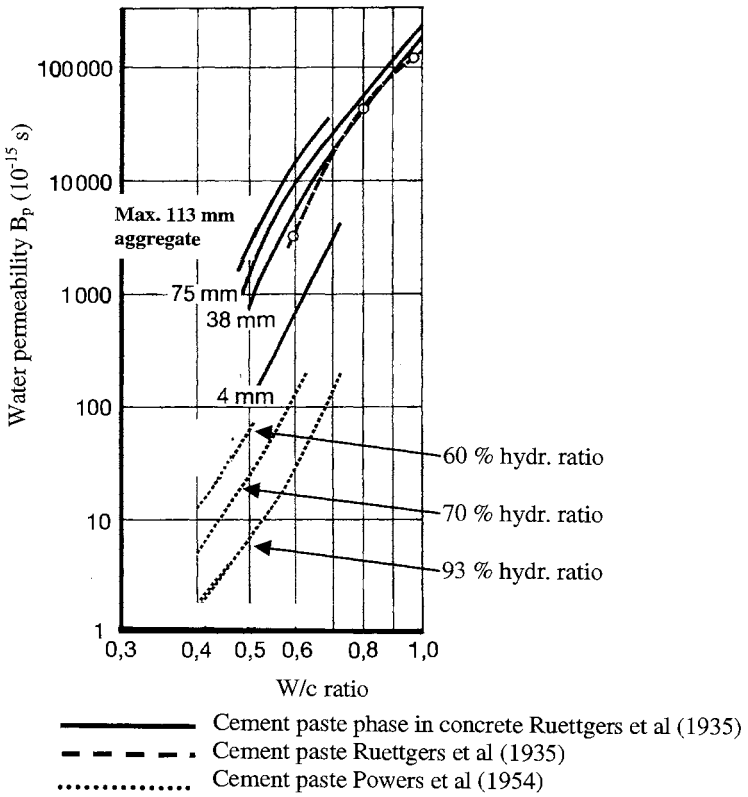

Figure 1-12 Water permeability for cement paste and the cement paste phase in concrete. Presented in Fagerlund (1980).

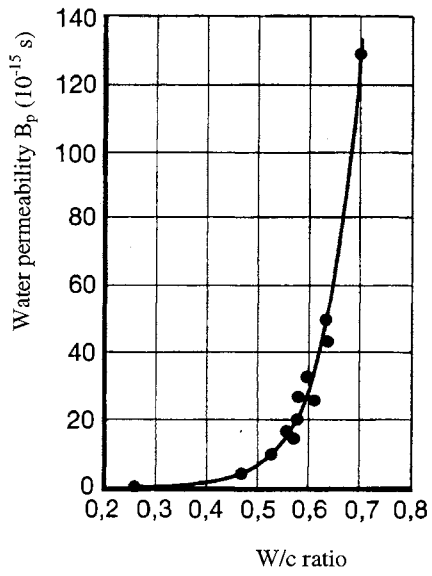

Figure 1-13 Permeability of cement paste in proportion to w/c ratio. Powers et al (1954), presented in Fagerlund (1980).

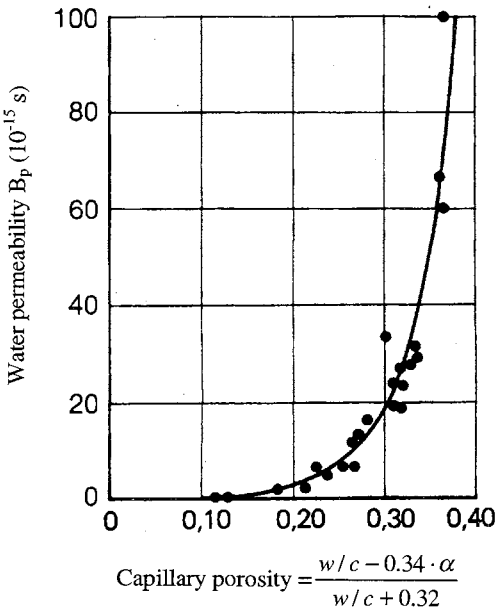

Figure 1-14 Permeability of cement paste in proportion to capillary porosity. Powers et al (1954), presented in Fagerlund (1980).

When there are cracks in the paste, mortar or concrete, the water flow is totally governed by the crack width. A way to calculate the leakage through a crack is to use the following variant of Hagen-Poiseuilles equation:

$$q_{w,crack} = \alpha \frac{w^3 \cdot \Delta P}{\mu \cdot \Delta x} \cdot L \qquad (1\text{-}21)$$

where:	$q_{w,crack}$	Leakage of water through a crack (m^3/s)
	α	"Surface roughness factor"; generally about 0.01-0.2.
	w	Crack width (m)
	$\Delta P/\Delta x$	Pressure gradient (Pa/m)
	μ	Dynamic viscosity (kg/ms)
	L	Length of the crack (m)

Edwardsen 1996) have studied the permeability in cracks in concrete under the influence of self-healing, see below under "Leaching effects on permeability". The initial flow for different crack widths and water pressure gradients followed the equation (1-21) with a roughness factor of about 0.21 (Figure 1-15).

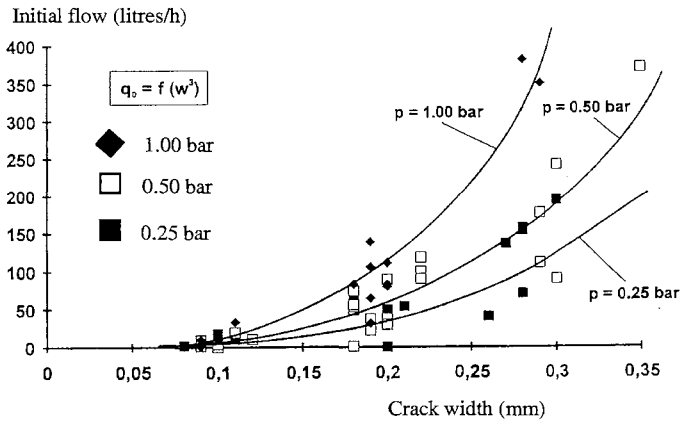

Figure 1-15 Initial flow of water as a function of the crack width from Edwardsen (1996).

Hearn and Morley (1997) found indications of increased leaching of Ca, K and Na compared to its virgin state when they dried 26-year old virgin concrete (Figure 1-16). They assume that the drying caused an exposure of previously unexposed soluble compounds. They found also that the concentration of Ca in the outflow water decreased during the test.

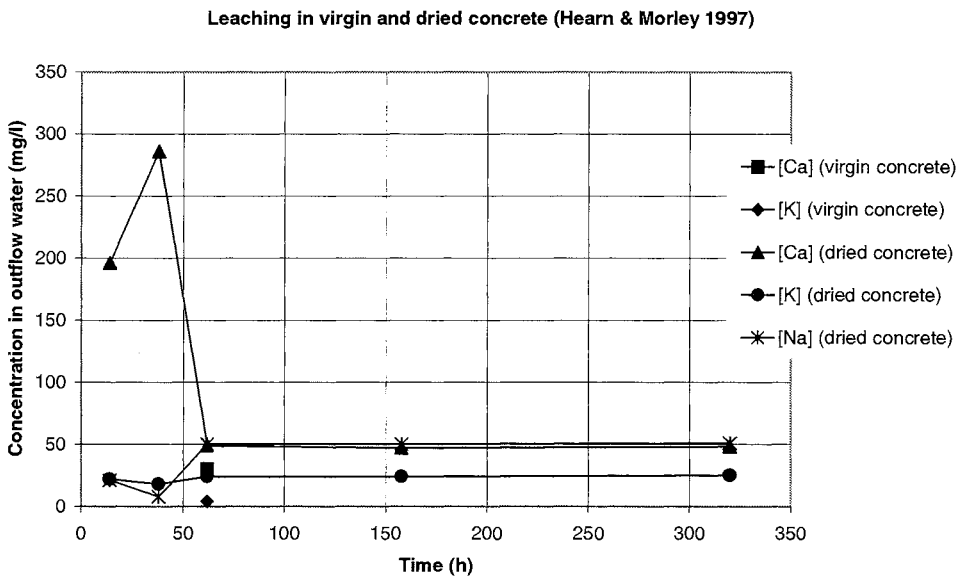

Figure 1-16 Typical changes in the outflow water during time for a permeability test Hearn & Morley (1997)

The less amount of dissolved ions there is in the pore water and the lower the pH value (e.g. due to aggressive CO_2 in the water), the more aggressive on concrete is the water. Water in many rivers is very soft with a pH value about 7.0. Comes the water from e.g. moor lands, it can also contain carbonic acid, which makes the water even more aggressive on concrete. Terzaghi (1940) means however, that aggressive carbonic acid mostly influences the leaching of concrete surfaces only and not so much the interior of the concrete.

In Table 1-3, mean values from water analyses in Swedish rivers are shown.

Table 1-3 Mean values of pH and aggressive CO_2 in Swedish rivers from Halvorsen (1966).

Location	pH	Aggressive CO_2 (mg/l)
Porjus	6.6	5.4
Knutsbro	6.8	7.9
Älvkarleby	6.5	6.2
Norrfors	6.5	6.7
Trollhättan	6.6	4.3
Edsele	6.6	5.0
Motala	7.2	3.0
Mean:	6.7	5.5

1.2.4 Leaching effect on permeability

Intuitively, one may presume that leaching shall give higher permeability when material is withdrawn from the pore space.

Halvorsen (1966) refers to work done by Ruettgers (1936), who claims that there is no increased permeability due to leaching, even for as much leaching as 1/3 of the total lime.

Meyers (1936), meant that for specimens of the type that Ruettgers used, the effect of carbonation was not regarded. CO_2 that has reacted with lime in pore solution, can both open and fill cavities and the permeability will change due to this.

Hearn and Morley (1997) performed a percolation study of 26-year old homogenous concrete in its virgin state and the same concrete after drying in order to find its self-healing properties. The result showed a constant permeability for the virgin concrete (Figure 1-17). The dried concrete got an increased permeability of about 100 times that in the virgin state, but it gradually decreased during the test. To facilitate the comparisons between water and other liquids, the authors has used a so-called "intrinsic" permeability k (m^2):

$$k = \frac{\mu}{\rho_w} \frac{q_w}{A} \frac{\partial P}{\partial x} \tag{1-22}$$

Where	k	"Intrinsic" permeability (m^2)
	μ	Dynamic viscosity (Pa·s)
	ρ_w	Density of water (kg/m^3)
	q_w	Rate of flow (m^3/s)
	A	Cross-section area (m^2)
	$\partial P/\partial x$	Pressure gradient (Pa/m)

Probably is the equation (1-22) wrongly written in Hearn and Morley. To have k in the unit m^2 and the pressure gradient written normal, the permeability k shall probably be written as D'Arcy's law (Scheidegger 1963):

$$q_w = \frac{k}{\mu} \frac{\partial P}{\partial x} A \tag{1-23}$$

The authors claim that the decrease in permeability was due to self-healing, caused of dissolution of soluble species such as $Ca(OH)_2$ in the upstream face and deposition and crystallisation of the same species at the downstream face. No self-healing due to continuing hydration of cement in the specimens was assumed. The deposition and crystallisation of species was assumed to occur when the pressure drops along the flow path. However, this presumes a pressure effect on the solubility of the species. In Constantiner and Diamond (1995), there was no significant pressure effect measured on the solubility for alkali and Calcium hydroxide.

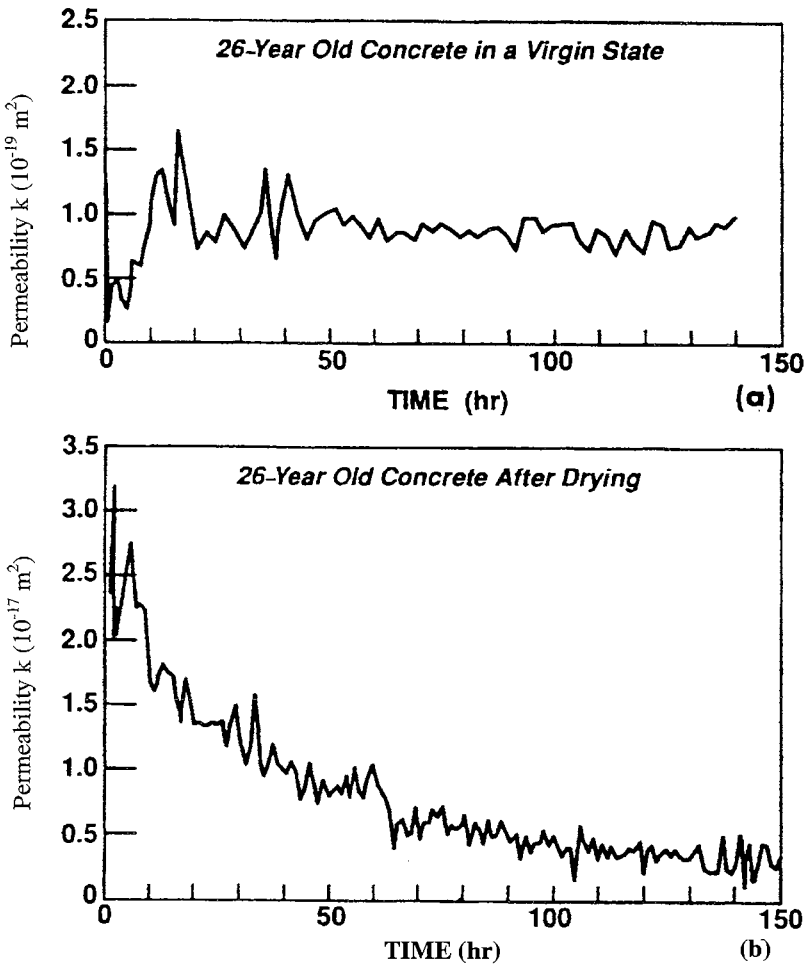

Figure 1-17 Typical variation of the permeability during testing of (a) 26-year old, never-dried concrete; and (b) the same concrete but oven-dried in +105°C and resaturated. Hearn and Morley (1996).

Edwardsen (1996) has studied the self-healing properties in concrete cracks. She found that:

- ✓ It was differences between stationary and mobile cracks. In Table 1-4 Edwardsen indicates crack widths that have a ability to self-heal.
- ✓ The main cause of self-healing was formation of $CaCO_3$ coming from reactions between dissolved $Ca(OH)_2$ and atmospheric CO_2. The growths of the $CaCO_3$ decreased by increasing crack width, with mobile cracks and by increasing water pressure.

In Figure 1-18, the healing rates for different crack widths and water pressure are showed Edwardsen (1996). The water flow in tests decreased rapidly due to self-healing. The author

means that the first time, Ca^{2+} are taken directly from the crack surface and the crystals of $CaCO_3$ can grow directly on the surface. But, due to the increasing layer of crystals on the surface, Ca^{2+} must diffuse both through the concrete and the formed crystal layer, and this will slow down further crystal growths and the self-healing rate.

Table 1-4 Recommendations by Edwardsen (1996) for maximum crack width for what autogenous healing at water-retaining structures with stationary and mobile cracks is possible.

Pressure gradient (m/m)	Crack width (mm)		
	Stationary cracks	Mobile cracks	
		Δw≤10 %	Δw≤50%
≤10	0.20	0.20	0.10
≤30	0.10	0.10	0.05

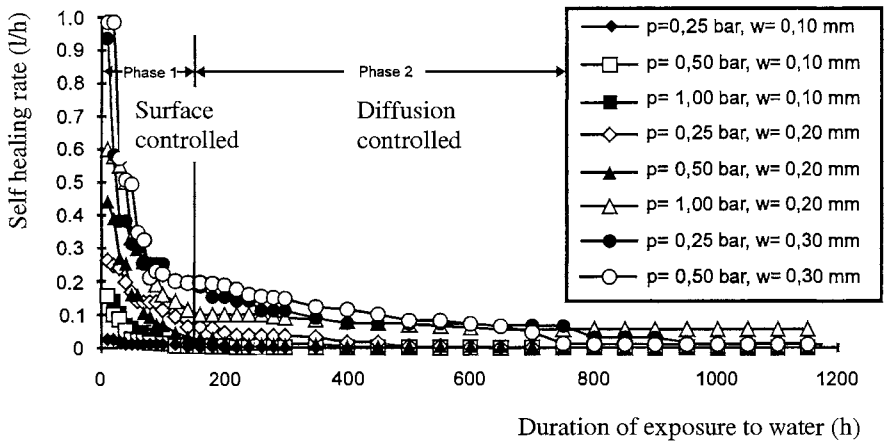

Figure 1-18 Healing rate for different crack widths and water pressure Edwardsen (1996).

1.2.5 Leaching effect on porosity

The work done by Bentz and Garboczi, mentioned above, have resulted in some possibilities of modelling leaching effect on porosity. It has not been possible to find any experimental data on the effect of leaching on porosity.

1.2.6 Leaching effect on strength

Spontaneously, one may presume that leaching shall give lower strength when material is withdrawn from the pore space.

Ruettgers (1936) performed comprehensive percolation studies on homogenous, very porous concrete and in Figure 1-19connections between leached content of CaO and the compressive strength are showed. Halvorsen (1966) and Mary (1937) have pointed out that the relation is

only valid for concrete with continuous pore system and not when the water percolation is concentrated to cracks or surfaces.
In Figure 1-19, results from Tremper (1931) and Terzaghi (1948) are also showed. The results show substantial higher reductions in strength than the Ruettgers data. One explanation given by Terzaghi, is that they used water with high content of aggressive CO_2 while Ruettgers used only pure water without carbon acid. Lime can very well have leached away from pore spaces in the upstream part, but re-crystallised as $CaCO_3$ again further downstream. The authors only measured the lime that came out of the specimens. Regarding that the total strength of the specimens probably was governed by theirs weakest link, in this case the leached upper part of the specimens, the measured leached ratio of CaO became too low in comparison to the measured strength.

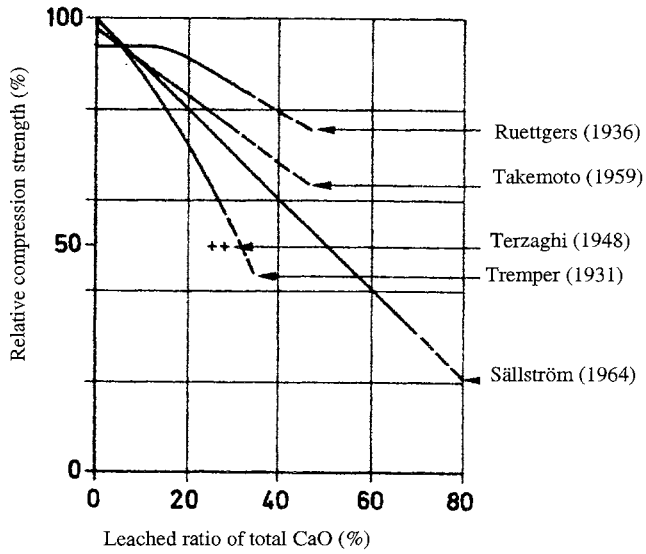

Figure 1-19 Relation between lime leaching and compressive strength. Results from different authors cited in Halvorsen (1966).

Terzaghi (1950) means that the main reduction in strength is caused by the dissolution of the cement gel.

On the other hand, Hallström (1934), cited in Halvorsen (1966), means that crystalline $Ca(OH)_2$ inside the concrete, contributes largely to the strength.

In Figure 1-20, a relation of loss of strength in proportion to loss of lime is shown from Moskvin (1980) with data from Ruettgers (1936). Moskvin stresses that the results behind the figures had a wide scatter and therefor not are altogether reliable.

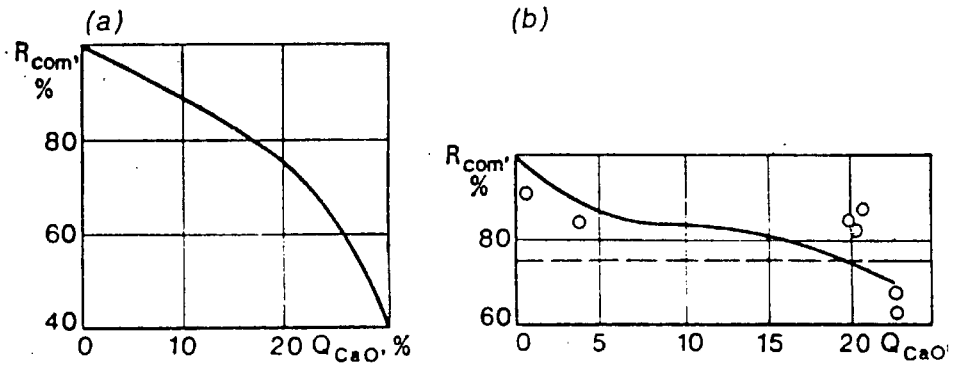

Figure 1-20 Loss of strength R_{com} in mortar (a) and concrete (b) as function of the amount of lime leached Q_{CaO}. Ruettgers (1936) presented in Moskvin (1980).

1.2.7 Synergy between leaching and other environmental attacks

No information about synergy effects between leaching and other environmental attacks have been found in the literature.

1.2.8 Concluding remarks

To summarise the literature survey one can say:

- ✓ In older literature before 1970, there have been mostly studies about percolation of water and homogenous leaching in concrete dams. Studies about leaching in cracks are missing. There are very few studies about mechanisms behind leaching.
- ✓ In later literature after 1970, there have not been so many leaching studies in percolated concrete, the few performed have been about self-healing effects. It has been more studies about leaching from cement paste and mortar in stagnant, pure water, where the dissolved hydration products have diffused to the water (extraction tests). Models of leaching due to diffusion of ions and models of changes in porosity and strength have been developed to some extent.

Many experiments have been carried out through the years, but these studies has mostly given curves for certain concrete types with certain curing condition, and for other certain conditions. The theory behind the whole leaching process has not been so much treated. This is only natural, because it is very difficult to look into a pore system – in any condition. There are no methods to visually look at the leaching process during time. It is both a micro-scale and a macro-scale involved and most of test methods destroys the specimens when they are used. Also, the statistical distribution of studied properties has not been so much treated.

1.3 Research needs

Today, there is a lack of knowledge regarding the following items:

- ✓ Statistical distributions of experimental data. By "statistical" is meant both distributions in space and time for a given property.

- ✓ Models for permeability in concrete, both for cracked and for homogenous concrete.
- ✓ Models for dissolving reactions in concrete. It should be of interest to simulate the dissolution of different hydration products in relation to each other's solubility and locations in the cement paste.
- ✓ Models for the whole leaching process including the flow of water, the dissolution of solid hydration products and the flow of dissolved ions due to both convection and diffusion.
- ✓ Changes of the pore size distribution when hydration products are leached away are not well known.
- ✓ Strength changes caused by increase in porosity due to leaching are not well known.

1.4 Short description of the present study

The purpose of the work

The purpose of the experimental work presented in this report was to study how de-ionised water flows through homogenous concrete and how the water effects the leaching process. Changes in *permeability*, *leaching rate* and *strength* were therefor studied.

The purpose of the theoretical work was to understand the theory behind leaching and perhaps find some models, by which estimations can be made about permeability, leaching rate and strength in concrete subjected to water percolation.

Limitations of the work

The experimental work has the following limitations:

- ✓ The w/c ratio was mainly 0.8, but a few specimens with w/c ratio 0.6 and 1.3 was used.
- ✓ The water pressure difference over the specimens was mainly 6 (bar) (60 meter water head).
- ✓ The water that was pressed through the specimens was de-ionised water with only atmospheric carbonic acid.
- ✓ The downstream face was not in contact with air below 100 % RH and have almost no contact with CO_2.
- ✓ There were no aggressive substances in the water (except atmospheric CO_2.
- ✓ The temperature was constantly +20°C.
- ✓ There was no influence from any other degradation mechanisms.
- ✓ There was no reinforcement in the specimens.

The modelling work has the following limitations:

- ✓ Water flow is assumed to occure in a number of *flow pipes* with an assumed size distribution and calculated by an assumed, reduced Hagen-Poiseuilles law.
- ✓ Only convection of transported Ca^{2+}-ions is regarded. Diffusion is not considered.
- ✓ The flow pipes are modelled with only one element through the concrete body, which means that no gradients of leaching effects can be calculated.
- ✓ Strength changes is assumed by an strength-structure relation, regarding only porosity, age, w/c-ratio and the amount of aggregate.

Experimental method

De-ionised water was pressed through a number of concrete specimens of different qualities. The flow of water and dissolved ions was measured in the drainage water. A chemical analysis was done of one leached specimen. A few cylinders that were drilled out of some leached specimens were tested of the compressive strength.

2 THE LEACHING PROCESS

2.1 General

A leaching process can be said to be the cause of an ambition to reach a lower energy level in a system. Chemical bonds are broken and solids are dissolved. In concrete, the pore solution stands in thermodynamic equilibrium with the solid material. If some parameters in the thermodynamic relation, such as temperature or pressure are changed, or if any of the dissolved material is carried away, the equilibrium is disturbed.
In figure 2-1, Moskvin (1980) gives a picture of the leaching rate in concrete. Between *a* and *b* the water flow is rather slow and the pore water is saturated. If the water flow increases, as at *b*, the pore walls become exhausted in lime and more lime must diffuse from the interior. The lime content in the water will in such a case decrease. In line segment *c-d*, the leaching rate is governed totally by the diffusion of $Ca(OH)_2$ from the interior to the main flow paths.

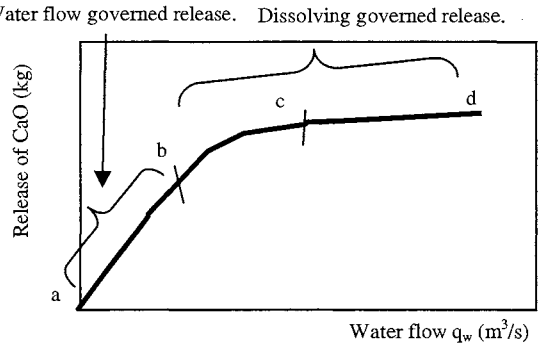

Figure 2-1 Lime leached from concrete vs rate of water percolation Moskvin (1980).

Concrete have certain *chemical* and *physical* properties, which make it more or less sensible to leaching.

Chemical properties depend on how the different compounds are built up, of what substances and how the different substances chemically interact with each other. How substances are built up or how they interact with each other is mainly a question how to reach a low, stable energy level.

Physical properties are related to how the hydration products are formed and connected to each other and the cavity between them, for example the geometrical size, connectivity and shape of the pores.

Chemical and physical properties interact with each other. The physical properties of a pore system decide how easy pure water can penetrate the pores. The chemical properties decide how easy the water, or in water dissolved aggressive substances, can react with the solid material inside the pore system. The reaction can for example be a dissolving reaction, as in leaching. Both physical and chemical properties govern the transportation of dissolved ions.

In figures 2-2 to 2-4, pictures taken by an ESEM microscope on one of the specimen that was tested in this work, is showed. In these pictures, the physical structure of the cement paste and the zone between the paste and the aggregate can to some extent be seen. The internal porosity of cement paste is very large, which appears in the pictures. The main constituents Calcium silicate hydrate (C-S-H), Calcium hydroxide (CH) and aggregate can be seen in the pictures. In a leaching process, it is mainly CH that is dissolved and transported away. When CH disappear, also C-S-H will starts to dissolve.

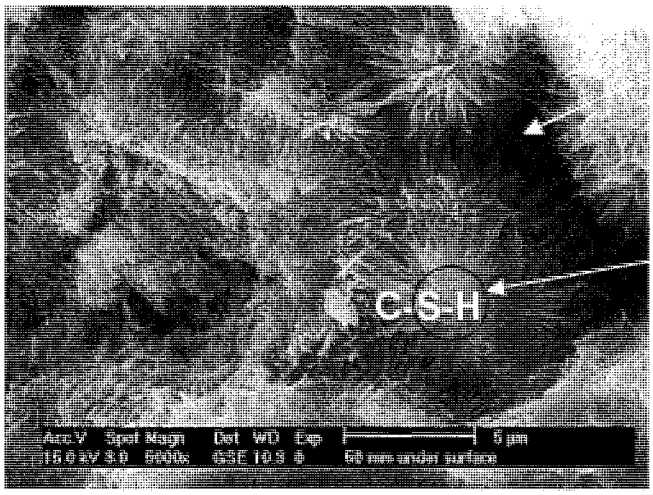

Capillary pores. Size ≈50Å to 1000Å.

Original border of the cement grain.

Figure 2-2 "Fluffy" Calcium-Silicate-Hydrate gel with capillary pores between. ESEM picture of one of the specimens tested in this study. Finger Institute at the University of Weimar.

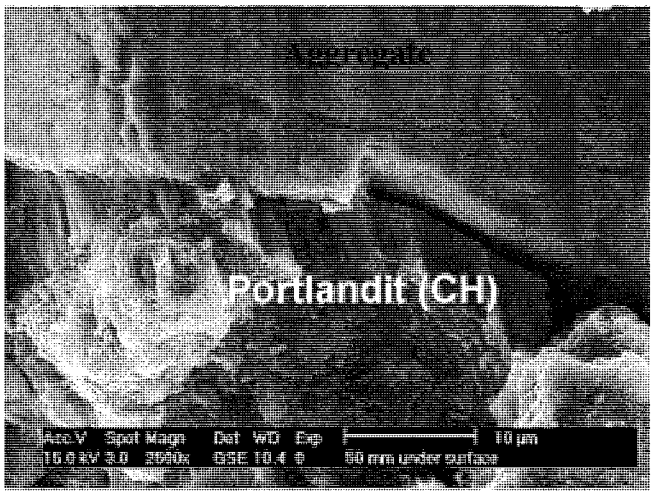

Figure 2-3 Calcium hydroxide formed close to the surface of an aggregate particle. ESEM picture of one of the specimens tested in this study. Finger Institute at the University of Weimar.

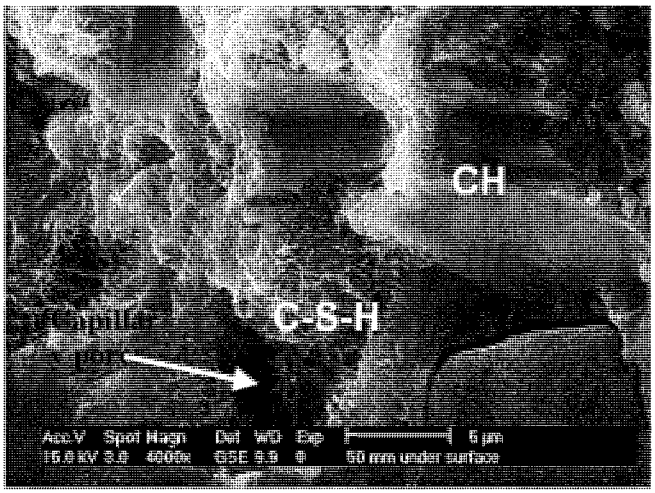

Figure 2-4 Calcium-Silicate-Hydrate gel with incorporated calcium hydroxide and capillary pores. ESEM picture of one of the specimens tested in this study. Finger Institute at the University of Weimar.

Most natural processes can be related to some sort of transforming (reaction) of energy inside a system or transport of energy through its border, see figure 2-5.

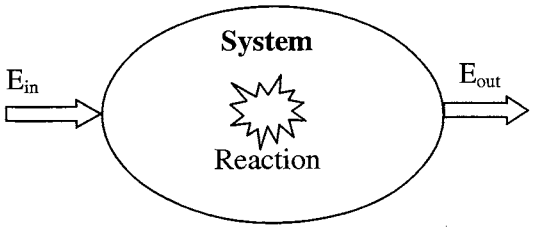

Figure 2-5 A principle picture over energy changes in a system.

In words, the transforming of energy can be written as: the change in energy is the change of heat plus the change of work done on a system.

$$dE = dq + dw \qquad (2\text{-}1)$$

where
- dE — Change in energy (J)
- dq — Heat change by radiation, convection or conduction (J)
- dw — Work done on the system, e.g. $w_{chemical}$, $w_{mechanical}$, $w_{kinetic}$, $w_{gravitional}$, $w_{interfacial}$ and $w_{electric}$. (J)

Transforming of energy inside a system or transport of energy through the border of the system may lead to transforming or transporting of mass inside the system or through its border. This is how lime leaching can be assumed to arise, pure water change the thermodynamic equilibrium in the concrete, solid mass is dissolved and transported away.

One way to describe a leaching process inside a saturated, porous material can be to see it as a balance of mass:

Change of mass = convection of mass + diffusion of mass + source or sink of mass through chemical reactions.

Or by a equation with masses rewritten to concentrations:

$$\dot{c}_i + \nabla(\mathbf{F}_{iv} + \mathbf{F}_{iu}) + Q = 0 \qquad \text{(Balance of ions in water)} \qquad (2\text{-}2)$$

$$\mathbf{F}_{iv} = \boldsymbol{v}_w c_i \qquad (2\text{-}3)$$

$$\mathbf{F}_{iu} = -\boldsymbol{k}_{ion(aq)} \nabla c_i \qquad (2\text{-}4)$$

where

	c_i	Concentration of dissolved ions (mole/m^3)
	$\dot{c}_i$	Changes of concentration during time *dc/dt* (mole/(m^3·s))
	$\boldsymbol{k}_{ion(aq)}$	Diffusion coefficient in pore solution (m^2/s)
	$\mathbf{F}_{iv}$	Convection flux of ions in pore solution (mole/(m^2·s))
	$\mathbf{F}_{iu}$	Constitutive relation of diffusion flux of ions in pore solution (mole/(m^2·s))
	Q	Mass source term, here as a dissolving reaction term (mole/(m^3·s))
	$\boldsymbol{v}_w$	Velocity of the water (m/s)
	∇	Nabla operator

The second term $\nabla \cdot \mathbf{F}_{iv}$ in the equation tells about how much of the substance that is carried away by a velocity field, e.g. ions transport in a water flow. The higher the velocity of the water, the more dissolved material is carried away by the water flow. The water velocity is very much influenced by the pore structure and the water pressure gradient.

The third term $\nabla \cdot (\mathbf{F}_{iu})$ tells about the ionic diffusion due to concentration gradients. Intermolecular forces in the pore solution between different ions and between dissolved ions and solid molecules influence the diffusion mobility. The larger the ion diffusivity, the more dissolved material is carried away by diffusion. Due to tortuosity of the pipes and intermolecular forces with other dissolved ions, or with solid material in the pipe walls, the diffusion coefficient in a real flow pipe, $k_{ion(aq)}$, is probably smaller than in the bulk water.

The fourth term Q tells about how much mass that is provided or lost due to chemical reactions with other substances. The reward in lower, more stable energy levels force different reactants to react with each other. Heat, pressure and chemical bonding energies influence these chemical reactions. A dissolving reaction may be looked upon as a matter of diffusion of reactants and products in a molecular scale. The purer the water, the larger the dissolving area, the higher the diffusivity at the pipe walls and the thinner the diffusion layer at the pipe walls, the larger is the dissolving reaction term Q and the more rapid will the leaching process be.

The flow of water can in the same manner be described by a balance equation:

$$\nabla \cdot (\mathbf{v}_w) = 0 \qquad \text{(Balance of water)} \qquad (2\text{-}5)$$

$$\boldsymbol{v}_w = -\boldsymbol{k}_w \nabla P_w \qquad \text{(Constitutive relation for water flux)} \qquad (2\text{-}6)$$

where

	$\boldsymbol{k}_w$	Water permeability coefficient (m/s)
	∇P_w	Water pressure gradient (m/m)

v_w Water flux (velocity) (m/s)

The wider the flow paths, the higher water permeability, and the higher is the water velocity.

In figure 2-6, a hypothetical leaching process in a small-scale fictitious flow path is showed. Pure water flows through concrete and tempts different hydration compounds to dissolve. If also aggregate consist of easy soluble compounds, these can also become dissolved. In which order solid materials are dissolved depends on theirs solubility and where they are situated in the pore system in relation to pure water and each other. Substances with lower solubility may be dissolved before other, more soluble substances, if they are surrounded by purer water (if all other terms in the energy balance, such as temperature, pressure, etc, are equal). When dissolved, the ions will diffuse towards water with less content of the ions. If they reach some main flow paths (flow pipe) where water flows through the concrete, the ions will be dragged along by the water. At the same time that the ions are carried away by the water flow, the ions may also diffuse towards purer water, which can be in the contra direction of the water flow.

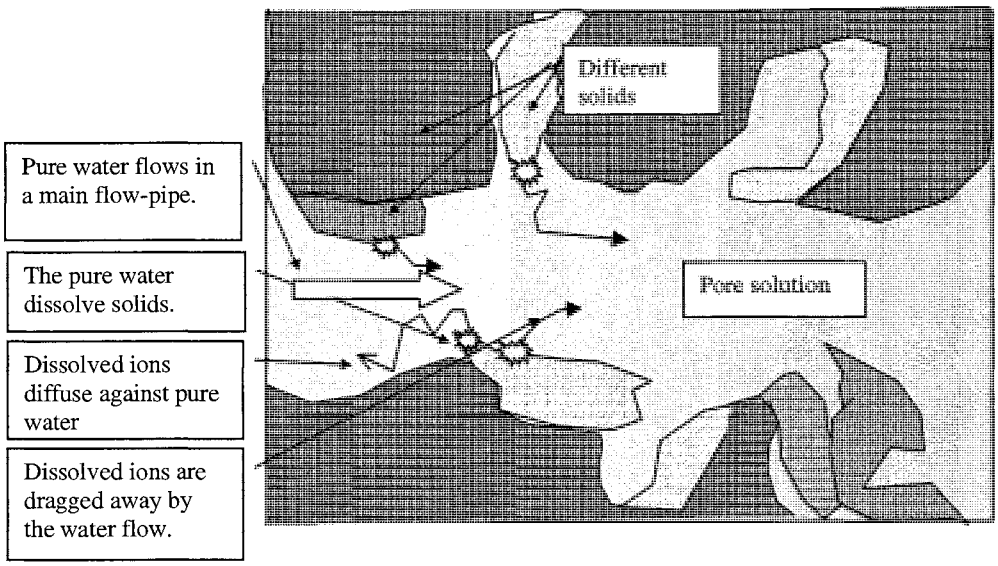

Figure 2-6 Principle how pure water in pore system dissolves substances of the pore walls.

Large internal, for water easy reachable surfaces, means a high leaching rate. If the water is aggressive (soft water or aggressive substances), the leaching rate will be even higher. High water permeability will not always cause a high leaching rate (kg/l). The concrete may have a few large flow pipes or cracks, enough for high permeability, but the pipe walls can quickly become exhausted in soluble ions and the leaching rate expressed in kg/l will be low. The maximum leaching effect arise probably when pure water is pressed through a pore system with many large flow-pipes leading through the concrete and with many short side pores into the pipe walls. The short side-pores brings ahead pure water to dissolve solid material and the large flow pipes is a supply of pure water that the dissolved ions can diffuse to.

Lime that are leached away by the pure water, comes mainly from crystals of Calcium hydroxide, $Ca(OH)_2$, due to its large amount and easy solubility. At the same time, but to a much less amount, as long there is $Ca(OH)_2$ left, lime will also be dissolved from the other

hydration products Calcium silicate hydrate (C-S-H), Calcium aluminium hydrates (C_3A) and Calcium aluminium iron hydrate (C_4AF).

$$H_2O + \left\{ \begin{matrix} Ca(OH)_2 \\ C\text{-}S\text{-}H \\ AFt \\ AFm \end{matrix} \right\} \Rightarrow Ca^{2+}(aq) \qquad (2\text{-}7)$$

Three different, large-scale common leaching processes can be sorted out:

CASE 1: Transport of ions governed by convection in very porous concrete with pure water and high pressure gradient. This case may lead to a rapid deterioration. See figure 2-7.

CASE 2: Transport of ions governed by diffusion in tight concrete with, pure water. This case may lead to a slow deterioration. See figure 2-7.

CASE 3: Concrete subjected to water with aggressive carbonic acid. This case may lead to a rapid deterioration. See figure 2-8.

With CO_2 in contact with the pore solution, possible reactions are:

$H_2O + CO_2 \leftrightarrow H_2CO_3$ carbon acid is formed (2-8)

$2H_2CO_3 + Ca(OH)_2 \leftrightarrow Ca(HCO_3)_2 + 2H_2O$ calcium hydroxide is dissolved (2-9)

$Ca(HCO)_2 + Ca(OH)_2 \leftrightarrow 2CaCO_3 + 2H_2O$ calcium carbonate is formed (2-10)

$CaCO_3 + H_2CO_3 \leftrightarrow Ca(HCO_3)_2$ calcium carbonate is dissolved (2-11)

In this work, there has been no aggressive carbonic acid in the water. Therefore, case 3 is not regarded further.

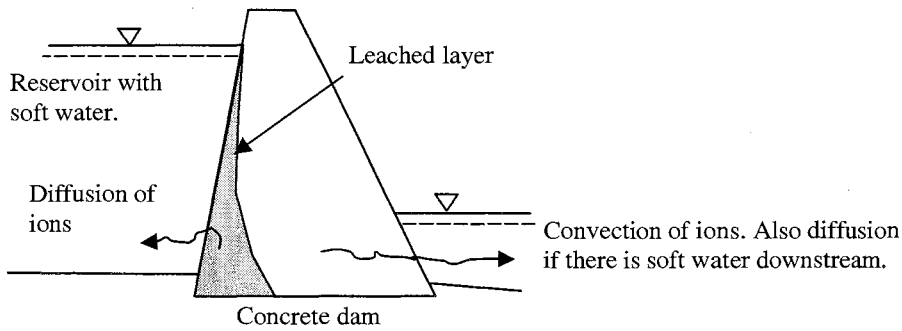

Figure 2-7 Schematic picture of leaching of ions by diffusion and convection from a concrete dam. The more permeable the dam is, the more of the dissolved ions are carried away downstream with the water flow (convection).

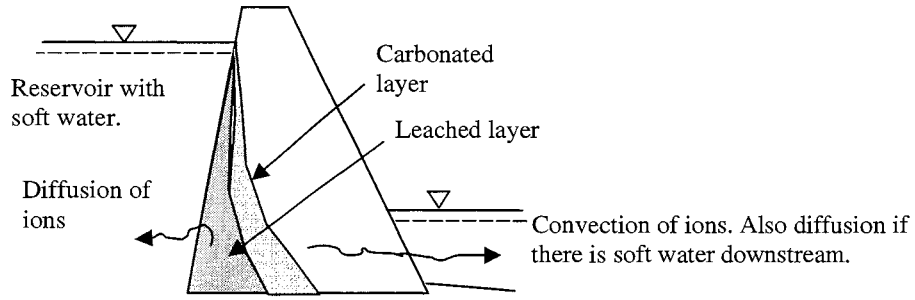

Figure 2-8 Schematic picture of leaching of ions from a concrete dam when the water contains aggressive carbon dioxide.

2.2 Chemical influences on the process

2.2.1 Chemical structure of concrete

The chemical composition of the cement used in this work is showed in table 6-1.

Ordinary Portland cement (OPC) is mainly made of raw material coming from limestone, sand and clay, The raw material are mixed, heated and grind and the resulting product is *cement*. In OPC, the main clinker minerals are C_2S, C_3S, C_3A and C_4AF, see table 2-1.

When cement is mixed in water, the most soluble compounds, such as K^+, Na^+, Ca^{2+}, SO_4^- and OH^-, dissolves in the water under heat release. In this mixture, with heat available and water molecules that willingly bond to the cement constituents, many new compounds are formed of the primarily cement constituents and the water. Crystals of $Ca(OH_2)$ and ettringite precipitates. Residual cement grains are covered by an increasing layer of hydration products, in which water diffuses and reacts with the cement. With increasing degree of hydration, less cement grains remains and more hydration products are formed. Most of the compounds forms amorphous or crystallite solids where water molecule, or part of the water molecule (H^+ and OH^-), is built in. These solid products are called *hydration products* and form the *cement paste*. Hydration products in hardened concrete have a very big internal surface in relation to its mass and form a porous complex. Some of the cement constituents remain to a great extent dissolved in the solution with the water, e.g. KOH(aq) and NaOH(aq). In concrete, are not only cement mixed with water, but also aggregates of different size. These aggregates are fixed within the hydration products, which form a thin "glue" between the aggregate particles.

Concrete is usually composed of about 75% aggregate and 25% cement paste. The dominant constituents of OPC cement paste are Calcium silicate hydrate (C-S-H), Calcium hydroxide (CH), Calcium aluminium hydrates (C_3A) and Calcium aluminium iron hydrate (C_4AF).

CH is formed as a by-product when C_3S and C_2S are hydrated. Under ideal conditions of crystallisation, CH forms hexagonal plates with weak bonding forces between every plate (Taylor 1990). A nature mineral that looks likes CH is Portlandite. The composition of the C-S-H gel may vary, but can approximately be written as $1.7CaO{\cdot}SiO_2{\cdot}xH_2O$, where x =1-4. The C-S-H structure in the inner part of the hydrated layer of the cement grain, is (Taylor 1990) more massive of almost no structure. The outer part formed in water-filled spaces, form columns of fibres radiating outwards. The older the cement paste becomes, the denser and more featureless the C-S-H gel becomes. Nature minerals that look like the C-S-H gel are Tobermorite and Jennit. The aluminium, ferrite and sulphate phases has the general composition $C_3(A,F){\cdot}xCaX{\cdot}yH$, where X can be different anions, e.g. SO_4^{2-}, OH^- or CO_3^-. For the AFm phase there are one (x=1) $CaSO_4$ and for the AFt phase there are three (x=3) $CaSO_4$. The AFm crystal looks similar to CH, but each third atom of Ca is changed to an atom of Al or Fe. Between each layer there are anions X that levels out the charge differences. Between each layer there are also

water molecules situated. Difference in size between the Ca atoms and the atoms of Al and Fe, makes the layer, which for CH was perfect plane, a little distorted. The AFt phase forms hexagonal prismatic crystals (Taylor 1990) with columns of $[Ca_3(A,F)(OH)_6 \cdot 12H_2O]^{3+}$ running parallel to the prism. Between the columns there are X-anions and H_8O.

Concrete is made up of a cement phase, aggregate, inter-facial zones between the paste and the aggregate and finally, air voids. The chemically structure of aggregate depends on the type of aggregate used. In Sweden, normally fractions of crushed granite and gneiss are used. This aggregate are hard, tight and not easy soluble. The inter-facial zone between the paste and the aggregate, become porous during the hydration and may also crack due to differences in modules of elasticity and strength. This zone has normally large contents of CH-crystals.

A life cycle for a concrete specimen from the source to a leached structure is described in figure 2-9.

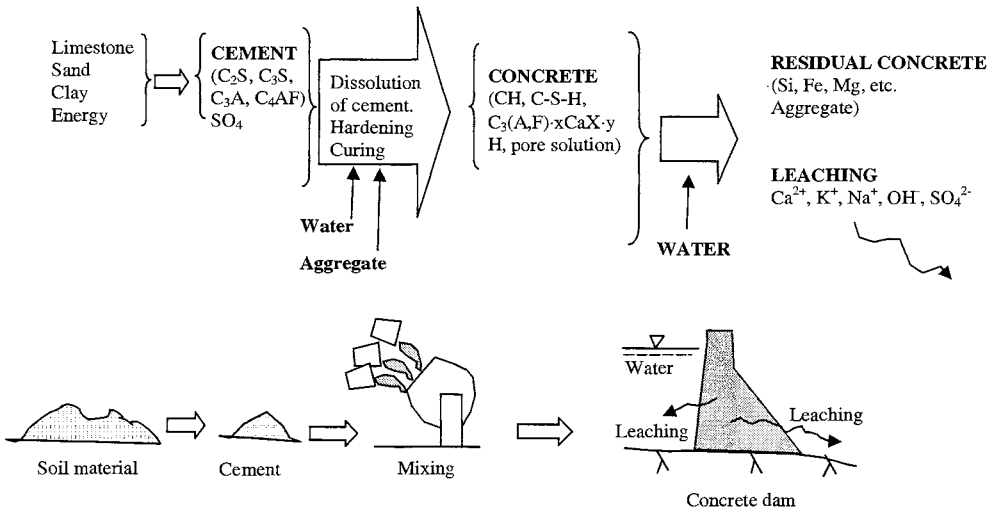

Figure 2-9 Cement is made of limestone, sand and clay during energy supply. Mixing cement, water and aggregate gives concrete. If the concrete structure is subjected to relatively pure water in the reservoir, soluble substances in the concrete will dissolve and diffuse away towards the reservoir. If the water at the same time percolates the dam body, the dissolved substances will also flow downstream and out of the dam.

Calcium is, together with oxygen and hydrogen, the most common element in concrete. There are calcium in several different types of compounds in the concrete, e.g. $Ca(OH)_2(s)$, C-S-H and AF-phases. These compounds stand for a large cause of the strength and the tightness of the concrete. These compounds are more or less soluble in water. NaOH and KOH are two very easily soluble compounds in concrete. Most of Na and K is therefor always dissolved in the pore solution. Not much solid phases of these compounds are available, so when there are concentration gradients or when the pore solution is pressed out of the concrete, NaOH and KOH will be washed out quickly. When NaOH and KOH are washed out, the concentration of OH^- will decrease in the residual pore solution and this make it possible for other, not so soluble, compounds consisting of OH^-, to be dissolved. Especially $Ca(OH)_2$, which have a rather high solubility and which there is a great extend of, are leached away. At the same time, but to much less extent, Ca^{2+} and OH^- from the C-S-H and AF-phases is leached away. The more porous the concrete are and the more CH in the concrete, the more sensitive is the concrete

against soft water attacks. The solubility of CH is further enhanced because it is concentrated to places like aggregate-paste interfaces and capillary pores, where also the porosity and permeability is larger (Grattan-Bellow 1990).

For notations and mole weights for common constituents in cement and cement paste, see table 2-1.

An example, of which hydration products that are formed when OPC is hydrated, is showed below. The example is rather realistic for the type of cement used later in this work. It is important to know how much of each hydration products that is formed so correct estimations can be done of residual contents after that the cement paste have been leached. For approximately weight parts of different hydration products in OPC reactions, see table 2-2.

Example 1 (estimated formed hydration products with the cement used in this work)
Assume cement with the following clinker composition ratios (Fagerlund 1997b):

$a \cdot C_3S + b \cdot C_2S + c \cdot C_3A + d \cdot C_4AF + e \cdot \overline{S}$

Where	a, b, c, d, e	Constants
	C_3S, C_2S, C_3A, C_4AF, $\overline{S}$	see table 2-1

The degree of hydration is assumed to be α=0.9 and the constants a, b, c, d and e to 0.557, 0.228, 0.021, 0.131 and 0.0207 respectively. These assumptions of a, b, c, d and e are received from the cement supplier for the cement used in this work. Assume that the amount of SO_4^{2-} results in half AFt and half AFm.

$0.9*(0.557 \cdot C_3S + 0.228 \cdot C_2S + 0.021 \cdot C_3A + 0.131 \cdot C_4AF + 0.0207 \cdot \overline{S})$ (kg/kg cement)

In this example, the following amount of hydration products is obtained.

m_{CSH} =0.9*(0.557*0.75 + 0.228*1.00) = 0.581 kg CSH/kg cement

m_{CH} = 0.9*(0.557*0.49 + 0.228*0.21 + 0.131*(-0.31) + 0.0207*(-1.0*74.08/40.08)) =

=0.218 kg CH/kg cement

m_{C3AH6} = 0.9*(0.021*1.40 + 0.131*0.78) = 0.118 kg CH/kg cement

m_{C3FH6} = 0.9*(0.131*0.90) = 0.106 kg CH/kg cement

m_{Aft} =0.9*0.5*0.0207*4.64 = 0.043 kg AFt/kg cement

m_{Afm} =0.9*0.5*0.0207*2.30 = 0.021 kg AFt/kg cement

Table 2-1 Notations for different compounds used in cement chemistry.

Chemical formula	Used notations	Mole weight (g)
CaO	C	56.08
SiO_2	S	60.09
H_2O	H	18
$Ca(OH)_2$	CH	74.08
SO_4^{2-}	$\overline{S}$	96.07
$3CaO{\cdot}SiO_2$	C_3S	228.33
$2CaO{\cdot}SiO_2$	C_2S	172.25
$3CaO{\cdot}2SiO_2{\cdot}3H_sO$	$C_3S_2H_3$ (C-S-H)	342.42
$3CaO{\cdot}Al_2O_3$	C_3A	270.2
$4CaO{\cdot}Al_2O_3{\cdot}Fe_2O_3$	C_4AF	485.98
$3CaO{\cdot}Al_2O_3{\cdot}6H_2O$	C_3AH_6	378.2
$3CaO{\cdot}Fe_2O_3{\cdot}6H_2O$	C_3FH_6	435.94
$CaSO_4$	$Ca\overline{S}$	136.15
$3CaO{\cdot}Al_2O_3{\cdot}3CaSO_4{\cdot}32H_2O$	$C_3A{\cdot}3Ca\overline{S}{\cdot}32H$ (AFt)	1254.65
$3CaO{\cdot}Al_2O_3{\cdot}CaSO_4{\cdot}12H_2O$	$C_3A{\cdot}Ca\overline{S}{\cdot}12H$ (AFm)	622.35

Table 2-2 Main Portland cement reactions of pure clinker compounds in water.

Reaction Weight parts		
$2\,C_3S + 6H$ 1.00 + 0.24	→	C-S-H + 3CH 0.75 + 0.49
$2\,C_2S + 4H$ 1.00 + 0.21	→	C-S-H + CH 1.00 + 0.21
$C_3A + 6H$ 1.00 + 0.40	→	C_3AH_6 1.40
$C_4AF + 2CH + 10H$ 1.00 + 0.31 + 0.37	→	$C_3AH_6 + C_3FH_6$ 0.78 + 0.90
$C_3(A,F) + xCaX + yH$ X = e.g. SO_4^{2-}, OH^-, CO_3^- x=3, y=32:		$C_3(A,F){\cdot}xCaX{\cdot}yH$ (general)
$C3(A,F) + 3Ca\overline{S} +$ 32H 1.0 + 1.51 + 2.13 x=1, y=12:	→	$C_3(A,F){\cdot}3Ca\overline{S}{\cdot}32H$ ettringite (AFt) 4.64
$C3(A,F) + Ca\overline{S} + 12H$ 1.0 + 0.50 + 0.80	→	$C_3(A,F){\cdot}Ca\overline{S}{\cdot}12H$ monosulphate (AFm) 2.30

In table 2-3 are the parts and the total amount of calcium (Ca), coming from the different hydration products, showed for the example. The total Ca, coming from the hydration products, is in the example 0.397 (kg/kg cement). If an assumed amount of free CaO of 0.07 (kg/kg) is included, the total Ca is 0.468 (kg/kg).

Table 2-3 The amount of hydration products and the amount of Ca in the hydration products for the example above.

	C-S-H	CH	C_3AH_6	C_3FH_6	Aft	AFm	Sum	CaO	Tot sum
	0.581	0.218	0.118	0.106	0.043	0.021		0.070	(kg/kg)
Mole weight	342	74	378	436	1255	622		56	
Mole weight Ca	3*40	40	3*40	3*40	6*40	4*40		40	
Ca	0.204	0.118	0.035	0.027	0.008	0.006	**0.397**		**0.47** (kg/kg)

The leaching process involves the dissolving reactions and the transport of dissolved ions. Regarding the dissolving reaction, the solubility is a main property (chapter 2.2.1). The transport of dissolved ions can be due to diffusion or convection. In chapter 2.2.3, the diffusion of ions is discussed. In chapter 2.3.2, the mobility of water, which is the cause to the convection flow, is discussed.

2.2.2 Dissolving reactions

For inorganic materials, such as cementitous materials, water is an excellent solvent. The purer and the more acid the water is, the more aggressive is the water. One can divide dissolving reactions in:

- ✓ Dissolving in stagnant water where the reaction can reach equilibrium
- ✓ Dissolving in mobile or stirred water where the reaction is not allowed to reach equilibrium

Dissolving in stagnant water where the reaction can reach equilibrium:

The dissolving of a *salt* in an aqueous electrolyte can be assumed as:

$$A_aB_b(s) \leftrightarrow aA^{b+} + bB^{a-} \quad (2\text{-}12)$$

Where A, B — Ions A and B
a, b — Stoichiometric coefficients

The *reaction quotient* R can be written:

$$R = [\gamma_a \cdot A^{b+}]^a [\gamma_b \cdot B^{a-}]^b \quad (2\text{-}13)$$

or

$$R = (\gamma_a \cdot m_A)^a \cdot (\gamma_b \cdot m_B)^b \quad (2\text{-}14)$$

Or if calculating with stepwise increasing dissolution:

$$R = (\gamma_a \cdot (m_A + a \cdot x))^a \cdot (\gamma_b \cdot (m_B + b \cdot x))^b \quad (2\text{-}15)$$

Where γ — A*ctivity coefficient* regarding the ion strength in the electrolyte (l/mole)
m — Amounts of the ions A and B (molarity) (mole/m^3)
a,b — Stoichiometric coefficients (-)
x — Stepwise added amount of ions (mole/m^3)

When a dissolving process is in equilibrium, there is a saturated solution and R is called the *solubility product* K_{sp}. The K_{sp} for some hydration products are shown in table 2-4 and 2-5.

If R is greater than K_p, there is a over-saturated solution and the dissolved salt will precipitate until K is reached. If R is smaller than K_{sp}, there is a under-saturated solution and the salt will dissolve until K_{sp} is reached.

One among many equations to calculate the activity coefficient, is the Güntelberg equation, which is said to be valid up to about 0.1 (mol/l):

$$\log \gamma_i = -\left(\frac{A \cdot z_i^2 \cdot \sqrt{I}}{1+\sqrt{I}} \right) \tag{2-16}$$

$$I = 0.5 \cdot \sum z_i \cdot m_i \tag{2-17}$$

$$A = 1.82 \cdot 10^6 (\varepsilon \cdot T)^{-1.5} \approx 0.5 \text{ for water at } 25°C \text{ (Stumm (1996))} \tag{2-18}$$

Where	I	Ion strength (mole/l)
	ε	Dielectric constant (F/m)
	T	Temperature (K)
	z_i	Valence of the ion (-)

As could be understood from equations (2-16), (2-15) and (2-13), the more dissolved ions in a solution, the higher the ion strength, the smaller the activity coefficients, and the smaller the reaction quotient, which means that more of the solid can dissolve before reaching K_{sp}. On the other hand, if there already are dissolved ions of the same type as those coming from the solid (m_A and m_B), the reaction quotient R will be larger and less solid can dissolve before reaching K_{sp}, known as the "common ion effect".

To show how the Güntelberg equation can be used, an example of a calculation scheme is presented below and compared with two solubility curves of measured data from Duchesne & Reardon (1995) and Fratini (1949) for Ca^{2+} in an aqueous solution of KOH (figure 2-10). K_{sp} is assumed from the literature. The calculated curve fit surprisingly well to the experimental data considering the high concentrations and the simplicity of the model. For solutions in equilibrium, an increase of KOH leads to a strong decrease in dissolved $Ca(OH)_2$ due to a much larger solubility product K_{sp} for KOH.

Example: calculation scheme "model Güntelberg":

1. Assume starting dissolved amounts of salts m_A, m_B, ...
2. Calculate ion strength and activity coefficients for each ion with equations (2-17) and (2-16).
3. Calculate the reaction quotient R with equation (2-15).
4. Check if R is <, = or > than K_{sp}.
5. Move against the saturation point (K_{sp}) by small steps of increase or decrease of the dissolved amount *x*.
6. Go to 2. again, until reaching the saturation points for all salts.

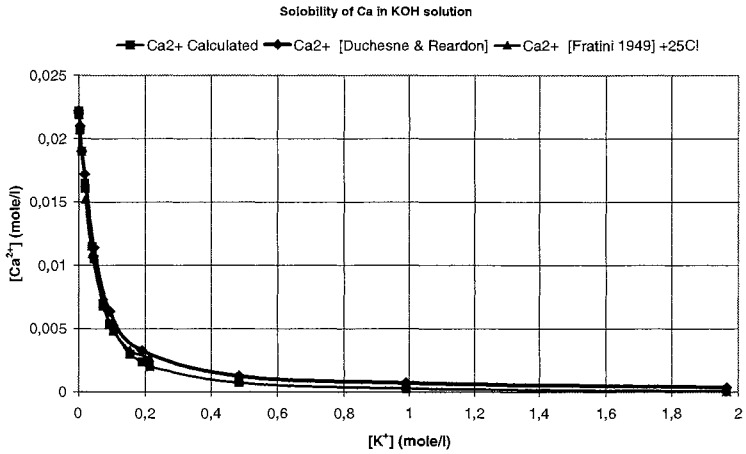

Fig 2-10 Calculated solubility of $Ca(OH)_2$ in aqueous solution of KOH compared with data from Duchesne & Reardon (1995), Fratini (1949). For the calculation, the solubility product K_{sp} was assumed to $10 \cdot 10^{-6}$ and 4.5 for $Ca(OH)_2$ and KOH respectively.

Table 2-4 Solubility data of different compounds in OPC.

Hydration product	Solubility (mole/l)	Solubility product K_{sp}
CH	S = (70.38-0.17 T)·10^{-3} (large crystals) Hedin (1955) e.g. 20.5·10^{-3} (+20°C) 21.0·10^{-3} (+19°C) Basset (1934) 22.2·10^{-3} Duchesne and Reardon (1995) 25.0·10^{-3} (cold water) 10.4·10^{-3} (hot water) 16.2·10^{-3} (+25°C) Aylward&Findlay (1994)	5.5·10^{-6} Atkins &Jones (1997) 6.4·10^{-6} Aylward&Findlay (1994)
C-S-H	See table 2-5, table 2-6, figure 2-4 and equation (2-19).	
C_3AH_6	See table 2-5	
C_3FH_6	See table 2-5	
$C_3(A,F)\cdot xCaX\cdot yH$	$CaSO_4$: S=15.3·10^{-3} [Chem. & Phys] $CaSO_4 \cdot 2H_2O$: S= 14·10^{-3} [Chem. & Phys]	$CaSO_4$: K=4.4·10^{-5} [Chem. & Phys] $CaSO_4 \cdot 2H_2O$: K=2.6·10^{-5} [Chem. & Phys].
KOH	Solubility S=119g/l/(39.1+(16+1))g/mol=2.12M Aylward&Findlay (1994)table 5.	
NaOH	Solubility S=114g/l/(22.99+(16+1))g/mol=2.85M Aylward&Findlay (1994)table 5.	

Table 2-5 Solubility for different concrete hydration products Moskvin (1980)

Compound	Solubility Stable at (g CaO/L)	Releasing
$Ca(OH)_2$	1.18	CH
$Ca(OH)_2$ supersaturated	1.6-1.9	CH
$Ca(OH)_2$ in 1 % Na_2SO_4 solution	2.14	CH
$Ca(OH)_2$ in 5g/l NaOH solution	0.18	CH
$2CaO{\cdot}SiO_2{\cdot}aq$	stable in saturated CH	CH
$3CaO{\cdot}2SiO_2{\cdot}aq$	stable in 1.1	CH
$Ca{\cdot}SiO_2{\cdot}aq$ (Wollasonite)	stable in 0.05	
$4CaO{\cdot}Al_2O_3{\cdot}19H_2O$ (C_4AH_{19})	stable over 1.15	CH
$3CaO{\cdot}Al_2O_3{\cdot}6H_2O$ (C_3AH_6)	stable between 0.315-1.15	CH
$C_{12}A_7$		CH and Al_2O_3 (A)
C_2AH_8		CH and A
$C_4F{\cdot}aq$ ($4CaO{\cdot}Fe_2O_3{\cdot}aq$)	stable over 1.15	
$C_2A{\cdot}aq$ ----- II -----	stable between 0.17-0.315	
$C_4F{\cdot}aq$ ($4CaO{\cdot}Fe_2O_3{\cdot}aq$)	stable over 1.15	
$CF{\cdot}aq$	stable between 0.64-1.15	

Ayora et al (1998) has given the following relation for the solubility of the C-S-H gel for all Ca/Si-ratios:

$$\log K_{CSH} = -13.863 + 1.743x - 0.937x^2 + 0.134x^3 \qquad (2\text{-}19)$$

where x $\log (Ca/Si)_{solution}$

$(Ca/Si)_{solution}$ The calcium-silicon ratio in the C-S-H gel

In figure 2-11, K_{CSH} is showed due to the equation (2-19). Such an equation can be useful when modeling the leaching process.

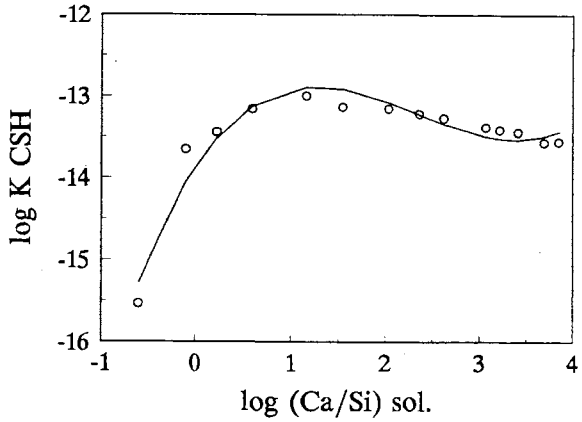

Figure 2-11 Solubility product K_{sp} for C-S-H gel Ayora et al (1998).

Adenot and Richet (1997) gives experimental data of the solubility of C-S-H, shown in table 2-6.

Table 2-6 Solubility product K_{CSH} for C-S-H of different composition from experimental data of Jennings (1986) and Berner (1988).

C/S of C-S-H	1.65	1.45	1.30	1.15	1.05	0.95	0.90	0.85
$pK_{CSH} = -\log_{10}(K_{CSH})$ of C-S-H	11.7	10.6	9.8	8.9	8.3	7.6	7.3	6.9

Dissolving in mobile water where the reaction not can go to equilibrium:

For mobile water, reaction rates and diffusion velocities become important. The kinetics of a dissolving reaction is very difficult to state. The steps in a reaction may be:

1) The time in which the reagents (e.g. water) move to the reaction place.
2) The chemical reaction (e.g. $Ca(OH)_2 \rightarrow Ca^{2+}+2OH^-$)
3) The time in which the products (e.g. Ca^{2+}, OH^-) can leave the reaction place.

The rate-determining steps are most probably 1) and 3). Most probably are chemical reactions of inorganic compounds very fast. In 1) and 3) lays both the diffusion velocities for the reagents and for the products, but also the influence from ion strength and common ion effect.

A dissolving reaction can be assumed as a diffusion process (Hedin 1962):

$$Q = rate(c_{sat} - c) = A_{solid} \frac{k_{ion}}{r}(c_{sat} - c) \qquad (2\text{-}20)$$

where
- Q Dissolving mass (mole/s)
- A_{solid} Surface from which the solid comes from (m^2)
- k_{ion} Diffusion coefficient (m^2/s)
- r Diffusion layer thickness (m)
- c_{sat} Saturation concentration ($mole/m^3$). Depended on the ion strength and common ion effect.
- c Concentration outside the diffusion layer t ($mole/m^3$)

In figure 2-12, the idea behind the equation is shown. Water molecules diffuse against the solid material, where they force the solid atoms or ions to break away from the solid and diffuse away against pure water or by any flow of water. If there are small diffusion layers, large concentration gradients and easily moving ions (high diffusion coefficient), the dissolving reaction is fast. If there are small volumes of water or the water is not exchanged with new, pure water often, the dissolving reaction will decrease rapidly.

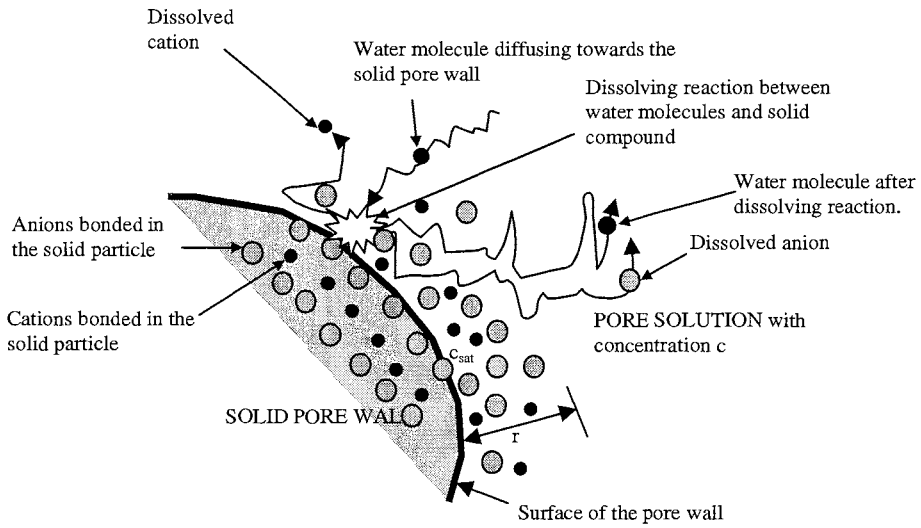

Figure 2-12 Principle of a dissolution process where water molecules diffuse to a solid pore wall and dissolve solid compounds. c = concentration (mole/l) in the pore solution outside the diffusion layer *t*. c_{sat} = saturation concentration of a compound (mole/l) in water.

Theoretically are all solid substances in concrete and in the pore solution in thermodynamic balance with each other and with the surroundings. When the balance is disturbed, as in leaching processes, the order of dissolution among the substances can be correlated to the solubility of the individual substances, but also to how close to the dissolving pure water each substance is. A substance *a,* which has a higher solubility than a substance *b*, but that is not so close to pure water, may be dissolved more slowly than substance *b* despite this has a lower solubility.

A model of the dissolving reaction in cement paste is presented in chapter 3.

2.2.3 Mobility of ions in concrete

In a concrete pore, ions are subject to different forces. The forces are the result of how the system wants to reach a low, stable level of energy. The forces may move ions, e.g. by convection or diffusion, in different directions.

Convection flow of ions is totally governed by the velocity field (the water flow) and is discussed in chapter 2.3.2. Most often, the quickest leaching degradation of a concrete structure happens when ions are leached by convection.

Diffusion flow of ions is probably influenced by concentration gradients, inter-molecular forces between dissolved ions and intermolecular forces between dissolved ions and solid walls.

Chemical interactions between ions and electrical forces between different charged ions may govern the mobility of ions (Marchand et al 1999). Also the shape, tortoise and connection of the pores influence the mobility (Delagrave et al 1997).

In this work not much effort is laid in study diffusion of ions. Used values are more or less taken from the literature.

2.3 Physical influences on the process

2.3.1 Physical structure of concrete

Here, only ordinary Portland cement (OPC) is treated and the structure of the concrete is assumed by a structure model described in Fagerlund (1994), which is largely based on works of Powers (1962).

When cement and water is mixed, the cement reacts with the water and forms a porous conglomerated mass of fine crystal-like gel particles or *cement paste*, see figure 2-2 to 2-4. The main volume of the gel consists of calcium-silicate-hydrate products with incorporated calcium hydroxide. The gel grows due to increasing porosity and water molecules that are chemically bounded in it. The rest of the original volume consists of the *capillary pores*, which are much coarser than the gel pores. If also aggregate is added, the results will be *mortar* or *concrete*, with fine or coarse aggregate respectively. Aggregate disturbs the structure. In the interfacial border between the cement paste and the aggregate, the properties are different compared to the cement paste and the aggregate. The porosity is higher, micro-cracks are common, water separation may have caused cavities under the aggregate, air voids may have been trapped and there are more crystals of calcium hydroxide (Fagerlund 1994). These properties make this zone weaker, more water permeable and more sensitive to leaching.

The physically structure of concrete is described by the shape and amount of the different phases in the concrete. A very important aspect regarding water permeability and leaching, is pore size distribution and connectivity. In figure 2-13 a principle figure is showed over the different types of pores in concrete, gel pores inside the cement gel, the capillary pores between the solids in the cement gel and finally, the pores between the cement gel and the aggregate. In addition to these, there can also be of air voids and cracks.

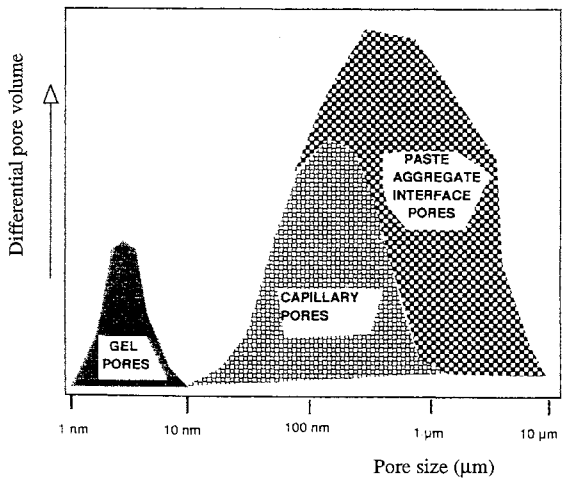

Figure 2-13 Diagram showing the large contribution of pores at the paste-aggregate interface to the total porosity in concrete. From Rohling and Nietner (1990) presented in Grattan-Bellew (1996)

In the model of cement paste it is assumed:

1) The density of the cement grains is 3100 (kg/m^3).
2) The chemically bound water in the hydration process is $0.25 \cdot \alpha \cdot C$.
3) The chemically bound water "decrease" in volume to 0.75 of the volume before the hydration.
4) The cement gel that is formed during hydration has a porosity of 28 %.
5) The air pores due to compaction or air-entraining agents are omitted. They are instead added on concrete level.

Where α Degree of hydration (-)
C Cement content (kg)

In figure 2-14, the constituents in concrete are showed principally.

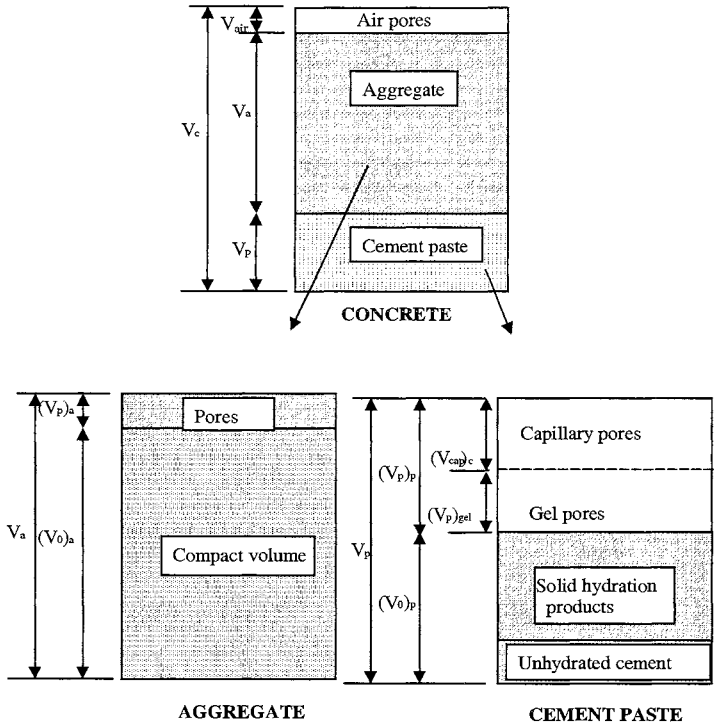

Figure 2-14 Schematic volume fractions of pores and solid materials in concrete.

The total pore volume $(V_p)_p$ of the cement paste is:

$$(V_p)_p = \frac{W - 0.75 \cdot W_n}{\rho_w} = \frac{W - 0.75 \cdot 0.25 \cdot \alpha \cdot C}{\rho_w} = \frac{W - 0.19 \cdot \alpha \cdot C}{1000} = \\ = \frac{C}{1000}(w/c - 0.19 \cdot \alpha) \qquad (2\text{-}21)$$

where $(V_p)_p$ Total pore volume of the cement paste (m^3)
W Mixing water content (kg)
W_n Chemical bound water (kg)
ρ_w Density of water (kg/m^3)
w/c Water to cement ratio

The compact volume, i.e. the solid volume without any pores, of the cement paste $(V_0)_p$ is

$$(V_0)_p = \frac{C}{\rho_c} + \frac{W_n}{\rho_w} = \frac{C}{3100} + \frac{0.19 \cdot \alpha \cdot C}{1000} = \frac{C}{1000}(0.32 + 0.19 \cdot \alpha) \quad (m^3) \tag{2-22}$$

where $(V_0)_p$ Compact volume of the cement paste (m^3)
ρ_c Density of cement (kg/m^3)

The total volume of the cement paste V_p is the sum of the pore volume and compact volume

$$V_p = (V_p)_p + (V_0)_p = \frac{C}{1000}(0.32 + w/c) \quad (m^3) \tag{2-23}$$

The total porosity of the cement paste P_p is

$$P_p = \frac{(V_p)_p}{V_p} = \frac{(w/c - 0.19 \cdot \alpha)}{(0.32 + w/c)} \quad (m^3/m^3) \tag{2-24}$$

The volume of the cement gel V_{gel} is

$$V_{gel} = \frac{C}{1000} \cdot 0.71 \cdot \alpha \quad (m^3) \tag{2-25}$$

The volume of the gel pores $(V_p)_{gel}$ is

$$(V_p)_{gel} = 0.28 \cdot V_{gel} = \frac{C}{1000} \cdot 0.20 \cdot \alpha \quad (m^3) \tag{2-26}$$

The volume of the capillary pores $(V_p)_{cap}$ in the cement paste is

$$(V_{cap})_p = (V_p)_p - (V_p)_{gel} = \frac{C}{1000}(w/c - 0.19 \cdot \alpha) - \frac{C}{1000} \cdot 0.20 \cdot \alpha = \\ = \frac{C}{1000}(w/c - 0.39 \cdot \alpha) \quad (m^3) \tag{2-27}$$

The capillary porosity $(P_{cap})_p$ of the paste is

$$(P_{cap})_p = \frac{w/c - 0.39\alpha}{0.32 + w/c} \quad (m^3/m^3) \tag{2-28}$$

The volume of the aggregate is

$$V_a = (V_0)_a + (V_p)_a = A/\rho_a \tag{2-29}$$

where V_c Volume of the concrete (m^3)
V_a Volume of aggregate (m^3)

V_{air}	Volume of air due to compaction or air additives (m^3)
$(V_0)_a$	Volume of the compact volume of the aggregate (m^3)
$(V_p)_a$	Volume of the pores of the aggregate (m^3)
A	Aggregate content (kg)
ρ_a	Density of the aggregate (kg/m^3)

The total volume of the whole concrete, air pores included, is

$$V_c = V_a + V_p + V_{air} \tag{2-30}$$

The porosity of the concrete is

$$P_c = \left[(V_p)_a + (V_p)_p + V_{air}\right] / V_c \tag{2-31}$$

Most often the porosity of the aggregate is negligible, and the porosity P_c of the concrete becomes:

$$P_c = \frac{0 + w/c - 0.19 \cdot \alpha + V_{air}}{V_a + w/c + 0.32 + V_{air}} \quad (m^3/m^3) \tag{2-32}$$

During the casting or afterwards during the curing, the concrete can receive cavities, which should be added to the above-mentioned porosity.

2.3.2 Mobility of water in concrete

Water can be transported either as vapour or as liquid. Driving forces for the movements can for example be; vapour content, vapour pressure, temperature, capillary under-pressure, over-pressure (e.g. hydrostatic, wind, gravity, osmotic pressure, etc). Water transport has a great influence on the durability of the concrete. Water itself can dissolve concrete and in freeze-thawing, water is a necessary ingredient. Different aggressive substances can move by diffusion or by convection through the concrete.

A flow of water through concrete is the sum of all small leakage ways. These ways can be of different shapes and origin. Concrete is constituted of cement paste and aggregate. Paste is a very porous material, but not all pores distributes any significant amount of water, they have to be of rather large size and they must be connected trough the concrete to do that. It is mainly the larger capillary pores and micro-cracks that stands for the main flow of water through the paste. Aggregate is very seldom so porous that any water flows through it. But between the paste and the aggregate, there are weak zones with micro-cracks and easy soluble hydration products, and here can the flow of water be quite large. In a large scale, there are also cracks and cavities due to compaction or curing. In this text, the flow paths (capillary pores, cracks or cavities), that distribute the main water are called *flow pipes*. The wider, the less tortuous, the less rough and the more connected the flow pipes are, the more water they can distribute.

In this work, only mobility of water due to hydrostatic over-pressure in saturated concrete is assumed. However, below is water flow due to other driving causes are shortly mentioned.

Transport of water at 0-45 % RH and no over-pressure:

In dry conditions, below 45 %RH, water vapour will *diffuse* due to differences in vapour concentrations through the more or less empty pore system (figure 2-15). The wider, straighter, smoother and more connected the pores are, the more easy goes the diffusion. Some of the water molecules will be absorbed on the pore walls, get stuck in very narrow pores or react chemically with substance in the pore walls.

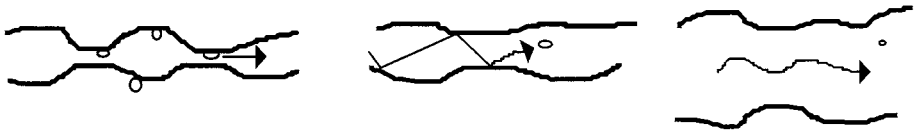

Figure 2-15 Diffusion in dry pores. The wider the pores, the less collision and attraction with the pore walls.

Transport of water at 45-99 % RH and no over-pressure:

When the humidity increases in pores, more water is adsorbed to the pore walls and after a while, water meniscus is formed in narrow passages causing capillary condensation. This happens at about 45 % RH. Now, the flow of water changes to the much more rapid *capillary suction* due to the curved meniscus. The transport becomes a combination of diffusion and capillary suction (figure 2-16). Between the water meniscus, the water is transported by diffusion to the next meniscus where the vapour condenses. The water is sucked through the meniscus to the next air-filled pore, where it is vaporised again and then diffuses again to the next meniscus. The higher humidity, the more of the transport is due to capillary suction.

Figure 2-16 Diffusion and capillary suction in the pores. The higher the humidity, the more of the water is transported by capillary suction.

Transport of water at 100 % RH and no over-pressure:

Near 100% RH, the material is filled almost completely with water and the transport is caused by capillary suction. Some pores are so isolated and difficult to reach, so they are filled with water first after a long time of water suction. When the pore system is completely filled with water, any transport of dissolved ions or gases goes by slow diffusion in the water.

Transport of water at 0-100 % RH and over-pressure:

The over-pressure may for example be applied as air over-pressure (e.g. hydrostatic pressure). The same principles as above for 0-100 % RH and no over-pressures is valid, but the transport of water is probably faster. The mobility of water differs depended on the content of water in the concrete (figure 2-17).

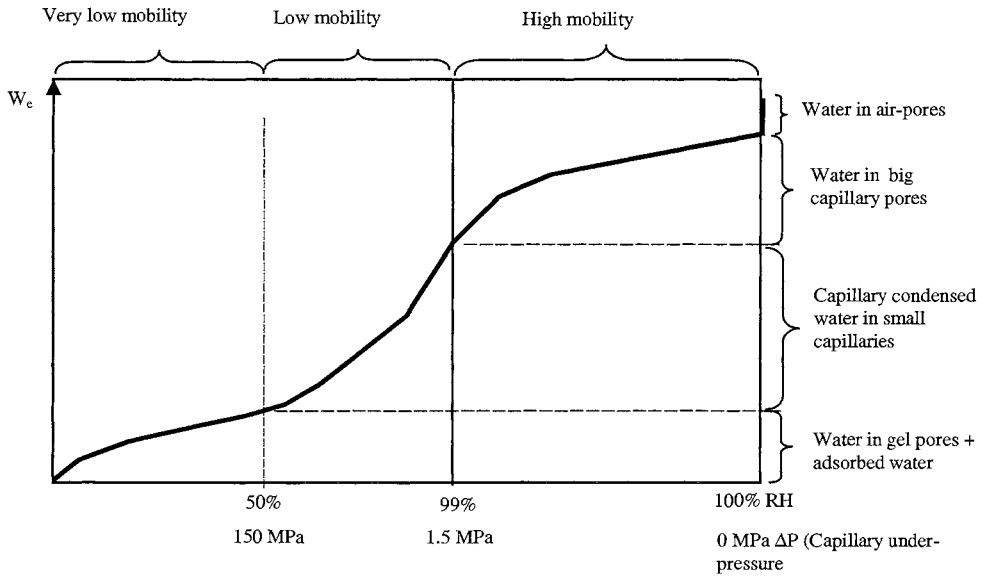

Figure 2-17 A principle picture of the mobility of water due to over-pressure effects in concrete for different relative humidity Fagerlund (2000).

Transport of water by over-pressure in saturated concrete:

This is the treated case in this work. The experimental set-up in this work gives this condition. The water pressure can generally be due to several reasons as: hydrostatic pressure, over-pressure in the vicinity of freezing water that expand, osmotic pressure, etc. The water is *pressed* through the pore system due to the over-pressure. The mobility of water is high, see figure 2-17 at 100 % RH. In figure 2-18, an example of water flow in saturated concrete in a cross-section of a fictive concrete dam is showed. In saturated concrete, the flow is stationary during time (if the pressure gradient is the same and no sources or sinks are located inside the body). The normal way to calculate a stationary flow of water in one dimension in a porous material is by using Darcy's law:

$$q_w = k_w \frac{dP_w}{dx} A_{tot} \tag{2-33}$$

where
- q_w Flow of water (m^3/s)
- k_w Water permeability coefficient (m/s)
- dP_w/dx The gradient of the piezometric water head (m/m)
- A_{tot} Cross section area (m^2)

Or in other units:

$$q_w = B \frac{dP}{dx} A_{tot} \tag{2-34}$$

where
- q_w Flow of water (kg/s)
- B Permeability coefficient (s)
- dP/dx Pressure gradient (Pa/m)

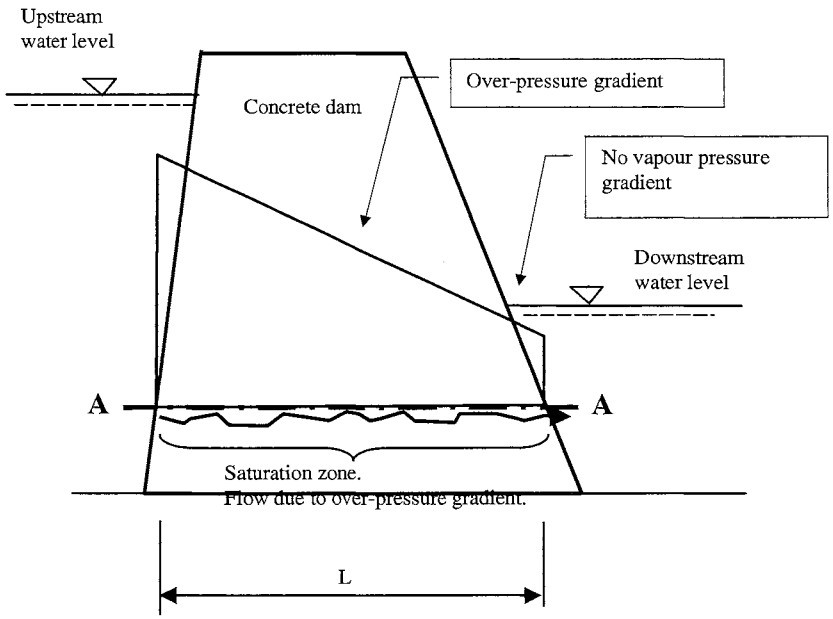

Figure 2-18 A principle sketch of a thick concrete dam and water flow due to over-pressure in saturated concrete in a section A-A. In the section A-A, both the upstream and the downstream faces are in water and the whole section is water saturated.

Influencing factors on the permeability of a concrete structure can be; Nilsson (1994) and Lawrence (1982):

- ✓ The permeability of the paste
- ✓ The permeability of the aggregate
- ✓ Type and size of aggregate
- ✓ More porous aggregate and larger aggregate made the concrete more permeable
- ✓ The permeability of the interfacial zone
  a) Pore size distribution of the zone
  b) Crystals in the zone (mainly $Ca(OH)_2$)
- ✓ Type of cement
  Ingredients in the cement that consumes CH decrease the short-term permeability. The long-term permeability is more uncertain. For example can the self-healing be less with less CH.
- ✓ Cracks or cavities during the casting work
- ✓ Micro-cracks due to shrinkage in the cooling period after casting, drying-shrinkage, temperature movements and elastic strain and creeping due to loads. These cracks exist mainly in the interfacial zone, but also in the paste. The larger the aggregate, the more and larger the micro-cracks, see figure 2-19. In dams with thick dimensions, cracks will easily be formed due to large temperature differences, if no actions are done to avoid them.
- ✓ Cracking during the life time of the structure
- ✓ Freezing
- ✓ Chemical attacks

- ✓ Leaching may lead to increasing permeability (flow pipes become wider) or decreasing permeability (self-healing in flow pipes).
- ✓ The shape and dimensions of the whole structure
- ✓ The influence of air- or water filled large pores. They exist mainly in the interfacial zone, but also in the paste. They exist very seldom in the aggregate.

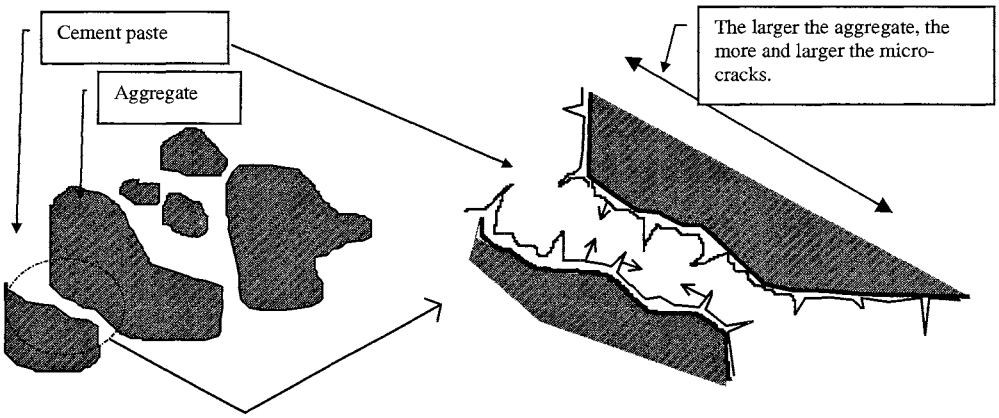

Figure 2-19 When the paste shrinks due to moisture or temperature changes, the aggregate will resist the movements and the paste will crack if the tensile strength is exceeded. The larger the aggregate, the larger will the micro-crack be and the bigger volume of micro-cracks are formed.

Because the flow of water approximately can be said to proportional to the pore diameter raised to 4, it is obvious that the flow increases rapidly for wider and more connected pores or cracks.

Combined water flow :
In reality, flow of water can be a combination of all the above mentioned transport types Fagerlund (1996) and Hedenblad (1993). For example, figure 2-20 shows a thick concrete dam where there is a hydrostatic pressure against the upstream face of the dam and the downstream face is exposed to air. The concrete is saturated and the internal water pressure is hydrostatic down to a point near the downstream face, where the humidity reaches 100 % RH. Further downstream, the internal relative humidity decreases down to the current climatic condition at the downstream face. A sunny summer day, the relative humidity at the downstream face can reach as low as about 30-40 % RH. The water transport is caused by a combination of over-pressure, suction and diffusion. Finally, at the downstream face, evaporation to the surrounding air occurs.

If there is water at the downstream face, water flow will of course be depended only on hydrostatic pressure all the way from the upstream to the downstream face.

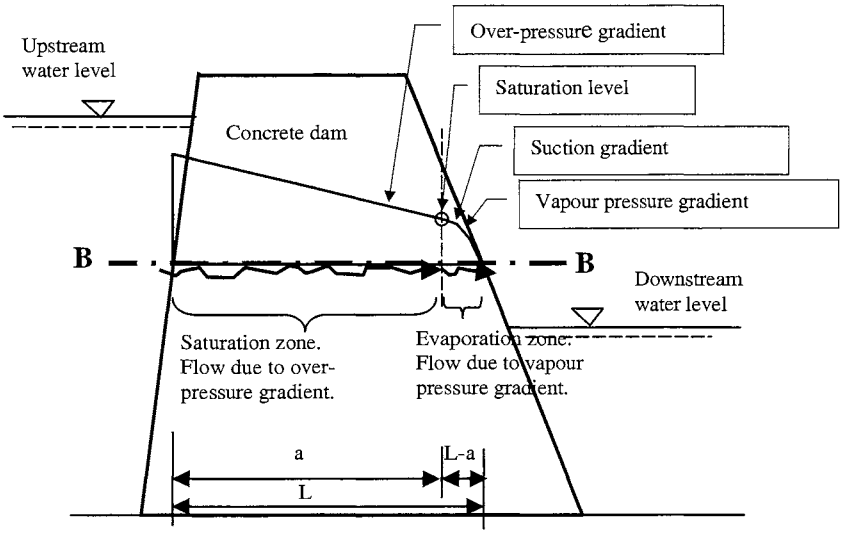

Figure 2-20 A principle sketch of a thick concrete dam and a combined water flow in a section B-B. In the section B-B, the upstream face is in water and the downstream face is in air. The section has one saturated zone and one evaporation zone Fagerlund (2000).

In a combined transport of water, the flux of water in the over-pressure part is, if assuming Darcy's law to be valid:

$$v_w = B\frac{dP}{a} \tag{2-35}$$

where v_w Water flux (kg/(m^{2}s))
B Permeability coefficient (s)
dP Pressure difference (Pa)
a Distance to the saturation level (see figure 2-20) (m)

This distance a can be written as; see Fagerlund (1996):

$$a = \frac{k_w \cdot dP \cdot L}{v_{w<100\%RH} \cdot H_{<100\%RH} + k_w \cdot dP} \tag{2-36}$$

where $v_{w<100\%RH}$ = measured flux of water below 100 % RH in laboratory (kg/(m^{2}s))
$H_{<100\%RH}$ = the thickness of the specimen tested in laboratory (m)
L = the total thickness of the dam (m)

In the example below, the point where the relative humidity reach 100% and the corresponding water flow is calculated for a fictive dam.

Example

A fictive concrete dam with a cross section thickness of L = 30 (m) is exposed to water pressure of $50 \cdot 10^4$ (Pa) (50 m water head) at the upstream face. Three different permeability coefficients (B) is assumed from figure 1-12 (Ruettgers 1935) for three different w/c ratios.

In table 2-7, data is taken from Hedenblad (1993) of $q_{<100\%RH}$ for different thickness $H_{<100\%RH}$ and for a relative humidity RH of 60% at the downstream face. Equations (2-35) and (2-36) are used. The result shows that the distance where the 100 % RH point is reached is very close to the downstream face for an ordinary concrete dam, 0.02 m for w/c ratio 0.8. It means that most often Darcy's law is enough for estimating water flows. The flow of water is little larger when calculated with a combined water flow than with pure over-pressure flow, due to the shorter dx in Darcy's law (a < dL). The higher the w/c ratio, the nearer the downstream face is the 100 % RH point.

Table 2-7 Calculation of water flux v_w in a fictive dam.

Type	W/c	B	DP	L	RH	$v_{w<100\%RH}$	$H_{<100\%RH}$	a	v_w (Darcy)	v_w (combined)
		10^{-15} (s)	10^4 (Pa)	(m)	(%)	(g/(m^{2}24hour)	(m)	(m)	(kg/(m^{2}s))	(kg/(m^{2}s))
Concrete	0.5	500	50	30	60	3.1	0.094	29.60	$8.333 \cdot 10^{-9}$	$8.446 \cdot 10^{-9}$
- II-	0.6	6 000	50	30	60	6.8	0.097	29.92	$100.0 \cdot 10^{-9}$	$100.2 \cdot 10^{-9}$
- II-	0.8	50 000	50	30	60	14.4	0.098	29.98	$833.3 \cdot 10^{-9}$	$833.9 \cdot 10^{-9}$

3 Leaching model used in this work

3.1 Introduction

The intention of the leaching model presented here is to find a tool that can be used in future structural check of concrete dams.

Nyame and Illston (1981) suggested that the main amounts of water flow in saturated concrete, exposed to over-pressure, occur in certain flow paths. Some preliminary results in the present work indicate also, that the flow of water goes mainly in such *flow-pipes*. In figure 3-1, the principle with water flow in flow-pipes is showed for a hypothetical dam. Water flows in tortuous pipes of different sizes and roughness. Between the pipes the concrete is assumed to be completely tight.

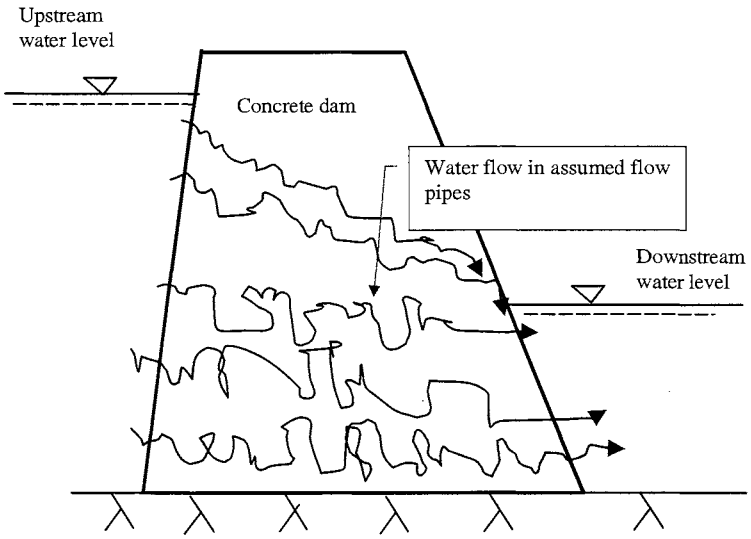

Figure 3-1 Water flow in assumed flow pipes in a concrete dam.

It must be said immediately that it is not an easy task to model a leaching process in concrete. Pore size distribution, tortuosity, connectivity and micro-cracks that govern the water permeability are difficult to model. How fast solid material is dissolved and transported away is difficult to model. Change in strength is probably strongly depended on where the leached material is taken from in the concrete. However, an attempt is done here to model the whole leaching degradation process (permeability, leaching of ions and strength reduction).

A short description of leaching can start with the dissolution of ions in the walls of the flow pipes. Dissolved ions must penetrate a diffusion layer in the walls of the pipe and then penetrate a diffusion layer in the pipe solution before they reach pure (or purer) water. In the pipes, ions will diffuse upstream or downstream towards even purer water. At the same time, ions will be transported by water flow (if any).

A total balance of mass for the solution in flow pipes can be assumed as:

$$\dot{c}_i + \nabla(\mathbf{F}_{iv} + \mathbf{F}_{iu}) + Q = 0 \qquad (2\text{-}2)$$

where c_i Concentration of dissolved ions (mole/m^3)

$\dot{c}_i$ Changes of concentration during time *dc/dt* (mole/(m^3·s))

$k_{ion(aq)}$	Diffusion coefficient in pore solution (m^2/s)
$\mathbf{F}_{iv}$	Convection flux = $v_w c_i$ of ions in pore solution (mole/(m^2·s))
$\mathbf{F}_{iu}$	Constitutive relation = $-k_{ion(aq)} \nabla c_i$ of diffusion flux of ions in pore solution (mole/(m^2·s))
Q	Mass source term, here as a dissolving reaction term (mole/(m^3·s))
v_w	Velocity of the water (m/s)
∇	Nabla operator

The equation describes how ions are dissolved from the solid (Q) and how the ions are transported away by convection ($v_w \nabla c$) or by diffusion ($\nabla \cdot (-k_{ion(aq)} \nabla c_i)$. In chapter 3.2, the leaching process is modelled in a simplified manner compared to equation (2-2). Leached material cause more a porous concrete when disappearing. Strength reduction due to leaching is treated in chapter 3.3. In chapter 3.4, leaching and strength models are combined to a degradation model. In chapter 3.5, a little more sophisticated model of the dissolving reaction Q is suggested for future calculations.

3.2 The leaching process

In figure 3-2, the assumed leaching model with certain flow pipes is showed for a small concrete part. The concrete is saturated and there is a water pressure gradient over the part. The part may for example be located somewhere inside a real dam. The model is very simple and the theory is rather easy to understand. However, many assumptions are made that ought to be checked against test results. This is done to some extent in chapter 8. The model is best suited for high-permeable concrete where most of the water flows in rather large paths that can be looked upon as *flow pipes*.

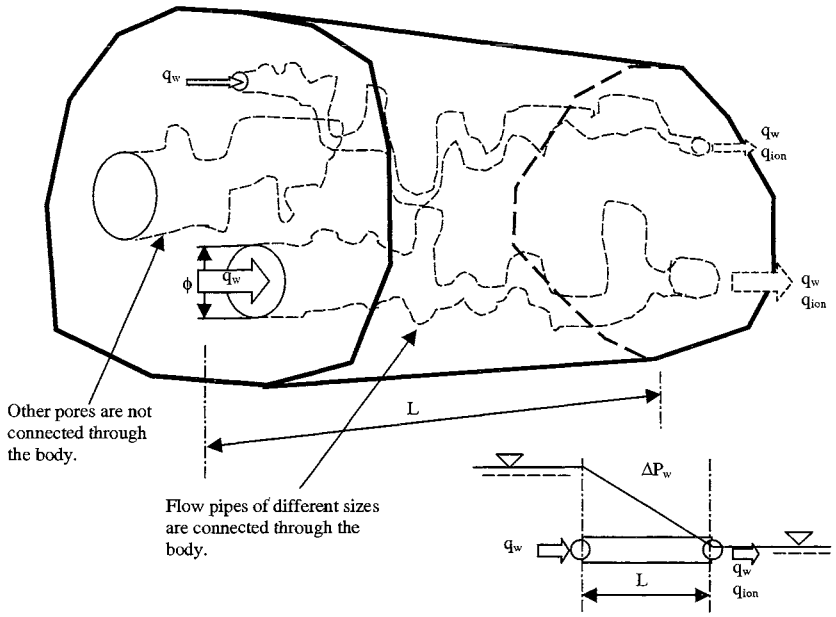

Figure 3-2 The assumed leaching model for a concrete specimen subjected to pure water pressure at the upstream face and a volume of drainage water at the downstream face without any pressure.

The model is based on the following assumptions:

Water flows through a number of tortuous *flow pipes* in a saturated continuous concrete body. The water dissolves solid material from the pipe walls. In this particular model, only dissolving of $Ca(OH)_2$ is regarded. It probably comes mainly from solid crystals of $Ca(OH)_2$, but also to some extent from other compounds that partly consist of $Ca(OH)_2$. Dissolved ions (Ca^{2+}, OH^-) are transported downstream and out of the body by the flow of water. No diffusion of ions in upstream direction is regarded! When solid material is taken from pipe walls, the pipe become wider and the water permeability increases and the strength decreases. Due to less available ions in the pipe walls, the dissolving rate is assumed to decrease. The body is here divided in only one element, so any gradients of leaching effects throughout the body can not be regarded. The model does not consider any self-healing effect, e.g. crystallisation of $CaCO_3$.

The flow of water through a number n_i of flow pipes of different average pipe diameters N, is assumed to be governed by a reduced Hagen-Poiseuilles law. The reduction is regarded by an assumed reduction coefficient r_w, regarding the deviation between flow in a real tortuous flow pipe and a perfect cylinder. The number n_i of each pipe size, is estimated from an assumed pore size distribution, see figure 3-3. In figure 3-3, the total pore volume is assumed for each of ten (10) different assumed pore diameters. Garboczi and Bentz (1996) have shown (figure 1-8) that only a fraction of the total pores are connected through the cement paste and have the ability to convey water. In the model presented here, only a certain portion (here called *share*) of the total pore volume is assumed to percolate water. The sum of the ten different pore volumes $V^i_{p/m}$ made up the total pore volume $V_{p/m}$. The figure is only hypothetical. The pore size distribution is however to some extent based on data from Winslow & Diamond (1970). From the total pore volume for each pore size, the total number n_i is calculated.

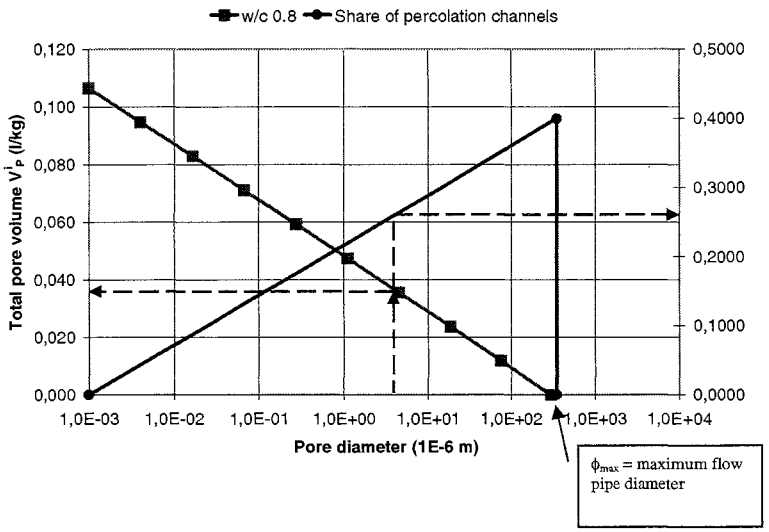

Figure 3-3 The pore size distribution model used. It is based on mercury porosimetry studies by Winslow and Diamond (1970). The figure shows an example with concrete with w/c 0.8.

In chapter 8 has the variables *rate*, *share*, r_w, and ϕ_{max} been varied to fit to experimental data. The total flow of water for pipes with a certain size i is:

$$q_w^i(t) = k_w^i(t) \cdot \frac{\Delta P_w}{L} \cdot A_i \tag{3-1}$$

The permeability for each pipe size *i* is:

$$k_w^i(t) = n_i \cdot \frac{(\phi_t^i)^2}{32\mu} \rho_w g \cdot r_w \tag{3-2}$$

The number of pipes of size *i* is:

$$n_i = \frac{\sum V_{pipe}^i(t_0)}{V_{one\ pipe}^i} = \frac{\sum V_{pipe}^i(t_0)}{\pi (\phi_0^i)^2 / 4 \cdot L} \tag{3-3}$$

The total volume of pipes of size *i* that are connected through the concrete and can lead water is:

$$\sum V_{pipe}^i(t_0) = V_{p/m}^i \cdot share \cdot m_{paste} \tag{3-4}$$

$$V_{P/m}^i = V_{p/m} / N \tag{3-5}$$

$$V_{p/m} = (V_p)_p / m_{paste} = \frac{(w/c - 0.19\alpha)}{1000(1 + 0.25\alpha)} \tag{3-6}$$

$$(V_p)_p = C(W - 0.19 \cdot \alpha)/1000 \tag{3-7}$$

$$m_{paste} = C(1 + 0.25 \cdot \alpha) \tag{3-8}$$

Where

$q_w^i(t)$	Total water flow for pipes with pipe size *i* at time *t* (m^3/s)
$k_w^i(t)$	Water permeability for pipe size *i* at time *t*, expressed by a reduced Hagen-Poiseuilles law (m/s)
ΔP_w	Water pressure difference between the ends of the pipe (m)
L	Length of the flow pipes (m)
A_i	Area of pipe size *i* at time *t* (m^2)
n_i	Number of flow pipes with pipe size *i* (nos.)
ϕ_0^i	Pipe diameter for pipe size *i* at time zero (m)
ϕ_t^i	Pipe diameter for pipe size *i* at time *t* (m)
ρ	Density of water (kg/m^3)
g	Acceleration of gravity (m/s^2)
r_w	Reduction coefficient due to deviation between flow in a real tortuous flow pipe and a perfect cylinder (-)
μ	Dynamic viscosity (Ns/m^2)
$\sum V_{pipe}^i(t_0)$	Initial total pipe volume for pipe size *i* at time zero (m^3)
$V_{one\ pipe}^i$	Initial volume of <u>one</u> pipe with pipe size *i* at time zero (m^3)
$V_{p/m}^i$	Total pore volume per kg paste for pipe size *i* at time zero (m^3/kg)
$V_{p/m}$	Total volume of the cement paste per kg paste (m^3/kg)
$share_i$	Share of the total pore volume with pipe size *i* that percolate water (-)
$(V_p)_p$	Total pore volume of cement paste (m^3)
m_{paste}	Weight of cement paste (kg)
N	Number of different pipe sizes in the body (nos.)

W	Content of mixing water (kg)
α	Degree of hydration (-)
C	Cement content (kg)

The mass of leached material from the pipe walls is assumed to be proportional to the flow of water, i.e. an instant dissolving reaction and then only convection flow of the dissolved ions are assumed. The concentration of dissolved material is assumed to be the same along the pipe-element.

$$dm_i = q_{ion} \cdot \Delta t = q_w^i(t) \cdot c \cdot \Delta t \tag{3-9}$$

where

dm_i	Mass of leached material for pipe size *i*. (kg)
c	Concentration of dissolved material in the drainage water (kg/m^3)
q_{ion}	Ionic flow (kg/s)
Δt	Time step (s)

As Unsworth et al (unknown), Moskvin (1980) and Hearn & Morley (1997) found, the leaching rate will probably decrease when the concrete have been leached for some while. As the walls of the flow pipes are assumed to be exhausted in soluble material, the concentration of ions in the drainage water is assumed to decrease:

$$c = c_0 \cdot \left[\frac{\phi_0^i}{\phi_t^i}\right]^{rate} \tag{3-10}$$

Where

c_0	Concentration of dissolved material at time zero in the drainage water (kg/m^3)
Rate	Rate at which the solubility decrease with increased pipe diameter

The volume of solid material that is leached in pipe size *i* is:

$$V_{pipe,leached}^i = dm_i / \rho_M \tag{3-11}$$

where

$V_{pipe,leached}^i$	Volume of leached $Ca(OH)_2$ during a time step Δt (m^3)
ρ_M	Density of the leached material (kg/m^3)

The pipe is assumed to grow wider as the solid material is leached away from the pipe walls.

$$V^i_{pipe,leached} = n_i \cdot (\phi_t^2 - \phi_{t-1}^2)\pi L/4 \tag{3-12}$$

Where

ϕ_{t-1}	Pipe diameter at the last time step (m)

Equations (3-11) and (3-12) gives a new flow-pipe diameter:

$$\phi_t^i = \sqrt{\frac{4 \cdot dm_i}{n_i \cdot \pi \cdot L \cdot \rho_M} + (\phi_{t-1}^i)^2} \tag{3-13}$$

The new total porosity of the cement paste in a leached concrete specimen is:

$$P_p(t) = \frac{(V_p)_p + \sum_i V_{pipe,leached}^i}{V_p} \tag{3-14}$$

$$(V_p)_p = w/c - 0.19 \cdot \alpha \qquad (3\text{-}15)$$

where $(V_p)_p$ Initial pore volume of the cement paste (m^3)

$V^i_{pipe,leached}$ Volume of leached material for all flow pipes (m^3)

V_{air} Pore volume due to mixing and any air additives (m^3)

3.3 Strength models for concrete

The strength of concrete depends on the amount and the strength of its solid constituents. Due to scatter in the distribution of hydration products, micro-cracks, stress concentrations, stress redistribution, different modulus of elasticity of hydration products and aggregate, etc, it is difficult to give any precise value of the strength by any theoretical model. Stress concentrations and micro-cracks around pores and in the not perfect homogenous solid phase lower the strength. Aggregates will probably to some extent "trap" micro-cracks and by that increase the strength. The smaller the size and higher the amount of the aggregate, the better crack-trapping ability and the higher strength is probably achieved. On the other hand, aggregate can result in more stress concentrations and stress re-distribution due to differences in elasticity and strength between the aggregate and the cement paste, and because of that aggregate can lead to decreasing strength. Larger sizes of the aggregate will probably mean higher stress concentration and lower strength. In Möller & Petersons (1994), the following influencing aspects on concrete strength are given; structure and porosity, the age of the concrete, w/c-ratio, any air-additives used, cement strength, additives, aggregate, curing condition, different strength in different directions, long term effects, temperature and temperature gradients, moisture gradients and the velocity of load placing and the duration of the applied load. In the model presented below, only influencing due to porosity is regarded.

From a leaching model, the amount of leached material is achieved. The amount of leached material gives a changed porosity in the cement paste phase in the concrete. Because the main effect of leaching is an increased porosity, it is tempting to use a strength model, which involve the porosity. It is also desirable to be able of relate the calculated strength of the cement paste to the strength of the whole concrete.

In the principles showed by figure 3-4, the strength of the concrete is assumed to approximately follow the strength of the cement-paste. In high w/c ratios, the aggregate probably increase the concrete's strength a bit compared to the paste's strength and vice versa for low w/c ratios Fagerlund (1987).

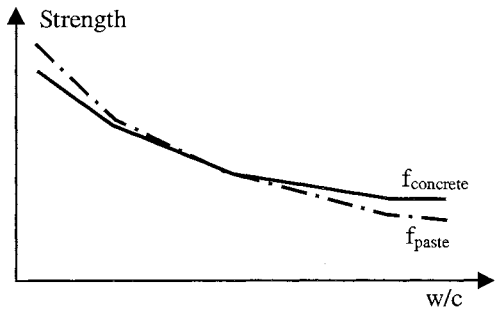

Figure 3-4 Principle relations between compression strength of concrete and paste. $f_{concrete} \approx f_{paste}$.

Two simple models for the strength of cement paste based on porosity are showed below.

Alternative 1: Compressive strength for cement paste
The solid phase $(V_0)_p$ of the paste, with solid gel and unhydrated cement, takes the entire load. Pores do not carry any load, see figure 3-5.

$$f_{pc} = f_0 (1 - P)^{K_1} \qquad \text{Bal'shin (1949) and Fagerlund (1995)} \qquad (3\text{-}16)$$

The porosity of the cement paste is defined as:

$$P = P_p = \frac{w/c - 0.19 \cdot \alpha}{w/c + 0.32} \qquad (2\text{-}17)$$

Where f_{pc} Compressive strength of cement paste (Pa)
f_0 Fictitious strength of the solid phase without pores (Pa)
K_1 Empirical parameter. Given as $2 \leq K_1 \leq 3.5$ in the literature (-)
P_p Porosity of the cement paste (no air pores are included) (m^3/m^3)
w/c Water to cement ratio (kg/kg)
α Degree of hydration (-)

Alternative 2: Compressive strength for cement paste
The cement gel V_{gel}, with gel pores, takes the entire load. Unhydrated cement and capillary pores takes no load, see figure 3-5.

$$f_{pc} = f_0' \cdot X^{K_2} \qquad \text{Powers (1958)} \qquad (3\text{-}18)$$

The gel space ratio is defined as:

$$X = \frac{V_{gel}}{V_{gel} + (V_{cap})_p} = \frac{0.71 \cdot \alpha}{0.32 \cdot \alpha + w/c} \qquad (3\text{-}19)$$

Where f_0' Fictitious strength of the cement gel, with gel pores included (Pa)
K_2 Empirical parameter. Given as $2 \leq K_1 \leq 3$ in the literature (-)
X Gel space ratio (m^3/m^3)
V_{gel} Volume of the cement gel (m^3)
$(V_{cap})_p$ Volume of the capillary pores in the cement paste (m^3)

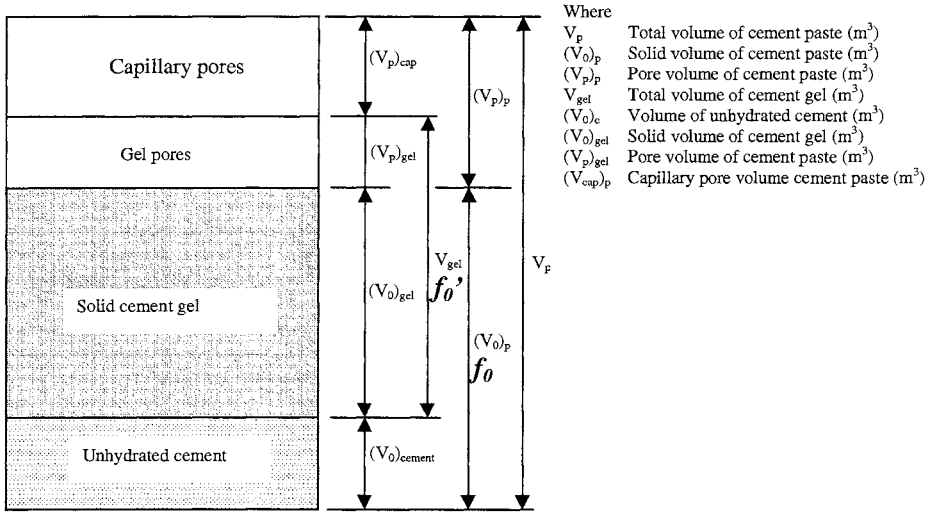

Figure 3-5 Schematic volume fractions in cement paste

The "fictitious" strength depend in alternative 1 on the strength of the solid phase without pores and in alternative 2 on the cement gel with gel pores included. Because the fictitious strength in the second alternative includes gel pores it should be lower than in the first alternative.

In figure 3-6, calculations of the compressive strength as a function of w/c ratio is showed for the strength-structure relations described by alternative 1 and 2 above. The parameters K_1 and K_2 are both chosen to 2.5. In the figure are also results from a laboratory test on the compressive strength f_{cc} of concrete made of Swedish standard cement and aggregate shown Ysberg (1979). No values of the fictitious strength are available in this work. The fictitious strength in the strength-structure relations has just been set to $f_0 = 210$ MPa and $f_0' = 100$ Mpa, so the curves fit well to f_{cc} given by Ysberg for w/c 0.7. It is interesting to note that the two alternative curves of the relations alternative 1 and 2, have very much the same shape. However, as it was assumed in figure 3-4, the curves for the strength-structure relations in figure 3-6, which describe the strengths of the cement paste, are little steeper than the curve for concrete presented by Ysberg.

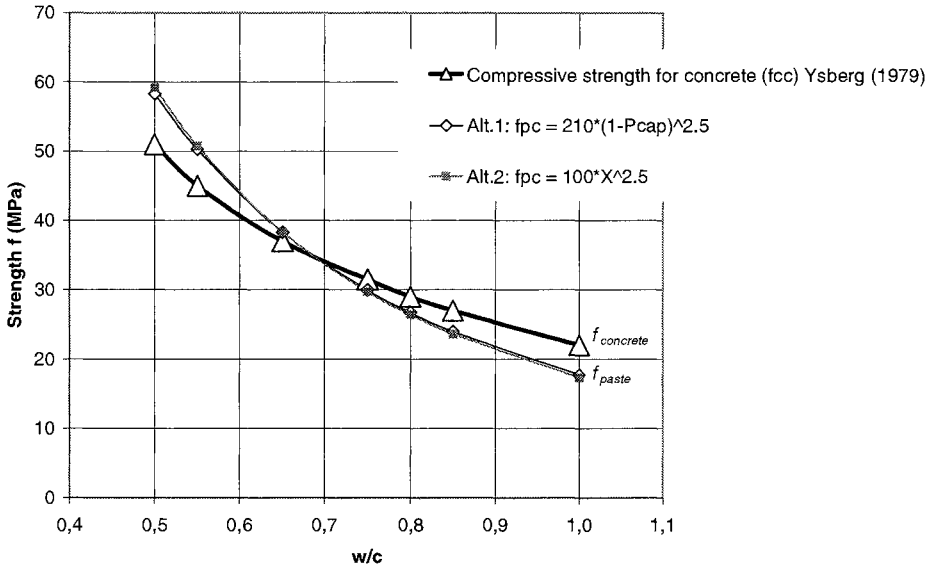

Figure 3-6 Calculated compressive strength relations (Alternative 1 and 2 from the text) compared with laboratory test results of compressive strength of Swedish concrete Ysberg (1979).

In figure 3-7, the strength-structure relations for the cement paste are modified to fit the whole curve of the concrete strength f_{cc} presented by Ysberg. The modifications are only pure curve fitting and transform the calculated strength of cement paste to an assumed strength of concrete. With a=1.2 and b=0.5 in the model g(f_{cc}) below, the relations turns out to be close to f_{cc} presented by Ysberg.

$$g(f_{cc}) = f_{pc} \cdot a \cdot (w/c)^b \qquad (3\text{-}20)$$

where
- g(f_{cc}) — Model describing the compressive strength of concrete (Pa)
- f_{pc} — Compressive strength of cement paste by any of the strength relations alternative 1 and 2 described above (Pa)
- a — Curve fitting parameter. a = 1.2 to fit f_{cc} in Ysberg (1979).
- b — Curve fitting parameter. b = 0.5 to fit f_{cc} in Ysberg (1979).

The strength model may be used for comparison with experimental results in this work and for static checks of real structures in the future. For such use, more verification must, however, be done.

An important reflection is that the strength of the concrete is rather similar to the strength of the cement paste. Is there, for example, a reduction by 10 % of the strength of the cement paste in the concrete (e.g. due to leaching), there will also be a reduction by 10 % of the strength of the whole concrete.

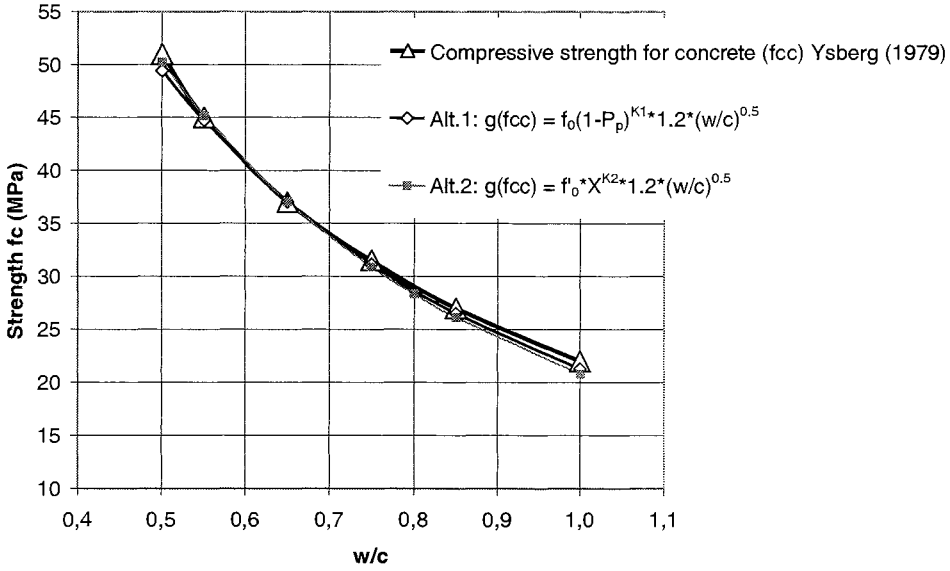

Figure 3-7 Modified compressive strength relations from figure 3-6 compared with laboratory test results of compressive strength of Swedish concrete Ysberg (1979).

3.4 Degradation model

The degradation of concrete due to leaching is assumed to occur according to the following line:

Leaching model in chapter 3.2 + strength model in chapter 3.3 ⇒ degradation model

A short description of a calculation scheme is showed below, which is a summary of chapter 3.2 and 3.3.

Calculation of degradation:

For t=1:T

For i=1:N

$$q_w^i(t) = k_w^i(t) \cdot \frac{\Delta P_w}{L} \cdot A_i \tag{3-1}$$

$$k_w^i(t) = n_i \cdot \frac{(\phi_t^i)^2}{32\mu} \rho_w g \cdot r_w \tag{3-2}$$

$$dm_i = q_{ion} \cdot \Delta t = q_w^i(t) \cdot c \cdot \Delta t \tag{3-9}$$

$$\phi_t^i = \sqrt{\frac{4 \cdot dm_i}{n_i \cdot \pi \cdot L \cdot \rho_M} + (\phi_{t-1}^i)^2} \tag{3-13}$$

$$P_p(t) = \frac{(V_p)_p + \sum_i V^i_{pipe,leached}}{V_p} \tag{3-14}$$

Next i

$$g(f_{cc}) = f_{pc} \cdot a \cdot (w/c)^b \tag{3-20}$$

Next t

In chapter 8, calculations is performed with help of the above calculation scheme. The calculations are to some extent calibrated against the test results.

3.5 Dissolving reaction

The dissolving model presented here is not used further in this work, but it is planned to be used in future works. The dissolving reaction Q is supposed to happen when water molecules diffuse into the pipe wall and dissolve hydration products that are fixed there. The dissolved ions diffuse out through the pipe wall into the pipe solution. The dissolving reaction presented here includes only the diffusion of dissolved ions out to the pipe solution (figure 3-8). For the further leaching process of ions out of the concrete, the equation (2-2) may be used.

$$\dot{c}_i + \nabla(\mathbf{F}_{iv} + \mathbf{F}_{iu}) + Q = 0 \tag{2-2}$$

where Q is the reaction term $\mathbf{Q}_{react}$ from equation (3-26) below for a one-dimensional pipe.

In a system with many ions, the calculation scheme "model Guntelberg" presented in chapter 2.2.2 may be used together with the model presented in this section. The reaction term Q is then depended on the ion strength and common ion effect between different ions.

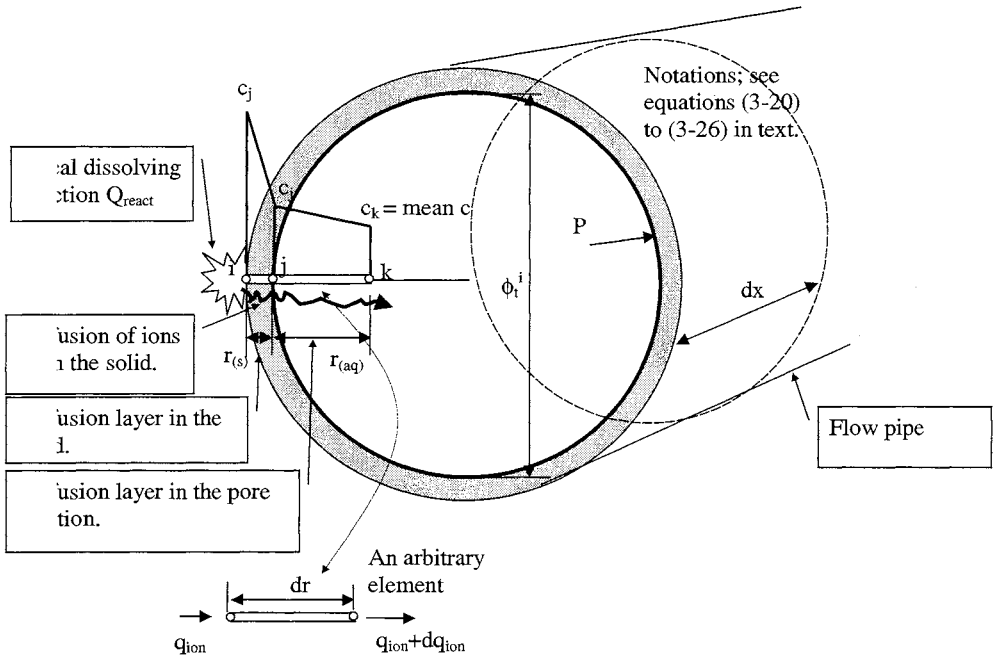

Figure 3-8 The reaction term Q_{pipe} is assumed as a diffusion process where new dissolved ions must penetrate the somewhat leached solid layer $r_{(s)}$ and out through the diffusion layer $r_{(aq)}$ in the pore solution in the flow pipe.

For diffusion in an arbitrary element, see lower left in figure 3-8, the mass balance can be written as:

$$\frac{d(q_{react})}{dr} = 0 \qquad (3\text{-}21)$$

Where q_{react} diffusion of dissolved ions from the pipe wall into the pipe solution (mole/(m·s))

dr infinitesimal length of the diffusion layer perpendicular to the wall (m)

Diffusion of dissolved ions from the pipe wall with the area A_{solid} and per meter pipe dx can be written as:

$$q_{react} = -k_{ion}\frac{A_{solid}}{dx}\frac{dc}{dr} = -k_{ion}\frac{P\,dx}{dx}\frac{dc}{dr} = -k_{ion}P\frac{dc}{dr} \qquad (3\text{-}22)$$

$$P = \pi\cdot\phi \quad \text{(for cylindrical pipes)} \qquad (3\text{-}23)$$

Where A_{solid} Area of the solid walls, that release ions to the flow pipe (m^2)

c Ionic concentration in the diffusion layer (mole/m^3)

dx infinitesimal length in the pipe direction (m)

k_{ion} Ion diffusivity coefficient (m^2/s)

ϕ Diameter of the flow pipe (m)

P wet perimeter (m)

The concentration distribution c over the element is approximated by Ottosen & Petersson (1992) and Zienkiewicz & Taylor (1989):

$$c = N\,\mathbf{a} \tag{3-24}$$

Where $\mathbf{a}$ Approximation of concentration c (mole/m^3)
N element shape functions (-)

The balance equation is reformulated by using the finite element method and the Galerkin method. The "diffusion resistance" for an arbitrary element is calculated as:

$$\mathbf{K}^e = \frac{P\,k_{ion}}{dr}\begin{bmatrix} 1 & -1 \\ -1 & 1 \end{bmatrix} \tag{3-25}$$

Where $\mathbf{K}^e$ "Diffusion resistance" matrix for element e (m^2/s)

The global FE formulation of the diffusion through the two diffusion elements in the wall and in the pipe solution is:

$$\mathbf{Ka}=\mathbf{Q}_{pipe} \tag{3-26}$$

$$\mathbf{K\,a} = \begin{bmatrix} K^1 & -K^1 & 0 \\ -K^1 & K^1+K^2 & -K^2 \\ 0 & -K^2 & K^2 \end{bmatrix}\begin{bmatrix} c_i \\ c_j \\ c_k \end{bmatrix} = \begin{bmatrix} -Q_i \\ 0 \\ Q_k \end{bmatrix} \tag{3-27}$$

$$K^1 = A_{solid}\;k_{ion(s)}\,/(dx\,r_{(s)}) = \pi\,(d+2r_{(s)})\,k_{ion(s)}\,/(dx\,r_{(s)}) \tag{3-28}$$

$$K^2 = A_{solid}\;k_{ion(aq)}\,/(dx\,r_{(aq)}) = \pi\,d\,k_{ion(aq)}\,/(dx\,r_{(aq)}) \tag{3-29}$$

Where $\mathbf{K}$ Global "diffusion resistance" matrix (m^2/s)
K^1 Diffusion "resistance" in the diffusion layer in the solid (m^2/s)
K^2 Diffusion "resistance" in the diffusion layer in the solution (m^2/s)
$k_{ion(s)}$ Diffusion coefficient in the solid diffusion layer (m^2/s)
$k_{ion(aq)}$ Diffusion coefficient in the pipe solution (m^2/s)
$\mathbf{Q}_{pipe}$ Global reaction matrix for a cylindrical pipe in one dimension (mole/(m·s))
r Diffusion layer thickness (m)
$r_{(s)}$ Thickness of the solid diffusion layer (m)
$r_{(aq)}$ Thickness of the diffusion layer in the pipe solution (m)
c_i Concentration in the un-leached solid wall (mole/m^3)
c_j Concentration in the leached surface of the pipe (mole/m^3)
c_k Mean current concentration in the flow pipe (mole/m^3)

The diffusion coefficient in the solid material, $k_{ion(s)}$, will probably decrease with the leaching ratio because it will be more difficult for the water to find any soluble substances. On the other hand, the solid structure is perhaps somewhat more porous after leaching, so the diffusion should be somewhat more rapid. When the substances are dissolved, the diffusion layer thickness, $r_{(s)}$, will increase.

4 SCOPE AND GENERAL LAYOUT OF THE EXPERIMENTAL WORK

To imitate a concrete dam subjected to soft water under pressure, a test equipment was built that pressed de-ionised water through a number of concrete specimens. The equipment consisted of a de-ionising aggregate, a storage tank for the de-ionised water, a pump, a pressure tank and a steel pipe system that carried the water to a number of stainless steel test cells in which "pressure specimens" of concrete were placed (4-1 to 4-4). The specimens were cast in cells of which the walls had a conical shape. Before starting the test, the specimens were remoulded from the cells and treated in different ways, see below. Then they were once again placed in the cells with latex-foil between the specimen and the cell. Foil was used to secure complete sealing. Any water that flowed through the concrete specimens after these were exposed to water pressure was collected in measuring vessels after the concrete specimens.

The *reference* specimens had the same size and were hardened and cured in the same way as the pressure specimens was. The only difference was that they were not conical shaped and they were not water pressed. The amount of the reference specimens was the same as the pressure specimens.

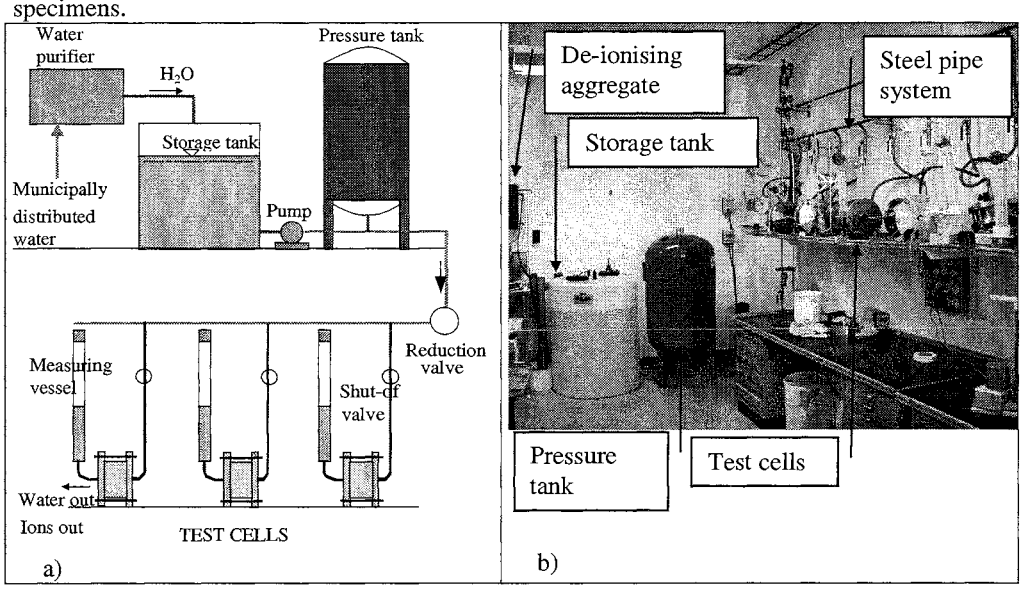

Figure 4-1 Test equipment. De-ionised water was pressed through a number of concrete specimens. 30 cells were used totally.

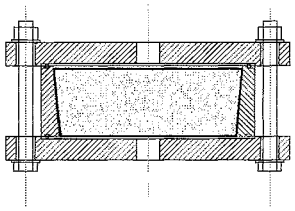

Figure 4-2 Test cell of steel with the *pressure* specimens of concrete inside. See drawing in appendix 5-1.

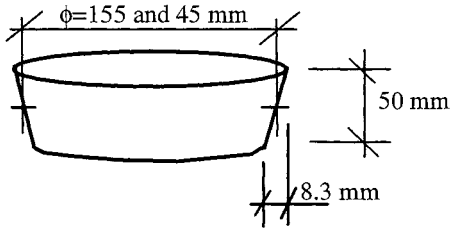

Figure 4-3 The pressure specimen for the pressure test. The reference specimens had the same dimensions, but were not conical.

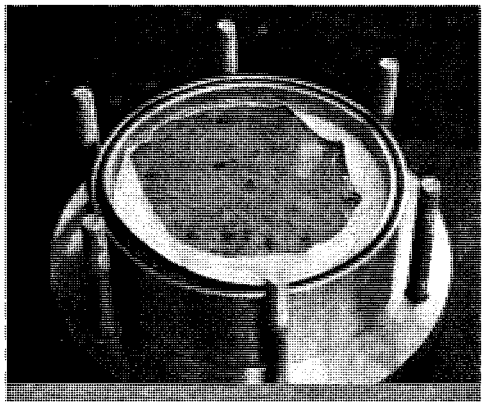

Figure 4-4 A specimen in a test cell after the leaching test.

The test equipment was intended to imitate concrete in a cross section A-A in figure 4-5 of a real dam. In such a section there is often water on both sides and the concrete is always more or less completely water saturated. There is almost no carbon dioxide (CO_2) that can influence the concrete. The leaching model used represents this case.

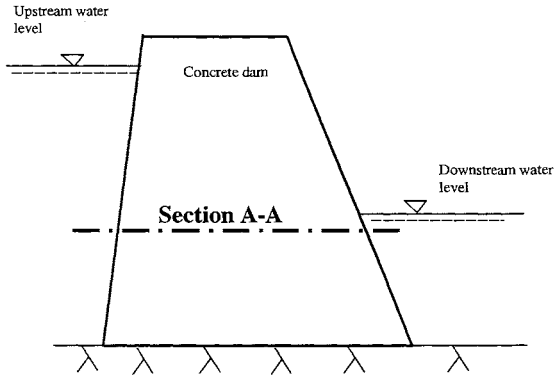

Figure 4-5 The test set-up is intended to imitate the saturated concrete inside a real dam in the cross section A-A.

The main properties that were studied were changes in water permeability, the leaching rate of water and Ca^{2+} and the strength changes.

Three types of experiments were performed, see below and figure 4-6.

Experiment 1

This was a test, to see how the test equipment worked and how large the water permeability was for this type of concrete. The concrete characteristics were: w/c 0.8, aggregate maximum 16 mm, 1 day of hardening in plastic bags in +20°C and then cured at +20°C for 3 months in lime saturated water. The specimens were then exposed to a water pressure of 6 bar for 2 months. This type of never dried concrete was called *virgin* concrete.

Nine specimens were tested:

- ✓ virgin concrete with diameter 155 mm: specimens 1-8 and specimen 10 (specimen 9 was abandoned)

Experiment 2

The resulting water flow in experiment 1 was very low. To get a larger leaching effect in a reasonable time, some specimens were *late-dried* to have the permeability increased. Concrete characteristic were: w/c 0.8 and 1.3, aggregate maximum 16 mm, 1 day of hardening in plastic bags at +20°C and then water cured for 6.5 months in +20°C. Half the number of the specimens were then dried 1 week at +55°C without plastic bags and then water saturated by vacuum treatment followed by water absorption.. Then all specimens were exposed to water pressure of 6 bar. At the end, the pressure was reduced to 1 bar. Water permeability, leaching of the most soluble ions (Ca^{2+}, K^{+}, Na^{+}, S) and the compressive strength in some specimen was measured in this experiment.

Ten specimens were tested:

- ✓ virgin concrete w/c 0.8 with diameter 155 mm: specimens 2 and 5 (specimen 2 was the same as specimen 2 in experiment 1)
- ✓ late-dried concrete w/c 0.8 with diameter 155 mm: specimens 1,3 and 4
- ✓ virgin concrete w/c 1.3 with diameter 155 mm: specimen 10
- ✓ late-dried concrete w/c 1.3 with diameter 155 mm: specimens 6, 7 and 8

Experiment 3

Some specimens were *early-heated* to imitate a more realistic curing condition in the interior of a thick dam, with much hydration-heat but no possibilities of drying. Concrete characteristics were: w/c 0.6 and 0.8, aggregate maximum 8 mm. The heating procedure was divided in 3 steps: (i) 1 day of hardening in plastic bags at +20°C, (ii) heating in plastic bags at +40°C (1 day for w/c 0.6 and 2 days for w/c 0.8), (iii) heating in plastic bags at +60°C for 2 days for w/c 0.6 and at +55°C for 3 days for w/c 0.8, (iiii) heating at +30°C (3 days for w/c 0.6 and 2 days for w/c 0.8). Then all specimens were stored in the same plastic bags for 52 days at +20°C. After the storing, all specimens were water saturated by vacuum treatment followed by water absorption. Then all specimens were exposed to water pressure in the leaching test. The pressure was a over-pressure of 6 bar, except for a short period (varied between one and eight weeks for different specimens) when the pressure was reduced to 3 bar.

23 specimens were tested:

- ✓ early-heated concrete w/c 0.6 with diameter 155 mm: specimens 1, 5, 6 and 7
- ✓ early-heated concrete w/c 0.8 with diameter 155 mm: specimens 8, 9 and 10
- ✓ early-heated concrete w/c 0.6 with diameter 45 mm: specimens 20 to 30
- ✓ early-heated concrete w/c 0.8 with diameter 45 mm: specimens 31 to 36

The de-ionising of the water and the test procedure are described in chapter 5.
The test specimens are described in more detail in chapter 6.

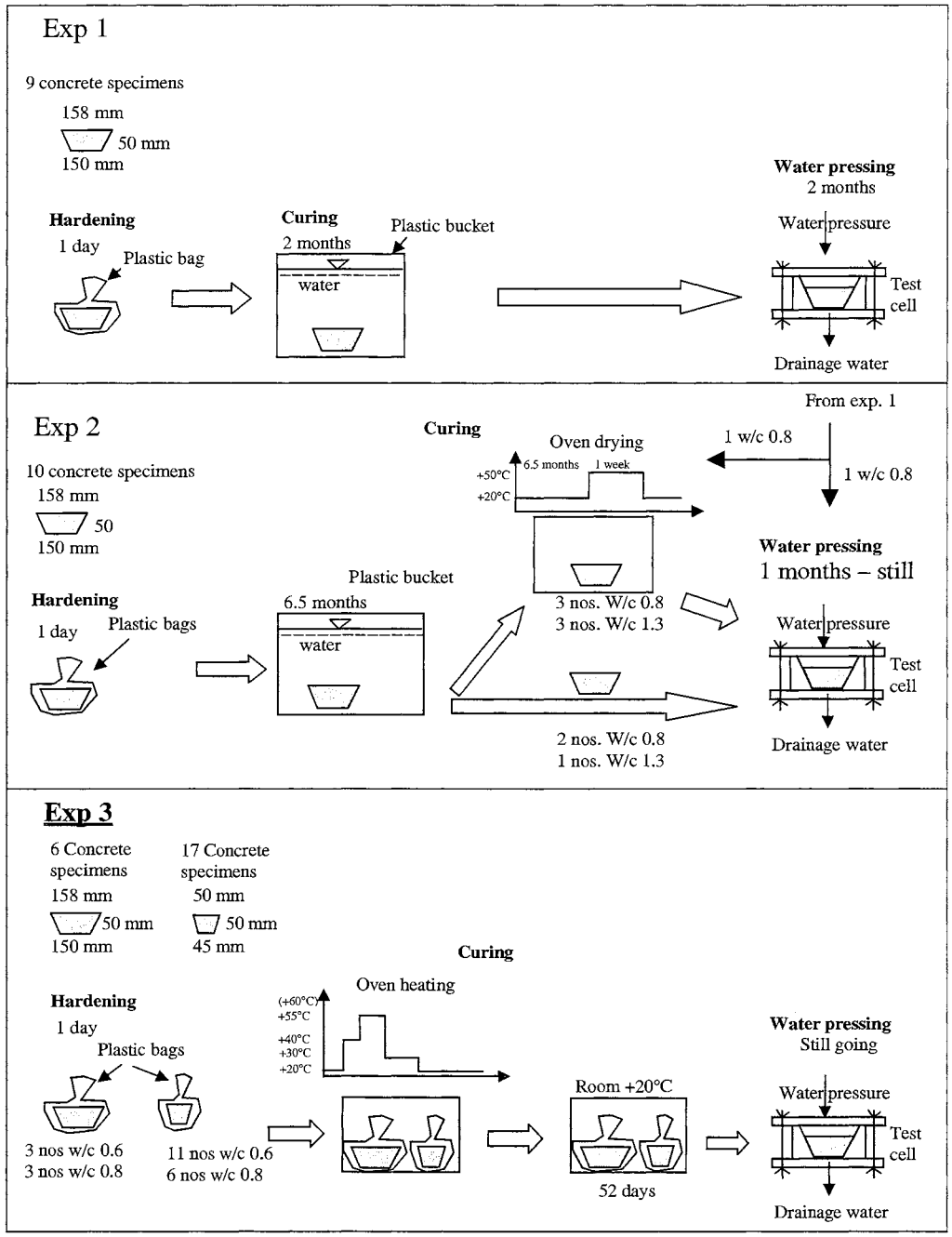

Figure 4-6 Three different experimental set-ups were used. The figure shows the *pressure* specimens. The *reference* specimens were hardened and cured in exactly the same way as the pressure specimens. The only difference was that they were not exposed to water pressure.

5 The experimental procedures

5.1 Test equipment

5.1.1 Test water

By *test water* is meant the water that was pressed through the concrete specimens during the experiment. Ordinary, municipally tap water was de-ionised in order to remove dissolved inorganic salts. A reverse osmosis water purifier was used. About 98 % of the inorganic ions are normally taken away according to the supplier. The conductivity was reduced from about 300 µS/cm to about 2-5 µS/cm according to the conductivity meter on the equipment. An analyses of the test water used was also performed, see table 5-1, which shows that a very pure (soft) water was received.

The water was de-ionised because of two things, (i) to have control over what was going in and what was going out from the specimens during the test, and (ii) soft water is more aggressive to concrete and results can be received more rapidly. The water was not de-aired.

Table 5-1 The properties of the de-ionised test water.

Property	Value
pH[1)]	6.25
Alkalinity[1)]	3.25 –4.5 mg $CaCO_3$/l
Hardness[1)]	0.20 mg $CaCO_3$/l
Conductivity[1)]	8.7 µS/cm (2-5 according to the ELGA's meter)
Ca[2)]	1.034 mg/l
Mg[2)]	0.045 mg/l
Na[2)]	1.337 mg/l
K[2)]	0.316 mg/l

1) Measured by titration and ion selective electrodes.
2) Measured by ICP-AES (5.2.3)

5.1.2 Pressure equipment

An over-view of the equipment is given in figure 4-1.

After the de-ionising aggregate, the water was stored in a plastic tank of 400 litre. The water was then pumped into ordinary pressure tank designed for houses that consisted of a rubber container inside a steel tank. When the rubber container was filled, the air pressure between the rubber container and the steel tank increased. The increased air pressure led to an increased water pressure in the rubber container. The pump was set to shut of when the water pressure reached 8 bar. The "water pressure" in this report means *over pressure* above the atmospheric pressure.

From the pressure tank, water flowed via a steel pipe to three pressure reduction valves. From each valve, water flowed further to test cells via a steel pipe. The valves were set to hold a certain pressure at the out-flowing side. With these valves, it was possible to have different pressures in each of the three steel pipes. When so much water had flowed out from the pressure tank that the pressure was lowered to a certain level, the pump started again and pumped in more water into the pressure tank.

Shut-off valves were placed before each test cells, so that the individual cells could be taken out of the system any time. The test cells was connected to the shut-off valves by a flexible tube.

Because of the very pure water, all parts in the system were made of acid-proof material.

5.1.3 Test cells

A number of test cells were made of acid-proof stainless steel. Two sizes was used, one for specimens with about ϕ155 mm diameter and one for specimens with about ϕ45mm in diameter. See figure 4-3 and Appendix 5-1.

Each test cell was composed of one cylindrical part and two end-plates. O-rings of rubber were placed between the plates and the cylinder. The concrete specimens were cast directly in the cylinders. The cylinders were conical inside so the water pressure applied during the leaching test should press down the concrete specimen and tighten it against the steel.

Entrapped air under the upstream lid was led out via a shut-off valve.

5.1.4 Outlet

Water that percolated through the concrete specimens (drainage water) was led via soft plastic tubes to measuring vessels. Three different types of measuring vessels were used, byretts for small water flow, measuring glasses for bigger water flow and 25 litres plastic drums for the real big flow.

5.2 Test procedure

5.2.1 Mounting in test cell and measurements of water flow

Concrete specimens that were exposed to water pressure are called *pressure specimens*. The mounting of the pressure specimens is described below. *Reference* specimens were stored in a water bucket during the whole test period.

A short (30-40mm), stiff plastic tube was applied to each bottom lid via a plastic nipple, see figure 5-1. A short (50-60mm), soft plastic tube was forced on each stiff plastic tube end. An o-ring was applied at the bottom end of each cylinder and the cylinders were placed on the bottom lids. De-ionised water was filled inside the cylinders, to stop carbon dioxide to come in contact with the downstream end of the concrete specimens and to avoid drying these ends.

The concrete specimens were taken from the curing water one by one. After about 2-3 minutes in the open air, silicon high vacuum grease was greased around the outer surface of each specimen. A latex rubber tube was forced around the surface. More silicon grease was applied on the latex tube and on the inside of the steel cylinders. This grease and latex tube were used for secure perfect sealing.

The concrete specimen was then placed inside the cylinder, entrapped air and some water from the bottom of the cylinder was pressed out during mounting of the specimen. The top lid with its o-ring was mounted and the cell was screwed together.

A tube, letting water in from the steel-pipe system, was screwed to the top of each lid and the water pressure was applied by the shut-of-valve. Trapped air, above the top lid, was released via air-valves.

The test cells were placed on a shelf on its cylindrical surface or on its flat surface and the measuring vessels were connected to the soft plastic outlet tubes.

To prevent moisture leakage from the byretts, rubber plugs and balloons were mounted on the outlet of the byretts. On the measuring glass, rubber balloons were mounted. On the drums, plastic tubes were placed around the soft plastic tube coming from the test cell and the hole in the drums.

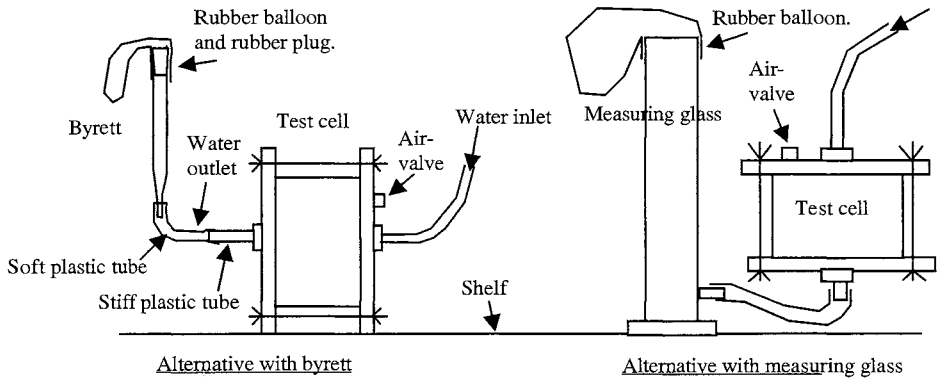

Figure 5-1 Test cells mounting, one on its cylindrical surface and one on its flat surface.

5.2.2 Permeability analysis

The *pressure* specimens were exposed to a water pressure of 6 bar on the upstream face during the test period. Sometimes the pressure was reduced, see chapter 7.

During the same period, the downstream face was exposed to water without any significant pressure.

The amount of water flowing through the concrete specimens, the *drainage water*, was measured manually by reading the water levels in byretts, measuring glass or plastic drums.

When the water-collecting vessel was full and after measuring the amount of water, it was emptied into the sink or it was gathered in small plastic or glass bottles, *test water samples*. The gathered water samples were later examined for pH and leached ion content.

The result of the permeability measurements is shown in chapter 7.2.

5.2.3 Chemical analysis in collected water samples

The gathered drainage water was checked regarding pH and ion concentration. pH was measured by an pH electrode and the concentration of calcium was measured by an Ca^{2+} selective electrode. At some occasion the concentration of Ca^{2+} and other ions in the out-flowing water were measured by a apparatus which use the technique of ICP AES, see below.

In real situations, with a large water reservoir against the upstream face of a dam, dissolved ions from the concrete will not influence the ion content in the reservoir very much. In the experiment, the small volume of the upstream water was rather quickly contaminated with dissolved ions that diffused upstream from the test specimens. To avoid this, the inlets were flushed through the air valves in the top lids every time the water level in the vessels was measured. In doing so, a rather pure water situation was maintained on the upstream face of each specimen, at least during the first one or two days after the flushing. The flushed volume was about 2 litre per specimen and occasion for the ϕ155 mm specimens and about 0.2-0.3 litre per ϕ 45 mm specimens. During the experiment 2, it was observed that this flushed water consist of relatively much ions that had diffused from the specimens. So, in experiment 3, the out-flushed water was occasionally gathered for some specimens (no 6, 7, 8, 9 and 10). The gathered water was then analysed in the same way as said above.

pH measured by pH electrode

An *Orion 720A ISE/pH meter* was used together with a *Beta Sensor pH Electrode model G-200-PC*. A magnetic stirrer was used to get quicker and more stable values. The temperature in buffers and collected water sample was the same, +20°C.

- *Calibration*. The pH Electrode was calibrated every measuring occasion against buffer solution with pH 7, 9 and 11.
- *Measuring*. The pH value was measured directly in the collected water sample.

Calcium measured by ion selective electrode

An *Orion 720A ISE/pH meter* was used together with a *Beta Sensor calcium selective electrode model ISE-400-P* and a *Beta Sensor reference electrode model R-860-S*. A magnetic stirrer was used to get quicker and more stable values. The temperature in standards and collected water sample was the same for both types of electrode.

- *Calibration*: The electrodes were calibrated in three different standards that was mixed of 40 ml 0.1M NaCl + 0.4 ml acetate buffer + *x* $CaCl_2$, where *x* was:

✓ x = 0.4 ml 0.001M ⇒ 0.39 mg Ca^{2+}/l ($0.4*10^{-3}*40\ 080/(0.4+40+0.4)=0.39$)
✓ x = 0.4 ml 0.01M ⇒ 3.9 mg Ca^{2+}/l ($0.4*10^{-2}*40\ 080/(0.4+40+0.4)=3.9$)
✓ x = 0.4 ml 0.1M ⇒ 39.3 mg Ca^{2+}/l ($0.4*10^{-1}*40\ 080/(0.4+40+0.4)=39.3$)

where 40 080 is the mole weight of calcium (mg)

Acetate buffer and sodium chloride was added to ensure that the test water samples and the standards have proper pH, similar ionic strength and to reduce the effect of interfering ions. The acetate buffer was made of acetic acid (CH_3COOH) and sodium acetate ($NaCH_3COO$). The acetate buffer buffers at $pH = pK_a + \log([A^-]/[HA]) = 4.75 + \log 1 = \underline{4.75}$.

Because an ion selective electrode only detects free ions, the pH must be rather low to avoid ion bonding between the ion studied and other ions. The measured pH was in the range 4.5 to 4.8 for both the calibration standards and the test specimens.

The ionic strength for both standards and test water sample was about 0.1, see table 5-2 and 5-3.

- *Measuring*: To have the same pH, ion strength and sensibility to interfering ions, the test water sample was composed of a solution of 20 ml 0.1 M CaCl + *x* of collected water + *y* acetate buffer (or multiples of it). x and y was most often chosen to x=0.4 and y=0.4 ml. The pH value was about 4.5 to 4.8.

The real ion concentration was given from the read value as:

$$[A] = \text{read value} * \frac{(V_{NaCl} + V_{collected\ water} + V_{acetate\ buffer})}{V_{collected\ water}} \qquad (5\text{-}1)$$

where
- [A] Real ion concentration in the test water (mole/l)
- read value Value read by the ion meter (mole/l)
- V_{NaCl} volume of NaCl solution used (ml)
- $V_{collected\ water}$ Collected test water volume (ml)
- $V_{acetate\ buffer}$ Volume of used acetate buffer (ml)

Calcium measured by ICP-AES

To check the reliability of the ion selective electrode measuring (chapter 5.4.3) and to measure other ions, analyses was also done with a *Purcin-Elmer Optima 3000 DV* which use a ICP AES technique (Inductive coupled plasma atom emission spectroscopy). The accuracy with this technique is +/- 5 % according to the test centre at the Plant ecology at Lund University. The

other elements checked, besides Ca were; Na, K, Al, Fe, S, Mg. The result of the chemical analysis is showed in chapter 7.3.

5.2.4 Chemical analysis of concrete

One specimen, specimen 3 in experiment 2, was analysed regarding chemical contents after the leaching test. One halves (piece 1) and one quarter (piece 2) of the specimen, was sliced into five slices each (figure 5-2). The procedure was:

1) The specimen was taken out of the leaching test.

2) The pieces 1 and 2 were cut in five slices, approximately 7 mm thick.

3) The still wet slices were measured by weight in air $\Rightarrow m_{wet,\ air}$

4) The slices were measured by weight under water $\Rightarrow m_{wet,\ water}$

5) The slices were dried in +105°C.

6) The slices were measured by weight in air $\Rightarrow m_{dry,\ air}$

The slices coming from piece 1 were then dissolved in HNO_3 and the solution was analysed chemically with regard to the most important elements. The dissolution of the slices gave also an insoluble rest. The procedure was:

7) The slices coming from piece 1 were boiled in a solution of water and HNO_3 for 2.5 weeks at 130°C. When the boiling was stopped, all except 80 ml was boiled away. The residual solution was diluted with de-ionised water to 1000 ml.

8) The solution was analysed with ICP AES (see chapter 5.2.3) with regard to the amount of the elements Al, Ca, Fe, K, Mg, Mn, Na, S and Si.

9) The dissolving of the slices gave also a residual solid part in the bottom of the measuring glass. This was dried and measured by weight

10) Because of the uncertainty of how much of the residual, not dissolved, part that came from the aggregate and how much that came from the cement paste, a new chemical analysis was done. In this new analyse, only aggregate was dissolved as described in 7) to 9) above.

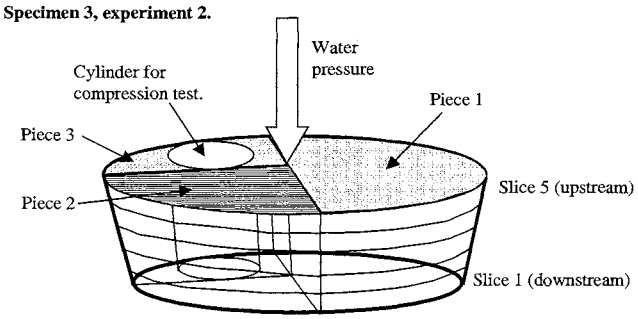

Figure 5-2 A chemical analysis of the residual content of elements was done for the piece 1 from the leached specimen 3 in experiment 2. Piece 2 was used for porosity measurements. An out-drilled cylinder from piece 3 was used for testing the compressive strength.

The result of the chemical analysis is showed in chapter 7.4.

5.2.5 Porosity analysis

The pore-structure of specimen 3 in experiment 2 was analysed.

The total porosity

From the same analyse point 1) to 6) in the above chapter 5.2.4, the total porosity of piece 1 and 2 from the specimen 3 was also received.

The volume V_c of the concrete slices was measured as:

$$V_c = \frac{m_{wet,air} - m_{wet,water}}{\rho_w} \tag{5-2}$$

where V_c volume of the concrete slices (m^3)
$m_{wet,air}$ Weight of the saturated slices in air (kg)
$m_{wet,water}$ Weight of the saturated slices beneath water (kg)
ρ_w Density of water (kg/m^3)

The dry bulk-density ρ_{dry} was measured as:

$$\rho_{dry} = \frac{m_{dry,air}}{V_c} \tag{5-3}$$

where ρ_{dry} Dry bulk-density of the concrete slices (kg/m^3)
$m_{,dry,air}$ Weight of the dried (+105°C) slices in air (kg)

The total porosity P_c of concrete that is reachable by drying in +105°C is

$$P_c = \frac{m_{wet,air} - m_{dry,air}}{\rho_w \cdot V_c} \quad (m^3/m^3) \tag{5-4}$$

The result is showed in chapter 7.5.

The pore size distribution

After the total porosity was determined as described above, the slices from piece 2 were water saturated again by vacuum treatment followed by water absorption. The test was carried out with help of a suction test, described in Janz (1997), see figure 5-3.

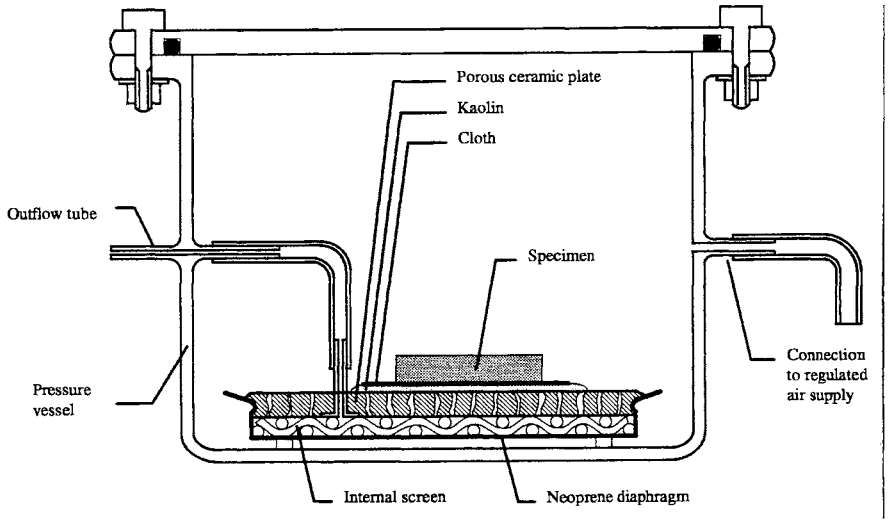

Figure 5-3 A sketch of a pressure plate extractor mounted in a pressure vessel. Excess water in the specimen is by overpressure forced out of the specimen through the cloth, kaolin clay, ceramic plate and then out of the vessel. The internal screen prevents the neoprene diaphragm to clog the underside of the ceramic plate when pressure is applied. The connection between the internal screen and the outside of the vessel (the outflow tube) produces atmospheric pressure underneath the ceramic plate. A high quality manifold pressure regulator regulates the applied overpressure Janz (1997).

The procedure was:

1) The wet weight was measured for all the slices.

2) The slices were put on a porous plate inside the suction apparatus described by Janz (1997) and an air pressure was applied to the chamber.

3) The pressure forced water out from the concrete pieces. Assuming the pores as circular tubes, the air pressure can be assumed to have a relation to the pore size according to the Laplace equation.

$$r_i = \frac{2 \cdot \sigma \cdot \cos\varphi}{P_i} \tag{5-5}$$

where r_i Circular pore radius (m)
σ Surface tension between liquid and air (N/m)
φ contact angle between the liquid and the solid tube walls
P_i Applied air pressure (Pa)

The surface tension $\sigma = 0.07275$ N/m at +20°C.
The contact angle φ is here assumed to be zero, i.e. the water will wet the solid surface completely. Radii between approximately 10 000 Å and 200 Å can be detected, which correspondence to a relative humidity RH of approximately 0.999 and 0.930 respectively according to the Kelvin equation.

$$\ln RH = -\frac{\sigma \cdot M_w}{R \cdot T \cdot \rho_w} \cdot \frac{1}{r_i} \tag{5-6}$$

where M_w Molar weight of water (0.018 kg/mole)
R Gas constant 8.314 (J/(mole*K))
T Temperature (K)

When equilibrium was reached the slices were taken out of the suction pot and measured by weight. The weight loss during each pressure step, correspondence to the volume of pores V_i with the assumed radius according to equation (5-4)

$$V_i = m_i/\rho_w \tag{5-7}$$

Where m_i Measured weight loss during each pressure step (kg)

The result is shown in chapter 7.5.

5.2.6 Analysis of mechanical properties

Compressive strength tests were performed on five of the leached specimens.

Small cylinders with diameter of 64 mm (specimens 1, 6, 8 and 10 in experiment 2) and of 40 mm (specimen 3 in experiment 2) were drilled out of the concrete specimens. At the same time, reference specimens of the same dimensions were tested. All cylinders were water saturated. If the cylinders had poor end surfaces, they were ground so that reasonably fine contact surfaces were received.
The geometry of the cylinders was measured and then they were tested in an ordinary strength-testing machine. The applied load was 1-2 kN/minute. The result is show in chapter 7.6.

The compressive strength, or modulus of elasticity modulus obtained, in this test can not be compared to such obtained at common standard tests, because of the difference in specimen sizes and procedure. But, anyhow, this test indicates changes in compressive strength and E-modulus for leached compared to un-leached concrete specimens.

5.2.7 Dissolving rate of $Ca(OH)_2$ in de-ionised water

Calcium hydroxide ($Ca(OH)_2$) is one of the mayor dissolved substance in the leaching process. To get an indication of the dissolving rate of $Ca(OH)_2$, a simple test was performed. 0.046 g powder of $Ca(OH)_2$ was instantly dissolved in 40 ml de-ionised water, and the change of pH was measured in the solution as function of time. The experiment started without a magnetic stirrer. To see the effect on the dissolving rate a magnetic stirrer was put in after 240 s. The pH-value correlates to the amount of OH^-, so by knowing the pH we know how much of the $Ca(OH)_2$ that has dissolved for each time step:

0.046 g in 40 ml is the same as 1.15 g/l or 1.15/74.08=0.0155 mole/l. If all the $Ca(OH)_2$ is dissolves, the pH value will be $14 + \log(2*0.0155) = 12.49$.

The result is shown in chapter 7.5.

5.3 Validity of the tests

The validity in this case tells how well the measured values from the tested concrete specimens can be compared to concrete somewhere inside a real dam in a real environment. Naturally, the test specimen cannot be of the same size as the real structure, but also the environment is very difficult to predict and imitate. Chemical, physical, mechanical and biological impacts from the environment can be more or less pronounced during a dam's lifetime. In real dams there are often more than one, degradation mechanisms at the time and sometimes they also working together by synergy, leading to a more rapid degradation.

The specimens, when placed inside the test equipment, are thought to be as much like as possible a real concrete dam, subjected to water on both sides and a pressure gradient between the two sides. The temperature was held constantly (+20°C). There was only a permanent load (the water pressure). The water was very pure with no chemical or biological aggressive constituents.

The intention with this work was not to grip over the whole spectrum of influences on the leaching process in a concrete dam. It would have been to many parameters at the same time.

So, compared with a real dam subjected to all possible impacts, the test method used was somewhat not valid in some aspects. Because leaching is strongly depended of the water permeability, most of the below mentioned aspects influence the permeability.

Our laboratory test was probably *accelerated* regarding:

- The pressure gradient
- The water to cement ratio
- The water aggressiveness
- No atmospheric CO_2 in contact with the concrete.

On the other hand, our laboratory test was *retarded* regarding:

- No aggressive ions in the water (CO_2, H^+, SO_4^{2-}, etc). Some CO_2 was however dissolved from the air into the water storage tank, leading to a pH value of about 6.
- The temperature was constantly 20°C
- Only permanent loads.
- No synergy degradation mechanisms.

To increase the value of this study, an additional field investigation of a real dam ought to be done.

Below, some factors that probably influence the validity are discussed.

1. Curing

Inside a real, thick dam during hydration, the temperature can rise quite high, 80 to 90°C (Fagerlund 1997c). The moisture in this location has no possibility to move away. The nearer the surfaces of the dam, the easier has the heat and moisture to flow out from the dam. The temperature will not rise so much here and if the surfaces are not water-cured, the concrete will also dry.

Three main curing conditions were used; virgin, late-dried, early-heated, see chapter 4.

Virgin specimens were never dried, except for some little drying the first day when they were hardening in plastic foil. The small specimen size and the fact that they were put in a water tank after unmoulding, led probably to few cracks in the specimens. The specimens had a high water to cement ratio, which means that the chemical drying was small, which means few micro-cracks. Stresses due to temperature changes and chemical reactions were small.

If concrete in real dams is very well cured (by water and cooling) and of the same w/c ratio as for the test specimens, the quality of the tested virgin specimens may be quite similar with such concrete.

Late-dried specimens, were dried about a week in +55°C after about 4 months in water. It means, that they were well cured and had a hydration ratio of about 0.9, when the drying started. +55°C is also a rather moderate drying temperature, especially when the concrete already had got a high tensile strength, due to the good curing conditions before the drying. If there are cracks, they will not heal easily due to lack of un-hydrated cement.

If concrete in real dams is very well cured (by water and cooling), of the same w/c ratio as for the test specimens and if it is later dried for some cause (e.g. stop of curing and very warm summer days at the same time), the quality of the tested late-dried specimens may be quite similar with such concrete.

Early-heated specimens were heated in plastic bags immediately after unmolding. The specimens probably received a realistic quality compared to concrete located in the interior of thick dams.

2. The pressure gradient

The pressure gradient over the 0.05-meter thick specimens in the experiment, ranged from 30 to 60 meter water head (mwh), i.e. 600 to 1200 (mwh/m.)

A *massive gravity dam* often has a pressure gradient of about 1.1 to 1.4 (mwh/m), i.e. a 100 m high dam is about 70 to 90 (m) at the base. Such a dam, can in a major part of its volume, have a water cement ratio (w/c) as high as the ones used in actual test. Only the upstream part and perhaps the downstream part usually have lower w/c. The pressure gradient in such a case is steeper over the tighter part and more flat over the more permeable, supporting part of the dam. For massive gravity dams *with a front slab,* the water pressure gradient over the front slab can be as high as about 40 (mwh/m).

Arc dams can have up to 20 (mwh/m) in pressure gradients. *Pillar dams* can have about 30 to 40 (mwh/m) over theirs tightening parts.

At joints and gate abutments, the pressure gradient can be even higher.

Massive dams with tight front layer, arc dams and pillar dams however have concrete of very good quality with low w/c, so their pressure gradient, which is often high, is not so dangerous. Around embedded parts such as joint band or gate folder, where it is difficult to cast, the concrete can however be of bad quality.

A high-pressure gradient can lead to:

- ✓ A higher percolation of water, leading to a more rapid leaching process.
- ✓ Chemical self-healing of the concrete will probably become impossible, because dissolved ions have no chance to precipitate due to high water flow.
- ✓ The high-pressure gradient can perhaps lead to internal erosion, i.e. particles inside the specimen can physically erode and follow the water out. The permeability can in such a case increase very much. On the other hand, the eroded particles perhaps get stuck or sediments somewhere downstream in the specimen and in such a case the permeability will decrease. However, the results from our experiments shows that the water velocity is very low even in porous concrete and therefore internal water erosion is not assumed to be of any significant value.

To **summarise;** it can be said that the gradients used in our experiments is much higher than usual for dams, even if it could be possible to reach the same height in some parts of a dam. The higher gradient leads to higher water flow and higher leaching rate. Different pressure gradients were used in our tests: Therefore the pressure influence can to some extent be understood.

3. Water to cement ratio

In the experiments, the water cement ratio used was 0.6, 0.8 and 1.3. These high values were chosen because a high permeability was wanted. For watertight structures, the w/c ratio shall not exceed 0.55 to 0.6. However in some structures or parts, in badly cast parts and in older structures there are possibilities for w/c ratios as high as 0.8. It is more doubtful if w/c ratios 1.3 exist, but perhaps they do in parts where the casting has failed or in older dams. Supporting parts in a dam, e.g. the main part in a RCC-dam or an old massif dam or the pillars in a pillar dam, may often have high w/c ratio. In such a case, damage of the tight front slab may lead to a high water leakage and leaching of hydration products trough the supporting parts. A high water to cement ratio means a greater permeability and that a bigger pore area is exposed to aggressive substances, like pure water.

It was rather difficult to cast concrete with such high w/c ratio as 1.3. Probably the specimens received flow paths due to water separation. A little amount of water separated to the top surface during casting and this water probably evaporated to some extent leading to a little lower w/c ratio than 1.3.

The intention was to imitate old, aged dams, which can very well have such poor concrete as these studied. The intention was also to study the leaching *process*, which probably is not so much influenced by the w/c ratio. It must also be admitted that, to finish the study in a reasonable time, the experiment must be accelerated, and high w/c ratios with resulting high permeability, was one way to go.

4. Water aggressiveness

De-ionised water was used. This has a very high ability to dissolve concrete. It is not unrealistic however, because much water in nature is fairly pure like water from melting snow or water flowing over or through insoluble ground material. These situations are rather common in mountainously terrain with granite or gneiss in the ground, such as in northern Sweden.

If also acids are dissolved in water, leaching effect on the concrete increases even more. In natural waters interacting with the atmosphere or coming from areas of decomposed organic matter, there is dissolved carbonic acid. Many natural waters contains ions, such as CO_2, H^+, SO_4^{2-}, which are aggressive to concrete and in most cases will increase the permeability in the long term. Myran (1967) gives a variation between pH 4.7 to pH 7.1 for thirty dam locations in Norway. The CO_2 content varied between 1.0 to 19.3 mg/l.

Marshy waters can content additional CO_2 and also other acids as humic acid, so pH can decrease, perhaps as low as pH 3-4. Moskvin (1980) gives example from Siberia of marshy waters that contain up to 50 mg CO_2/l. It is not uncommon to have plenty of carbonic acid in the water due to the atmosphere or to any surrounding decomposing organic material. There was no such water in contact with our specimens and therefor the experiment was retarded compared to some, real structures. Some CO_2 was however dissolved from the air into the water storage tank, leading to a pH value of about 6.

The partial pressure P of carbon dioxide at 25°C and 1.00 atm is $P = 3.04*10^{-4}$ atm (Atkins & Jones 1997 p. 535). At such condition, the solubility S of CO_2 is:

$S = k_H*P = 2.3*10^{-2}$ mole $l^{-1}atm^{-1}*3.04*10^{-4}$ atm $= 7.0*10^{-6}$ mole/l or $44\,000*7*10^{-6}$=0.31 mg CO_2/l.

Where k_H Henry's constant (mole/(l·atm))

For dilute water this leads to:

$H_2O + CO_2$	↔	H_2CO_3	↔	HCO_3^-	+	H_3O^+
		a-x		x		x

$x^2/(a-x) = K_{a1} \Rightarrow x = -K_{a1}/2 + ((K_{a1}/2)\text{^}2 + K_{a1}*a)\text{^}0.5$

For $a = S = 7.0*10^{-6}$ mole/l and $K_{a1} = 10^{-6.35}$ gives

$H^+ = x = 1.6*10^{-6}$ mol/l

pH=-log x = **5.81**

So, the measured pH-value of 6.25 in our test water seems reasonable.

To **summarise**; it can be said that the experiments used a rather aggressive water condition at the upstream face but a non-aggressive water condition at the downstream face in relation to a real dam.

5. No atmospheric CO_2 in contact with the concrete

Surfaces of real dams, are usually in contact with atmospheric CO_2. This CO_2 together with leached $Ca(OH)_2$ from the dam, often form calcite curtains at the downstream faces and thereby the permeability is somewhat reduced at the surface. The concrete specimens used in this work have no contact with atmospheric CO_2. Compared to dams with surfaces in contact atmospheric air the test method is therefore to same degree accelerated.

6. The temperature was constantly 20°C

In real concrete dams, the temperature differs depended on the size of the dams and the location in the dam. At the upstream face, the temperature is the same as the water temperature, somewhere between 4 to 10°C. At the downstream face, the temperature follows the air temperature, or the water temperature if below water surface. The air temperature may differ much during the year. The thicker the dam is, the more influence will the ground temperature have on the interior temperature of the dam. Inside the dam, the temperature varies between the temperature of the upstream face, the ground and the downstream face. Any temperature changes at these faces only slowly influence the interior. Most probably the interior temperature is about 5 to 10°C during most of the year. When the temperature in thinner dams changes, the concrete may expand or shrink, and the resulting tensions can cause cracking in the concrete.

The test equipment was placed in a room with the constant temperature +20°C. Solubility of solid material in concrete differs with the temperature. For calcium hydroxide, $Ca(OH)_2$, the most important constituent regarding leaching, the solubility increases with lower temperature. Due to the rather high temperature in the experiment compared to real dams and due to the fact that the temperature was constant during test, the test method must be said to somewhat retarded.

7. Loads

In real dams there are stresses due to external or internal forces. These stresses may lead to cracks and a higher permeability. If the stresses vary in intensity, the cracks also vary and any possible self-healing may be hindered.

The present specimens were supported at the circumference. The water pressure forces the specimens down and outwards due to the conical shape of the specimen and the steel cylinder in which the specimen is mounted. The water pressure cause bending moment and normal stresses in the specimens. In our experiments the stresses were always constant.

8. Synergy between degradation mechanisms

In reality, there are many other degradation mechanisms acting simultaneously (e.g. leaching, freeze-thawing, erosion). Frost damage can cause substantial cracking in concrete and the

permeability is of course increased in such a case. No other degradation mechanisms than leaching were exposed on our experiments.

9. Cast direction

In the test specimens, the water flow direction during the leaching test was in the same direction as the cast direction. The upstream face was the same as the top face during casting. In real dams the cast direction often is perpendicular to the water flow direction.

10. End effects

There may be an end effect when pressing water through a specimen, which made short specimens less permeable per unit length than longer specimens (Ruettgers et al (1935) p. 408).

11. Summary of validity

The experiment was accelerated regarding; (i) the high water pressure, (ii) the high water to cement ratio, (iii) the aggressive water.

5.4 Reliability of the tests

5.4.1 Introduction

The reliability of a test depends on the accuracy of used test methods. It is quantified with variation coefficients from a large amount of test results. Low variations coefficients imply a good reliability of the test method. Any source of errors shall be regarded in estimating the reliability. The reliability can be divided in:

- ✓ *Repeatability*: The variation in test results when the test is repeated for the same material batch, by the same test equipment and by the same test personnel.
- ✓ *Reproducibility*: The variation in test results when the test is repeated for the same batch of material, but in another laboratory by other test equipment and other test personnel.

In this report, only repeatability is regarded. The reproducibility for this test method has not been checked in another laboratory. The reliability of the whole test depends on the reliabilities of the different test methods used for determining leaching and permeability.

5.4.2 Permeability analysis

In the following, different parameters influencing reliability are treated.

1. Undesired water leakage

Any possible leakage of water between the concrete specimen and the steel cylinder and not through the concrete specimen will give wrong results. If there is evaporation from the measuring vessels, it will also give wrong results.

(i) Water leakage between specimen and steel cylinder:

The very uniform water flows in the experiments indicate that all or almost all water volume permeates through the concrete and not trough the boundary between the specimen and the cell wall. If water had flown through the boundary, it should probably not have been so uniform. The silicon grease that was used at the boundary should in case of leakage probably have been eroded and the water flow should have increased with time. In many cases there was an increased water flow, but in these cases distinct *flow pipes* through the concrete specimens were always observed. No sign of increased water flow through the slot between the specimen and steel cylinder was ever observed. When dismantled, no concrete specimens showed any sign of

corrosion on the surface that had been placed against the steel cylinder. The surface was smooth and there was no visible sign of leaching of the surface, even for the specimens that have had very much water flowing through them.

In order to test the tightness of the boundary between the specimen and the cell wall, the top surface of one concrete specimen and its side was covered by a tight latex "foil". No water flow was observed indicating that the boundary was completely tight.

(ii) Evaporation from measuring vessels:

If the collected water evaporates, the measured water flow would give too small values and the measured contents of dissolved ions may give too high values. If CO_2 comes into the collected water, the carbon dioxide will react with the dissolved calcium in the water and calcite will be produced and the pH value will sink. The later examination of the Ca^{2+} and pH will in such a case give wrong results. So, it is important that there is a diffuse tight layer between the air and the vessel that collect the water. For tight specimens with low flow of water, this is especially important.

The soft plastic tube leading collected water from the test cells to the byretts was made as short as possible. When byretts were used as measuring vessels, a rubber plug and a rubber balloon was placed on the top of byrett to prevent moisture diffusion to the air and CO_2 diffusion from the air.

The specimens with measuring glass as measuring vessels had the same short soft plastic tube and rubber balloon in the top.

The very permeable specimens that had plastic drum to collect the drainage water had a longer soft plastic tube from test cells to the drums, about 0.5m. But in this case, with high water flow, moisture evaporation or CO_2-dissolving in the water was not so important as with the other specimens.

Permeability tests on the rubber plug-balloon used for the byretts, and on the balloon used for measuring glass was performed. The result points to a nearly insignificant leakage. The largest measured evaporation together with the smallest measured drainage water flow has a ratio of 1 to 30. In such a case the measured drainage water flow was in the reality about 1/30=3.3% larger and the measured ion content in the drainage water was about 3.3% less in the reality. The result can be seen in appendix 5-2.

2. Water pressure.

When byretts were used as measuring vessels, the water level in the byretts was sensitive to the applied water pressure. If the pressure had risen above the decided level, the water level in the byrett showed a little to high level. The pressure was checked every time a measurement of the flow was made.

3. Decrease in flow area.

When the specimens were taken out from the test cell after the test was stopped, it could be seen that in some cases *the latex tube* around the concrete had been pressed out 1-2 cm on the top and bottom end of the specimen. However, the out-pressed tube was so loose that the flow area had not decreased.

4. Carbonation

It is always a risk that atmospheric *carbon dioxide* CO_2 will come in contact with calcium hydroxide in the concrete, either via the water inlet side or via the water outlet side, causing carbonation. If the concrete is carbonated, the permeability will probably decrease. Also the

drainage water in the outlet side can be carbonated if CO_2 leaks into the measuring vessel. If the drainage water become carbonated, the content of ions and the pH value will be too low.

(i) Water at the inlet side:

Some CO_2 from the atmosphere have probably been dissolved in the water of the storage tank. It is not easy to say how the permeability will be influenced by the CO_2 in the inlet water. In chapter 5.3, it was estimated that about 0.31 mg/l of atmospheric CO_2 dissolves in water at ordinary partial pressure. This 0.31 mg CO_2 means that $0.31 \cdot 10^{-3}$ g/44 g/mole = $7.0 \cdot 10^{-6}$ mole H_2CO_3 is formed in each litre water according to equation (2-8).

With CO_2 in contact with the pore solution, possible reactions are:

$H_2O + CO_2 \leftrightarrow H_2CO_3$ carbon acid is formed (2-8)

$2H_2CO_3 + Ca(OH)_2 \leftrightarrow Ca(HCO_3)_2 + 2H_2O$ calcium hydroxide is dissolved (2-9)

$Ca(HCO)_2 + Ca(OH)_2 \leftrightarrow 2CaCO_3 + 2H_2O$ calcium carbonate is formed (2-10)

$CaCO_3 + H_2CO_3 \leftrightarrow Ca(HCO_3)_2$ calcium carbonate is dissolved (2-11)

As can be seen in equation (2-9), one mole of H_2CO_3 may dissolve ½ mole of $Ca(OH)_2$ and produce ½ mole of $Ca(HCO_3)_2$. The ½ mole of calcium bicarbonate produced may flow out of the concrete by convection or diffusion or it will react with one mole $Ca(OH)_2$ and form one mole of $CaCO_3$ (equation 2-10).

Later, perhaps more, H_2CO_3, will reach this $CaCO_3$, dissolve this and then perhaps flow through and out of the concrete, equation (2-11). If only $Ca(OH)_2$ is leached, the capillary porosity and the permeability may increase. But if also $CaCO_3$ is formed, the permeability may decrease again.

Example

An example of the influence on the permeability if reaction equations (2-9) and (2-10) happen is given for specimen 3, experiment 2 (dried w/c 0.8).

At the end of the leaching test, 12 litre of water had penetrated through the specimen 3. The dimension of the specimen was $V_{specimen} = \pi * 0.155^2/4 * 0.050 = 9.4 \cdot 10^{-4}$ m^3. The capillary pore volume for of the specimen is assumed as $V_{cap} = (w/c - 0.39\alpha) * C/1000 * V_{specimen} = (0.8 - 0.39 * \alpha) * 245/1000 * 9.4 \cdot 10^{-4} = 0.110$ m^3/m^3* $9.4 \cdot 10^{-4}$ m^3 = $1.0 \cdot 10^{-4}$ m^3.

The molar weight for $Ca(OH)_2$ and $CaCO_3$ is $74.08 \cdot 10^{-3}$ and 100.08 kg/mole respectively. The density for $Ca(OH)_2$ and $CaCO_3$ is 2300 and 2700 kg/m^3 respectively.

If only equation (2-9) happens, the volume of dissolved calcium hydroxide will approximately be:

$$V_{Ca(OH)2,leach} = n_{Ca(OH)2} \cdot M_{Ca(OH)2} / \rho_{Ca(OH)2} \cdot V_w = ½ * 7 \cdot 10^{-6} \cdot 74.08 \cdot 10^{-3} / 2300 \cdot 12 = 13.6 \cdot 10^{-10} \text{ m}^3$$

The calcium bicarbonate formed may flow out of the concrete by convection or diffusion or it will react with more $Ca(OH)_2$ and form $CaCO_3$. If this happens, equation (2-10), and no backward reaction happens, the volume of formed calcium carbonate will approximately be:

$$V_{CaCO3,leach} = n_{CaCO3} \cdot M_{CaCO3} / \rho_{CaCO3} \cdot V_w = 7 \cdot 10^{-6} \cdot 100.08 \cdot 10^{-3} / 2700 \cdot 12 = 31.1 \cdot 10^{-10} \text{ m}^3$$

Both the capillary volume increases due to leaching of $Ca(OH)_2$ and capillary volume decreases due to crystallisation of $CaCO_3$ as the theoretical example shows above, is insignificant little compared to the capillary volume of $9.4 \cdot 10^{-4}$ (m^3) and can not influence the permeability.

However, if the water has percolated through only a few main flow pipes, there may be a significant increase in permeability. Let us hypothetically assume hundred flow pipes with an

initial diameter of 0.1 mm which make the volume of these pipes to $V_{100\ pipes} = 100 \cdot \pi \cdot (10^{-4})^2/4 * 0.05 = 393 \cdot 10^{-10}$ m^3. If the water only have leached away $Ca(OH)_2$ due to equation (2-9), the diameters of the hundred pipes may have increased to $(4 \cdot (13.6+393) \cdot 10^{-10}/(100 \cdot \pi \cdot 0.05) - (10^{-4})^2)^{0.5} = 0.14 \cdot 10^{-3}$ m (see equation 3-3) and with Hagen-Poisuilles law, the permeability may increase $(0.14/0.1)^4 = 4$ times. So, if there are very few flow pipes, the permeability can be influenced. With the same discussion, formed $CaCO_3$ may decrease the permeability significantly, if only a few flow-pipes is regarded.

(ii) At the outlet side, the drainage water is in contact with the concrete all the time. The vessels in which, the drainage water is stored in, are sealed from the atmospheric CO_2 by balloons. When the balloons were removed to empty the vessel, some CO_2 came in contact with the drainage water, but the emptying is too fast for any significant amount of CO_2 to be dissolved. However, when the vessels are emptied some CO_2 is trapped inside the vessel.

Assuming a trapped volume of 1 litre, a total pressure of 1 atm, 25 °C and a partial pressure of CO_2 to $3 \cdot 10^{-4}$ atm, (Atkins & Jones 1997 p. 535):

$$n = PV/(RT) = 3 \cdot 10^{-4} * 1/(8.206 \cdot 10^{-2} * 293) = 12 \cdot 10^{-6} \text{ mole} \quad (5\text{-}8)$$

Where	n	Number of CO_2 molecules (mole)
	P	Partial pressure of CO_2 (atm)
	V	Volume of trapped air (litre)
	R	Gas constant
	T	Temperature (K)

According to equation (2-8) to (2-9), this amount of CO(aq) can carbonate about $0.5 \cdot 12 \cdot 10^{-6} = 6 \cdot 10^{-6}$ mole Ca(OH)(aq) to $CaCO_3$. However, in one litre drainage water there is about $15 \cdot 10^{-3}$ mole $Ca(OH)_2$, so the drainage water will act as a big buffer that trap any CO_2 before it reach the concrete. Any leakage of CO_2 in to the outlet side is therefore assumed not to influence the permeability.

5. *Effect of* air-filled pores *in the concrete*

Some of the concrete specimens were not saturated when the test started, by the vacuum saturation method described in paragraph 6.7. However, they had been stored in a water tank all the time, so they were probably almost completely saturated. From the air measurement of the concrete when it was cast, the air content was typically about 0.6- 1.3 % of the volume of the concrete. For the specimens with the dimensions of ϕ 155 mm * 50 mm, this means that there was about 1.0%*0.155^2*pi/4*0.055 = 9.4 ml air for each specimen. During the experiment, air bubbles were sometimes observed when escaping to the water surface in the outlet water. This could mean that not all air had been removed before the test started. However, the water flow during the test was very uniform, indicating that the air bubbles had already been saturated in the water storage stage before the test started.

6. *Effect of air in the inlet water*

Air bubbles released in the concrete specimen due to the gradually lower water pressure in the specimen from the top to the bottom may decrease the permeability. However, the water used for the test was in contact only with air under ordinary atmospheric pressure. The water pressure was risen from the atmospheric pressure by a pump and again released to the atmospheric pressure when the water flowed through the concrete specimen. So, there shall not

be any decrease in the permeability due to released air bubbles inside the concrete specimen, because the pressure never drops below the pressure where the air first was dissolved, 1.0 atm.

7. Swelling of the concrete

Swelling of the concrete specimens occurs when it is resaturated after drying. The specimens were probably almost completely saturated when the test started and therefore swelling can be neglected.

8. Dissolution and deposition of dissolved substances

Dissolution and deposition of soluble species might occur along the flow path. Any solid material that is dissolved and carried away from its location by the water, increases the local permeability. If the dissolved material is deposited in any other place, the permeability will decrease in that place. It is hard to say what the resulting change in the global permeability of the specimen will be. Since the solubility of the species in the specimen is not pressure dependent, since the temperature was not changed through the specimen or during the time, since the whole specimen was saturated with water, since the concrete was not carbonated and since no other property, that influences the solubility was changed, there was probably no deposition of already dissolved material. So, with only dissolution and no deposition of material, this must mean that the permeability was increased.

9. Stresses in the specimen.

As mentioned in chapter 5.3, bending moment and supporting tension at the circumference against the steel cylinder, can perhaps change the permeability.
The bending moment in the ϕ155 (mm) circular specimen exposed to 6 bar water pressure is:

$$M = \frac{qr^2(3+\nu)}{16} = 600\ \text{kN/m}^2 * 0.0775^2\ \text{m}^2 * (3+0.2)/16 = 0.72\ \text{kNm/m}$$

The stress due to this moment is:

$\sigma_M = \pm$ M*6/W = ± 0.72 kNm/m*6/(1 m*0.05^2 m^2) = ± 1730 (kPa)

The normal stress in the specimen due to the supporting force at the circumference is (see figure 5-4):

σ_N = q*upstream face area/(tan θ*circumference area) =
600kN/m^2*π*0.155^2/4m^2/(8.3/50*π*0.155*0.05) = 2790 kPa

where	M	Bending moment (kNm/m)
	q	Water pressure (kPa)
	r	Radius (m)
	ν	Poisson's ratio
	W	Bending resistance (m^3)
	σ_N	Normal stress (kPa)

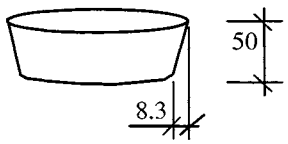

Figure 5-4 The conical shape of the specimens.

The total normal stress σ in upstream face is:

$\sigma = \sigma_M + \sigma_N = +1730 + 2790 = +4520$ kPa (compressive stress)

The total normal stress in downstream face is:

$\sigma = \sigma_M + \sigma_N = -1730 + 2790 = +1060$ kPa (compressive stress)

If a elasticity modulus of about 30 GPa is assumed, the strain ε_c of the whole concrete specimen is:

$\varepsilon_c = \Delta V/V_c = \sigma/E = 4520 \cdot 10^3$ Pa$/30 \cdot 10^9$ Pa $= 0.15 \cdot 10^{-3}$

If only the capillary pores in the cement paste, $(V_{cap})_p$ are assumed to be compressed, the initially capillary pore volume will decrease as:

$\Delta V = \varepsilon_c \cdot V_c / (V_{cap})_p = \varepsilon_c \cdot 1000/(C \cdot (w/c - 0.39 \cdot \alpha))$

where	ε_c	Strain in the specimen (m^3/m^3)
	ΔV	Change in capillary volume due to normal stresses (m^3)
	V_c	Volume of the whole specimen (m^3)
	$(V_{cap})_p$	Capillary volume of the paste (m^3)
	w/c	Water to cement ratio
	C	Cement content (kg)
	α	Degree ofhydration

Example

For the w/c 0.8 specimen 3 in experiment 2 it is assumed: $\Delta V = 0.15 \cdot 10^{-3} \cdot 1000/(245 \cdot (0.8 - 0.39 \cdot 0.9)) = 1.36 \cdot 10^{-3} = 0.14$ % of the initial capillary pores, which is not much!

For the test cell types of ϕ 45 mm, the same value is about 0.03%.

As was also seen, both the upstream and the downstream side of the specimen was compressed, so no cracks may appear and therfore the permeability will not increase due to cracking.

10. Continued hydration of residual clinker.

The concrete specimens in experiment 1 (virgin w/c 0.8) were water cured for about 90 days before the leaching test started. The specimens in experiment 2 were water cured for 58 days (late-dried w/c 1.3) and 201 days (late-dried w/c 0.8), see chapter 4 and 6.

Probably the hydration ratio α was about 0.9 when the late-drying process or the leaching test started. In such high ratios not much cement was left for continued hydration.

The situation was probably different for the specimens in experiment 3. These specimens were air cured for about 60 days and had no access to outer free water, see chapter 4 and 6. Therefore, a considerable amount of unhydrated cement might have been left in the specimens when they were exposed to water pressure. The cement hydrated when water flowed through the specimen.

In conclusion, there was probably no hydration during the leaching test for specimens in experiment 1 and 2 but probably a marginal hydration in specimens in experiment 3.

11. Summary of reliability

The discussion performed above indicates that the reliability in the permeability test probably was quite high.

5.4.3 Chemical analysis of drainage water

1. Undesired water leakage

This has already been discussed in chapter 5.4.1. No significant amount of water leakage occurred, and therefore the measured content of ions in the leakage water must be assumed as quite reliable.

2. Contamination by alkalis in the inlet water

The water did not only leach ions from the concrete specimens downward due to convection. Ions also moved up-streams due to diffusion. After a while, especially if the water flow was small, the de-ionised water at the inlet side becomes saturated with dissolved ions and the water consequently becomes less aggressive to the concrete. This was solved by occasionally flushing out the water from the inlet side through the air-valve.

3. Carbonation.

CO_2 in the inlet or outlet water can may react with $Ca(OH)_2$ and form $CaCO_3$. This can influence the ion profile in the specimen if the specimen is studied by chemical analyses, see more in chapter 5.4.1 about carbonation.

CO_2 coming in from the outlet, into the drainage water can also influence the content of free Ca^{2+} and the pH value. There is typically a content of Ca^{2+} of 20 mg/l to 800 mg/l in the drainage water.

In the chapter 5.4.2 about Carbonation it was mentioned that dissolved CO_2 in the drainage water will react with approximately $140 \cdot 10^{-9}$ kg Ca^{2+}/l, or in other units 0.14 mg/l, to form $CaCO_3$. This is very little compared to the measured content of 20 mg/l to 800 mg/l. During the chemical investigation of the collected water, acetate acid was added, which decrease the pH to about 4.7, which probably released the Ca in $CaCO_3$ to free Ca^{2+}- So the CO_2 in the drainage water have probably not disturbed the measurement of Ca^{2+}.

The produced H_3O^+ ion from atmospheric CO_2 was discussed in chapter 5.3 Water aggressiveness to be about $1.6 \cdot 10^{-6}$ mole/l. If the pH value in the drainage water was typically about 12.5, without regard to the CO_2, then the pH is reduced to about $pH = 14 - \log(10^{-(14-12.5)} - 1.6 \cdot 10^{-6}) \approx \underline{12.5}$, i.e. the pH in the drainage water was not significantly reduced by atmospheric CO_2.

4. Measurement of ions in the drainage water

The error due to different ion strength is with the Güntelberg equation and table 5-2 and 5-3:

$$\text{Error} = \frac{\left(\frac{m}{\alpha}\right)^{test\ sample}}{\left(\frac{m}{\alpha}\right)^{standard}} = \frac{\left(\frac{m}{\gamma \cdot m}\right)^{test\ sample}}{\left(\frac{m}{\gamma \cdot m}\right)^{standard}} = \frac{(\gamma)^{test\ sample}}{(\gamma)^{standard}} = \frac{10^{-\frac{A \cdot z^2 \sqrt{I_{test\ sample}}}{1+\sqrt{I_{test\ sample}}}}}{10^{-\frac{A \cdot z^2 \sqrt{I_{standard}}}{1+\sqrt{I_{standard}}}}} \qquad (5\text{-}9)$$

$$I = 0.5 \cdot \Sigma z^2 \cdot m. \qquad (5\text{-}10)$$

$$-\log \gamma = 0.585 \cdot z^2 \cdot \sqrt{I}/(1+\sqrt{I}) \qquad \text{(the Güntelberg equation)} \qquad (5\text{-}11)$$

Where Error — Error due to different ion strength
m — Molarity (mole/l)

α	Chemical activity (mole/l)
γ	Activity coefficient
I	Ionic strength
z	Valence of the ion

$$\text{Error} = \frac{10^{-\frac{0.585 \cdot 2^2 \cdot \sqrt{0.097}}{1+\sqrt{0.097}}}}{10^{-\frac{0.585 \cdot 2^2 \cdot \sqrt{0.098}}{1+\sqrt{0.098}}}} = 1.0055, \text{ i.e. } 0.55\ \%, \text{ no matter the measured contents.}$$

Where 0.097 and 0.098 is the ion strength in the standards and the test sample respectively. The error is 0.55%, which is not large. Only type of ion matter in the calculation. If the measured concentration of Ca^{2+} in table 5-3 decreases to 0.6 g/l, the error become: Error=0.60%

So, the error changes from 0.55% to 0.60% for changes in concentration of Ca^{2+} from 0.7 to 0.6 (mole/l), which is not much. The measuring seems not to be so sensitive for different ion content in the test water sample.

Table 5-2 Ionic strength for standards with 40 ml 0.1 M NaCl, 0.4 ml 0.01 M CaCl and 0.4 ml 0.1 M Acetate buffer. ($[Ca^{2+}]$=3.9mg/l/40080mg/mole = $9.8 \cdot 10^{-5}$).

	Ca^{2+}	H^+	OH^-	Na^+	Cl^-	**ion strength**
real molarity m (mol/l)	9,80E-05	1,58E-05	6,31E-10	9,80E-02	9,81E-02	
charge z	2	1	1	1	1	**0,098**
activity coefficient γ_i	0,327	0,756	0,756	0,756	0,756	
activity α (mol/l)	3,21E-05	1,20E-05	4,77E-10	7,41E-02	7,42E-02	

Table 5-3 Ionic strength for a typical test sample with 20 ml 0.1 M NaCl, 0.4 ml collected water sample and 0.4 ml Acetate buffer.

	Ca^{2+}	H^+	OH^-	Na^+	Cl^-	K^+	$(SO_4)^{2-}$	Al^{3+}	**ion strength**
Known added content (mol/l)				0,1	0,1				
Measured content in a typical collected sample (g/l)	0,7			0,13		0,475	0,012	0,001	
atom weight (g/mol)	40,08	1	17	22,99		39,1	32,07	26,98	
measured molarity m (mol/l)	3,36E-04	1,58E-05	6,31E-10	9,63E-02	9,62E-02	2,34E-04	7,20E-06	7,13E-07	
charge z	2	1	1	1	1	1	2	3	**0,0970**
activity coefficient γ_i	0,329	0,757	0,757	0,757	0,757	0,757	0,329	0,082	
real molarity (mol/l)	1,02E-03	2,09E-05	8,33E-10	1,27E-01	1,27E-01	3,09E-04	2,19E-05	8,71E-06	

The error for interfering ions can be calculated as Kriz (1991):

$$\text{Error} = \frac{-\log([A^{n+}] + K_{A,B}[B^{m+}]^{n/m}) + \log[A^{n+}]}{-\log[A^{n+}]} * 100\% \qquad (5\text{-}12)$$

where

A	Studied ion with its charge n.
B	Interfering ion with its charge m.
$K_{A,B}$	Interfering ions selectivity constant.

For the standards in table 5-2: [A] = $9.8 \cdot 10^{-5}$ Ca^{2+}, [B] = $9.8 \cdot 10^{-2}$ Na^{+} and $K_{A,B}$ = 0.003 Kriz (1991) and the error = -2.6 %. But the content in the standard is known, so the value set is the right one.

For the test sample in table 5-3, the ion concentrations is [A] = $3.4 \cdot 10^{-4}$ Ca^{2+}, [B] = $9.6 \cdot 10^{-2}$ Na^{+} and $K_{A,B}$ = 0.003 and the error is -0.9 %.

When calibrating by the standard, a volume of about 0.9 % (0.0-0.9) to low is obtained for the test sample.

A comparison with ICP AES was also permformed. The deviation when measuring with the electrodes was usually about +/- 0-10 % (sometimes about 20 %) compared to measuring by ICP AES. The error with ICP AES is normally within the range +/- 5 % according to the test centre at the Plant ecology at Lund University.

5.4.4 Chemical analysis in concrete

Only specimen 3 in experiment 2 was examined with regard to the chemical content which is too few.

Dissolving the leached concrete in HNO_3 as described in chapter 5.2.4 also might have caused certain dissolution of the aggregate. Determining the solubility of the pure aggregate compensated for this error.

5.4.5 Porosity analysis

Only specimen 3 in experiment 2 was examined with regard to porosity. For porosity studies it is important to examine such large pieces so the influence from unrepresentative sample due to the aggregate can be neglected.

For the total porosity study, one half of the specimen (about 100 cm^2) and one quarter (about 50 cm^2) were examined. These two parts were sliced in 5+5 slices of about 7 mm thickness. These 10 slices were examined, see chapter 5.2.5. Only one specimen is too small for a statistically safe. On the other hand, the total area of the slices from this separate specimen was large enough to get a good reliability for this specimen.

5.4.6 Mechanical properties

The compression tests were made on rather few specimens. Therefore the test are probably not totally statistically significant. The size of the samples was also much smaller then for common standard tests. But the intention was only to compare leached concrete with un-leached concrete of the same size, the same recipe, and that was cast and cured in the same way. However, larger amount of samples ought to be tested in the future to get higher statistical precision.

6 CONCRETE

6.1 Introduction

The concrete specimens used were of two types, *leaching specimens* and *reference specimens*, see chapter 4 for an overview. The leaching specimens were exposed to a water pressure gradient. The reference specimens lay in stagnant water without any water pressure. The leaching specimens were produced from rather normal concrete used for hydraulic structures. However, unusually high w/c ratios were used to get permeable concrete.

6.2 Cement

A low alkali, sulphate resistance Portland cement with moderate heat of hydration ("Degerhamn anläggningscement) of the type CEM I 42,5 was used for all three experiments, see table 6-1.

Table 6-1 Chemical composition of cement.

Cement	Oxides %									Clinker minerals			
Type	CaO	SiO_2	Al_2O_3	Fe_2O_3	K_2O	Na_2O	MgO	SO_3	Cl	C_3S	C_2S	C_3A	C_4AF
Experiment 1 and 2 Analysed by CEMENTA Period 970101-971231	65.5	22.7	3.56	4.32	0.57	0.05	0.45	2.07	0.02	55.7	22.8	2.1	13.1
Experiment 3 Analysed by CEMENTA Period 980101-981231	65.4	22.7	3.5	4.2	0.6	0.1	0.7	2.1	0.0	57.3	21.8	2.1	13

6.3 Admixtures and additives

No admixtures or additives were used.

6.4 Aggregate

The sieve curves for the different aggregate fractions used are shown in figure 1 in Appendix 6.

Due to the suppliers, the compact density of the aggregate is:

- ✓ *Hardeberga quartzite* 2630-2640 (kg/m^3).
- ✓ *Åstorp sand* 2550 (kg/m^3)

Both types of aggregate are non-porous. This leads to the same bulk density as the compact density. The size distribution of the aggregate used in the different concrete recipes is shown in figures 6-1 and 6-2. Two limiting size distributions curves for good workability and thereby good homogeneity are also shown in the figures. Generally, it can be said that the smaller size and the smoother the size distribution of the aggregate, the more watertight will the concrete be. The gradation curves used are quite normal for Swedish concrete. No optimum curve with regard to impermeability was searched for.

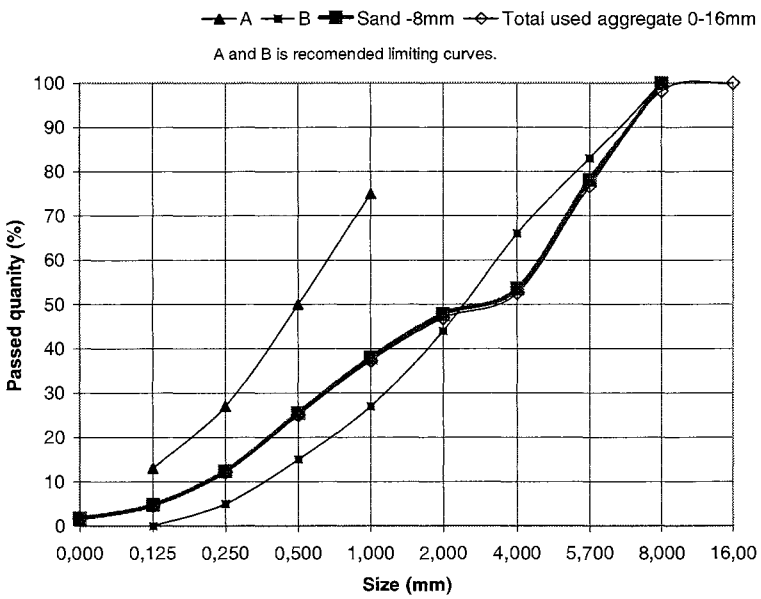

Figure 6-1 Size distribution for sand 0-8 mm and the total aggregate 0-16 mm for experiment 1 and 2.

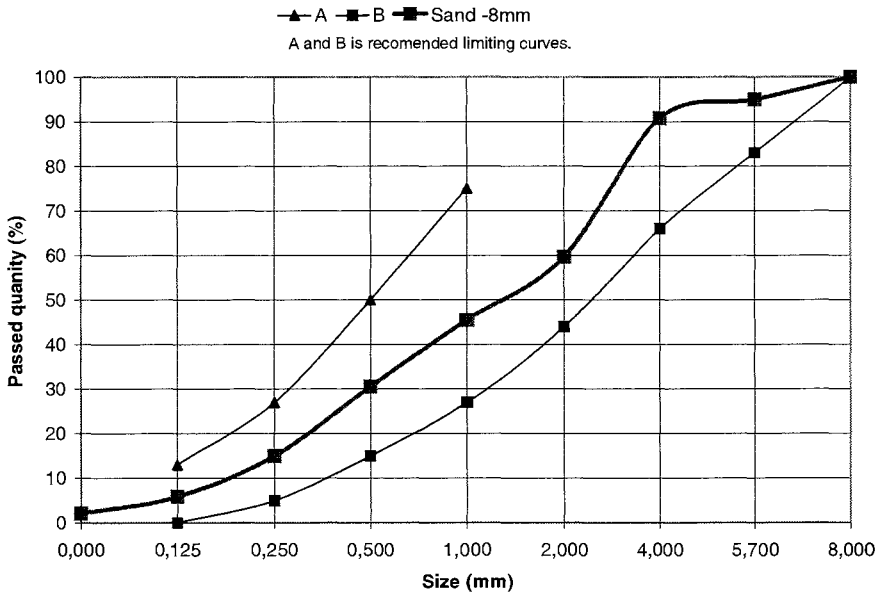

Figure 6-2 Size distribution for sand 0-8 mm for experiment 3.

6.5 Mixing and curing water

Ordinary municipal tap water was used both as mixing water and curing water.

6.6 Recipes

The recipes for the different types of concrete that were used are shown in tables 1 to 5 in appendix 6.

6.7 Casting

The concrete was mixed in an ordinary laboratory concrete mixer. Cement and aggregate were mixed first for about 3 minutes. Then water was added and the mixing continued for about 3 minutes more.

For the leaching specimens, the concrete was cast in steel cylinders (figure 6-3) placed on fibreboard and vibrated on a vibrating table for approximately 15-20 seconds. The steel cylinders were the same cylinders as were used later in the leaching test. The thickness of the specimen was adjusted for the correct value using a piece of wood.

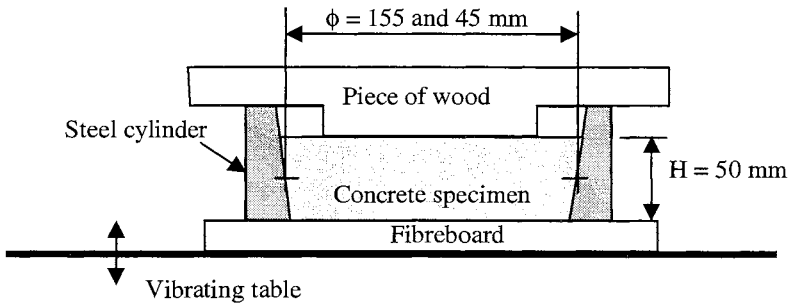

Figure 6-3 Casting of the leaching specimens.

The reference specimens were cast in 300 mm long steel tubes with diameter 150 mm. The concrete cylinders were later cut in 50 mm slices.

After about 24 hours in plastic bags, all the specimens and cylinders were unmolded.

6.8 Curing

The experimental specimens were divided in three groups:

- ✓ Experiment 1 was a feasibility study to see if the test equipment worked and to see which concrete quality to use. The concrete quality was *virgin* (undried) w/c 0.8 concrete.
- ✓ Experiment 2 was an outcome of experiment 1 and included specimens with much higher permeability. Virgin concrete with w/c 0.8 and 1.3 were used together with *late-dried* specimens with the same w/c ratios.
- ✓ Experiment 3 was an attempt to use a more normal curing, *early-heating,* and to study the lower w/c ratio of 0.6.

A more precise specification over the casting and curing conditions are shown in tables 6 to 9 in appendix 6. See also chapter 4 for an overview.

After the pressure and reference specimens were unmolded, they were either put in a water storage tank (experiment 1 and experiment 2) or put in plastic bags and in an oven (experiment 3). The specimens, which went to the water storage tank, were later, either put in the pressure

cells (virgin specimens) or dried in an oven (late-dried specimens). The specimens that were dried were water saturated by vacuum treatment followed by water absorption before they were mounted in the pressure cells.

The specimens that were put in oven directly after unmolding (experiment 3), were stored in the same plastic bags in room temperature until they were exposed to water pressure. Before the specimens were mounted in the pressure cells, they were water saturated by vacuum treatment followed by water absorption. The virgin (never-dried) specimens were assumed to be water saturated without vacuum treatment.

The curing water was saturated with lime to prevent any leaching of lime from the specimens during the curing.

7 RESULTS OF EXPERIMENTAL WORKS

7.1 Permeability

All results from the leaching test regarding water flow permeability are shown in Appendix 7. A summary is shown below in figures 7-1 to 7-7.

Generally, the water flow was different for different concrete qualities (w/c 0.6, 0.8 and 1.3) and for different curing histories (virgin, early-heated and late-dried).

- ✓ Virgin = never dried concrete, see a short description in chapter 4 and 6.7.
- ✓ Early-heated = heated in oven directly after un-molding, see chapter 4 and 6.7.
- ✓ Late-dried = virgin specimens that was dried after 6.5 months, see chapter 4 and 6.7.

The results show three different water flow pattern; a constant water flow, an accelerating water flow or a retarding water flow. Observe that the last observed flow of water for each specimen in the figures, is no final water flow, but the water flow at just that time when respective specimen were taken out of the pressure cell.

Below a summary is made of the observed effect of w/c-ratio and pre-curing history, see also figure 7-7 for an schematic over-view.

The water flow for the specimens with **virgin w/c 0.8** (figure 7-1 and specimens 2 and 5 in figure 7-2) was constant of about 10^{-11} m^3/s. However, one of the specimens had an increased water flow of 100 times after some time, to about 10^{-9} m^3/s.

The water flow for the specimens with **late-dried w/c 0.8** (specimens 1, 3 and 4 in figure 7-2) was constant of about 10^{-9} m^3/s, which is approximately 100 times larger compared to the virgin state. However, one of the specimens had a further increased water flow of 100 times after some time, to about 10^{-7} m^3/s

The water flow for the specimens with **virgin w/c 1.3** (specimens 10 in figure 7-2) was initially constant of about 10^{-9} m^3/s for the one tested specimen, which is 100 times higher than virgin concrete with w/c 0.8. Later the flow increased 100 times to about 10^{-7} m^3/s.

The water flow for the specimens with **late-dried w/c 1.3** (specimens 6-8 in figure 7-2) was constant of about 10^{-8} m^3/s, which is approximately 10 times larger compared to the virgin state. Later, the water flows for all these specimens increased about 100 times to about 10^{-6} m^3/s.

The water flow for the specimens with **early-heated w/c 0.6** was initially about 0.5 to 1.0 10^{-9} m^3/s for the specimens with a diameter of 150 mm (specimens 1, 5-7 in figure 7-3), but rather fast it decreased 10 times down to about 10^{-10} m^3/s. After 12 000 hours, the water flow had decreased about 100 times to 10^{-11} m^3/s. The specimens with a diameter of 45 mm (specimens 20-30 in figure 7-4) had the same development, but only 30% of the flow of the larger specimens, if converted to the same diameter.

The water flow for the specimens with **early-heated w/c 0.8** was initially about 0.5 to 1.0 10^{-9} m^3/s for the specimens with a diameter of 150 mm (specimens 1, 5-7 in figure 7-3), but rather fast it decreased 10 times down to about 10^{-10} m^3/s. After 12 000 hours, the water flow had decreased about 100 times to 10^{-11} m^3/s. The specimens with a diameter of 45 mm (specimens 31-36 in figure 7-5) had the same development, but only 50% of the flow of the larger specimens, if converted to the same diameter.

Thus, the water permeability differed by about 100 000 times from the lowest initially water flow value of virgin concrete with w/c ratio of 0.8, to the highest flow after about 30 days in the late-dried concrete with w/c ratio of 1.3.

The early-heated concrete had permeability that was about 50 times higher compared to the virgin concrete, but after some time it was reduced to about 5 times as high as the virgin concrete, probably by self-healing.

When the water flows increased for some concrete specimens, they were dismantled to see if there were any visual changes. At the upstream face of the concrete specimens, small brown

areas were always observed. The brown areas consisted of compounds containing Al, Fe, Si and some Ca, probably residual parts of leached C-S-H and AF phases. In the centre of the brown areas, small pipes leading into the concrete were observed. Probably these holes were the so-called main *flow pipes,* in which the main water flows had occurred.

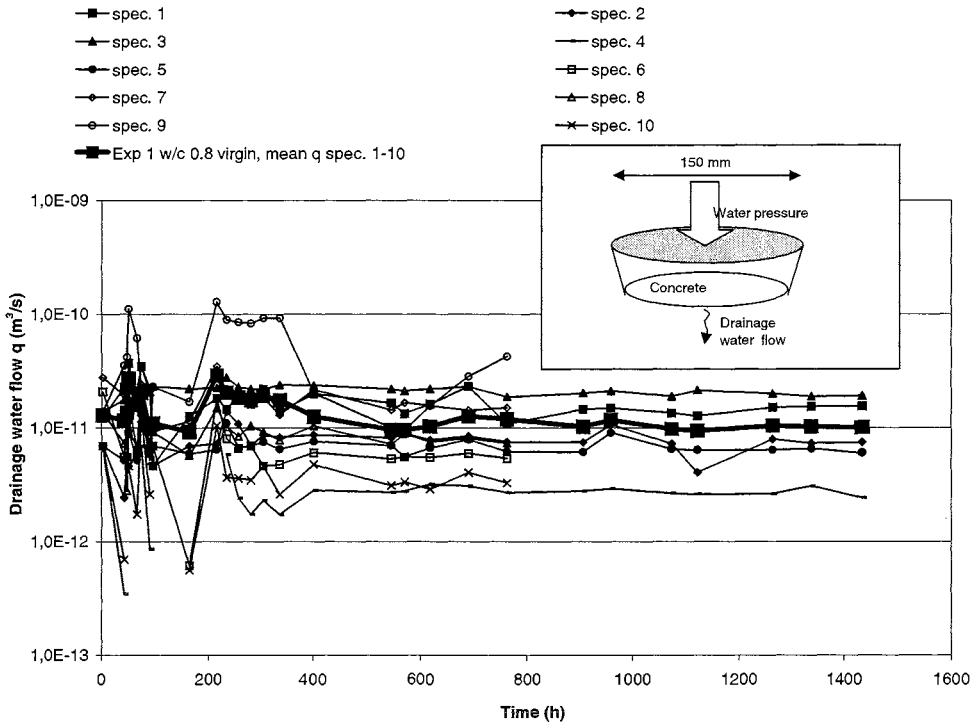

Figure 7-1 Water flow in experiment 1: virgin concrete w/c 0.8 (spec. 1-10). The mean flow for the same specimens is also

given.

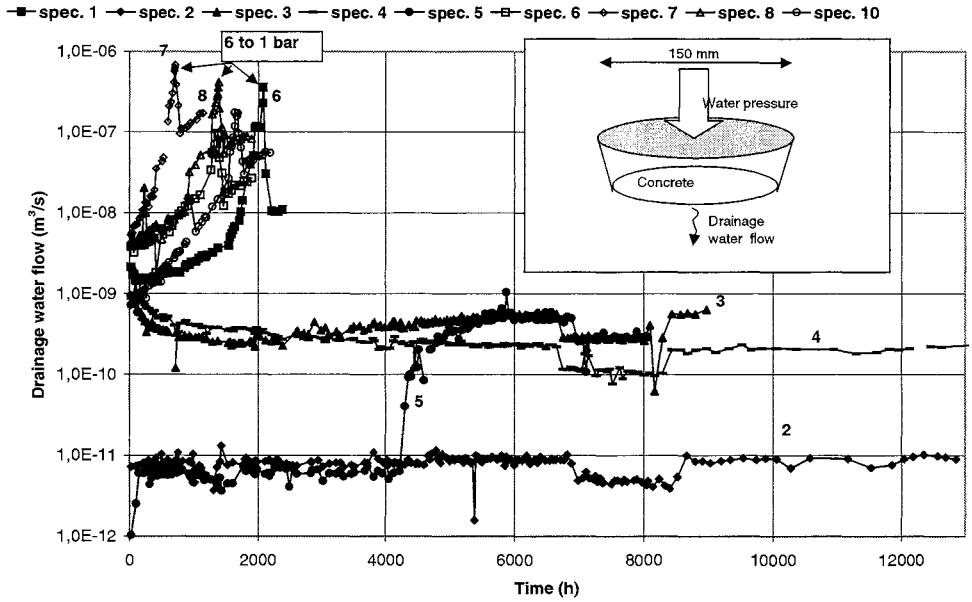

Figure 7-2 Water flow in experiment 2: virgin concrete w/c 0.8 (spec. 2 and 5), late-dried w/c 0.8 (spec. 1,3 and 4), virgin w/c 1.3 (spec. 10) and late-dried w/c 1.3 (spec. 6-8). Observe that the water pressure for specimens 1, 6-8 and 10 was reduced from 6 to 1 bar because of large water volumes.

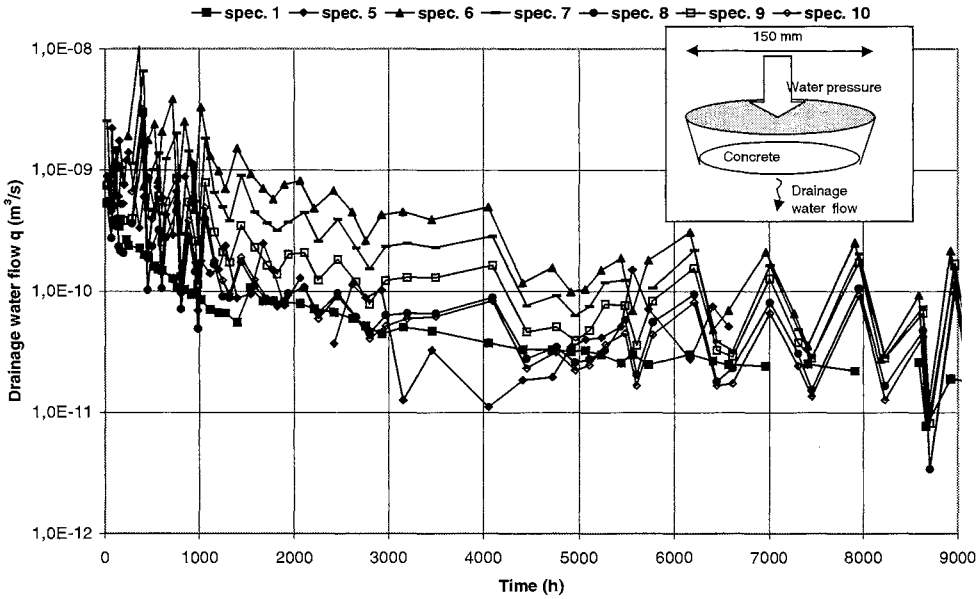

Figure 7-3 Water flow in experiment 3: early-heated concrete w/c 0.6 (spec. 1, 5-7), early-heated w/c 0.8 (spec. 8-10).

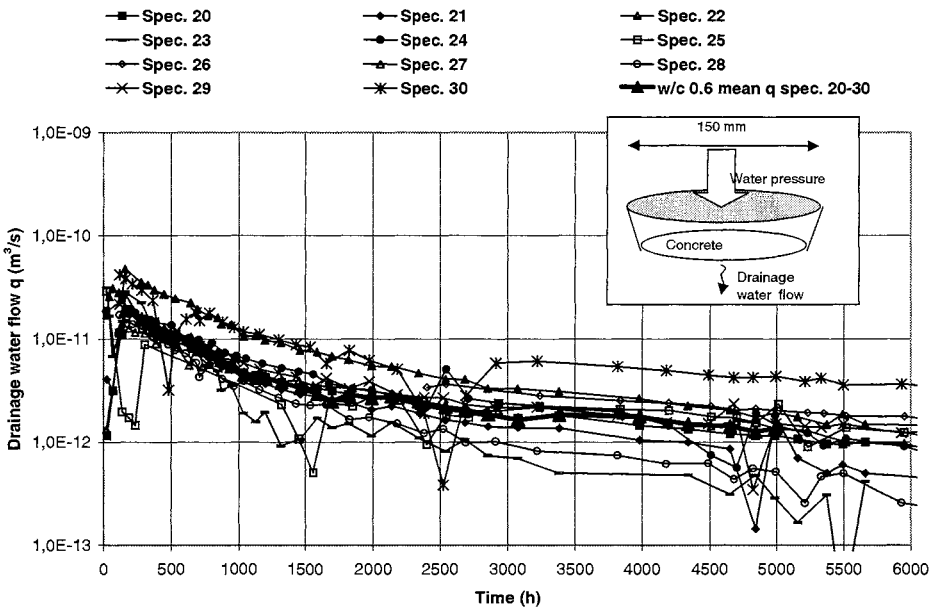

Figure 7-4 Water flow in experiment 3: early-heated concrete w/c 0.6 (spec. 20-30). The mean flow for the same specimens is also given.

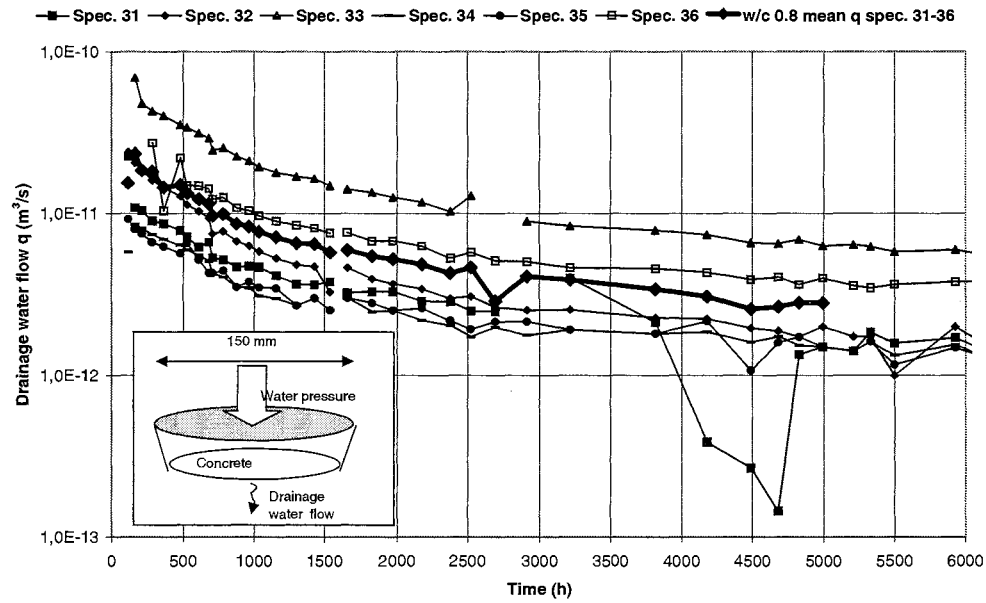

Figure 7-5 Water flow in experiment 3: early-heated concrete w/c 0.8 (spec. 31-36). The mean flow for the same specimens is also given.

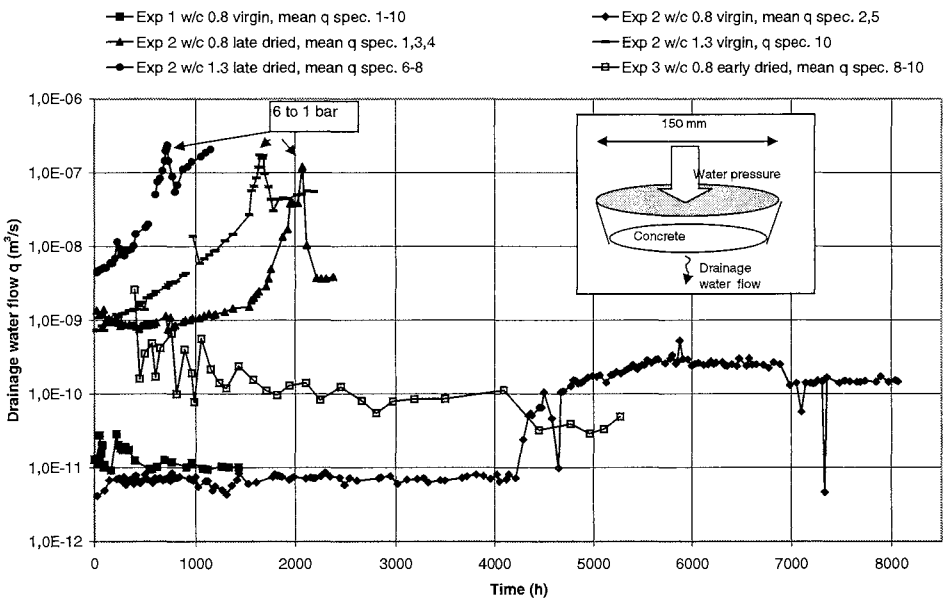

Figure 7-6 Mean water flow μ[q] for experiment 1 (specimens 1-10), experiment 2 (specimens 1-8 and 10) and experiment 3 (specimens 6-10).

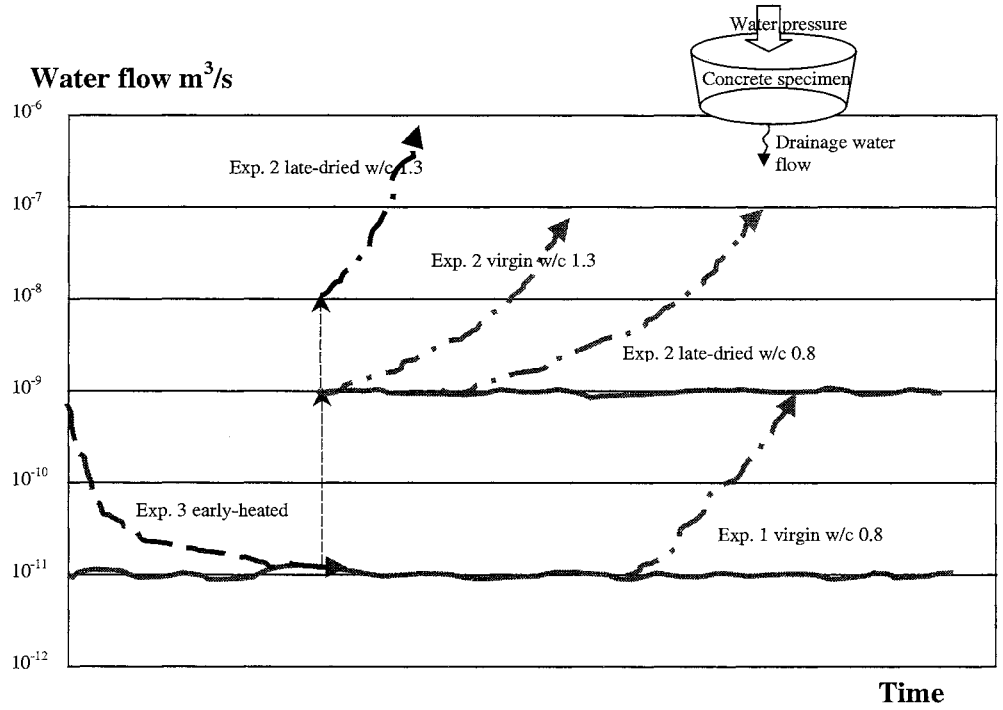

Figure 7-7 A schematic picture over the flow of outlet water in experiments 1-3.

7.2 Chemical analysis of the drainage water

7.2.1 General

The test procedure and the concrete specimens are described in chapter 4, 5 and 6. The water that was pressed through the concrete specimens, here called the drainage water (sometimes called the outlet water), was analysed regarding its chemical contents. Only data from experiment 2 (late-dried w/c 0.8 and 1.3) is shown. In this chapter an overview of the result is given. The results of the chemical analysis are also shown in appendix 7-4 to 7-7.

The experiments show three types of leaching behaviour:

- ✓ Leaching in homogenous concrete with constant flow.
- ✓ Leaching in homogenous concrete with increasing water flow.
- ✓ Leaching in homogenous concrete with decreasing water flow.

As mentioned in chapter 7.1, there was a constant drainage water flow in specimens with low w/c ratio and for virgin (non-dried) specimens. Increasing water flow appeared for high w/c ratios and for late-dried specimens. Finally, the decreasing water flow appeared for the early-heated specimens.

Some ions diffused upstream, against the water flow, towards the inlet water. This is treated in chapter 7.3.

7.2.2 Leaching of Ca

When the water flow was **constant**, the concentration of leached calcium in the drainage water was also constant with a mean value of about μ[Ca] = 0.6 g per litre drainage water, (figure 7-8). The leaching rate of Ca expressed as the product of the water flow and the concentration in the drainage water; $\Sigma m^3/s \cdot kg/m^3 = kg/s$, was also constant because of the constant flow of water.

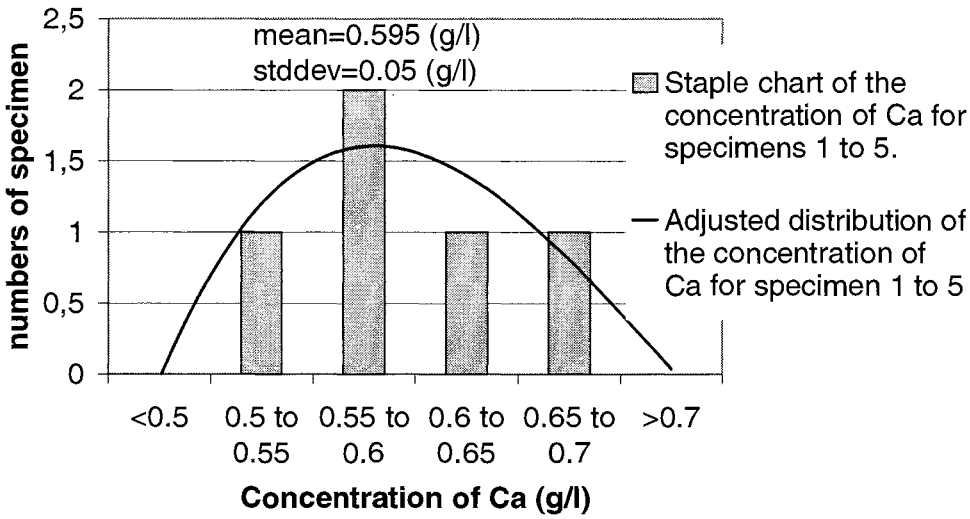

Figure 7-8 Variation in Ca concentration in the drainage water for five specimens of virgin and late-dried w/c 0.8 concrete, before any rapid increase in water flow occurred.

When the water flow was **increasing**, the concentration of calcium in the drainage water decreased from the above mentioned 0.6 g/l down to as lowest measured 0.005 g/l. The leaching rate expressed as kg/s was however quite constant.

When an accumulated water flow of about 1 to 10 litres had percolated each specimen, the concentration of Ca began to decrease in the drainage water, see figures 10 to 12 in appendix 7-4. A specimen of the size ϕ155 (mm)*50 (mm) has an initial content of cement of:

w/c 0.8 exp. 1 and 2: $m_c = V^*C = \pi \cdot 0.155^2/4 \cdot 0.05\ m^3 \cdot 241\ kg/m^3 = 0.227$ kg cement

w/c 1.3 exp. 2: $m_c = V^*C = \pi \cdot 0.155^2/4 \cdot 0.05\ m^3 \cdot 158\ kg/m^3 = 0.149$ kg cement

1 litre percolated water for these two concrete types correspond to:

w/c 0.8 exp. 1 and 2: 1/0.227 = 4.4 l/kg cement

w/c 1.3 exp. 3: 1/0.149 = 6.7 l/kg cement

When the water flow was **decreasing**, the concentration of calcium in the drainage water was constant, but a little bit higher than when the water flow was constant, 0.8 to 1.2 g Ca per litre drainage water. The leaching rate expressed by kg/s decreased due to the decreasing flow of water.

The residual content of Ca in the specimens, decreased by rates that differs only a little among the same type of concrete/curing method.

7.2.3 Leaching of K and Na

Both the concentration (kg/l) and the leaching rate (kg/s) of K and Na in the drainage water decreased when water was pressed through the specimens. This was the case for all the three types of flow patterns; constant, decreasing and increasing water flow. The concentrations began to decrease when approximately 0.1 litre had flown through the specimens.

7.2.4 Leaching of S

The initial concentration of leached sulphate in the drainage water was quite high (0.02 g/l). It slowly decreased during the test.

7.2.5 Leaching of Mg, Fe and Si

The leaching of Mg was typically about 0.01 to 0.1 mg per litre drainage water. The initial concentration of Mg in the cement was according to the cement supplier about 0.45 % MgO per kg cement, i.e. approximately about 600 mg/specimen (e.g. for specimen 2: 0.0045*24.31 g/mole/40.31g/mole*245*10^6 mg/m^3*π*.155^2/4*0.05 m^3 = 630 mg/specimen). The maximum observed leaching of Mg occurred in specimen 7 (late-dried w/c 1.3) and was about 1 mg Mg, which is a fairly low value.

The leaching of Fe was typically about 0.01mg per litre drainage water. The initial content of Fe was according to the cement supplier about 4.32 % Fe_2O_3 per kg cement, i.e. approximately about Fe(s) = 0.0432*55.85*2(g/mole)/159.7(g/mole)*245*10^6(mg/m^3)*π*.155^2/4*0.05(m^3) = 6900 mg/specimen for the w/c 0.8 specimens. The maximum drainage appeared in late-dried specimen 1 and was about 17 l*0.01 mg/l= 0.2 mg, i.e. 0.2/6900, which is a very low value.

7.2.6 Changes in pH

The pH value of the drainage water decreased when its content of K^+ and Na^+ decreased. It decreased from about 13.2 –13.4 to about 12.5, corresponding to the pH-value of a saturated $Ca(OH)_2$ solution. For the very permeable specimens where much water was percolated, the pH decreased even more. The lowest observed value was 10.25 in specimen 1, experiment 2.

7.2.7 Summary

There were three types of leaching behaviour (figure 7-9) that were strongly correlated with the concrete type (w/c 0.8 or w/c 1.3) and the curing history (virgin, late-dried or early-heated). As described in chapter 7.1, the water permeability was different for these concrete types. When the water flow was constant, there was a constant concentration in the drainage water of leached Ca of about 0.7 to 1.2 g/l for the early-heated specimens, and about 0.6 g/l for the rest. The concentration of K and Na in the drainage water rapidly decreased for all specimens. Due to the decrease of K and Na in water, the pH-value in the drainage water fell somewhat at the beginning. When the water flow increased, especially when it increased rapidly, there was a rapid decrease in the concentration of Ca and pH. The concentration of S had a slowly decreasing rate, more or less unaffected by the water flow.

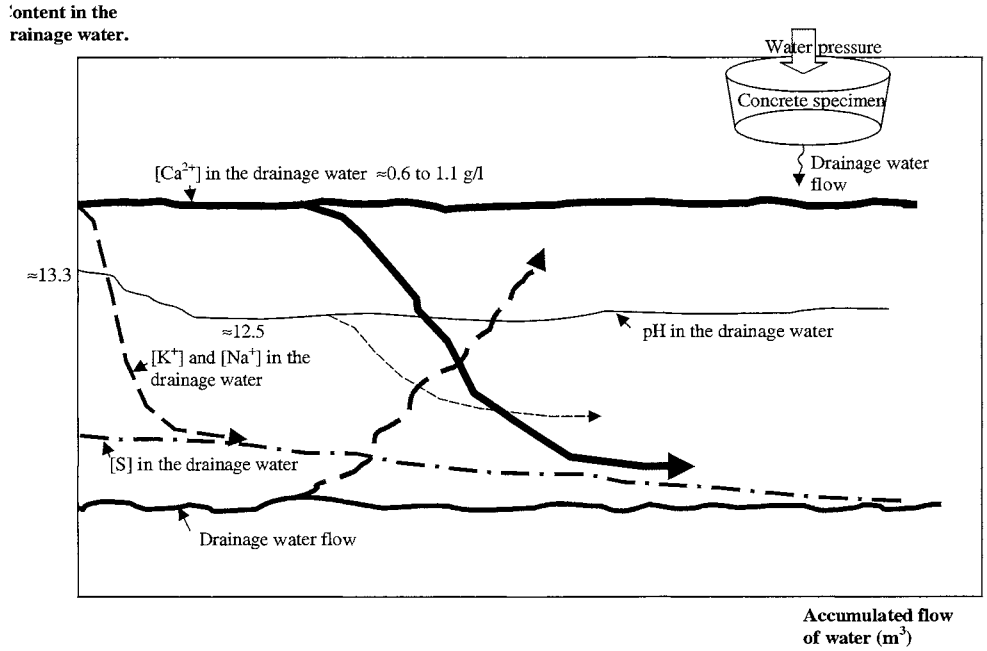

Figure 7-9 A schematic picture over the effect of leaching on the ion content and pH-value of the outlet water in experiment 1-3.

7.3 Chemical analyses of the water at the upstream face

The test procedure and the tested concrete specimens are described in chapter 5 and 6.

As mentioned before, the inlet-water leading to each specimen, was de-ionised. The whole upstream surface of each concrete specimen was exposed to this pure water. Because of the large gradients in concentration of ions between the concrete surface and the water, the diffusion of ions from the concrete surface to the purified water was probably quite large. The dissolved ions from the specimens made the inlet-water less de-ionised as it was meant to be. To maintain pure water condition water was flushed out from the inlet side at every measurement occasion. But, by doing so, the dissolved ions were also flushed away. Even if the concentration was low, the diffusion upstream should be included in the total loss of leached material from the concrete specimens.

Between every flushing, the inlet-water was again gradually refilled by dissolved ions from the concrete. No systematic measurement of the ion concentration of the inlet water was made. Only a few measurements of the pH-value and the concentration of Ca^{2+} in the out-flushed water were performed. By this, a rough estimation was made of the removed ions due to diffusion in the upstream direction.

In figure 7-10 an estimation of the amount of Ca-ions leached upstream is shown. It is based on measurements of out-flushed water from specimens 6 to 10 in experiment 3. At every measurements of water flow, about 2 litre of water was flushed per specimen of size ϕ155 mm and about 0.3 litre per specimen of size ϕ45 mm.

The diffusion upstream of Ca^{2+} decreased from initially about 0.03 g/l for the first 2 litres of collected water per concrete specimen, to about 0.01 g/l at 400 hours (see figure 7-10). At 400 hours to 500 hours the concentration was measured in three different samples, in the first litre

(0.05 g/l), in the second litre (0.02 g/l) and in the third litre that was flushed (0.008 g/l). At 850 hours the concentration was measured for two different samples, for the first 0-1.5 litre (0.03 g/l) and for the next 1.5 –3 litre (0.01 g/l) that came out by the flushing. This shows that it was concentration gradients in the inlet water, from the specimens and in the upstream direction in the steel pipe system.

In figure 7-11, the measured pH values from the inlet water that was flushed from specimens 6 to 10 in experiment 3, is showed.

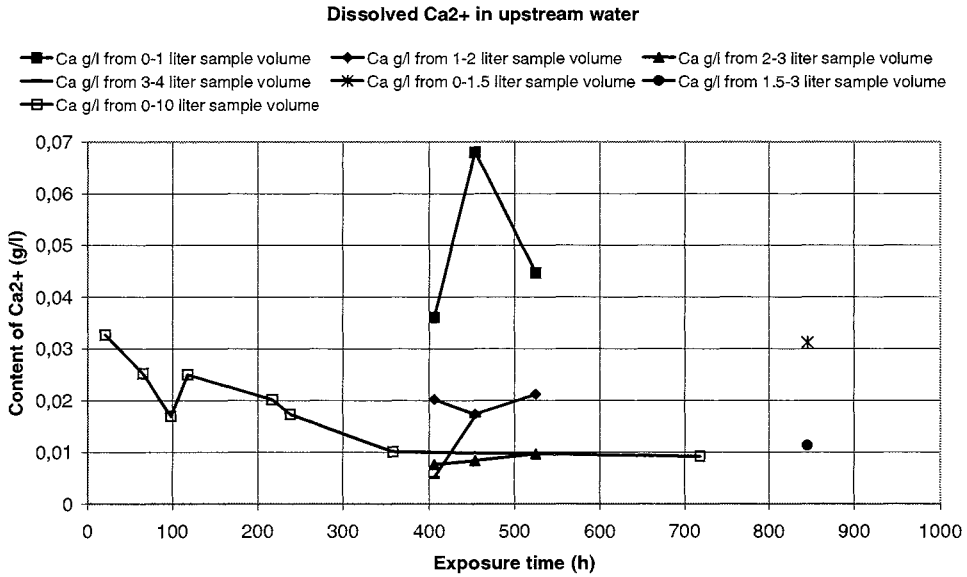

Figure 7-10 Measured content of Ca^{2+} in the out-flushed water from the inlet side of specimens 6-10 in experiment 3.

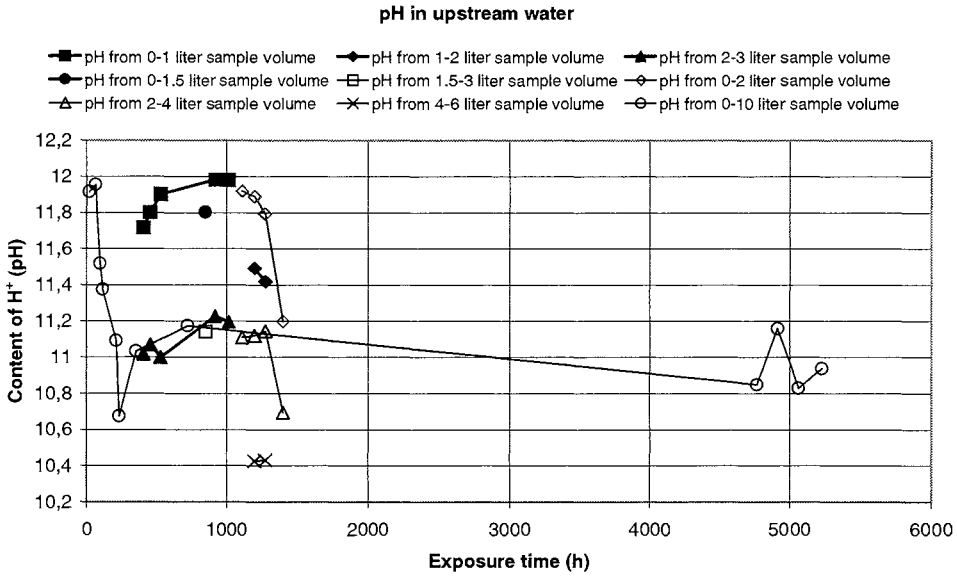

Figure 7-11 Measured content of H^+ (pH) in collected water from the upstream face of specimens 6-10 in experiment 3.

Some brown, soft areas were always observed at the upstream face of concrete specimens having a rapidly increased permeability (see chapter 7.1). A chemical analysis of this brown substance was performed. The result is shown in table 7-1. The results can not be treated quantitatively because a certain amount of the brown material was analysed together with some of the upstream water. Therefore, the unit mg/litre can only be regarded as an indication of which elements the brown powder consists of and of the proportions of elements.

Table 7-1 Measured content in mg of element per litre of water in the sample. The sample was taken from observed brown areas in the upstream face of specimen 7.

	Al	Ca	Fe	K	Na	S	Si
Water sample from experiment 2, specimen 7	15.2	39.2	93.0	0.9	0.7	4.0	20.2

7.4 Chemical analysis of the leached concrete

A chemical analysis was performed for one specimen; specimen 3 in experiment 2.

The contents of different residual elements in five slices taken from the leached concrete were examined. The result is shown in table 7-2 and in figure 7-12. The chemical analysis was made by the method described in chapter 5.2.4.When the slices were dissolved in the HNO_3, a solution and a solid rest at the bottom were obtained.

The dissolved elements in the solution probably emanated from the cement paste, but also to some extent from the aggregate. The solid rest probably emanated from the aggregate, but also to some extent from the cement paste.

In order to estimate how much of the dissolved elements that came from the paste and how much that came from the aggregate, a second study of only the aggregate was performed. The second study was performed in the same way and with the same type and amount of aggregate that was used for the concrete specimen 3. See table 7-3.

Table 7-2 The chemical composition of the dissolved matter from one half (piece 1) of specimen 3 in experiment 2. The specimen was cut in 5 slices. Slice 1 is closest at the downstream face and slice 5 closest at the upstream face. The position of the slices is shown in figure 7-12. The content of elements is in mg element per mg of the total slice. The aggregate content is in weight percent of the total slice weight.

	Measured residual Al piece 1 (mg/mg)	Measured residual Ca piece 1 (mg/mg)	Measured residual Fe piece 1 (mg/mg)	Measured residual K piece 1 (mg/mg)	Measured residual Mg piece 1 (mg/mg)	Measured residual Mn piece 1 (mg/mg)	Measured residual Na piece 1 (mg/mg)	Measured residual S piece 1 (mg/mg)	Measured residual Si piece 1 (mg/mg)	Measured residual solid piece 1 (%)
Slice 1	6,460	44,756	11,466	1,251	1,128	0,315	0,225	1,507	0,105	82,3
Slice 2	5,419	37,550	10,767	1,197	1,014	0,259	0,191	1,247	0,089	83,5
Slice 3	5,794	43,461	10,142	1,189	0,968	0,278	0,191	1,704	0,092	83,5
Slice 4	6,129	45,242	10,526	2,222	1,205	0,298	0,178	1,771	0,157	82,6
Slice 5	6,235	41,375	11,550	1,285	1,266	0,359	0,247	1,588	0,127	80,6

Table 7-3 The chemical composition of the dissolved matter from the same aggregate that was used in table 7-2 after dissolution in HNO_3 acid. The aggregate content is in weight percent of the total slice weight.

	Measured residual Al piece 1 (mg/mg)	Measured residual Ca piece 1 (mg/mg)	Measured residual Fe piece 1 (mg/mg)	Measured residual K piece 1 (mg/mg)	Measured residual Mg piece 1 (mg/mg)	Measured residual Mn piece 1 (mg/mg)	Measured residual Na piece 1 (mg/mg)	Measured residual S piece 1 (mg/mg)	Measured residual Si piece 1 (mg/mg)	Measured residual aggregate piece 1 (%)
Sand 0-8	4,271	3,708	13,930	0,082	1,439	0,291	0,000	0,031	0,022	94,90
gravel 8-16	1,602	0,620	2,087	0,644	0,187	0,025	0,245	0,158	0,000	98,72

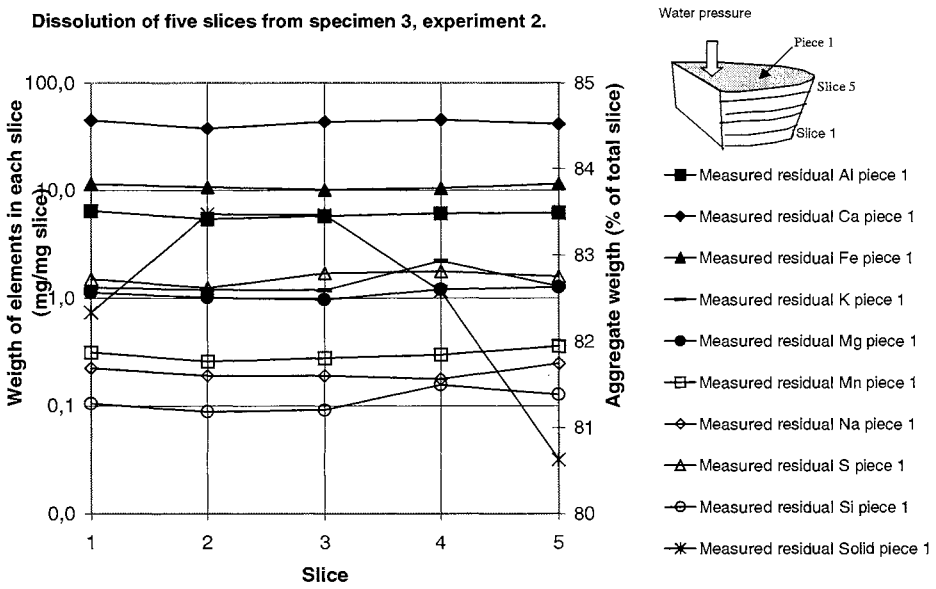

Figure 7-12 The chemical composition of the dissolved matter from one half (piece 1) of the specimen 3 in experiment 2. Slice 1 is closest at the downstream face and slice 5 closest at the upstream face. Observe the log scale.

7.5 Porosity

7.5.1 Total porosity

Only one specimen was analysed for porosity after terminating leaching test, specimen 3 in experiment 2 (late-dried w/c 0.8). The porosity was measured by the method described in chapter 5.2.5. The porosity after the specimen had been leached for 306 days is showed in figure 7-13. Piece 1 is one half of the specimen and piece 2 is a quarter of the specimen. The specimen was also cut in 5 slices, slice 1 closest at the outlet surface and slice 5 closest at the inlet surface.

From the measurement of the porosity, also the density was obtained, see figure 7-14.

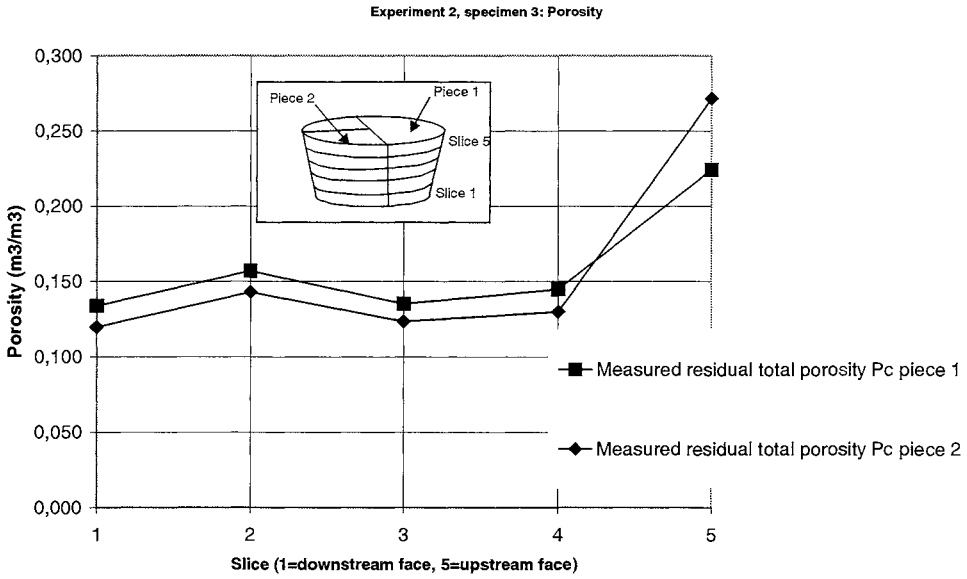

Figure 7-13 Porosity of the leached specimen 3 in experiment 2. The initial total porosity is assessed in chapter 8.4, see figure 8-8, where also the measured residual total porosity of piece 1 in the above figure is shown.

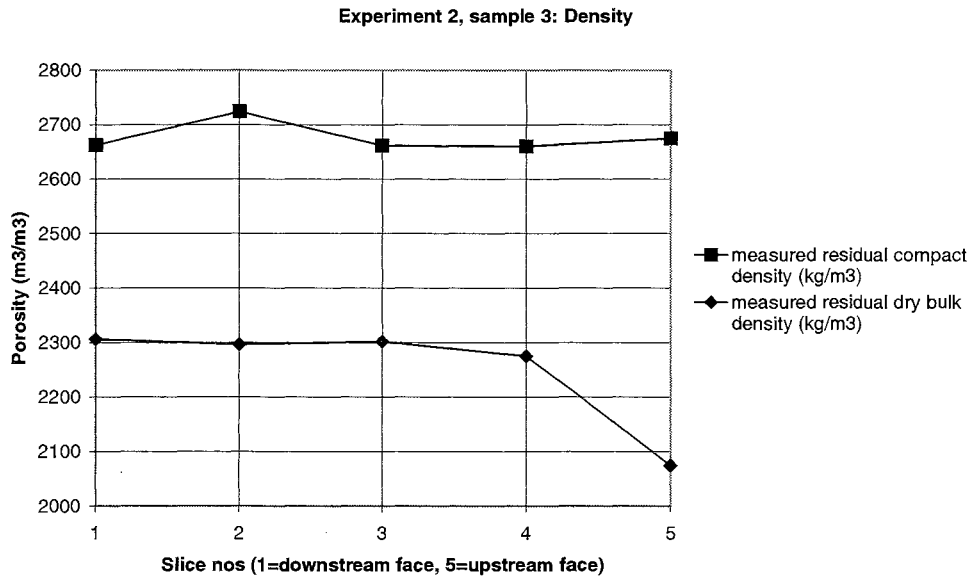

Figure 7-14 The compact density and the dry bulk density for piece 1 of the specimen 3, experiment 2.

7.5.2 Pore size distribution

The pore-size distribution of specimen 3, experiment 2 (late-dried w/c 0.8) was studied. The porosity after the specimen had been leached for 306 days is shown in figure 7-15. The distribution was measured by the method described in chapter 5.2.5. Unfortunately the measurement was interrupted when the air pressure was changed to 100 bar because the air was flowing so rapidly in the test cell that the small concrete slices were pulverised.

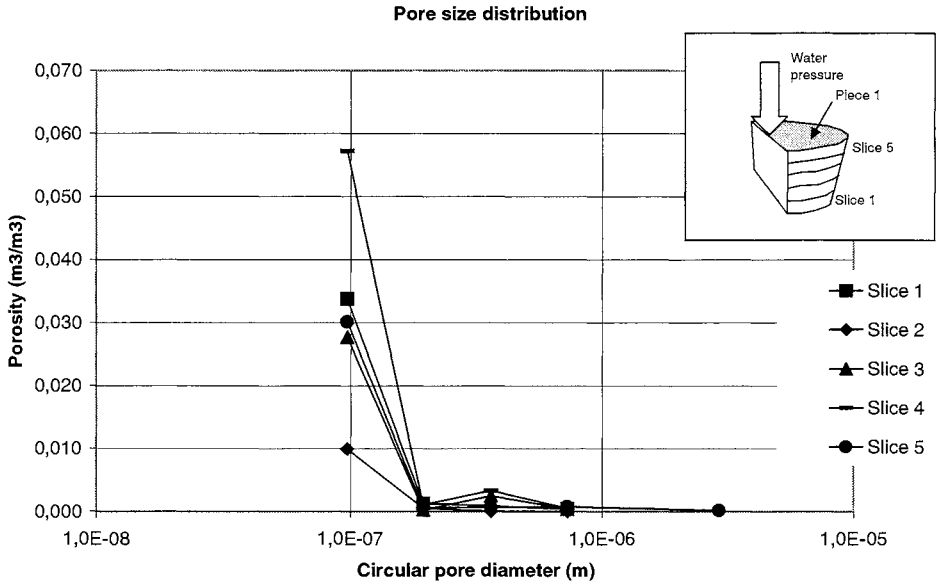

Figure 7-15 Pore size distribution in the leached specimen 3, exp. 2. The pore size distribution is not complete due to the problem described above.

7.6 Mechanical properties

7.6.1 Compressive strength

Small cylinders were drilled from five leached specimens coming directly from the leaching test. The cylinders were all water saturated. The same number of cylinders were drilled from reference specimens. All cylinders were tested in a compressive machine. Some of the leached cylinders had lower compressive strength than the un-leached cylinders.

Specimens 1, 3, 6, 8 and 10 from experiment 2 were strength tested directly after they were taken out of the test cell. See table 7 in appendix 6 for the time history for the specimens. The un-leached reference specimens had the same history, but were stored in lime-saturated curing water, without any pressure gradients during the same time as the comparing specimens were leached.

Specimens, which have had a large increase in water-flow during the water-pressing test, were in a very bad shape after the leaching test. Specimen no 7 fell completely apart when trying to drill cylinders. So from this specimen, no cylinder was available. Also one drilled cylinder from specimen no 8 was discarded since many small pieces fell from that cylinder. Many of the other cylinders also obtained minor damage during drilling. But after grinding, reasonable fine test surfaces were obtained.

In chapter 7.1, the observation of small brown areas in the upstream face of same specimens was mentioned. In these brown areas, it was also observed *flow pipes* leading into the specimen,

where the main water flow evidently had taken place and at the same time probably leached solid material. It was observed during the compressive test, that cylinders with many such brown areas and flow pipes, had lost much more of their strength. Around some larger flow pipes leading through the specimens, so much hydration products were lost, that the concrete no longer had any cohesion. Cylinders from leached specimens without such brown areas and flow pipes had almost the same strength as the reference specimens. So the influence of leaching on the compressive strength was very much a local effect.

In table 7-4, figure 7-16 and in appendix 7-8, the concrete compressive strength is shown. The value "29 MPa" for the unleached specimen 3 seems too low, compared to the strength of the other specimens, but there is unfortunately no explanation to this.

Table 7-4 Compressive strength for un-leached and leached concrete specimens from experiment 2.

Specimen	Compressive strength (Mpa)			
	Un-leached specimen		Leached specimen	
	Mean	Stddev	Mean	Stddev
1 (virgin w/c 0.8)	46	0.8	36	14.8
3 (late-dried w/c 0.8)	29	3.5	33	-
6 (late-dried w/c 1.3)	19	0.3	16	4.7
8 (late-dried w/c 1.3)	18	5.0	12	-
10 (virgin w/c 1.3)	21	7.2	18	2.5

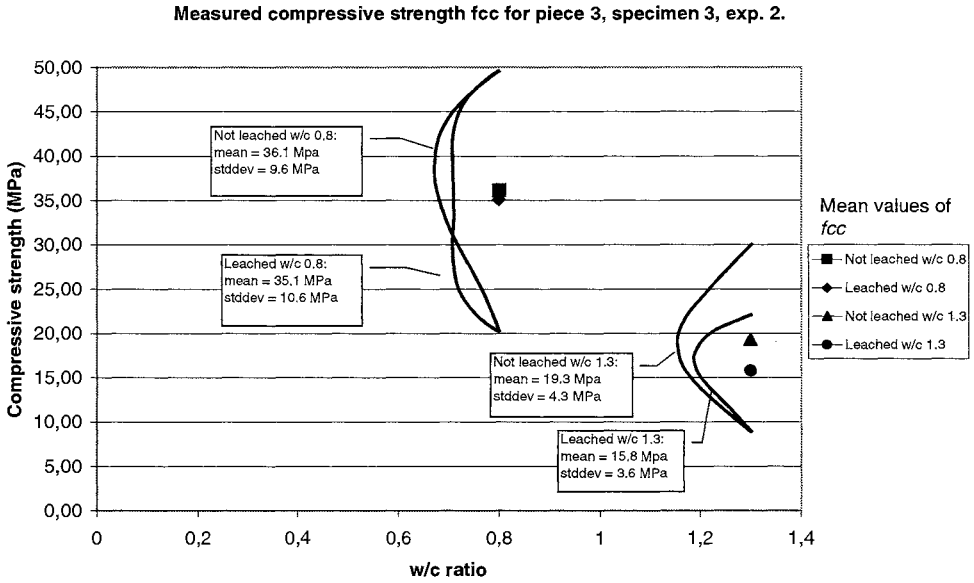

Figure 7-16 Mean value and standard deviation of the compressive strength for piece 3 coming from specimen 3 in experiment 2.

7.6.2 Elastic modulus

From the figures in appendix 7-8 over measured data of applied stress and deformation, the modulus of elasticity E is calculated and presented in table 7-5.

$$E = \Delta\sigma \cdot L/\Delta L \qquad (7\text{-}1)$$

Where E = modulus of elasticity (Pa)

$\Delta\sigma$ = a change in applied compressive stress for a certain change in deformation ΔL. Obtained from the steep part of the measured curves in appendix 7-8. (Pa)

L = the length of the tested cylinders (m)

ΔL = the deformation change for the change in stress $\Delta\sigma$ (m)

Table 7-5 Elastic modulus for un-leached and leached specimens.

Specimen	Elastic modulus E (Gpa)			
	Un-leached specimen		Leached specimen	
	Mean	Stddev	Mean	Stddev
1 (virgin w/c 0.8)	3.4	0.9	2.4	0.8
3 (late-dried w/c 0.8)	4.5	2.7	19.7	-
6 (late-dried w/c 1.3)	1.2	0.2	0.7	0.1
8 (late-dried w/c 1.3)	1.4	0.4	0.6	-
10 (virgin w/c 1.3)	1.8	0.2	1.1	0.4

7.7 Dissolving rate of $Ca(OH)_2$ in de-ionised water

A simple test of the dissolution of $Ca(OH)_2$ in de-ionised water was done, see also chapter 5.2.7.

Figure 7-17 shows the result. Initially the solution was not stirred, but after 240 seconds a magnetic stirrer was placed in the solution. Without stirring, an asymptote was reached at approximately 0.4 g of dissolved Ca^{2+} per litre, i.e. 0.01 mol/l. The rest of the $Ca(OH)_2$ remains un-dissolved. When beginning to stir the solution, the reaction re-started, reaching 0.46 g Ca^{2+}/l. The reaction rate was rapid, especially at the beginning when the water was pure.

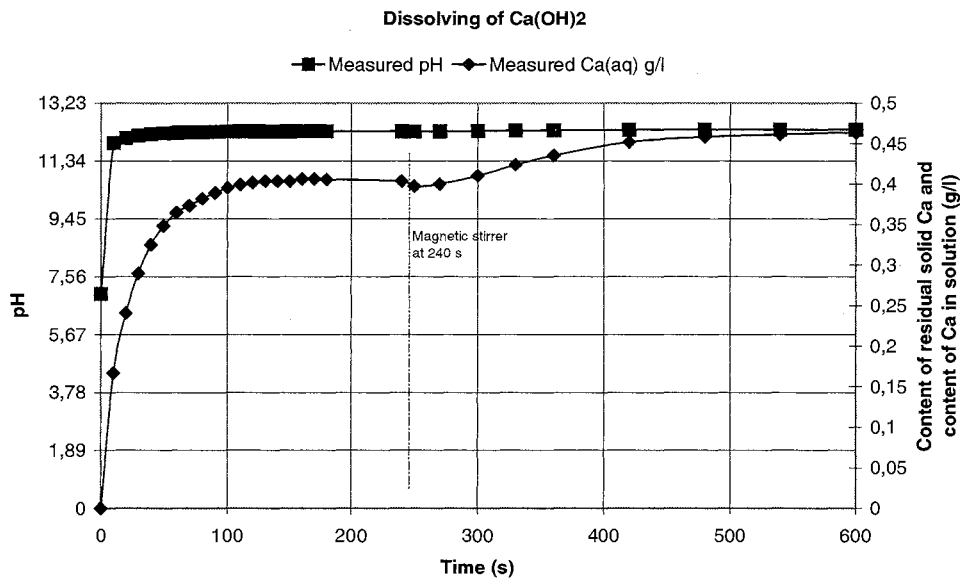

Figure 7-17 Experimental result of dissolving powder of $Ca(OH)_2$ in de-ionised water.

8 DISCUSSION OF RESULTS AND MODELLING OF THE LEACHING PROCESS

8.1 Introduction

In the experiments presented in this report, pure water under pressure was applied to the upstream face of the concrete specimens. On the outlet side, drainage water without any pressure was coming out of the specimen.

The experimental results show that pure water percolating through concrete has an ability to dissolve hydration products, mainly $Ca(OH)_2$, and also to carry the dissolved ions out of the specimen. The transport of the dissolved ions can occur as diffusion upstream to the bulk of pure water at the inlet side or as convection in a downstream direction by the flow of water. Depending on the w/c ratio and the curing history, leaching develops in different ways. Mature concrete with a high hydration ratio or mature concrete that was dried (late-dried) was more porous and permeable. If the specimens were early-heated, the water permeability became high at the start but it quickly decreased due to restarted hydration and self-healing.

In the high-permeable concrete, water seems to have flowed in a rather few, distinct flow pipes. In these pipes, water had dissolved solids, mainly $Ca(OH)_2$, and thereby grew wider. Therefore the water flow increased further, which caused more leaching in a accelerated process. Finally, the pipe walls became so exhausted in solids (lime) that the leaching rate and the water flow increased only slowly. Around these pipes the concrete became very disintegrated with almost no continuous cementitious material left to maintain strength and tightness.

Between the flow pipes, or in not so permeable concrete, the leaching was governed by diffusion to the flow pipes or to the bulk of soft water at the upstream end.

The permeability is related to the number and size of the flow pipes, and the permeability is therefore increased when the flow pipes become wider in the leaching process. The leached layer at the upstream face does probably not have a big effect on the permeability.

The measured residual content of substances in the leached specimens approximately well corresponded to the measured ionic flow in the drainage water flow.

When the OH^--ions were leached, the pH value decreased in the drainage water and probably also in the pore solution; anyhow in the main flow pipes.

The results also show that when solid material is leached, the porosity increases and the strength decreases due to less load-bearing solid material. The number of specimens that were tested with regard to strength, were however too small for really reliable results.

In the following sections, the following parameters are discussed: (i) permeability, (ii) leaching in the upstream face, (iii) leaching through the specimen, (iv) residual content of substances in the leached specimen, (v) porosity, (vi) strength.

8.2 Discussion of permeability results

A number of concrete specimens (chapters 4 and 6) were exposed to water pressure and the flow of the drainage water out of the specimens was measured (chapter 7.1).

The results show that there are three different types of water flow:

- ✓ a constant water flow.
- ✓ an accelerating water flow
- ✓ an retarding water flow

A **constant** water flow always appeared at the beginning of the test for all specimens. The late-dried and the early-heated specimens had an about 100 times higher initial permeability than in the virgin state. Some specimens maintained a constant flow but others obtained flow that changed with time. The main reasons for a constant water flow were probably:

- ✓ the test time was not long enough. If there are no self-healing effects (e.g. formation of calcite), probably all concrete specimens exposed to water pressure will sooner or later be so leached that the permeability increases.
- ✓ In case of virgin specimens, the concrete was well cured with few micro-cracks and a low permeability. Probably, the water flowed slowly in a large amount of flow pipes of small diameters. Since the water flow was so low, the leaching of solid material from the pipe walls was so low that the permeability remains the same.

Two cases of **increased** water flow appeared, (i) late-dried and early-heated concrete got an instantly higher permeability compared with the virgin state, (ii) some specimens got an increased flow during time. The reasons were probably:

- ✓ The initially rise in water flow was due to much more formed micro-cracks when the concrete was dried and heated.
- ✓ The rise of flow during time was probably because the main flow occurred in rather few pipes that quickly became leached. The higher w/c ratio and if the concrete was late-dried, the greater was the probability for an increased water flow. Due to leaching, the flow pipes became wider and because the water flow is approximately proportional to the diameter of the pipes raised to four, the flow increased very quickly. From visual observations of the upstream face of the concrete, small round, brown areas were seen. In these areas the solid was soft and small distinct pipes leading into the concrete could be imagined. The observed leaching in the upstream face due to diffusion of ions to the bulk water in the inlet, was probably not any great cause of increased permeability. The late-dried concrete had probably only a small amount of unhydrated cement available for continuous hydration that could have tightened the concrete.

A **decreasing** water flow appeared rather quickly for early-heated concrete specimens. The main reasons were probably:

- ✓ The concrete was heated when had not yet reached high strength. The swelling due to the increase in temperature in the oven and the shrinkage due to the decrease in temperature when taken out of the oven, lead to micro-cracking of the concrete. These cracks increased the permeability, but also increased the possibility for unhydrated amount to react. During the whole curing, the concrete specimens were placed in plastic bags. No more water was therefore available for continuous hydration. When penetrating water during the leaching test reached unhydrated cement, much of the cement was probably hydrated. The new hydration products filled up the pore system and caused a decrease in the permeability.

The measured permeability was calculated by the coefficients k_w and B in the relations:

$$q_w = k_w \frac{dP_w}{dx} A_{tot} \tag{2-33}$$

$$q_w = B\, g \frac{dP_w}{dx} A_{tot} \tag{8-1}$$

Where A_{tot} Total cross section area of the specimen perpendicular to the water flow at the middle height of the specimen, i.e. $A_{tot} = \pi(\phi_1^2+\phi_2^2)/8$, where ϕ_1 and ϕ_2 is the diameter at the top and bottom end respectively (m^2)

B Permeability coefficient in (s)

dP_w/dx Water pressure gradient (m/m)

k_w Water permeability (m/s) of the concrete specimens with the

pressure gradient expressed as water-head per m specimen)

q_w Water flow. In this case measured in the experiments (m^3/s)

The relation between the permeability expressed as k_w and B is $k_w = g \cdot B \approx 10 \cdot B$.

The permeability relations above assumes a one-dimensional flow, a steady-state flow, no damping effects, no source or sink of water inside the specimens and an isotropic permeability, i.e. the coefficient of permeability is the same in all directions and locations.

In figures 8-1 and 8-2, the resulting permeability, expressed as B, from the experiment in this work are compared to values from literature. In figure 8-1, all values until a test period of 400 hours have been summarised to a mean value for each specimen. These mean values are presented in the figure by mean and standard deviation for certain groups of specimens. The relatively short period of 400 hours, make these permeability values to a sort of initial permeability.

In figure 8-2, the measured values of B is a sort of mean value of the permeability during the whole test time, including water pressure from time zero to as shortest 762 hours and as longest 5300 hours. Therefore, the values also include changes in permeability during the test time.

For w/c 0.8, the mean value and standard deviation is given for each curing type and specimen size.

The curves from Ruettgers (1935) are taken from Fagerlund (1980) and show the permeability of only the cement paste in concrete. These curves are here multiplied with an assumed paste share of 0.25 in order to give the permeability for the whole concrete so a comparison could be made with the present experimental results. The concrete of Ruettgers was probably dried to some extent.

The curves from Hearn and Morley (1996) are based on concrete that was virgin (not dried) and that was 26 year old (w/c=0.9).

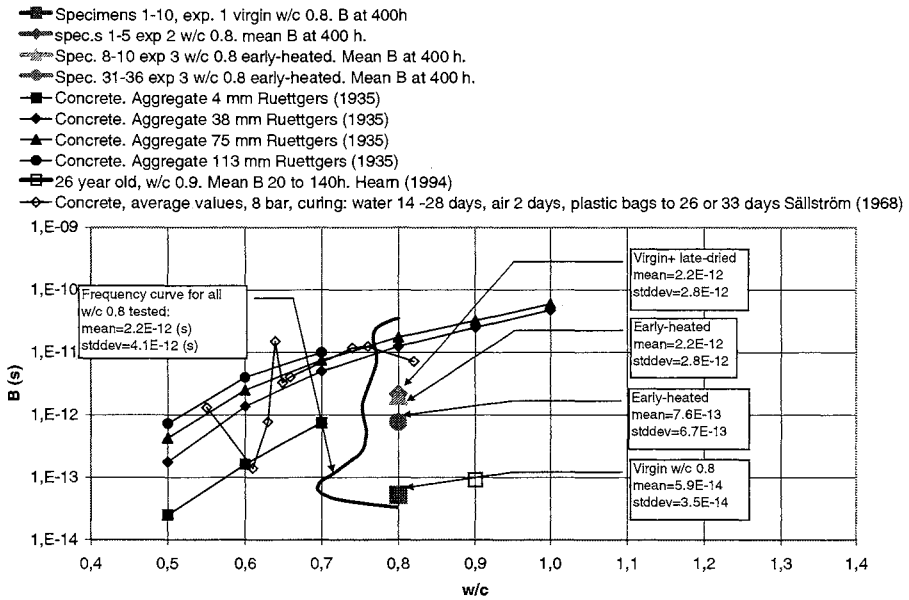

Figure 8-1 Initial water permeability B (s) for concrete specimens in this work and some values from literature. Specimens in this work were subjected to water pressure for a short time (t=400 hours).

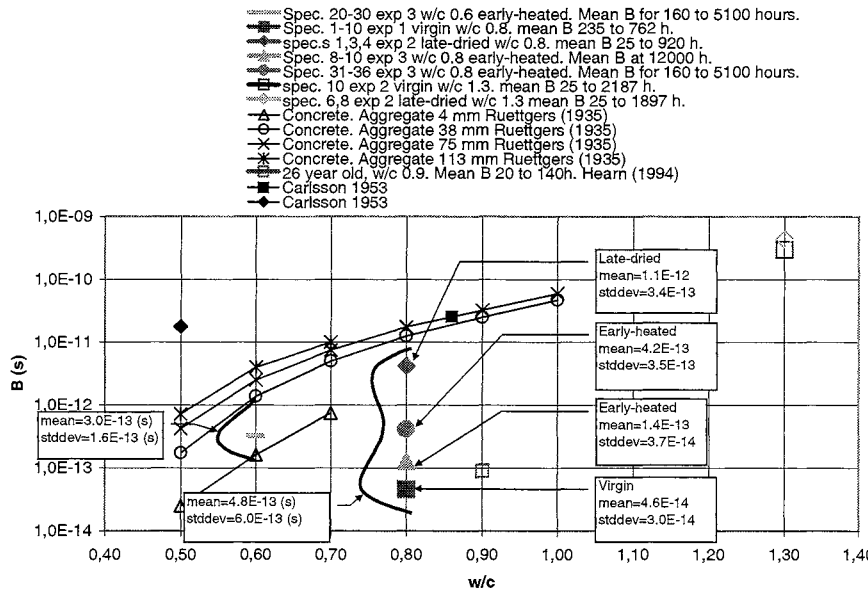

Figure 8-2 Long-term water permeability B (s) for concrete specimens in this work and some values taken from the literature. Specimens in this work were exposed to water pressure for 25 to 5300 hours, see the head in the above figure.

The **early-heated** concrete from experiment 3 in this work has a maximum aggregate size of 8 mm, but 90 % was below 4 mm. In figure 8-2, it can be seen that concrete with w/c ratio 0.6, has a permeability of about 2 times respective 1/4 the permeability of concrete with aggregate size 4 mm and aggregate size 32 mm respectively from the test of Ruettgers (1935). This seems to be a good compliance. For concrete with w/c 0.8, the initial permeability (figure 8-1) was about the same as for concrete with aggregate size 4 mm from Ruettgers, but it decreased during time (figure 8-2) down to about 15 times lower than the permeability for aggregate size 4 mm.

The **late-dried** concrete in this work had maximum aggregate size of 16 mm, but 98 % was of 8 mm or smaller. In figure 8-2, it can be seen that concrete with w/c ratio 0.8, has a permeability of about 2 times respective 1/2 the permeability of concrete with aggregate size 4 mm and aggregate size 32 mm respectively from the test of Ruettgers (1935).

The **virgin** concrete used in this work has about the same permeability as the virgin concrete used by Hearn (1994). Certainly, Hearn's concrete had a w/c ratio of 0.90 compared with 0.80 in this work. On the other hand Hearn's concrete was 26 years old and the concrete in this work only 3 months old. Therefore, the high w/c-ratio in Hearn's is compensated for by the higher maturity.

For the specimens in this work with w/c ratio of 0.8, the standard deviation of the permeability was larger than for the w/c 0.6 specimens. This is because the deviation for w/c 0.8 was calculated for all three types of cured specimens; virgin, late-dried and early-heated, but for w/c 0.6 specimens only early-heated specimens were considered in calculation of standard deviation (table 8-1).

Table 8-1 Permeability expressed in B (s) defined by equation (8-25) from experiment 1, 2 and 3 in this work.

Concrete	Mean permeability $\mu(B)$ (s)	Standard deviation $\sigma(B)$ (s)	Coefficient of variation $v=\sigma/\mu$ (-)
Early-heated w/c 0.6 ϕ 45 mm	$3.0 \cdot 10^{-13}$	$3.0 \cdot 10^{-13}$	1,00
Early-heated w/c 0.8 ϕ 45 mm	$4.2 \cdot 10^{-13}$	$3.5 \cdot 10^{-13}$	0,83
Early-heated w/c 0.8 ϕ 155 mm	$1.1 \cdot 10^{-12}$	$3.4 \cdot 10^{-13}$	0,31
Virgin w/c 0.8 ϕ 155 mm	$4.6 \cdot 10^{-14}$	$3.0 \cdot 10^{-14}$	0,65
Late-dried w/c 0.8 ϕ 155 mm	$1.7 \cdot 10^{-12}$	$4.2 \cdot 10^{-13}$	0,25
Total for all w/c 0.8	$4.8 \cdot 10^{-13}$	$6.0 \cdot 10^{-13}$	1,25

In chapter 8.5, test results are compared with the leaching model from chapter 3.

8.3 Leaching of substances

8.3.1 Introduction

A number of concrete specimens (chapter 4 and 6) were leached and the drainage water coming out from the specimens was measured with regard to leached ions (chapter 7.2). The following tests were made:

- ✓ chemical analyses of the inlet water at the upstream face were done for some specimens at some occasions.
- ✓ chemical analyses of the drainage water during the leaching experiment were done for all specimens in experiment 2 and 3.
- ✓ chemical analyses of specimen 3 in experiment 2 were done after it had been leached.

The chemical reaction (Q) between the constituents of the cement paste and the water, has not been examined except for a simple study of the dissolution of $Ca(OH)_2$ powder in de-ionised water. However, from the data of drainage water flow, ion content in drainage water and some measurements of the composition of the inlet water, some tendencies can be seen as how to water dissolves solid cement paste material as function of time or accumulated water flow. The different levels of dissolved ions in relation to each other in the examined water samples can be explained by different solubility of different substances and by how much of the different ions that are available in the concrete.

8.3.2 Leaching of ions to water at the upstream face

At the upstream face, the concrete was exposed to pure water with very low content of ions. Because of the large concentration gradient between the pore solution inside the specimen and the pure inlet water, the diffusion of dissolved ion upstream probably was large. By the repeated flushing of the upper surface, the dissolved ions were removed. Therefore, the upstream water was rather pure all the time making big diffusion upwards possible. Diffusion of dissolved ions from the upper concrete face to the inlet water, was probably a big cause of the total loss of material from this upper part of the specimen. This was not expected when the test procedure was decided, and afterwards it can be said that not enough effort was laid on measuring the ion

content and flushed water volumes from the water inlet side. However, the test equipment was not built in such a way that such, extensive measurement on the inlet side could be done during the experiment.

During the leaching test, 2 l of the inlet water from each specimen was flushed out regularly. The concentrations of Ca^{2+} in the flushed-out water decreased from initially about $3.5 \cdot 10^{-3}$ mole/l (0.03 g/l) to about $2.5 \cdot 10^{-4}$ mole/l (0.01 g/l) at 800 hours of testing. Still after 5200 hours, the concentration was estimated to be about $1 \cdot 10^{-4}$ mole/l (0.005 g/l). The result of the chemical analyses of the inlet water at the upstream face of the concrete specimens 6 to 10 in experiment 3 is presented in figures 8-3 and 8-4. More precisely, the analysis was made for the flushed-out water from the inlet side. In figure 8-4, the measured concentration of Ca^{2+} and H^+ in the inlet water is shown.

At the moment, no data of the concentration of Ca^{2+} in the upstream water after 850 hours of leaching is available. However, some pH measurements up to 5200 hours were performed. These pH values are transformed into concentration of Ca^{2+} below.

The concentration of OH^- that force the pH to high levels mainly comes from the dissolution of KOH, NaOH and $Ca(OH)_2$ as described in the equation below.

$$[K^+] + [Na^+] + 2*[Ca^{2+}]/M_{Ca} = (10^{-(14-pH)} - 10^{-7}) \text{ mole/l} \qquad (8\text{-}2)$$

Where M_{Ca} Mole weight for Ca (g/mole)
[ ] Concentration (g/l), (mole/l)

Until 718 hours of leaching the concentrations of K^+ and Na^+ were estimated to be the measured OH^- (pH) minus the measured concentration of Ca^{2+} from the equation above.

After 718 hours of leaching the concentration of K^+ and Na^+ was assumed to be about $5 \cdot 10^{-4}$ mole/l together and decreasing down to $2.5 \cdot 10^{-4}$ mole/l at 5000 hours. The concentration of Ca^{2+} after 718 hours is estimated from the measured pH and the assumed K^+, Na^+ from equation above. See figure 8-4. Despite all the assumptions, there is a clear picture of the amount of leached Ca^{2+} from the upstream face of the concrete specimen.

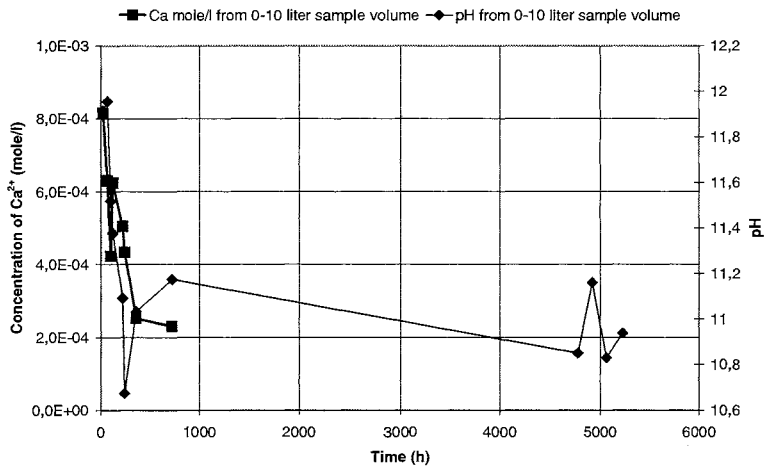

Figure 8-3 Measured contents of Ca^{2+} and H^+ (pH) in collected water from the upstream face of specimens 6-10 in experiment 3.

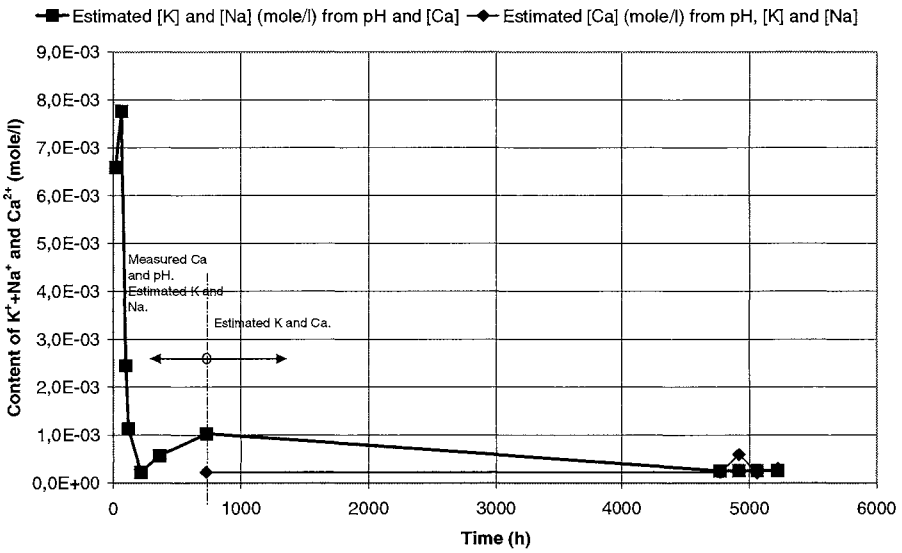

Figure 8-4 Estimated concentrations of K^++Na^+ and Ca^{2+} in collected water from the upstream face of specimens 6-10 in experiment 3.

To obtain an understanding of the total amount of flushed-out Ca^{2+} an example is given for the first 1400 hours of leaching test. During these 1400 hours there were several flushing occasions *n*. 2 litres was flushed every occasion. The loss of mass $V_{flushed}$ in the flush water is:

$V_{flushed}$ = *n* times*2 litre/time = 2*n litre per specimen

The flushed-out mass $M_{flushed}$ of Ca^{2+}, if $5 \cdot 10^{-4}$ mole/l is taken as a mean value between time zero and 1400 hours, is:

$M_{flushed}$ = 2**n* litre*~ $5 \cdot 10^{-4}$ mole/litre*40.08 g/mole = 0.04*n g per specimen.

In table 8-2, it can be seen that the diffusion through the upstream face accounts for a great part of the whole loss of Ca from the concrete specimens. With time the diffusion upstream will probably decrease since the thickness of the diffusion layer in the upstream part of the concrete will increase. More measurements must be done after a longer time to see the development of this diffusion through the upstream face. A reasonable assumption is that the diffusion ratio is inversely proportional to the square-root of the exposure time.

Table 8-2 Assumed and measured loss of Ca (g) through the upstream face and measured loss of Ca (g) through the downstream face.

	Spec. 6	Spec. 7	Spec. 8	Spec. 9	Spec. 10
Number of flushing occasions until 1400 hours of test.	20	22	23	19	21
Estimated loss of Ca (g) from the upstream face until 1400 hours of test.	0.80	0.88	0.92	0.76	0.84
Measured loss of Ca (g) from the downstream face until 1400 hours if test.	5.89	3.80	0.37	1.55	1.42

An estimation of the relation between diffusion upstream and convection downstream of ions is given in two examples. In the first example, the water flow is given from experimental results and in the second example, the water flow is calculated by a reduced Hagen-Poiseuille law.

Example 1 (diffusion and convection of ions in two specimens with real water flow given)

The diffusion and convection of $Ca(OH)_2$ in specimen 1 (high water flow) and 2 (low water flow) from experiment 2 is calculated. Due to intermolecular forces between the pore wall and water and the tortuous pore system, the diffusion coefficient $k_{ion(aq)}$ in the pore solution is assumed to be only about 10 % of the free water diffusion, $k_{ion(aq)} \approx 0.1*10^{-9}$ (m^2/s) = 10^{-10} (m^2/s). It is also assumed that the layer dx over which the concentration drops from saturated concentration of 0.02 mole/l to zero, to be 0.010 m. The cross-section area of the specimen is $A_{tot} = \pi \cdot \phi^2/4 = \pi \cdot 0.155^2/4 = 18.9 \cdot 10^{-3}$ m^2.

Then, the diffusion upstream is:

$$q_{ion\ diff} = k_{ion(aq)} \cdot \frac{dc}{dx_i} \cdot A_{tot} = 10^{-10} \frac{m^3}{s} \cdot \frac{20\,mole/m^3}{0.01\,m} \cdot 18.9 \cdot 10^{-3}\,m^2 = 4 \cdot 10^{-9} \frac{mole}{s}$$

The convection flow for specimen 1 at the beginning of the test was:

$$q_{ion\ conv} = A_{tot} v_w \nabla c \approx A_{tot} v_w c = A_{tot} \frac{q_w}{A_{tot}} c = 2 \cdot 10^{-9} \frac{m^3}{s} \cdot 20 \frac{mole}{m^3} = 4 \cdot 10^{-8} \frac{mole}{s}$$

and for specimen 2:

$$q_{ion\ conv} = A_{tot} v_w \nabla c \approx A_{tot} v_w c = A_{tot} \frac{q_w}{A_{tot}} c = 1 \cdot 10^{-11} \frac{m^3}{s} \cdot 20 \frac{mole}{m^3} = 2 \cdot 10^{-10} (\frac{mole}{s})$$

For specimen 1, the diffusion of dissolved ions upstream was about 10 times *less* than the convective flow of ions downstream.

For specimen 2, the diffusion of ions upstream was about 10 times *greater* than the convective flow of ions downstream.

This means, as long the part of the specimen that is close to the upstream face still contain a large amount of dissoluble substances, the loss of ions by diffusion upstream was about the same as the loss downstream by convection in the drainage water.

However, when diffusion layers increases, diffusion will of course also decreases. This is valid both for diffusion from individual flow pipe walls, as for the whole upstream face of the specimen.

The circumstances was probably different for the really large water flows in some specimens, (up to $4 \cdot 10^{-8}$ m^3/s). Here convection of ions downstream in the flow pipes probably dominated. However, in the concrete between the flow pipes, where the water permeability was much smaller, the diffusion of ions upstream from the slice nearest the inlet water was probably still large compared to any convection flow downstream.

In order to relate the radius of the flow pipes to type of ionic flow, convection or diffusion, a calculation is given.

Example 2 (diffusion and convection of ions in two specimens with calculated water flow)

The flow of ions due to diffusion is described by:

$$q_{ion\ diff} = A_i\, k_{ion(aq)}\, dc/dx \qquad (8\text{-}3)$$

and the flow of ions due to convection is described by:

$$q_{ion\ conv} = A_i\, v_w\, c \qquad (8\text{-}4)$$

where	$q_{ion,diff}$	Ionic flow by diffusion (mole/s)
	$q_{ion,conv}$	Ionic flow by convection (mole/s)
	A_i	Cross-section area of a flow pipe i (m^2)
	$k_{ion(aq)}$	Diffusivity of ions in the flow pipe solution (m^2/s)
	c	Ion concentration in the pipe solution ($mole/m^3$)
	dc/dx	Ion gradient in x-direction ($mole/(m^3 \cdot m)$)
	v_w	Velocity of the water flowing in the assumed flow pipes (m/s)

The velocity v_w of the water flow in the flow pipes is calculated with a reduced Hagen-Poiseuille's law. The reduction is done with an assumed reduction coefficient r_w, due to deviation of a real, tortuous flow pipe and a perfect cylinder.

$$v_w = k_w \nabla P = r_w \frac{\phi^2}{32\mu} \rho_w g \frac{\Delta P_w}{L} \tag{8-5}$$

where	v_w	Velocity of the water flowing in the assumed flow pipes (m/s)
	k_w	Water permeability (m/s)
	ΔP_w	Difference in water pressure between the inlet and outlet face (m)
	L	Length of the flow pipe (m)
	r_w	Assumed reduction coefficient due to the tortuosity and pore wall-water interactions in the flow pipes (-)
	ϕ	Diameter of the flow pipes (m)
	μ	Dynamic viscosity of water (Ns/m^2)
	ρ_w	Density of water (kg/m^3)
	g	Acceleration of gravity (m/s^2)

In figure 8-5, ion flow by diffusion versus convection for some in-data in the equations above is given. It can be seen that for flow-pipes with diameter less than 10^{-7} m, ionic diffusion dominates and for flow pipes with diameter above 10^{-7} m convective flow of ions dominates. According to the figure, the convective and diffusive flows are equal at a pipe diameter of approximately 10^{-7} (m).

volume of the capillary pores of specimen 3 is $V_{cap} \approx 241(0.8\text{-}0.39\cdot0.9)\cdot\pi\cdot0.155^2/4\cdot0.05 = 0.10$ litre. The passed 0.41 litre in table 8-3 corresponds to about four times the volume of the capillary pores V_{cap}. According to figure 1-3, showing work by Unsworth et al (unknown), the concentration of Ca reaches its top value of about 0.53 g/l, only when the concentration of K and Na had decreased to about 0.2 g/l. The value of 0.53 g/l in Unsworth (unknown) was measured after that a water volume corresponding to six pore volumes (6 PV) had passed the specimen, which is about the same as the amount of water passed per capillary volume at the first measuring occasion for specimen 3.

This confirms that the high amount of Ca depends on previous leaching of amount of K and Na.

Table 8-3 Measured contents of K, Na, S and Ca, compared with calculated contents of Ca in specimen 3 from experiment 2. For the calculation was the solubility products for KOH, NaOH, $CaSO_4$ and $Ca(OH)_2$ assumed to be 4.5, 8.1, $4\cdot10^{-6}$ and $9\cdot10^{-6}$ respectively.

Measuring occasion	K (g/l) measured	NaOH (g/l) measured	$CaSO_4$ (g/l) measured	Ca^{2+} (mol/l) calculated	Ca^{2+} (g/l) measured
Spec. 3, Q=0.41 liter	0.223	0.034	0.025	0.75	0.742
Spec. 3, Q=5.18 liter	0.013	0.005	0.021	0.84	0.552

The calculated values in table 8-3 correspond rather well with the measured values of Ca. For a total penetrated water volume of 5.18 litre, the concentrations of KOH and NaOH had decreased so much that, due to the common ion effect, more $Ca(OH)_2$ can be dissolved than when the passed water content was low, Q=0.41 litre. The measured amount of Ca was however smaller when 5.18 litre had passed. This can perhaps be explained by the fact that the specimen had been leached for 4200 hours at this time and therefore, the flow pipe walls might have been exhausted in Ca.

Ca was probably dissolved mainly from $Ca(OH)_2$, but also to some extent from AFt, AFm and C-S-H. There are much more of Ca compounds in concrete available than K and Na and therefore the total amount of dissolved Ca will be big, even if the solubility of Ca-compounds is lower than of K and Na compounds. Probably the great amount of $Ca(OH)_2$ in the concrete was the main contributor to the high level of Ca in the drainage water. When the flow pipes at last became exhausted in Ca, the Ca content in the drainage water also decreased.

In figure 10 in Appendix 7-4 showing w/c 0.8 specimens 1-5 from experiment 2, it can be seen that somewhere between 2 and 10 litre of accumulated flow of water, the concentration of Ca in the drainage water decreased rapidly. For specimen 5, the concentration of Ca decreased already after about 0.15 litre had passed.

For the specimens 6 to 10 (w/c 1.3) from the same experiment 2, the concentration of Ca in the drainage water decreased after about 6 to 10 litre had passed through the specimens (figure 11 in Appendix 7.4).

The rapid decrease in the concentration of Ca after a certain accumulated water flow was probably caused by the flow pipe walls became exhausted in Ca. The differences between different specimens may be due to different number and size of the flow pipes. The flow of water is more or less proportional to pipe diameter ϕ raised to 4, but the area of the pipe walls is proportional to ϕ only. In the case of specimen 5, the flow pipes may have been fewer but wider and the layer with available calcium in the pipe walls was also probably thinner than for the

other concrete specimens with w/c 0.8. The permeability became almost the same but the pipes were more rapidly exhausted in calcium.

The water flow was about 100 times greater for concrete of quality w/c 1.3 than for concrete with w/c 0.8 (cured in the same way). This means that the number of flow pipes, or the diameter of the pipes (or both) was bigger for the concrete with w/c 1.3. The decreasing leaching rate after about 6 to 10 litres for the concrete with w/c 1.3, indicates that the pipes were wider and the layer with available calcium in the pipe walls was thinner than for concrete with w/c 0.8.

In figure 1-4 from Moskvin (1980), the decrease in leached Ca appeared when approximately 10 to 60 (litre/kg cement) of water had seeped through. Transforming the values from the present investigation to this unit gives:
For specimens 1-5: $m_C = C*\pi\phi^2/4*L = 241*\pi*0.155^2/4*0.05 = 0.23$ kg cement which means 2/0.23 to 10/0.23 = 9 to 44 l/kg cement.

For specimens 6-10: $m_C = C*\pi\phi^2/4*L = 158*\pi*0.155^2/4*0.05 = 0.15$ kg cement, which means 6/0.15 to 10/0.23 = 40 to 67 l/kg cement.

In figure 8-6, it can be seen that the result from the present work fits quite well with data from Moskvin (1980).

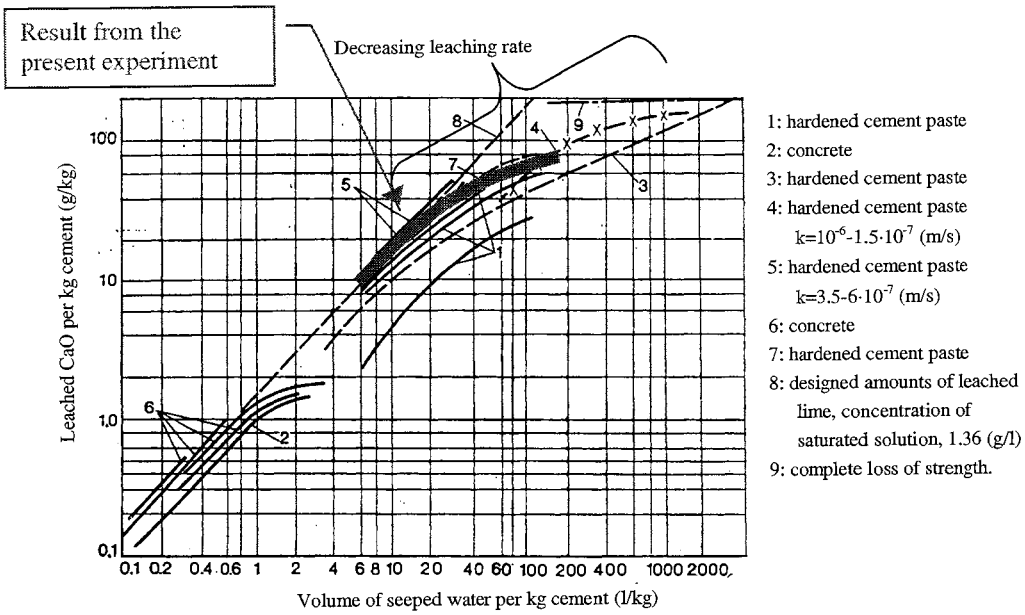

Figure 8-6 Quantity of lime leached from cement mortar or concrete vs volume of percolated water. Data from the present work and data based from several authors and presented in Moskvin (1980). k = permeability (m/s)

Lea (1983) reported from a study that the concentration of calcium in the drainage water coming out from concrete exposed to water pressure was saturated until a calcium content corresponding to 10-15 % of the cement weight was leached. In the present study, the concentration of calcium in the drainage water was saturated until a content of calcium corresponding to about 2-4 % of

the cement weight was leached for specimens 1 to 4 (w/c 0.8) and to 3-5 % for specimens 6 to 10 (w/c 1.3). The specimens that Lea used was probably more porous than in the present study.

Figure 13 to 19 in appendix 7-4, shows how the estimated residual content of Ca decreases in the leached specimens 1 to 10 in experiment 2. The residual content is estimated from an assumed initial content minus the observed leaching to the drainage water. It is hard to say from which compound calcium is taken; CH, C-S-H or AF phases. The leached amount of calcium in relation to the total initial content of calcium in the specimens was about 6 % for specimens 1 to 5 (w/c 0.8) and about 39 % for specimens 6 to 10 (w/c 1.3).

The leached amount of calcium in relation to the total initial content of calcium hydroxide in the specimens was about 20 % for specimens 1-5 (figure 16 in Appendix 7-4), and from 77 % to over 100 % for specimens 6-10 (figure 19 in Appendix 7-4). The high ratios indicate that calcium probably is taken from C-S-H and AF phases also.

In figure 13 to 15, data from Sällström (1964) and Ruettgers (1936) are also showed. For low accumulated flow of water, the measured residual content of Ca from Ruettgers are about the same as for the w/c 0.8 concrete specimen 1-5 in this text. For high-accumulated flow, the specimens in this text were not so much leached that the specimen of Ruettgers and Sällström. Probably, their specimens were more porous.

In figures 1 and 2 in Appendix 8-1, two relations that describe the concentration of Ca in the drainage water for two specimens (1 and 10) in experiment 2 is presented. Pure curve fitting have been used to develop the relations. One of the relations involves the accumulated flow of water and the other relation involves the increase in water flow. The relations may be used in future leaching models. The relations are:

✓ Concentration of calcium in the drainage water for **specimen 1** (Late-dried w/c 0.8):

$$\text{Relation 1): } [Ca] = \left(\frac{1}{\sqrt{[Ca]_0}} + 0.15 \cdot Q_w \right)^{-2} \tag{8-6}$$

$$\text{Relation 2): } [Ca] = [Ca]_0 \cdot \left[\frac{q_{w0}}{q_w} \right]^{1.5} \tag{8-7}$$

✓ Concentration of calcium in the drainage water for **specimen 10** (Virgin w/c 1.3):

$$\text{Relation 1): } [Ca] = [Ca]_0 \cdot e^{-0.23 \cdot Q_w} \tag{8-8}$$

$$\text{Relation 2): } [Ca] = [Ca]_0 \cdot \left[\frac{q_{w0}}{q_w} \right]^{0.6} \tag{8-9}$$

Where	[Ca]	Concentration of Ca in the drainage water (g/l)
	$[Ca]_0$	Initial concentration of Ca in the drainage water (g/l)
	Q_w	Accumulated water flow (l)
	q_w	Water flow (l/s)
	q_{w0}	Initial water flow (l/s)

Due to the decrease of potassium and sodium and the corresponding decrease in OH^-, the pH value was somewhat reduced in the beginning. See also the principles in figure 7-9.

Leaching of S

The concentration of sulphate (S) in the drainage water was low and constant in all tests.

S was observed in the drainage water by a low, but stable concentration for a long time. It probably comes from AFt and AFm compounds. There is less S than Ca in concrete and the solubility of sulphate compounds is lower than that of the others compounds. Therefore, the content of S in the drainage water was lower than that of K, Na and Ca, but it was constant and lasted longer then K and Na. As can be seen in figure 1 in appendix 7-6, the estimated residual content of S in the leached specimens 1 to 5, is about 95 to 99 % of the initial content.

Leaching of Mg, Fe, Si

The content of magnesium (Mg), iron (Fe) and silicon (Si) in the drainage water was very low in all test. The leaching of Mg, Fe and Si do not at all follow the other, more soluble elements Ca, K, Na and S. It was hardly possible to detect any concentration of Mg, Fe and Si in the drainage water. The hydration products mainly lost Ca, Na, K and S. The residual products probably consist of a leached, porous, weak skeleton of these, insoluble compounds containing Mg, Fe and Si.

Leaching of OH^-

The leaching of hydroxide ions (OH^-) of course strongly follows the leaching of K, Na and Ca, since it comes from the same dissolving reactions. See appendix 7-7. When Ca, K and Na are removed from the pores, the hydroxide ions are also removed.

8.3.4 Unleached components in the specimen

The aim with this study was to estimate the residual contents of calcium, but also other elements, in different parts in the water flow direction, of a leached specimen.

One half of the leached specimen, no 3 (late-dried w/c 0.8) in experiment 2, was cut in five slices perpendicular to the flow direction, see figures 5-2 and 8-6. The slices were dissolved in HNO_3 and then examined regarding the elements of Al, Ca, Fe, K, Mg, Mn, Na, S, Si by ICP AES technique, see chapter 5.2.4. The chemical contents of the elements above and also the porosity were measured in each slice.

When the slices of the half specimen 3 was dissolved, a solid rest appeared at the bottom of the container. This solid part came probably mainly from the aggregate, but also to some extent from the cement paste. To estimate the amount of aggregate that was dissolved in the HNO_3, a second test was performed in the same way, but now was only aggregate dissolved.

The measured residual elements for each slice in the specimen 3 are compared with an assumed initial content of the same elements. The residual content of calcium (Ca) is also compared to observed leached content of Ca in the drainage water from the same specimen.

The following assumptions is made:

- ✓ The structural model according to Powers is used (see chapter 2.3.1 for abbreviations).
- ✓ There are no pores in the aggregate.

From the measure of porosity described in chapter 7.3, the volume of the analysed concrete slices is known. The total volume of each concrete slice is the sum of the volume of aggregate, cement paste and the volume of air due to compaction or air additives in them:

$$V_c = V_a + V_p + V_{air} \quad (2\text{-}30)$$

The volume of aggregate V_a in the concrete slices is assumed as the observed solid rest after the dissolution test minus estimated part of silicon from the cement paste and with regard to that a certain part of the aggregate was probably dissolved during the test:

$$V_a = (m_{residual} - (Si(t_0) - Si(aq))/(\rho_a \cdot (1-S_a)) \quad (8\text{-}10)$$

Where	$m_{residual}$	Solid rest that was not dissolved in HNO_3 for each slice in specimen 3 (kg)
	$Si(t_0)$	Assumed initial content of Si in each slice in specimen 3 (kg)
	$Si(aq)$	Observed content of Si in the solution of HNO_3 and the slices from specimen 3 (kg)
	S_a	Solubility of used aggregate in HNO_3 (weight %)
	ρ_a	Density of aggregate (kg/m^3)

When dissolving the concrete slices, all the contents of Si in the paste except the measured content $C_{Si}(aq)$ in the solution is assumed to belong to the measured residual $m_{residual}$.
The initial content of Si in the cement paste is assumed:

$Si(t_0) = 0.1061 \cdot C$ (from the cement manufacturer)

Where C Cement content (kg)

The separate test of the solubility of the aggregate in HNO_3 indicated that $(1-S_a) = 94.0$ % by weight of the aggregate 0-8 mm and 98.72 % of the aggregate 8-16mm by weight. The mean value was 96.36%. The density ρ_a is 2550 (kg/m^3) for the 0-8 fraction and 2630-2640 (kg/m^3) for the 8-16 (mm) fraction (figures given by the supplier). If the total concrete volume, the content of air and the volume of the aggregates is known, the volume of cement paste can be estimated:

$$V_p = \left[\frac{C}{1000}(0.32 + w/c)\right] = \\ = V_c - V_a - V_{air} = V_c - \frac{(m_{residual} - (0.1061 \cdot C - Si(aq)))}{\rho_a \cdot (1 - S_a)} - V_{air} \quad (8\text{-}11)$$

Reformulating the equation gives:

$$C = \frac{\left(V_c - \frac{m_{residual} + Si(aq)}{\rho_a \cdot (1 - S_a)} - V_{air}\right)}{\left(\frac{0.32 + w/c}{1000}\right) - \frac{0.1061}{\rho_a \cdot (1 - S_a)}} \quad (8\text{-}12)$$

The content of different elements in the cement is known, see table 6-1 for experiment 2. The amount of calcium in concrete is:

$$Ca = 0.655 \cdot C \cdot M_{Ca}/M_{CaO} = 0.47 \cdot C \cdot 40/56 = 0.47 \cdot C \quad (8\text{-}13)$$

Where	Ca	Content of calcium in the concrete (kg)
	M_{Ca}	Molar weight of calcium (40 g/mole)
	M_{CaO}	Molar weight of calcium oxide (56 g/mole)

The w/c ratio and the volume of air due to insufficient compaction are assumed to be the same throughout the cement paste.

The upstream end of the specimen (slice 5) had a higher initial content of Ca than the rest of the specimen (figure 8-6). It was probably some separation of aggregate during casting and therefore, the upstream part became richer in cement paste.

The loss of Ca is defined as the difference between the assumed initial content and the measured residual content. For specimen 3, the loss of Ca using this assumption is estimated to be 3.6 (g). The measurements of the inlet water for specimens 6 to 10 in experiment 3, indicates

how much calcium is leached upwards, see chapter 8.2.1. If the diffusion between each flushing is assumed to be $1 \cdot 10^{-4}$ mole/l for specimen 3, the loss of Ca is 10^{-4} mole/l ·40.08 g/mole ·179 flushing occasions = 0.72 g. The measurements in the drainage water described in chapter 8.2.2 gave a loss for specimen 3 to 6.8 g.

The estimated loss of Ca in the leached specimen of 3.6 g (see above), is somewhat lower than the measured total loss in the inlet and outlet water which is 0.72+6.8 = 7.5 g. But the relations described above are rather sensitive, for example if the content of Ca in the cement instead is 0.5·C kg and if the solubility of aggregate in HNO_3 is $(1\text{-}S_a)$= 99%, the loss had been 7 g, which is almost the same as the measured value 7.5 g.

Specimen 3 lost calcium due to leaching. Most was lost in the upstream part (slice 5) but also in slice 2 in the downstream part. The loss of calcium from slice 5 at the upstream part is probably caused by the fact that it was exposed to aggressive pure water and that it contained a large initial content of Ca.

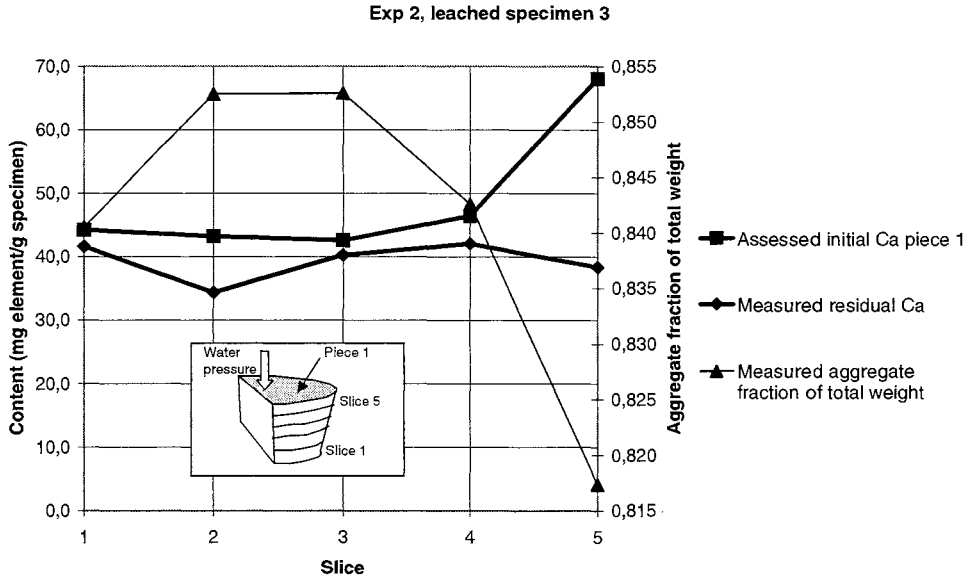

Figure 8-7 The figure shows the initial and residual content of Ca and the content of aggregate in concrete specimen 3, experiment 2. The assumed, initial content of Ca in the specimen is valid just before the leaching test started. The residual content of Ca in the leached specimen has been measured.

8.4 Porosity

The initial total porosity is estimated and compared to the measured total porosity. The initial total porosity P_c of the concrete specimen 3 in experiment 2, just before the water-pressing test started, is estimated with:

$$(V_p)_p = \frac{C^{assumed}}{1000}(w/c - 0.19\alpha) \quad (m^3) \tag{8-14}$$

$$P_c = \left[(V_p)_p + V_{air}\right] / V_C^{measured} \quad (m^3/m^3) \tag{8-15}$$

Where $(V_p)_p$ Total volume of the pores in the cement paste (m^3)

$C^{assumed}$	Cement content from the chemical analyses in chapter 7.4 (kg)
w/c	Water to cement ratio (kg/kg)
α	Degree of hydration (-)
P_c	Total porosity of the concrete (m^3/m^3)
V_{air}	Volume of air pores due to air additives or compaction (m^3)
$V_c^{measured}$	Measured volume of the concrete slice (m^3)

The residual total porosity P_c in the leached specimen 3 is measured (chapter 7.5). The specimen became more porous in the upstream slice no 5, when the specimen was leached, see figure 8-7. The increases in porosity in this part make sense. It is evident that more leaching has occurred at the upstream part of the specimen. This indicates that leaching is not homogenous over the entire volume but that leaching occurs as a sort of "moving boundary". The reason probably is that when water flows in the downstream direction from the upstream part, it became saturated by lime and therefore cannot dissolve more lime. A contributing factor is that diffusion upstream might have occurred making the dissolution bigger at the upstream part. The tighter the upstream face is, i.e. no, or very few and small flow pipes, the more is lost due to diffusion in upstream direction. When the flow pipes are wider, the water flows more easily in downstream direction, carrying more dissolved material with it.

The measured residual porosity minus the estimated initial porosity gives the solid volume that has leached during the leaching experiment. Data from figure 8-7 gives:

$V_{leached} = 1.4 \cdot 10^{-6}$ (m^3)

Where $V_{leached}$ Volume of leached solid material as the measured residual $(V_p)_p$ including the V_{air} minus assumed the initial $(V_p)_p$ (m^3)

In chapter 8.2.3, the total loss of Ca to the drainage water was estimated to be some where between 3.6 and 7.5 g. Assuming Ca coming only from $Ca(OH)_2$ and calculate with 3.6 g of Ca loss the following volume of solid material is leached:

$V'_{leached} = 3.6 \text{ g} / 40 \text{ g/mole} \cdot 74 \text{ g/mole} / \sim 2300 \cdot 10^3 \text{ g/m}^3 = 2.9 \cdot 10^{-6} \text{ m}^3$

The estimated loss of material in this study ($1.4 \cdot 10^{-6}$ m^3) seems to be in rather good agreement with the estimated loss of material from the study of leached ions in the drainage water ($2.9 \cdot 10^{-6}$ m^3).

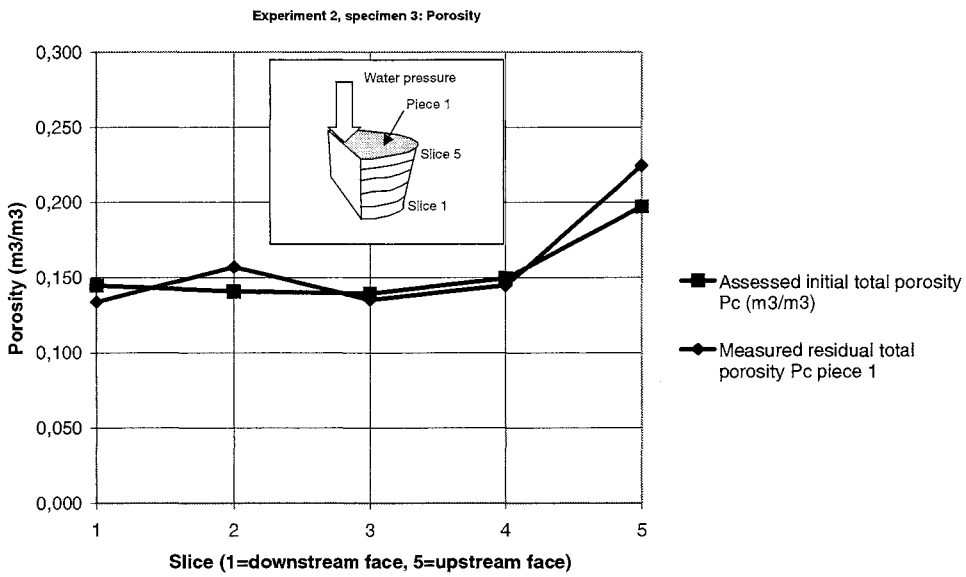

Figure 8-8 Initial and residual total porosity P_c of concrete specimen 3 in experiment 2.

Not only the total porosity is interesting to know but, even more interesting is it to estimate the effect of leaching on the pore size distribution. Comparison between the initial pore size distribution after leaching give important information for an analysis of the leaching process; how water permeability is related to the pore distribution, from which pores the leached material is taken, and how the size of these pores has changed.

One measurement of the pore size distribution was made (chapter 7.5). The test was unfortunately interrupted, so no data is available above air pressure 30 (bar) corresponding to 0.049 μm of pore diameter or a relative humidity (RH) of 97.8 %. The capillary volume $(V_{cap})_c$ of the concrete specimen is approximately:

$(V_{cap})_c = 241/1000*(0.8-0.39*0.9) = 0.108\ (m^3/m^3)$

The measured pore volumes in figure 7-15 of about 0.03 to 0.06 m^3/m^3 are therefore reasonable. The shape of the distribution up to 10 (μm) agrees fairly well with figure 2-12 from Grattan-Bellew (1996).

It is quite clear that determination of the pore size distribution by the technique used here or by mercury porosimetry is promising methods to use in future experiments.

8.5 Mechanical properties

8.5.1 Compressive strength

The compressive strength for five leached specimens 1, 3, 6, 8 and 10 (see chapter 4 and 6 for description of the specimens) was performed, using a strength test machine.
Generally it can be said, that the number of tested cylinders was too low for any safe statistical determination of the initial and residual compressive strength. The standard deviation for the different concrete types was too large. Anyhow, some trends can be seen. Leached specimens have lost some of their strength compared to the reference specimens. All specimens, except

specimen 3, got a reduced strength after they had been leached, see chapter 7.6.1 and Appendix 7-7.
More data will be available in the near future.

8.5.2 Elastic modulus

All tested cylinders, except the one from specimen 3, have a reduced E-modulus when they were leached, see Appendix 7-8.

8.6 Leaching model 1 versus the experimental results

The observed leaching process in the experiments is compared with the leaching model described in chapter 3.2 and the strength model described in chapter 3.3. The model gives the flow of water by a reduced Poiseuille flow in assumed flow pipes with a reduction factor due to the deviation between a real flow pipe and a perfect cylinder. The leaching and strength models seem to give rather correlating results using the measured data from the experiments performed.

However, the input variables are in many cases simply estimated and ought to be studied more in future studies. Besides, the model does not regard diffusion of ions or balance of ions in the pore solution in the flow pipes. The assumption of no diffusion is a large simplification considering the great concentration gradient in the upstream part of the concrete specimens due to the pure inlet-water.

The model is calculated for specimens 1, 2, 7 and 10 from experiment 2 and the results are compared with measured values. For some specimens, more than one calculation is made with different input variables. The different calculation is in such cases denoted "run 1", "run 2", etc.

Input data used for the leaching model and strength model and the results is shown in the figures 8-8 to 8-13. The calculation of water flow, leaching of solid material and changes in compressive strength is performed by the equation scheme below. Observe that only the most important equations is showed here, some more equations from chapter 3.2 is needed to achieve the equations below.

The reduction factor r_w, the maximum pipe diameter ϕ_{max}, the solubility parameter *rate* and the *share* of the total porosity that convey water is set so that the permeability at time zero (k(0)), the permeability at the test stop (k(stop)) and the shape of the calculated permeability curve between this two times fits the observed time-permeability curves for specimens 1, 2, 7 and 10 in Appendix 7-1. The calculations were made, using the spreadsheet program Excel.

For t=1:T
  For i=1:N

$$q_w^i(t) = k_w^i(t) \cdot \frac{\Delta P_w}{L} \cdot A_i \tag{3-1}$$

$$k_w^i(t) = n_i \cdot \frac{(\phi_t^i)^2}{32\mu} \rho_w g \cdot r_w \tag{3-2}$$

$$dm_i = q_{ion} \cdot \Delta t = q_w^i(t) \cdot c \cdot \Delta t \tag{3-9}$$

$$\phi_t^i = \sqrt{\frac{4 \cdot dm_i}{n_i \cdot \pi \cdot L \cdot \rho_M} + (\phi_{t-1}^i)^2} \tag{3-13}$$

$$P_p(t) = \frac{(V_p)_p + \sum_i V^i_{pipe.leached}}{V_p} \quad (3\text{-}14)$$

Next i

$$g(f_{cc}) = f_{pc} \cdot a \cdot (w/c)^b \quad (3\text{-}20)$$

Next t

Where t Time step (hour)
T Total calculation time (hour)
i Calculation for pipe size *i*
N Number or different pipe sizes (nos.)

See chapter 3 for explanation of the notations used in the equations and in the figures.

Specimen 1, experiment 2:

Two different calculation runs was performed for specimen 1, run 1 (figure 8-9) and run 2 (figure 8-10).

In run 1, the input variables *rate, share,* r_w, and ϕ_{max} was set to 1.5, 0.4, 10^{-4} and 257 μm respectively. The received permeability from this run 1 was in good correlation with the measured permeability. The initial value was calculated to $4.7 \cdot 10^{-11}$ m/s against the measured $8 \cdot 10^{-11}$ m/s and the value at 2000 hours was calculated to $1.5 \cdot 10^{-8}$ m/s against the measured $1.6 \cdot 10^{-8}$ m/s. The permeability between these two times was about the same. The measured curve is however steeper at the time when the permeability accelerated.

In run 2, the input variables *rate, share,* r_w, and ϕ_{max} was set to 1.5, 0.0004, 10^{-3} and 91 μm respectively. The received permeability from this run 2 was also in good correlation with the measured permeability, except the initial value. The initial value was calculated to $7 \cdot 10^{-14}$ m/s against the measured $8 \cdot 10^{-11}$ m/s and the value at 2000 hours was calculated to $1.2 \cdot 10^{-8}$ m/s against the measured $1.6 \cdot 10^{-8}$ m/s. The permeability between these two times correlated better than for run 1 with a steeper acceleration.

In run 1 the flow pipes are coarser (ϕ_{max}=257 μm) and a larger share of the pipes lead water (*share* =0.4) compared to run 2 where ϕ_{max} was 91 μm and the *share* was 0.004. On the other hand, water is assumed not to flow so easy through the specimen in run 1, the reduction due to tortuous pipes r_w is $r_w=10^{-4}$ compared with 10^{-3} for run 2. So, the more and larger but less permeable flow pipes in run 1 cause almost the same evolution of water flow during time as the fewer and smaller, but more permeable flow pipes in run 2. The permeability curves in both run follows the measured flow of water quite good. Run 2 however, gives a much lower initial permeability and also a more rapid increase in water-flow. By setting the fictitious strength f_0 to 340 Mpa, the initial values of the compressive strength fit to the measured value for both runs. At the stop time 2060 h for the test, the strength is too low (29 MPa) in run 1 and too high (46 MPa) in run 2 compared to the measured values (36 MPa). All input and output data are shown in the figures.

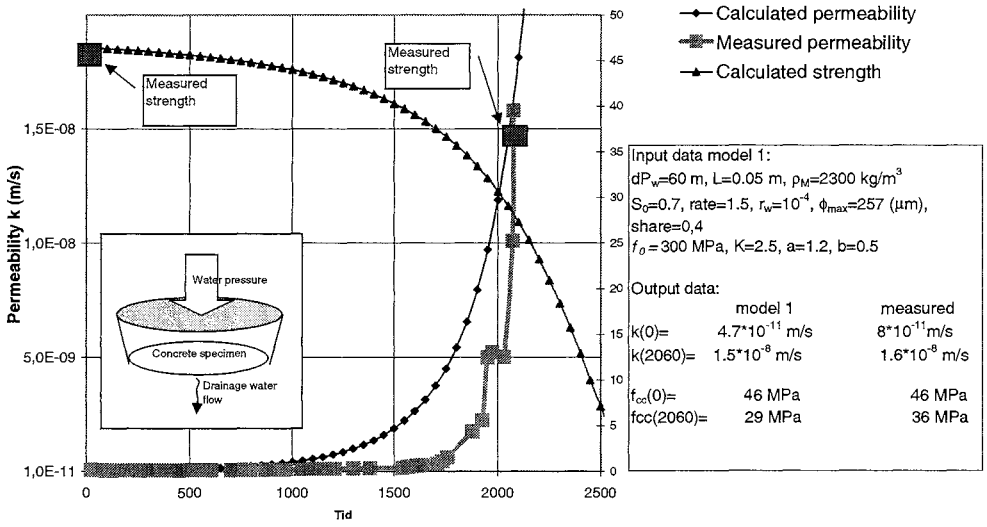

Figure 8-9 Specimen 1, exp. 2; Late-dried w/c 0.8. A comparison of permeability and strength between model 1 and measured values. See chapter 3 for explanation of used notations.

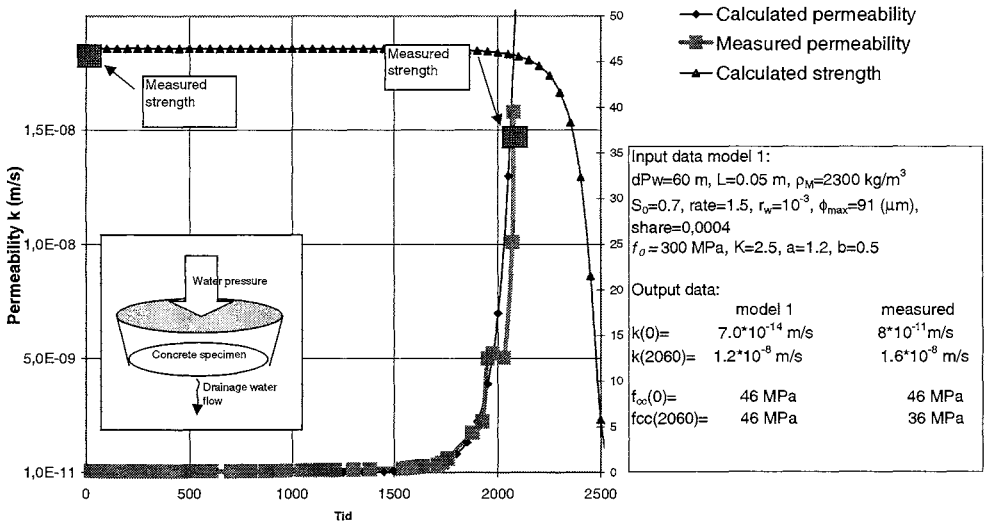

Figure 8-10 Specimen 1, exp. 2; Late-dried w/c 0.8. A comparison of permeability and strength between model 1 and measured values. See chapter 3 for explanation of used notations.

Specimen 2, experiment 2:

Two different calculations were performed for specimen 2, run1 (figure 8-11) and run2 (figure 8-12). In run1, the flow pipes were supposed to be almost as coarse (ϕ_{max}) as for run 1 for

the late-dried specimen 1 and the *share* of the flow pipes that can lead water is also the same. The difference is that the reduction parameter r_w is set much smaller, so the calculated permeability became the 100 times smaller permeability that was observed in the experiment. The time evolution of the water-flow follows the measured rather well in run 1. In run 2, the *share* of water flow in the flow pipes in relation to the total flow is decreased to 0.04 and the reduction due to deviation between a real pore and a perfect cylinder r_w is increased to 10^{-5}. The initial permeability k(0), is the same as in run1, but the time evolution is not the same and does not at all follow the measured curve.

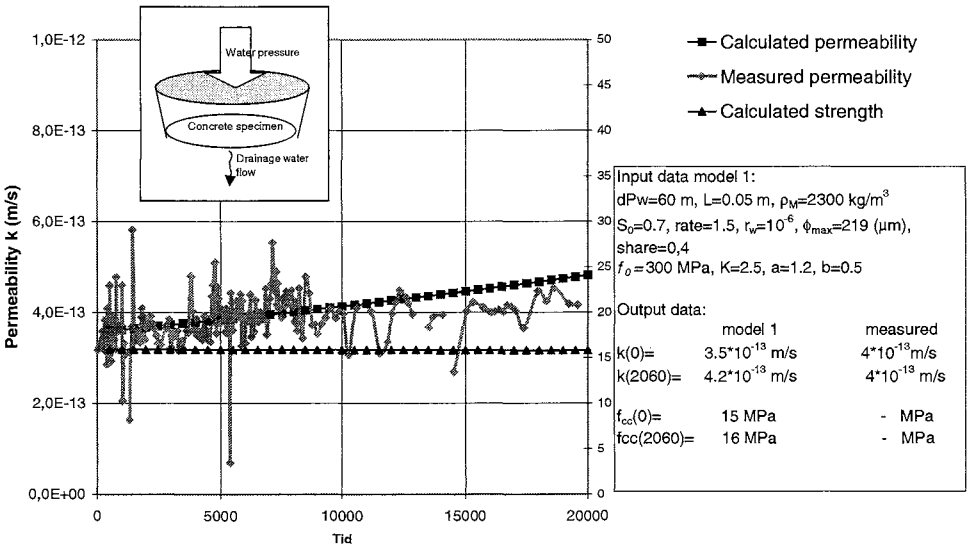

Figure 8-11 Specimen 2, exp. 2; Virgin w/c 0.8. A comparison of permeability and strength between model 1 and measured values. See chapter 3 for explanation of used notations.

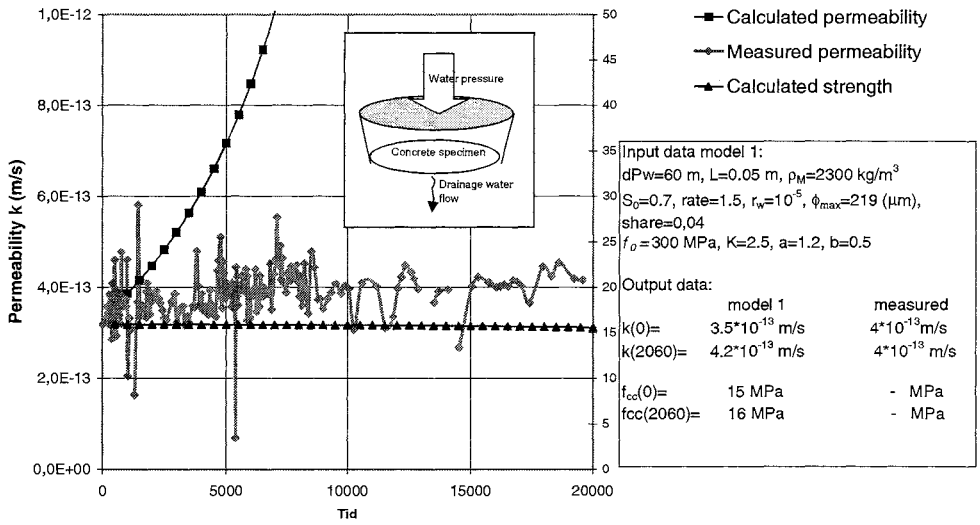

Figure 8-12 Specimen 2, exp. 2; Virgin w/c 0.8. A comparison of permeability and strength between model 1 and measured values. See chapter 3 for explanation of used notations.

Specimen 7, experiment 2:

For late-dried w/c 1.3 specimen 7 in figure 8-13, the flow pipes (ϕ_{max}) are rather coarse and there are also many pipes that can percolate water; i.e. the *share* of water flow in pipes is high. This leads to a good fitting to the measured permeability curve. The exponent K in the strength relation in equation (3-16) is changed to 1.9 to have a good fitting to the measured initial strength.

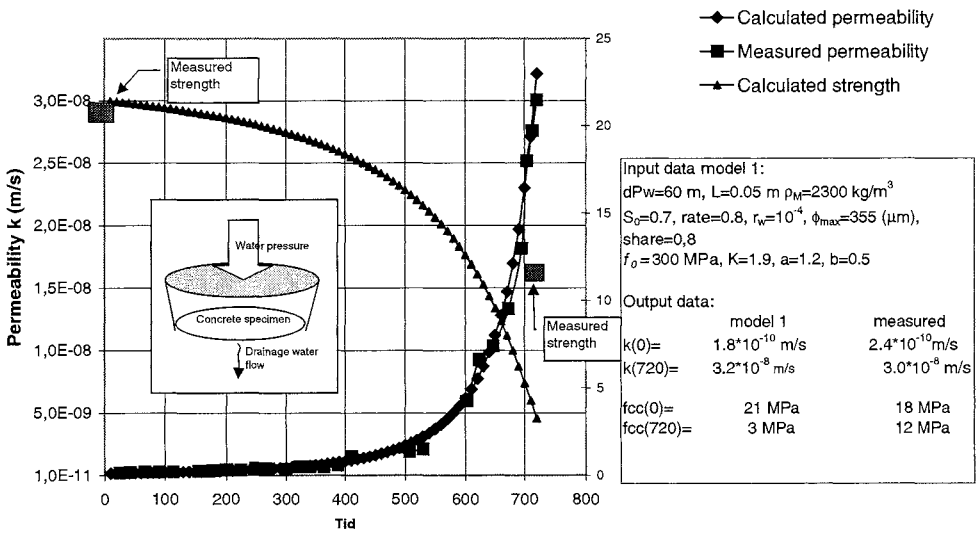

Figure 8-13 Specimen 7, exp. 2; Late-dried w/c 1.3. A comparison of permeability and strength between model 1 and measured values. Input data due to table 4, model 1a. See chapter 3 for explanation of used notations.

Specimen 10, experiment 2:

For virgin w/c 1.3 specimen 10 in figure 8-14, the assumed size of the flow pipes is assumed to be the same (ϕ_{max}) as for the late-dried variant of w/c 1.3 (specimen 7). In the calculations of specimens 1 and 2 (w/c 0.8) that is showed above, the selected value of ϕ_{max} was a little lower for the virgin than for the late-dried variant, but here it is the same (ϕ_{max}=355μm). There is a somewhat smaller selected *share* of the pipes that can lead water in specimen 10 (*share*=0.4) than in specimen 7 (*share*=0.8) and the pipes are selected approximately the same permeable (r_w) for specimen 10 and specimen 7. This leads to a good fitting to the measured permeability curve. The exponent K in equation (3-15) is 1.9, as for specimen 7, to have a good fitting to the measured initial strength.

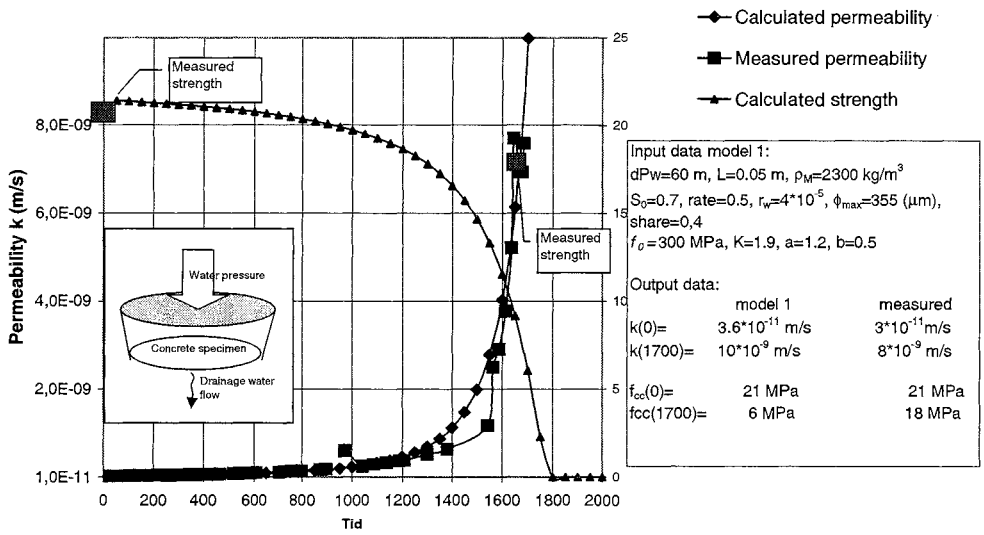

Figure 8-14 Specimen 10, exp. 2; Virgin w/c 1.3. A comparison of permeability and strength between model 1 and measured values. See chapter 3 for explanation of used notations.

Conclusion

Leaching model 1 described in chapter 3.2 and the strength model in chapter 3.3 have a simple and physically reasonable basis. The parameters used C, W, V_{air}, dP_w, L and c_0 are determined by the experiment while the parameters ϕ_{max}, *share*, r_w, and *rate* are selected to fit the experimental results of permeability. With these input parameters, the model and the experimental data corresponds very well with each other.

The chose of variables must however be discussed more before it can be said to be a good model. So far input data concerning the flow pipe size and the share of water flowing in these pipes are selected so that a good correlation with experiments is obtained. In a good model, the data should be based on observations.

A weak point of the model is that it only considers flow of Ca-ions due to convection (by the water flow). Diffusion must be regarded where there are large concentration gradients and when the concrete is of high quality with small flow pipes. Besides, the mass balance between different ions in the pore solution is not regarded in model 1. This is of minor importance for high permeable specimens with many, coarse flow pipes, because $Ca(OH)_2$ almost directly after start of the test becomes the main dissolved compound. The other compounds in cement paste have either already leached out due to their high solubility and small initial content (KOH and NaOH), or they have a low solubility.

8.7 Dissolution of $Ca(OH)_2$ in pure water

As can be seen in figure 8-15, the measured dissolving process was very rapid at the beginning. The measured dissolution should have been even more rapid if the solution had been stirred from the beginning. Now, stirring started after 240 seconds.

The dissolving reaction is also calculated (figure 8-14) by the calculation scheme "model Guntelberg" in chapter 2.2.1 and with the method in chapter 3.5, which describes a dissolving reaction.

Calculation simulates the dissolution in cavities between particles. The following data were used in the model; the particle diameter ϕ is $2 \cdot 10^{-4}$ m, the diffusion coefficient in the pore solution in the cavities $k_{ion(aq)}$ is 10^{-10} m^2/s, the diffusion layer in each solid particle $t_{(s)}$ is 10^{-9} m and the diffusion coefficient in the diffusion layer in the solid particle to $k_{ion(s)}$ is 10^{-11} m^2/s. The variables used are assumed, but quite reasonable.

The calculation gives surprisingly good agreements with the measured values (figure 8-14). One calculation used the solubility product $K_{sp} = 4 \cdot 10^{-6}$ and the other calculation used $K_{sp} = 6 \cdot 10^{-6}$. The one with $K_{sp} = 4 \cdot 10^{-6}$ fitted the measured dissolution curve before the stirring and the other with $K_{sp} = 6 \cdot 10^{-6}$ seems to fit a measured curve if it had been stirred from the start. The stirring made of course the solubility increase.

Due to Atkins & Jones (1997) and Aylward & Findlay (1994), the K_{sp} should be about $6 \cdot 10^{-6}$, so the used values of K_{sp} seems reasonable.

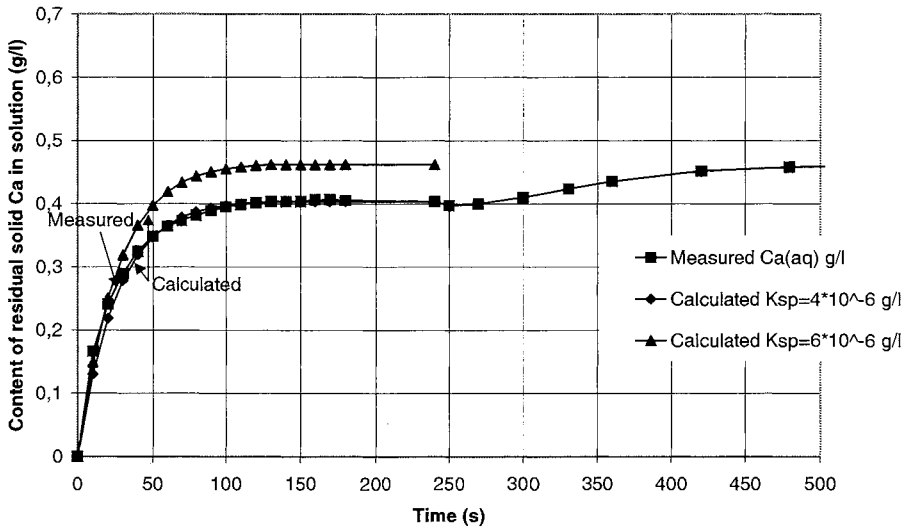

Figure 8-15 Measured and calculated dissolving of $Ca(OH)_2$(s) in pure water.

8.8 Conclusions

8.8.1 Experiments

The purpose of this work was to study the flow of de-ionised water under pressure through homogenous concrete of different qualities and curing history and the leaching effect of this water flow.

The laboratory test was *accelerated* regarding (i) the pressure gradient which is about 100 times higher than in a real structure, (ii) the water to cement ratio which is not below 0.80 although the normal value in structures is 0.55 to 0.60, and (iii) the water aggressiveness; de-ionized. On the other hand, the test was *retarded* since there were no aggressive ions in the water (CO_2, H^+, SO_4^{2-}, etc) and the temperature was constant at 20°C.

The experimental results show that percolating pure water through concrete specimens have an ability to dissolve hydration products, probably mainly $Ca(OH)_2$, and also to carry the dissolved ions out of the specimen by diffusion or convection.

Depending on the w/c ratio and the curing history, the permeability was different. A high hydration ratio made the specimens more porous with higher water permeability.

Virgin specimens had a low and constant permeability with small deviations between the specimens. However, one w/c 0.8 and one w/c 1.3 had a rapidly increased permeability after some time. Probably the same will happen with the other specimens after longer time of leaching.

Late-dried specimens, became 100 times more permeable than in the virgin state. This was probably caused by micro-cracks during the drying. Because of the high hydration ratio almost all cement had been consumed and there was not much cement left for any self-healing. These specimens had often a rapidly increased permeability after some time.

Early-heated specimens, had a about 100 times higher initial water permeability than in the virgin state. Then, the permeability rapidly decreased due to a restarted hydration and a resulting self-healing to near the same value as in the virgin state. Probably these specimens will also reach the point where the permeability rapidly increase. It is only a matter of time.

In the high-permeable concrete, the water seems to have flowed in a rather few, distinct flow pipes. In these pipes, the water had dissolved solids, probably mainly $Ca(OH)_2$) and the pipes grew wider. Then, the water flow increased further and even more solid material was leached. Finally, the pipe walls became so exhausted in lime so that the leaching rate and the water flow increased only slowly. The dissolution of the pipe walls was a diffusion process from the interior of the solid and towards the pipe wall. Around these pipes the concrete became very disintegrated with almost no continuos cementitious material left to maintain strength and tightness.

Between the flow pipes, or in less permeable concrete, more of the leaching seemed to be governed by diffusion to the inlet water at the upstream end.

A detailed analysis of one specimen, showed that most calcium was leached from the upstream part of the specimen. This was probably due to diffusion in the upstream direction. Another possibility is that the permeating water became saturated with lime already at the upstream part due to dissolution of lime there. Therefore, its dissolving ability was very much reduced when it reached the deeper parts of the specimen. Another part of the specimen, which lost quite lot calcium, was where the aggregate content was high. The cause of the leaching in this part was probably due to water percolation in porous and easily soluble areas. Because of leaching, the porosity was increased in these parts of the specimen.

The measured residual content of substances in the leached specimens corresponded fairly well to the measured ionic flow in the drainage water flow.

The results also show that when solid material is leached, the porosity will increase and the strength will decrease due to less load-bearing solids. The strength reduction due to leaching, was to a high degree a local phenomenon. In parts of the specimen, where much solid material had been leached, the strength was very much reduced. But if these parts were small compared to the whole specimen, the average strength of the whole specimen was not much influenced. The number of specimens used for strength testing were however too few for any more detailed analysis.

8.8.2 Modelling

The leaching model 1 is very simple, but despite this, it gave interesting results. This model imitates leaching by assuming that there are a certain number of flow pipes in the concrete. The flow of water was assessed by a "reduced" Hagen-Poiseuille law.

However, the pipes were modelled with only one element through the whole body and because of this, no gradients of the leaching effects could be predicted. Another weak point in the model is that no diffusion in the upstream direction is regarded. The experiment shows that diffusion upstream to the pure water at the inlet was strong. Also, the dissolving reaction term was modelled in a very simplified manner. The model is simply calculated using an Excel file. It can easily be connected to ordinary static calculations for estimations of the safety marginal for a concrete dam during time.

8.8.3 Future research

The following additional research ought to be made:

- ✓ A more precise study of the diffusion of ions upstream in addition to the study performed in this work of the convection of ions downstream.
- ✓ Future experiments should regard leaching in cracks or larger flow pipes. These can be artificially be produced in the concrete specimens before the leaching test starts.
- ✓ ESEM and MIP studies from the leached cracks or flow pipes should be used for investigating chemical and physical changes of the structure.
- ✓ A comprehensive study of the strength of leached specimens.
- ✓ Development of more sophisticated models that take consideration to the more complicated features in the leaching process. For example, the balance of mass (equation 2-2) can be formulated and solved by the Finite Element Method. This requires development of the individual terms in the equation and also verification by experiments.

References

Adenot, F., Richet, C. (1997), *Modelling of the chemical degradation of a cement paste,* Mechanisms of chemical degradation of cement based systems, E & FN Spon, London.

Alemo, J., Johansson, N., Bronner, N. (1988), *Dissolution of cement grout by flowing water,* Vattenfall Utveckling och Miljö, 1988, Råcksta, Vällingby.

Atkins, P., Jones, L. (1997), *Chemistry Molecules, Matter, and Change*, 3rd edition, W. H. Freeman and Company, New York.

Aylward, G., Findlay, T. (1994), *S I Chemical Data (SICD)*, John Wiley & Son, 3rd edition.

Ayora, C. et al (1998), *Weathering of iron sulfides and concrete alteration: Thermodynamic model and observation in dams from central Pyrenees, Spain,* Cem. & Concr. Res. Vol. 28, no. 9, pp 1223-1235.

Bal´shin (1949), *Relation of mechanical properties of powder metals and their porosity and the ultimate properties of porous metal-ceramic materials,* Dokl. Akad. Nauk. SSSR, 67, 5.

Beckman O., Kjöllerström B., Sundström T. (1986), *Basic thermodynamics for college studies,* (in Swedish), Almqvist & Wiksell, Sweden.

Bentz, D. P., Garboczi, E. J. (1991a) *A digitized simulation model for microstructureal development,* Advances in Cementitious Materials, Ceramic Transactions Vol. 16, pp. 211-226.

Bentz, D. P., Garboczi, E.J. (1991b) *Percolation of phases in a three-dimensional cement paste microstructural model*, Cement and Concrete Research, Vol. 21, pp. 325-344.

Bentz, D. P., Garboczi, E. J. (1992), *Modelling the leaching of calcium hydroxide from cement paste: effects on pore space percolation and diffusivity,* Materials and Structures, Vol. 25, 523-533.

Bentz, D. P. (1999), *Modelling cement microstructure: Pixels, particles, and property prediction,* Materials and Structures, Vol. 32, 187-195.

Berner, U. R. (1988), *Modelling the incongruent dissolution of hydrated cement minerals*, Radiochimica Acta, 44/45, pp. 387-393.

BBK 94, *Concrete structures*, (in Swedish), Boverket 1994.

BTG M, *The concrete Handbook Material ed. 2*, (in Swedish), Svensk Byggtjänst, Stockholm 1994.

Carde, C., Francois, R. (1997), *Aging damage model of concrete behavior during the leaching process*, Materials and Structures Vol. 30, pp 465-472.

Carde, C., Francois, R. (1997), "Effect of ITZ leaching on durability of cement-based materials", Cement and Concrete Research, Vol. 27, pp 971-978.

Carde, C., Francois, R., Torrenti, J-M. (1996), *Leaching of both calcium hydroxide and C-S-H from cement paste: Modelling the mechanical behaviour*, Cement and Concrete research, Vol. 26, No. 8, pp. 1257-1268.

Carde, C., Francois, R., Ollivier, J-P. (1995), *Microstructural changes and mechanical effects due to the leaching of calcium hydroxide from cement paste.* Proceedings of the Materials Research Society's Symposium on Mechanisms of Chemical Degradation of Cement-based Systems, Boston, 27-30.

Carde, C., Francois, R., Ollivier, J-P (1997), *Microstructural changes and mechanical effects due to the leaching of calcium hydroxide from cement paste.* Mechanisms of chemical degradation of cement based systems, E & FN Spon 1997, London.

Carde, C., Francois, R. (1997), "Effect of the leaching of calcium hydroxide from cement paste on mechanical and physical properties", Cement and Concrete Research, Vol. 27, pp 539-550.

Cederwall, K. (1979), *Hydraulics for civil engineers,* (in Swedish), Liber läromedel, Malmö.

Constantiner, D., Diamond, S. (1995), *Pore solution analysis: Are there pressure effects?*, Proceedings of the Materials Research Society's Symposium on Mechanisms of Chemical Degradation of Cement-based Systems, Boston, 27-30.

Davis R. E. (1950), *"Permeability and Triaxial Tests of Lean Mass Concrete"*, Corps of Engineer.

Delagrave, A., Gerard, B., Marchand, J. (1997), *Modelling the calcium leaching mechanisms in hydrated cement pastes,* Mechanisms of chemical degradation of cement based systems, E & FN Spon, London.

Duchesne, J., Reardon, E. J. (1995), *Measurement and prediction of portlandite solubility in alkali solutions,* Cement & Concrete Research, vol. 25, no. 5, pp 1043-1053.

Edvardsen, C. (1996), *Water permeability and autogenous healing of cracks in concrete*, (in German), Heft 455, Deutscher Ausschuss für Stahlbeton, Berlin.

Ekström, T. (2000), *Leaching of concrete Experiments and Modelling,* Licentiate thesis report TVBM – 7153, Div. of Building Materials, Lund Institute of Technology.

Engkvist, I., Albinsson, Y., Johansson Engkvist, W. (1996), *The long term stability of cement – Leaching tests*, SKB technical report 96-09, KTH, Göteborg.

Eriksen, K., *Cores from the Storfinnforsen dam,* (in Danish), Statens Vejlaboratorium, Roskilde, Denmark.

Fagerlund, G. (1980), *Moisture-mechanical properties*, (in Swedish), The concrete Handbook Material, Svensk Byggtjänst, Stockholm.

Fagerlund, G. (1987), *Relations between the strength and the degree of hydration or porosity of cement paste, cement mortar and concrete,* Seminar on Hydration of Cement, Aalborg Portland, Aalborg.

Fagerlund, G. (1989), *Concrete for hydraulic structures*, (in Swedish), CEMENTA, Danderyd.

Fagerlund, G. (1991), *Freeze testing of concrete from the Storfinnforsen dam,* (in Swedish), Div. of Building Materials, Lund Institute of Technology.

Fagerlund, G. (1994), *Structure and development of structure*, (in Swedish), The concrete Handbook Material, Svensk Byggtjänst, Stockholm.

Fagerlund G. (1996), *Service life prediction of concrete structures*, (in Swedish), report TVBM-3070, Lund.

Fagerlund, G. (1997), *Deterioration, service life and repair of concrete structures-knowledge and research needs*, Div. of Building Materials, Lund Institute of Technology.

Fagerlund, G. (1997a), *Composite models and composite formulas*, (in Swedish), Compendium in Building Material Div. of Building Materials, Lund Institute of Technology.

Fagerlund, G. (1997b), *The chemistry of cement based binder*, (in Swedish), Compendium in Building Material Div. of Building Materials, Lund Institute of Technology.

Fagerlund, G. (1997c), *Temperature development in concrete*, (in Swedish), Compendium in Building Material Div. of Building Materials, Lund Institute of Technology.

Fagerlund, G. (2000), *Leaching of concrete*, contribution to EU-project CONTECVET, Div. of Building Materials, Lund Institute of Technology.

Faucon, P., Bonville, P., Adenot, F., Genand-Riondet, N., Jacquionot, J., Virlet, J. (1997), *^{57}Fe Mössbauer study of cement water degradation*, Advances in Cement Research, 9, No 35, pp. 99-104.

Faucon, P., Gerard, B., Jacquinot, J., Marchand, J. (1996), *Leaching of cement: study of the surface layer*, Cement and Concrete Research, vol. 26, no. 11, pp 1707-1715.

Faucon, P., Adenot, F., Jacquionot, J., Petit, J., Cabrillac, R, Jordan, M. (1998), *Long-term behaviour of cement pastes used for nuclear waste disposal: Review of physico-chemical mechanisms of water degradation*, Cement & Concrete Research, vol. 28, No.6, pp. 847-857.

Freeze, R. A., Cherry, J. A. (unknown), *Groundwater*, Dep. Of Geological Sciences, Univ. Of British Columbia, Vancouver.

Garboczi, E. J., Bentz, D.P. (1992), *Computer simulation of the diffusivity of cement-based materials,* J. Mater. Sci. 27.

Garbotczi, E. J., Bentz, D. P. (1996), *Multi-Scale Picture of concrete and its transport properties: Introduction for non-cement researchers*, NISTIR 5900, Gaitersburg, U.S.A.

Garboczi, E. J., Bentz, D.P. (1998), *Modelling Analytical/Numerical theory of the diffusivity of concrete,* Advances in Cement Based Materials 1998;8:77-88.

Granholm, H., Werner, D., Giertz-Hedström, S. (1934), *Investigation of the suitability of concrete pipes for road drainage*, (in Swedish), Betong, 1934(19):1, p.1-84.

Grattan-Bellew, P. E. (1996), *Microstructural investigation of deteriorated Portland cement concretes*, Construction and Building Materials, Vol. 10, No. 1, pp. 3-16.

Grube, H. and Rechenberg, W. (1989), *Durability of concrete structures in acidic water*, Cement and Concrete Research, Vol. 19, pp. 783-792.

Halvorsen, U. (1966), *Corrosion of steel and leaching of lime near cracks in concrete structures*, (in Swedish), Bulletin 1, Div. of Building Technology, Lund Institute of Technology.

Hearn, N., Detwiler, R. J., Sframeli, C. (1994), *Water permeability and microstructure of three old concretes*, Cement and Concrete Research, Vol. 24, No. 4, pp. 633-640.

Hedenblad, G. (1993), *Moisture Permeability of Mature Concrete, Cement Mortar and Cement Paste*, report TVBM-1014, Div. of Building Materials, Lund Institute of Technology.

Hedin, R. (1962), *Processes of Diffusion, Solution and Crystallistation in System* $Ca(OH)_2 - H_2O$, Swedish Cement and Concrete Research Institute, Stockholm.

ICOLD (unknown), *Deterioration of dams and reservoirs, examples and their analysis,* Paris, France.

Imhof-Zeitler, C. (1996), *Fließverhalten von Flüssigheiten in durchgehend gerissenen Betonkonstruktionen,* (in German), Heft 460, Deutscher Ausschuss für Stahlbeton, Berlin.

Janz, M. (1997), *Methods of measuring the moisture diffusivity at high moisture levels*, Report TVBM 3076, Div. of Building Materials, Lund Institute of Technology.

Janz, M., *Retention curve and pore size distribution measured with pressure plate and pressure membrane extractiors, Methods a nd calibration*, Report TVBM-9050, Div. of Building Materials, Lund Institute of Technology.

Jennings, H.M. (1986), *Aqueous solubility relationships for two types of Calcium silicate hydrates*, Journal of the Ceramic Society, 69, pp. 614-618.

Johannesson, B. (1998), *Modelling of transport processes involved in service life prediction of concrete; important principles,* Licentiate thesis report TVBM – 3083, Div. of Building Materials, Lund Institute of Technology.

Koenders, E. (1997), *Simulation of Volume Changes in Hardening Cement-Based Materials.* Delft University Press, Netherlands.

Kriz, D. (1991), Laboratory product handbook, Chemel analys AB, Lund.

Lagerblad, B., Trägårdh, J. (1994), *Conceptual model for concrete long time degradation in a deep nuclear waste repository,* SKB Technical report 95-21, Swedish Cement and Concrete Research Institute, Stockholm.

Lawrence, C. D. (1982), *Permeability measurements on concrete,* Cement and Concrete Association.

Lea, F. M. (1983), *The chemistry of cement and concrete,* third edition, Edward Arnold (Publishers) Ltd, London.

Marchand, J., Samson, E., Maltais, Y. (1999), *Modelling ionic diffusion mechanisms in saturated cement based materials – an overview,* CRIB-Department of civil engineering, Laval Univ., Quebec, G1P4r7.

Mary, M. (1936), contribution to the discussion with Ruettgers, Proceedings of the ACI, vol. 32, pp. 125-129.

Mason P.J. (1990), *The effects of aggressive water on dam concrete,* Water Power & Dam construction.

Melander, R. (1997), *Betongdammars kondition och beständighet,* Licentiate Thesis, Div. of Hydraulic Engineering, Royal Institute of Technology, Stockholm.

Meyers, S. L. (1936), contribution to the discussion with Ruettgers, Proceedings of the ACI, vol. 32, pp. 230-233.

Moskvin, V. (1980), *Concrete and reinforced concrete deterioration and protection,* Mir Publishers, Moscow.

Möller, G., Petersons, N. (1994), *Strength,* (in Swedish), The concrete Handbook Material, Svensk Byggtjänst, Stockholm.

The Swedish National Encyclopaedia, (1989-2000) Sweden.

Nilsson, L.-O. (1994), *Moisture and Concrete,* (in Swedish), The concrete Handbook Material, Svensk Byggtjänst, Stockholm.

Nyame, B. K., Illston, J. M. (1981), "*Relationships between permeability and pore structure of hardened cement paste*", Magazine of Concrete Research, Vol. 33, No. 116.

Ottosen, N., Petersson, H. (1992), *Introduction to Finite Element Method*, Prentice Hall Europe.

Pitzer, K. S. (1991), *Activity coefficients in electrolyte solutions*, p. 75, CRC Press, Boca Raton, FL.

Powers, T. C. (1962), *Physical properties of cement paste,* From: Chemistry of cement. Proceedings of the 4th International Symposium, Washington, 1960. Washington D.C., 1962. National Bureau of Standards, Monograph 43, vol. II, pp. 577-613, 1962.

Powers T. C. (1958), *The physical structure and engineering properties of concrete.* PCA Research & Development Laboratories, Bulletin 90, Chicago.

Persson, B. (1992), *"Högpresterande betongs hydratation, struktur och hållfasthet"*, Report TVBM-1009, Div. of Building Materials, Lund Institute of Technology.

Roehling, S. and Nietner, M., *A model to describe the kinetics of structure formation and strength development*, VTT Symp. 115, ed. Heikki Kukko, 1990 Microstruct. Prop. Concr., 1990, pp.5-51.

Roy, D. M. and Jiang, W. (1995), *Concrete chemical degradation: Ancient analogues and modern evaluation*, Proceedings of the Materials Research Society's Symposium on Mechanisms of Chemical Degradation of Cement-based Systems, Boston, USA, 27-30.

Ruettgers, A. (1936), final reply in discussion, Proceedings of the ACI, vol. 32, pp. 337-389.

Ruettgers, A., Vidal, E. N., Wing, S. P. (1935), *An investigation of the permeability of mass concrete with particular reference to Boulder Dam*, ACI Journal, Proceedings 1935(31):4, pp. 382-416.

Ryshkewitch, T. (1953), *Compression strength of porous sintered alumina and zirconia.* Journal of the American Ceramic Society, vol. 36.

Scheidegger, A. E., (1963) *The physics of flow through porous media*, University of Toronto Press

Seidell, A. (1965), *Solubilities of inorganic and metal-organic compounds*, Princeton.

Seveque, J., Cayeux, M., Elert, M., Nouguier, H. (1992), *Mathematical modelling of redioactive waste leaching*, Cement and Concrete Research. Vol. 22, pp477-488.

Stronach, S. A., Glasser, F. P. (1997), *Modelling the impact of abundant geochemical components on phase stability and solubility of the CaO-SiO_2-H_2O system at 25 °C: Na^+, K^+, SO_4^{2-}, Cl^- and CO_3^{2-}*, Advances in Cement Research, vol. 9, No. 36, pp. 167-181.

Stumm W., Morgan J. J. (1996), *Aquatic chemistry*, John Wiley & Sons, Inc., U.S.A.

Sällström, S. (1964), Investigation of the durability of porous cement mortar exposed to continuing water percolation, (in Swedish), Statens Vattenfallsverk, Preliminary report, Stockholm.

Sällström, S. (1991), The *Storfinnforsen dam; investigation of the status and repair demand of the concrete,* (in Swedish).

Takemoto, K, Takahashi, H., Takagi, S. (1959), *Leaching of lime from various kinds of cement mortar and its effect on the strength*, Japan Cement Engineering Ass., Review of the 13th Cement Meeting, Tokyo.

Terzaghi, R. D. (1948), *Concrete deterioration in a shipway*, Proceedings of the ACI, vol. 44, pp. 977-1005.

Terzaghi, R. D., answer to K. Mather regarding the paper "*Leaching of lime from concrete*, ACI February 1950, pp. 475-477.

Thaulow, T. and Jakobsen, U. H. (1995), *The diagnosis of chemical deterioration of concrete by optical microscopy*, Proceedings of the Materials Research Society's Symposium on Mechanisms of Chemical Degradation of Cement-based Systems, Boston, 27-30.

Taylor H. F. W. (1990),*"Cement chemistry"*, Academic Press, London.

Tremper, B. (1931), *The effect of acid waters on concrete*, Proceedings of the ACI, vol. 28, pp. 1-32.

Trägårdh, J., Lagerblad, B. (1998), *Leaching of 90-year old concrete mortar in contact with stagnant water*, SKB Technical report TR-98-11, Swedish Cement and Concrete Research Institute, Stockholm.

Unsworth, H. P., Lota, J. S., Hubbard, F. H. (unknown magazine and year), *Microstructural and chemical changes during leaching of cementitious materials.*

Wallin, M. (1988), *A fundamental analysis of the Rate of Limestone Dissolution from a Plane geometry*, Licentiate thesis, Department of Chemical Engineer, University of Lund.

Wang, K., Jansen, D., Shah, S. (1997), *Permeability of cracked concrete,* Cement and Concrete Research, Vol. 27, No. 3, pp. 381-393.

White, Frank M. (1979), *Fluid mechanics*, McGraw-Hill.

Winslow, D. N., Diamond S. (1970), *A mercury porosimetry study of the evolution of porosity in portland cement paste.* Journal of Material, 1970(5):3, pp. 564-585.

Ysberg, G. (1979), *Connection between water cement ratio/water-air-cement ratio and compressive strength,* report Ra 3:79, Swedish Cement and Concrete Research Institute, Stockholm.

Young J. F. (1985), *Hydration of portland cement*, Ed. Roy D. M. Institutional Modulus in Cement Science, Materials Research Laboratory, University Park, Pennsylvania State University, Pennsylvania.

Zamorani et al (1986), *Calcium release from cement samples of different size*, Cement and Concrete Research, vol. 16, pp 394-398.

Zienkiewicz, O. C., Taylor, R. L., (1989), *The Finite Element Method,* 4th edition, McGraw-Hill, New York.

APPENDIX TO CHAPTER 5

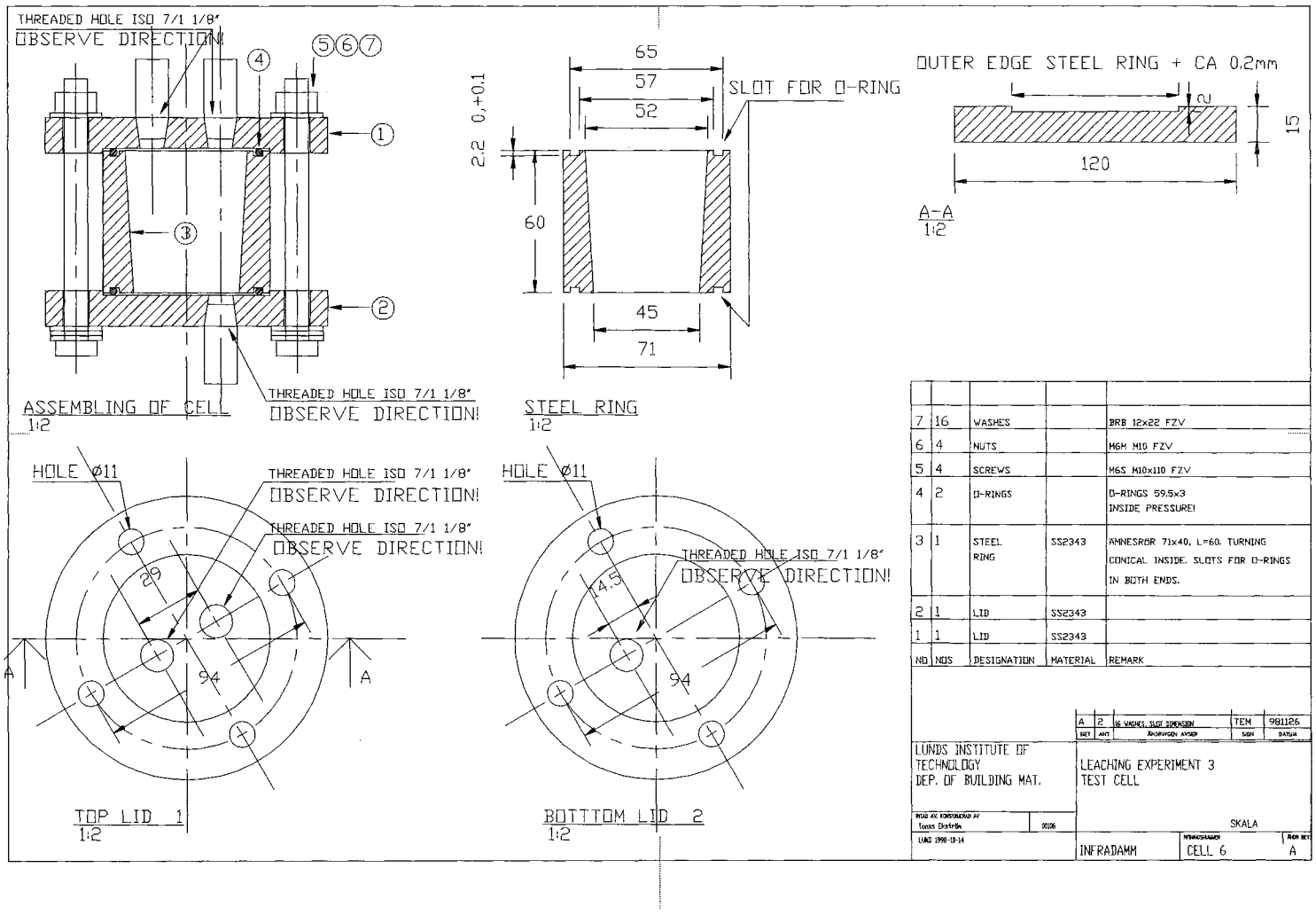

7	16	WASHES		BRB 12x22 FZV
6	4	NUTS		M6M M10 FZV
5	4	SCREWS		M6S M10x110 FZV
4	2	O-RINGS		O-RINGS 59.5x3 INSIDE PRESSURE!
3	1	STEEL RING	SS2343	AMNESRÖR 71x40, L=60. TURNING CONICAL INSIDE. SLOTS FOR O-RINGS IN BOTH ENDS.
2	1	LID	SS2343	
1	1	LID	SS2343	
ND	NOS	DESIGNATION	MATERIAL	REMARK

A	2	16 WASHES, SLOT DIMENSION	TEM	981126
RÄT	ANT	ÄNDRINGEN AVSER	SIGN	DATUM

LUNDS INSTITUTE OF TECHNOLOGY
DEP. OF BUILDING MAT.

UTAD AV KONSTRUERAD AV: Tomas Ekström — 0026
LUND 1998-10-14

LEACHING EXPERIMENT 3
TEST CELL

SKALA

INFRADAMM | CELL 6 | A

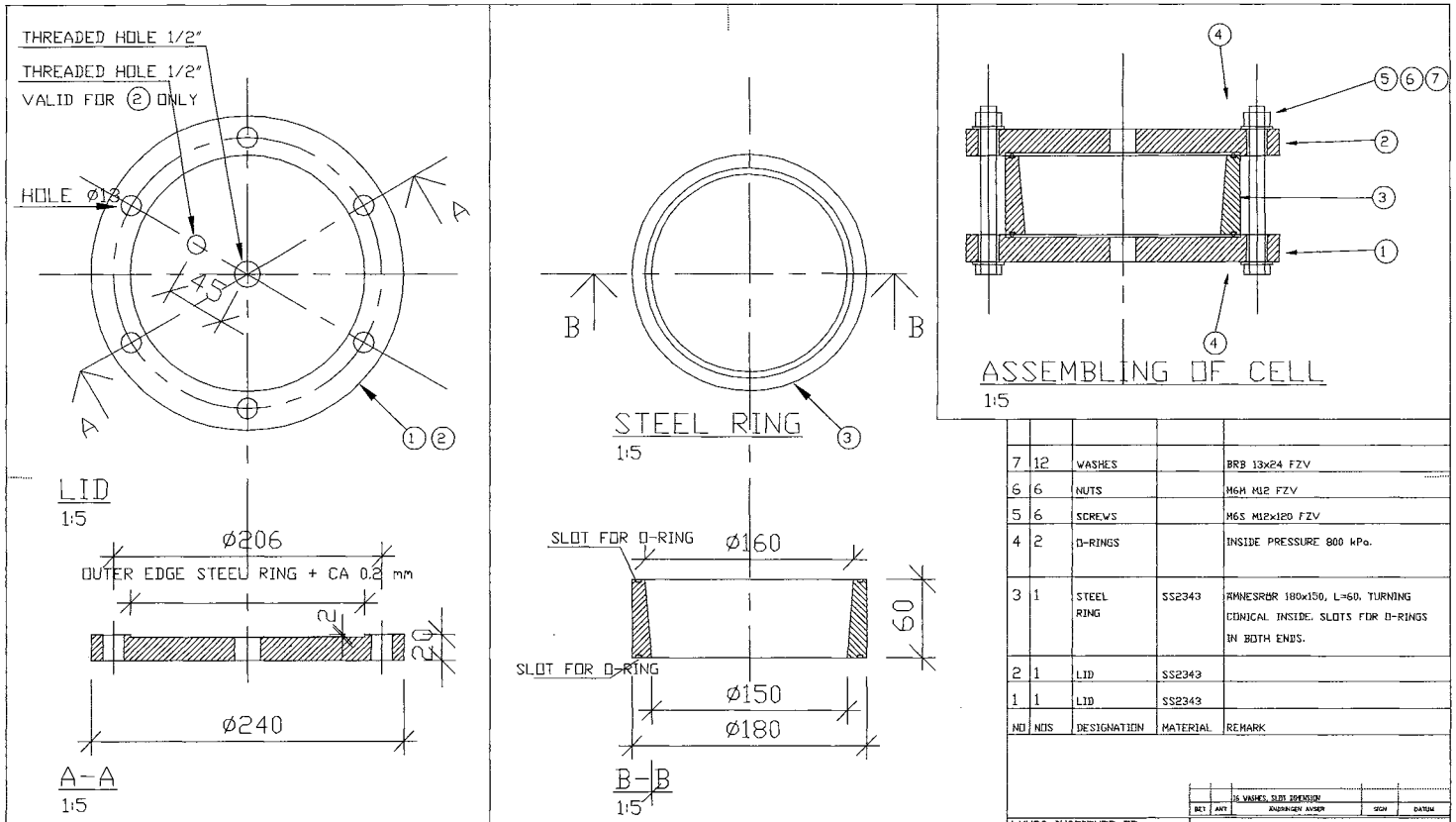

NO	NOS	DESIGNATION	MATERIAL	REMARK
7	12	WASHES		BRB 13x24 FZV
6	6	NUTS		M6M M12 FZV
5	6	SCREWS		M6S M12x120 FZV
4	2	O-RINGS		INSIDE PRESSURE 800 kPa.
3	1	STEEL RING	SS2343	RÖRNESRÖR 180x150, L=60, TURNING CONICAL INSIDE. SLOTS FOR O-RINGS IN BOTH ENDS.
2	1	LID	SS2343	
1	1	LID	SS2343	

BET	ANT	ÄNDRINGEN AVSER	SIGN	DATUM
		16 WASHES, SLOT DIMENSION		

LUNDS INSTITUTE OF TECHNOLOGY
DEP. OF BUILDING MAT.

LEACHING EXPERIMENT 3
TEST CELL

- RELATIONSRITNING
- ARBETSRITNING
- FÖRFRÅGNINGSUNDERLAG
- BYGGNADSLOVSRITNING
- FÖRHANDSKOPIA

RITAD AV, KONSTRUERAD AV: Tonas Ekström — 9606
LUND 1998-10-14

SKALA

INFRADAMM | CELL 6 | A

In the leaching experiment were rubber plugs and rubber balloons used to stop flow of vapor and air to and from the measuring vessels. A permeability test was performed for these plugs and balloons. The leakage appeared to be negligible, see figure 1.

Figure shows that the evaporation was about 200 times less than the smallest measured drainage water flow.

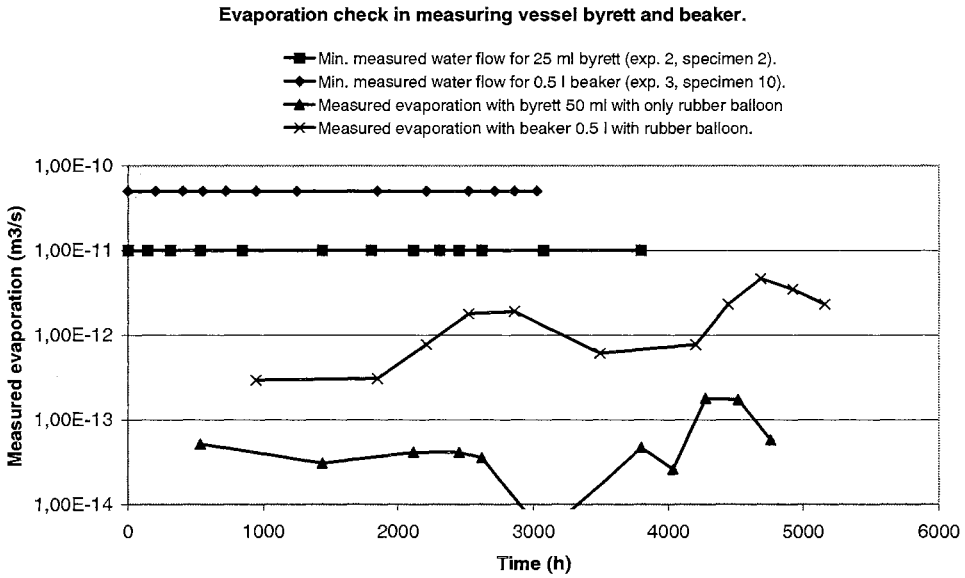

Figure 1 Check of evaporation from measuring vessels.

APPENDIX TO CHAPTER 6

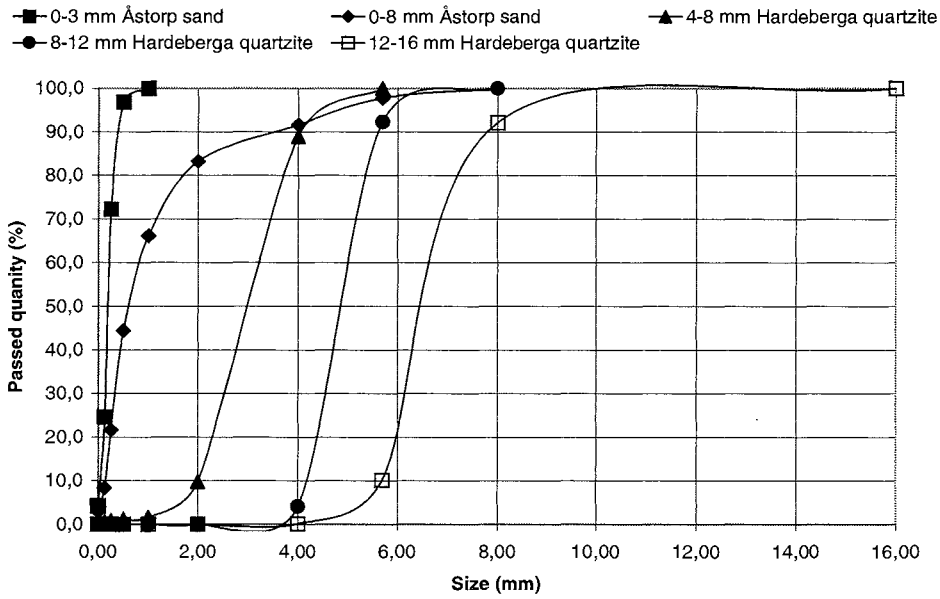

Figure 1 Sieve analyse of aggregate.

Table 1 Concrete recipe for all the specimens in experiment 1 and for specimens 1-2 in experiment 2.

Concrete w/c 0.80	Solid wet mass (kg)	Vapor content (%)	Solid dry mass (kg)	Water mass (kg)	Solid dry mass (kg/m^3)	Water mass (kg/m^3)
Cement			10,98	-	241	-
Mixing water			-	8,21	-	180,4
Aggr. 0-8mm	42,87	0,4	42,70	0,171	938	3,8
Aggr. 8-12mm	21,37	0,11	21,35	0,024	469	0,5
Aggr. 12-16mm	21,73	1,76	21,35	0,382	469	8,4
SUM			96,37	8,79	2117	193,0
w/c			**0,800**			
Aggr. Content of total solid mass			0,89			
Air content (%)			0,6			
Volume (l)			45,52			
Density (kg/m^3)			2310	2375	(measured)	

Table 2 Concrete recipe for specimens 3-5 in experiment 2.

Concrete w/c 0.80	Solid wet mass (kg)	Vapor content (%)	Solid dry mass (kg)	Water mass (kg)	Solid dry mass (kg/m^3)	Water mass (kg/m^3)
Cement			10,98	-	241	-
Mixing water			-	8,48	-	186,0
Aggr. 0-8mm	42,89	0,44	42,70	0,189	936	4,1
Aggr. 8-12mm	21,4	0,11	21,38	0,024	469	0,5
Aggr. 12-16mm	21,4	0,39	21,32	0,083	467	1,8
SUM			96,37	8,78	2113	192,5
w/c			**0,799**			
Aggr. Content of total solid mass			0,89			
Air content (%)			0,8			
Volume (l)			45,60			
Density (kg/m^3)			2306	2370	(measured)	

Table 3 Concrete recipe for specimens 6-10 in experiment 2.

Concrete w/c 1.30	Solid wet mass (kg)	Vapor content (%)	Solid dry mass (kg)	Water mass (kg)	Solid dry mass (kg/m^3)	Water mass (kg/m^3)
Cement			7,2	-	177	-
Mixing water			-	9,08	-	223,2
Aggr. 0-8mm	37,4	0,40	37,25	0,150	916	3,7
Aggr. 8-12mm	18,7	0,20	18,66	0,037	459	0,9
Aggr. 12-16mm	18,7	0,10	18,68	0,019	459	0,5
SUM			81,79	9,29	2010	228,2
w/c			**1,290**			
Aggr. Content of total solid mass			0,91			
Air content (%)			0,8			
Volume (l)			40,69			
Density (kg/m^3)			2239	2317	(measured)	

Table 4 Concrete recipe for specimens 1, 6-7, 20-30 in experiment 3.

Concrete w/c 0.60	Solid wet mass (kg)	Vapor content (%)	Solid dry mass (kg)	Water mass (kg)	Solid dry mass (kg/m^3)	Water mass (kg/m^3)
			9	-	335	-
Mixing water				3,4		126,6
Aggr. 0-3mm					0	0,0
Aggr. 0-8mm	35	5,5	33,08	1,925	1232	71,7
Aggr. 4-8mm	15	0,7	14,90	0,105	555	3,9
SUM			56,97	5,43	2122	202,2
w/c			0,603			
Aggr. Content of total solid mass			0,84			
Air content (%)			1,3			
Volume (l)			26,85			
Density (kg/m^3)			2324			

Table 5 Concrete recipe for specimens 8-10, 31-36 in experiment 3.

Concrete w/c 0.80	Solid wet mass (kg)	Vapor content (%)	Solid dry mass (kg)	Water mass (kg)	Solid dry mass (kg/m^3)	Water mass (kg/m^3)
			9		289	
Mixing water				5,75		184,5
Aggr. 0-3mm					0	0,0
Aggr. 0-8mm	38	3,3	36,75	1,254	1179	40,2
Aggr. 4-8mm	18	1,1	17,80	0,198	571	6,4
SUM			63,548	7,202	2039	231,0
w/c			0,800			
Aggr. Content of total solid mass			0,86			
Air content (%)			1,3			
Volume (l)			31,17			
Density (kg/m^3)			2270	2325		

The air content was measured by the pressure method in an apparatus of type *Bluhm und Feurherdt* containing 8.0 litre.

The volume in the tables were calculated as:

$$V = \frac{C/\rho_{cem} + (W_{mix} + W_{agg})/\rho_w + (Agg_{0-8} + Agg_{8-11} + Agg_{11-16})/\rho_{agg}}{1 - Air}$$

I.e. for concrete table 1:

$$V = \frac{10.98/3.1 + 0.6/1 + 42.7/2.55 + (21.35 + 21.35)/2.64}{1 - 0.006} = 45.5 \ l$$

The cement content per m^3 then become C=10.98/0.0455=241 kg/m^3 which is used in table 1.

To the right of the calculated density is also one measured given.

Table 6 Experiment 1. Casting, curing and leaching test.

Specimen	W/c	Water curing	Water pressing
1	0.8	83 days	77 days
2	0.8	96 days	64 days
3	0.8	96 days	64 days
4	0.8	96 days	64 days
5	0.8	93 days	61 days
6	0.8	91 days	42 days
7	0.8	90 days	41 days
8	0.8	91 days	42 days
9	0.8	92 days	43 days
10	0.8	96 days	44 days

Table 8 Experiment 2. Casting, curing and leaching test.

Speci-men	W/c	Water curing	Oven +55°C	Vacuum sucking in water	Vacuum sucking in air	Leaching test				Water pressing stop
						6 bar	3 bar	2 bar	1 bar	
1[1)]	0.8	119 days	14 days	1 day	1.5 hour	87 days	No	No	13 days	After 100 days
2[1)]	0.8	127 days	No	No	No	497 days[2)]	68 days	No	No	Still running
3	0.8	201 days	14 days	1 day	1.5 hour	306 days	68 days	No	No	After 374 days
4	0.8	201 days	14 days	1 day	1.5 hour	487 days[2)]	68 days	No	No	Still running
5	0.8	201 days	No	No	No	287 days	68 days	No	No	After 355 days
6	1.3	58 days	7 days	1 day	1.5 hour	71 days	2 days	1 day	18 days	After 92 days
7	1.3	58 days	7 days	1 day	1.5 hour	71 days	2 days	1 day	15 days	After 89 days
8	1.3	58 days	7 days	1 day	1.5 hour	71 days	2 days	1 day	18 days	After 92 days
9	1.3	58 days	No	No	No	No	No	No	No	Abounded
10	1.3	75 days	No	No	No	79 days	2 days	1 day	18 days	After 100 days

[1)] Sample 1 and 2 were tested in an earlier *Experiment 1* between 13/1 and 31/3 1998. In that test, they were situated in water all the time. A small amount of deionized water, 100 ml for sample 1 and 50 ml for sample 2, was pressed through the samples during that test period.

[2] At 30/11-99

Table 9 Experiment 3. Casting and curing.

Concrete type	Oven +40°C	+55°C	+60°C	+30°C	Room curing in +20°C	Vacuum sucking in water	Vacuum sucking in air
W/c 0.6	1 day	No	2 days	3 days	52 days	1 day	1.5 hour
W/c 0.8	2 days	3 days	No	2 days	53 days	1 day	1.5 hour

Table 10 Experiment 3. Leaching test.

Specimen	W/c	Water storing	Water pressing 3 bar	Water pressing 6 bar	Water pressing stop
1	0.6	7 days	60 days	210 days[1]	Still running
5	0.6	47 days	20 days	-- II --	Still running
6-7	0.6	7 days	11 days	259 days[1]	Still running
8-10	0.8	3 days	11 days	259 days[1]	Still running
20-23	0.6	7 days	6 days	264 days[1]	Still running
24-27	0.6	18 days	No	264 days[1]	Still running
28-30	0.6	19 days	No	264 days[1]	Still running
31-36	0.8	15 days	No	264 days[1]	Still running

[1] At 30/11-99

APPENDIX TO CHAPTER 7

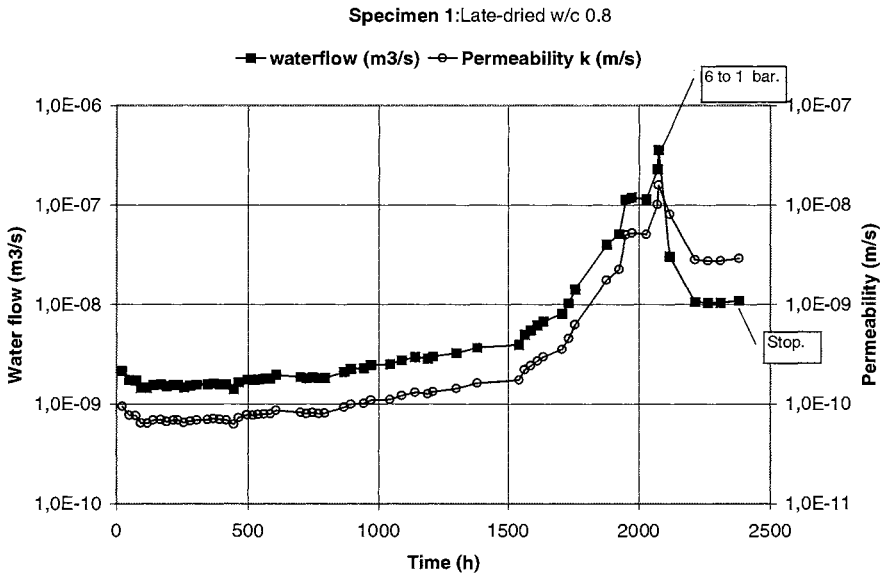

Figure 1 Measured water flow for concrete **specimen 1, exp. 2**. Late-dried w/c 0.8 concrete with thickness of 50mm. The water pressure was 6 bar except for the last 300 hours of the test. Specimen 1 had been leakage tested before in *Experiment 1* for 1434 hours, as virgin concrete. In *Experiment 1* the water flow was about 1.5E-11 m^3/s for 6 bar, i.e. 120 times less then now when the specimen had been dried. As can be seen in the figure, the flow increased rapidly between 1500 and 2100 hours. After 2100 hours the water pressure had to be decreased in order to manage the big water volumes.

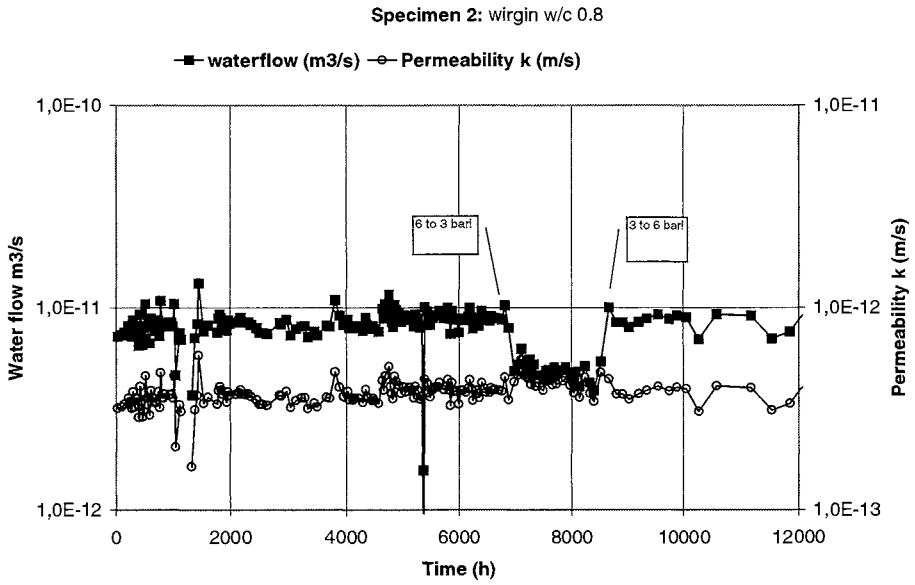

Figure 2 Measured water flow for concrete **specimen 2, exp. 2.** Virgin w/c 0.8 concrete with thickness of 50mm. The water pressure was 6 bar except for a period between 6800 and 8700 hours. The flow of water has been uniform all the time. The test is still running when this figure is drawn.

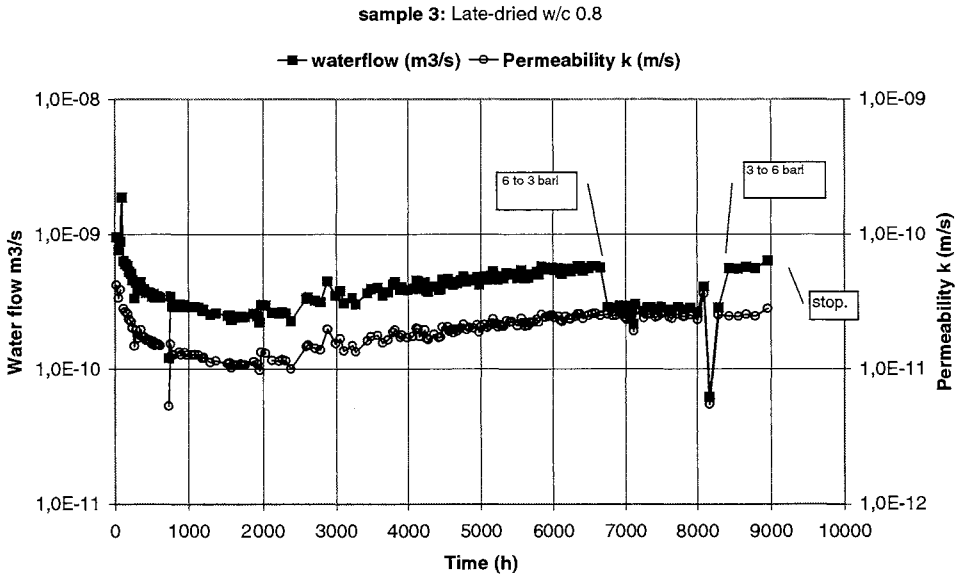

Figure 3 Measured water flow for concrete **specimen 3, exp. 2.** Late-dried w/c 0.8 concrete with thickness of 50mm. The water pressure was 6 bar except for a period between 6600 and 8400 hours. The flow of water decreased a while the first period, but then it leveled out. The flow was somewhat increased from 3000 hours until the test was stopped.

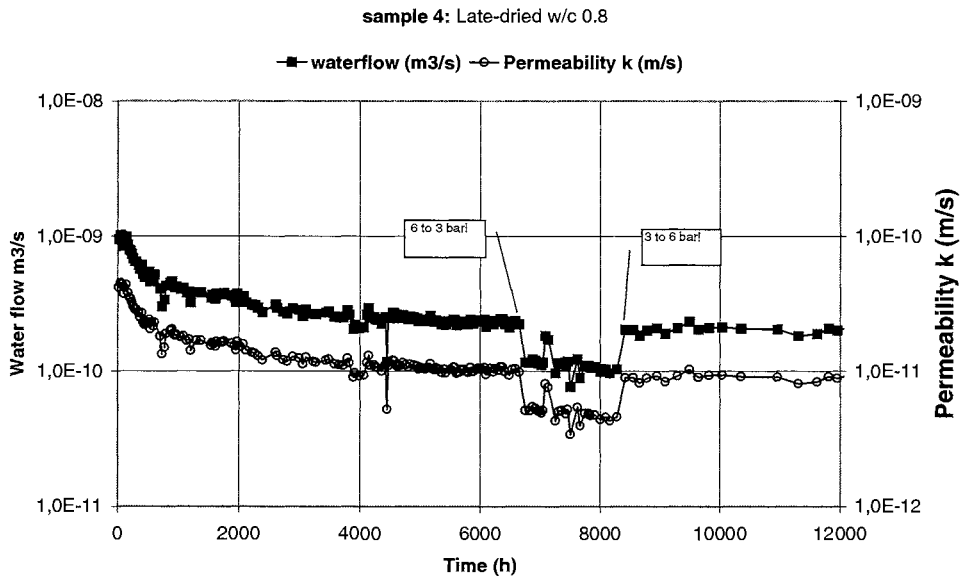

Figure 4 Measured water flow for concrete **specimen 4, exp. 2.** Late-dried w/c 0.8 concrete with thickness of 50mm. The water pressure was 6 bar except for a period between 6600 and 8400 hours. The flow of water decreased a while the first period, but then it leveled out.

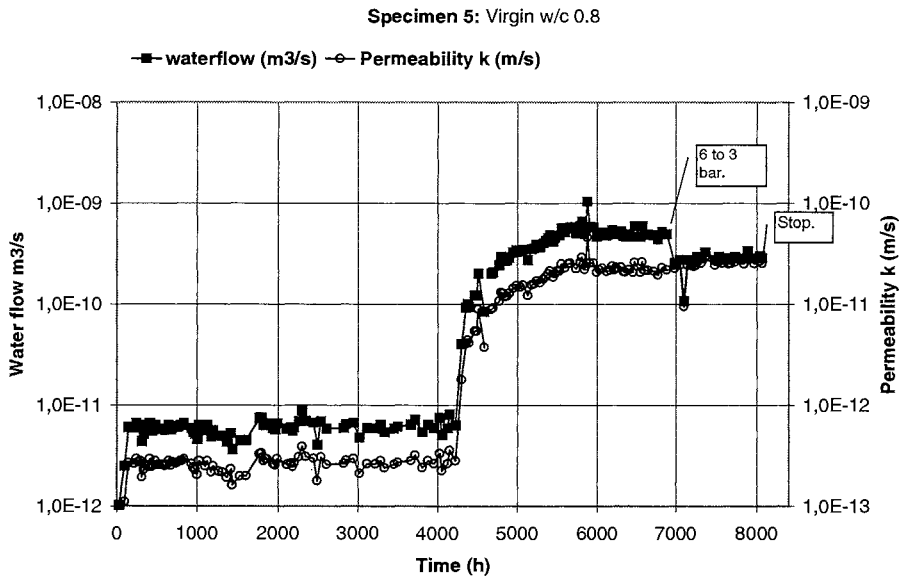

Figure 5 Measured water flow for concrete **specimen 5, exp. 2.** Virgin w/c 0.8 concrete with thickness of 50mm. The water pressure was 6 bar except for a the last period. The flow of water was uniform and about the same as for spec. 2 the first 4000 hours. Then it was rapidly increased up to about 100 times higher flow where it leveled out.

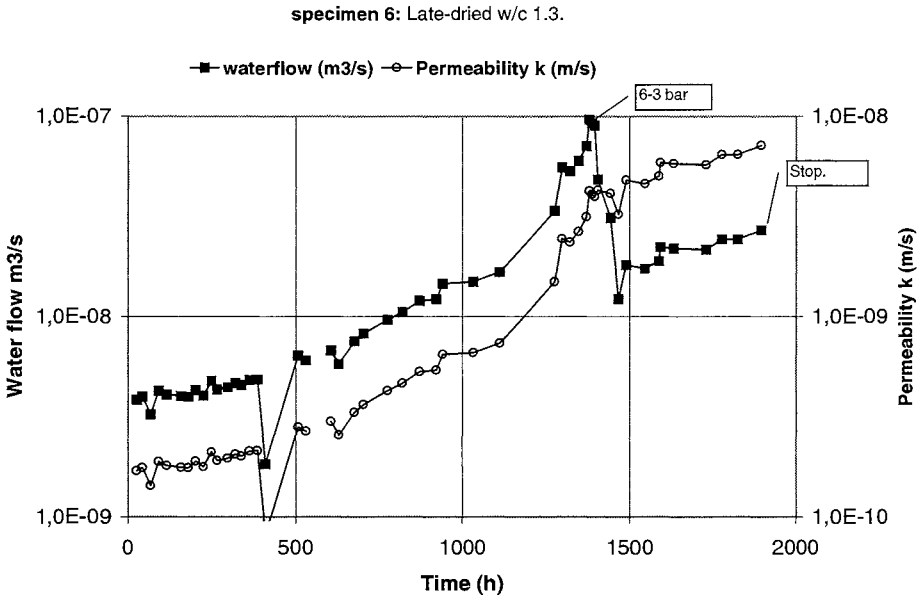

Figure 6 Measured water flow for concrete **specimen 6, exp. 2.** Late-dried w/c 1.3 concrete with thickness of 50mm. The water pressure was 6 bar except for the last periods. The flow of water increased rapidly by about 25 times after about 800 hours.

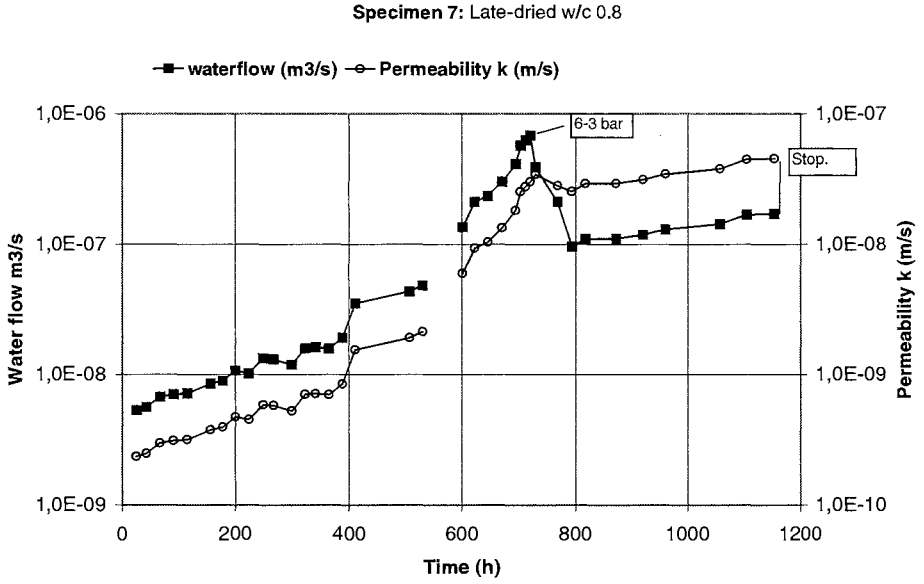

Figure 7 Measured water flow for concrete **specimen 7, exp. 2.** Late-dried w/c 1.3 concrete with thickness of 50mm. The water pressure was 6 bar except for the last periods. The flow of water increased rapidly by about 130 times after about 200 hours.

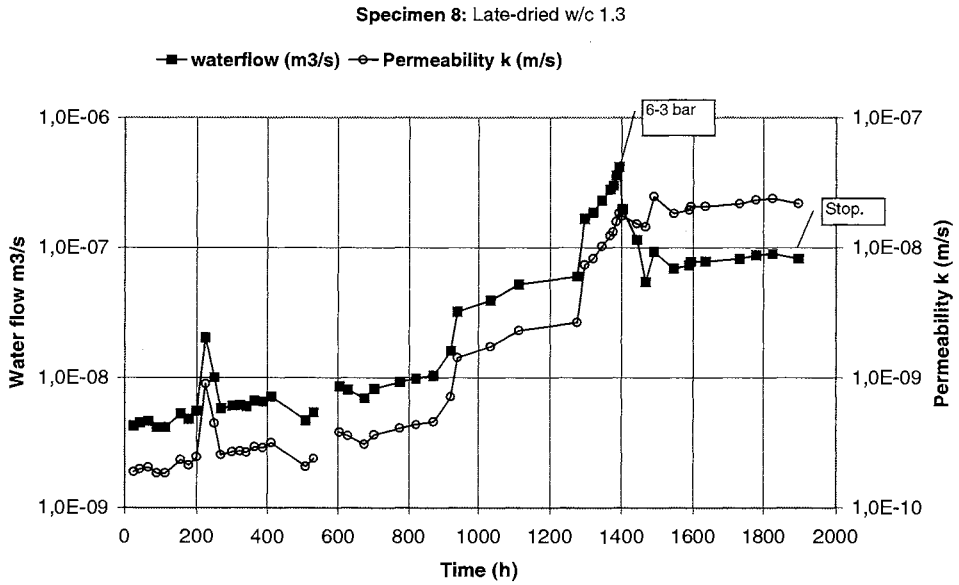

Figure 8 Measured water flow for concrete **specimen 8, exp. 2.** Late-dried w/c 1.3 concrete with thickness of 50mm. The water pressure was 6 bar except for the last periods. After a uniform beginning, the flow of water increased rapidly by about 90 times after about 800 hours.

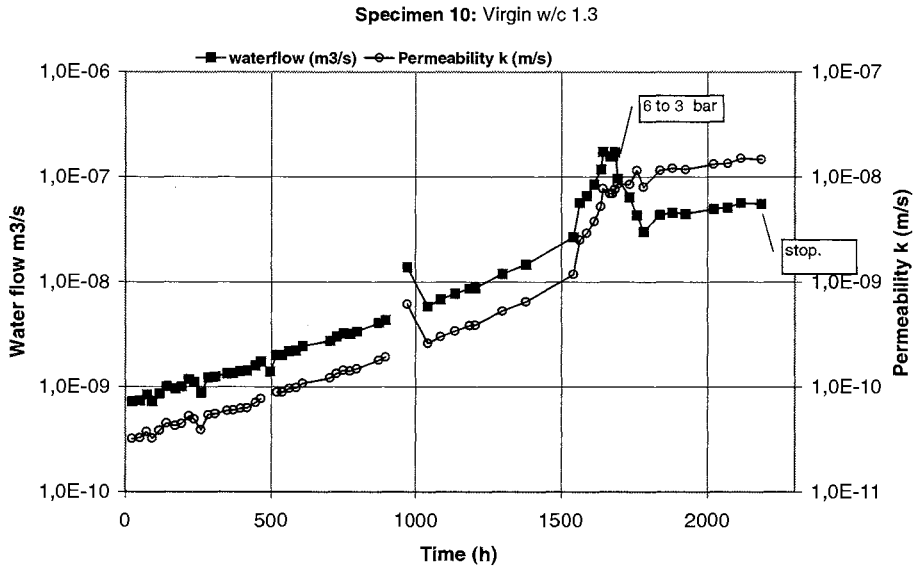

Figure 9 Measured water flow for concrete **specimen 10, exp. 2.** Virgin w/c 1.3 concrete with thickness of 50mm. The water pressure was 6 bar except for the last period. The flow of water increased gradually during the entire test period. After 1500 hours, the increase was more rapid. The increase was about 240 times in total.

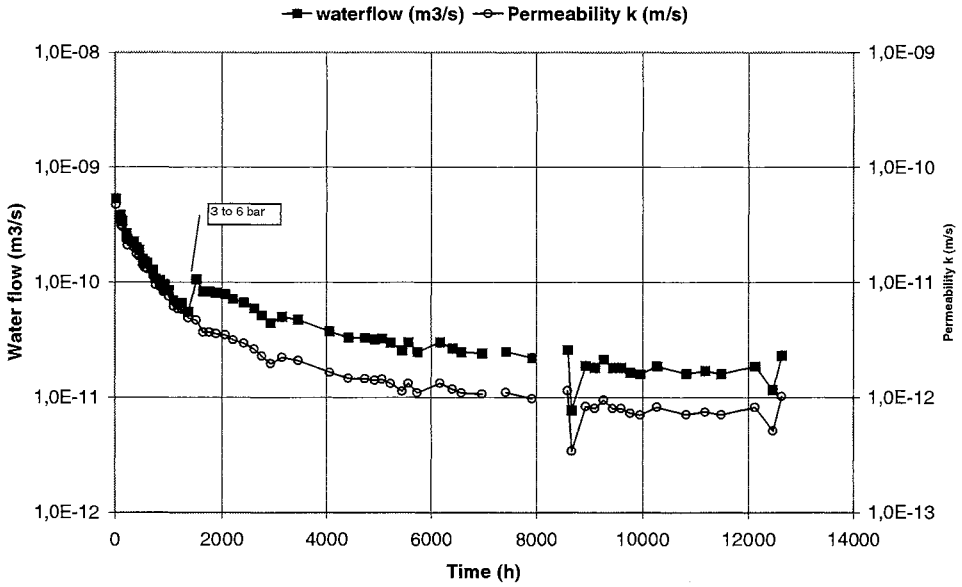

Figure 1 Measured water flow and permeability for concrete **specimen 1, exp. 3**. Early-heated w/c 0.6 concrete ϕ155x50mm. The water pressure was 6 bar except the first period.

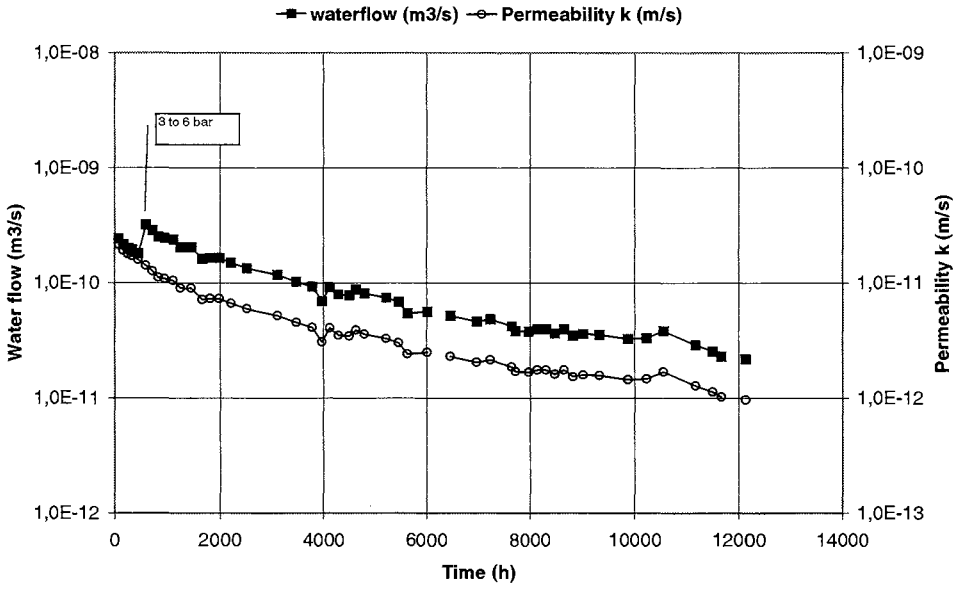

Figure 2 Measured water flow and permeability for concrete **specimen 5, exp. 3**. Early-heated w/c 0.6 concrete ϕ155x50mm. The water pressure was 6 bar except the first period.

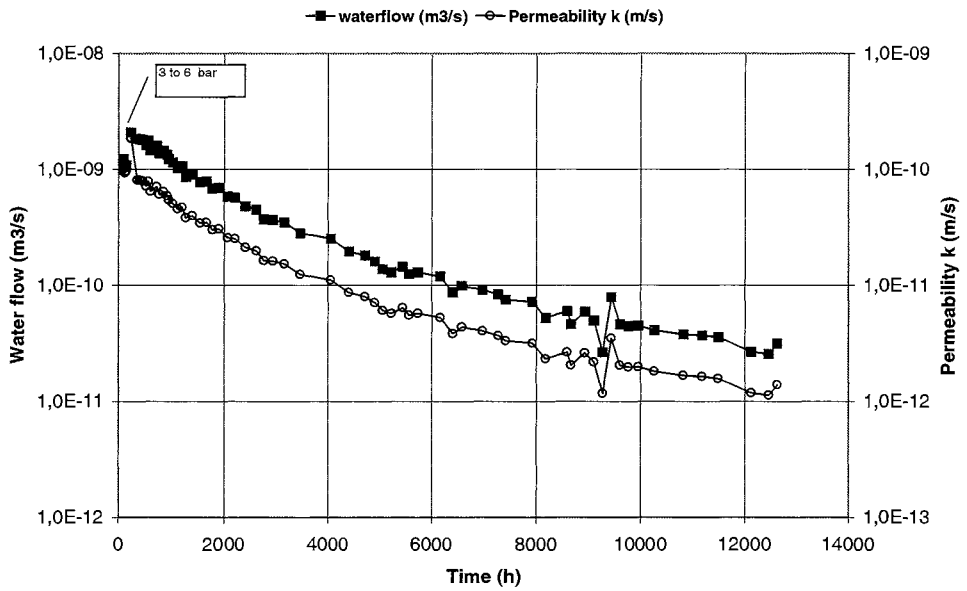

Figure 3 Measured water flow and permeability for concrete **specimen 6, exp. 3**. Early-heated w/c 0.6 concrete ϕ155x50mm. The water pressure was 6 bar except the first period.

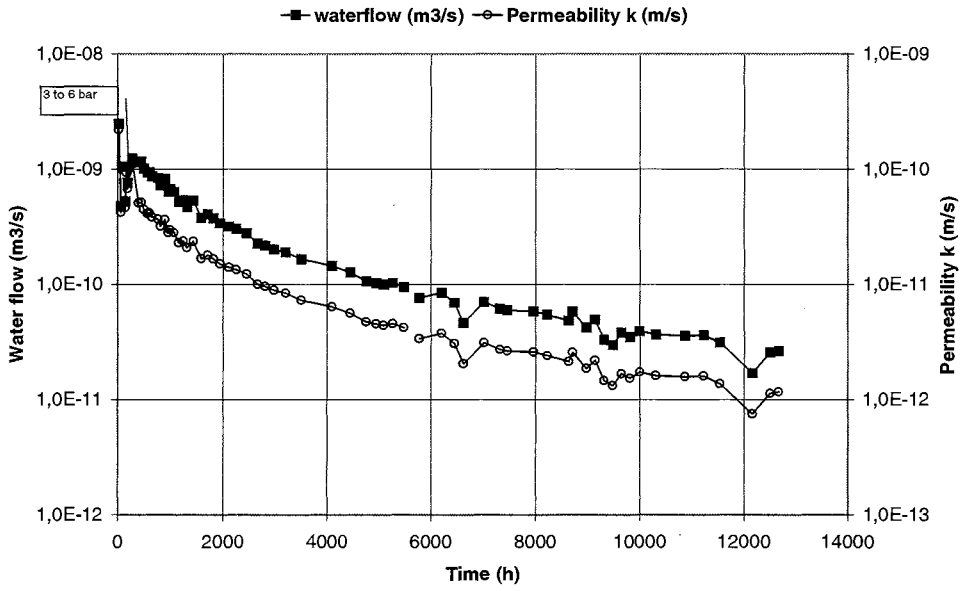

Figure 4 Measured water flow and permeability for concrete **specimen 7, exp. 3**. Early-heated w/c 0.6 concrete ϕ155x50mm. The water pressure was 6 bar except the first period.

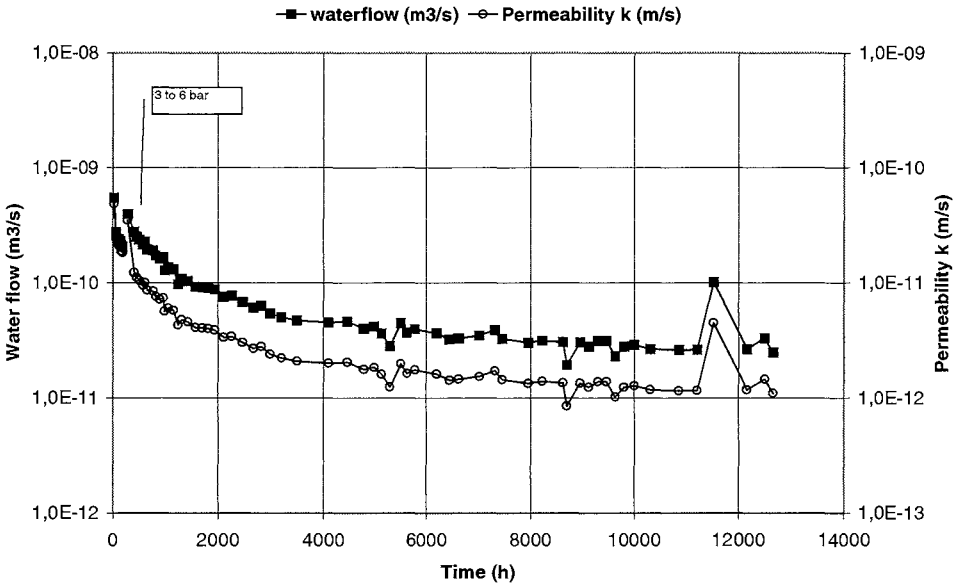

Figure 5 Measured water flow and permeability for concrete **specimen 8, exp. 3**. Early-heated w/c 0.8 concrete ϕ155x50mm. The water pressure was 6 bar except the first period.

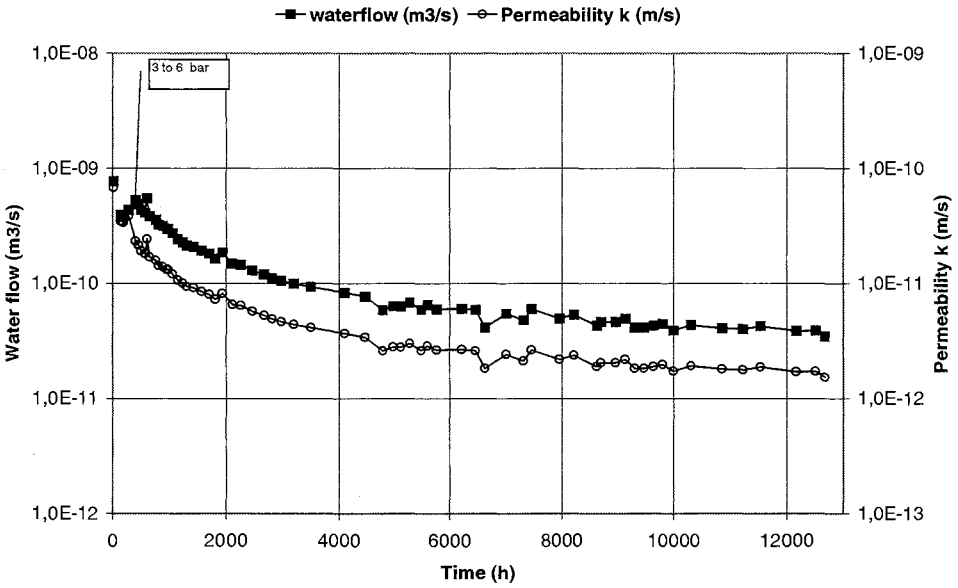

Figure 6 Measured water flow and permeability for concrete **specimen 9, exp. 3**. Early-heated w/c 0.8 concrete ϕ155x50mm. The water pressure was 6 bar except the first period.

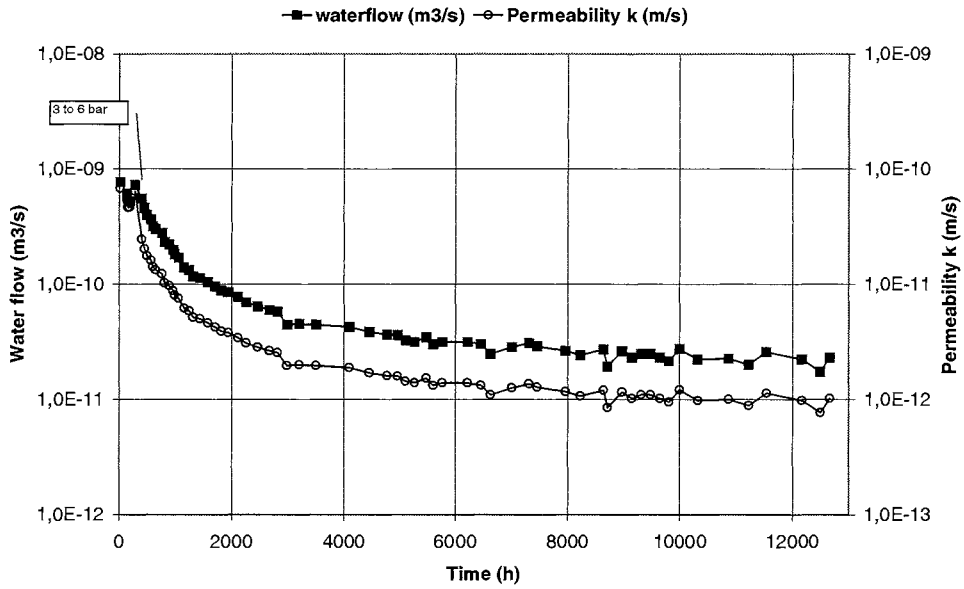

Figure 7 Measured water flow and permeability for concrete **specimen 10, exp. 3**. Early-heated w/c 0.8 concrete ϕ155x50mm. The water pressure was 6 bar except the first period.

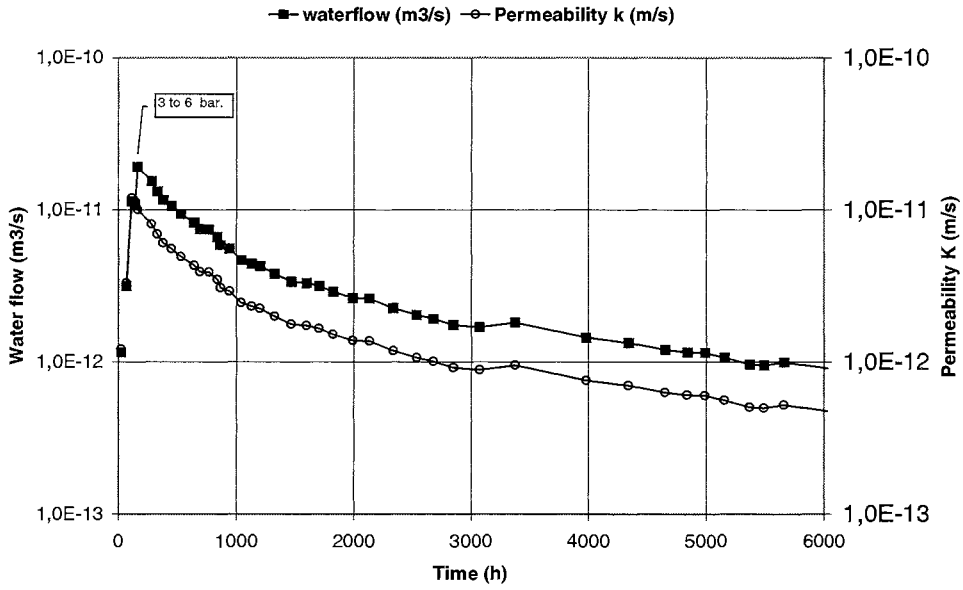

Figure 8 Measured water flow and permeability for concrete **specimen 20, exp. 3**. Early-heated w/c 0.6 concrete ϕ45x50mm. The water pressure was 6 bar except the first period.

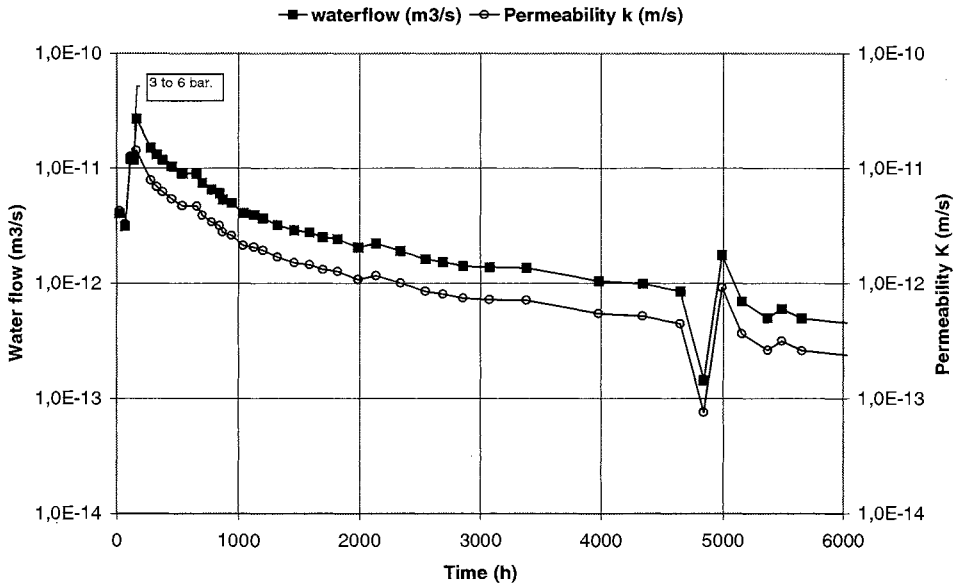

Figure 9 Measured water flow and permeability for concrete **specimen 21, exp. 3**. Early-heated w/c 0.6 concrete ϕ45x50mm. The water pressure was 6 bar except the first period.

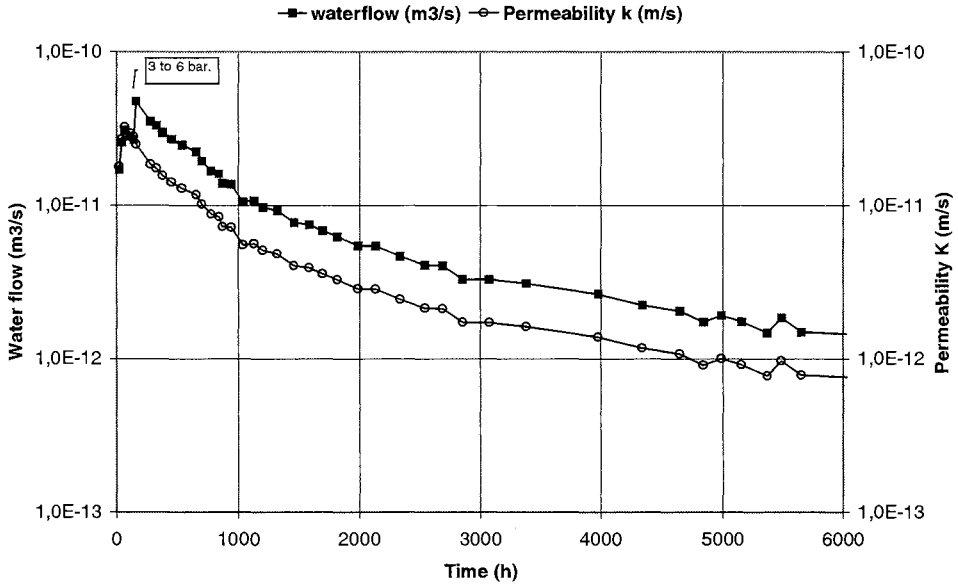

Figure 10 Measured water flow and permeability for concrete **specimen 22, exp. 3**. Early-heated w/c 0.6 concrete ϕ45x50mm. The water pressure was 6 bar except the first period.

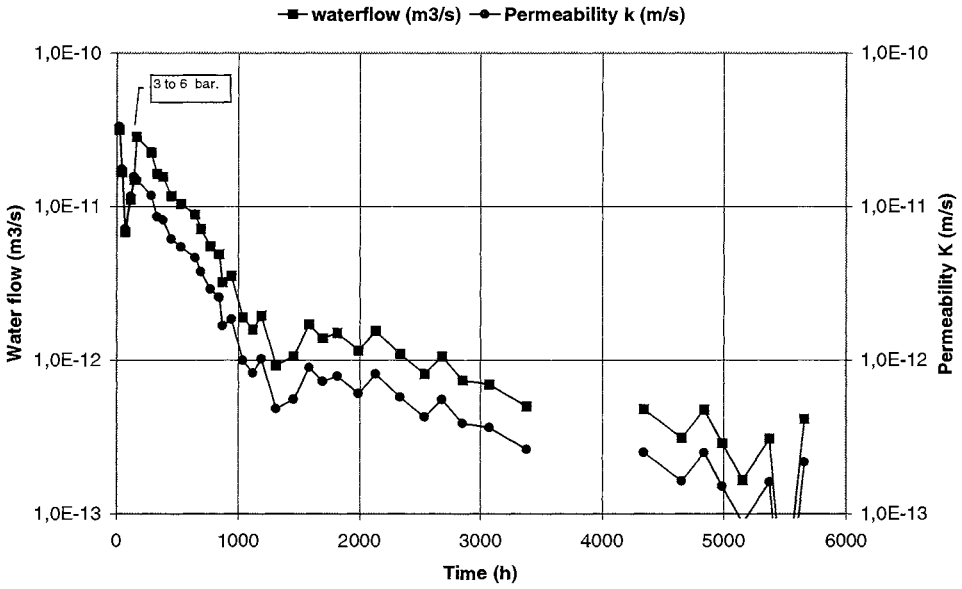

Figure 11 Measured water flow and permeability for concrete **specimen 23, exp. 3**. Early-heated w/c 0.6 concrete ϕ45x50mm. The water pressure was 6 bar except the first period.

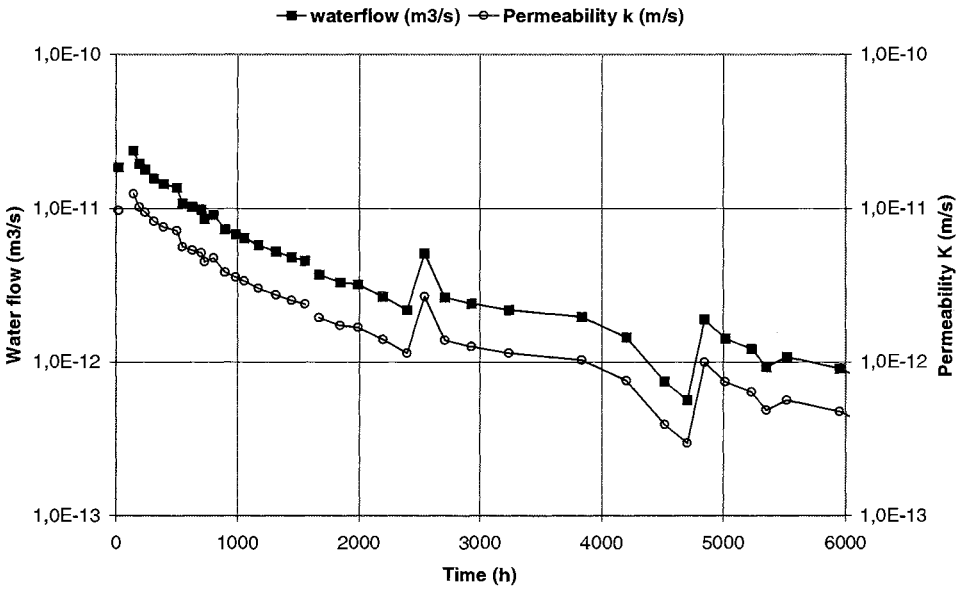

Figure 12 Measured water flow and permeability for concrete **specimen 24, exp. 3**. Early-heated w/c 0.6 concrete ϕ45x50mm. The water pressure was 6 bar.

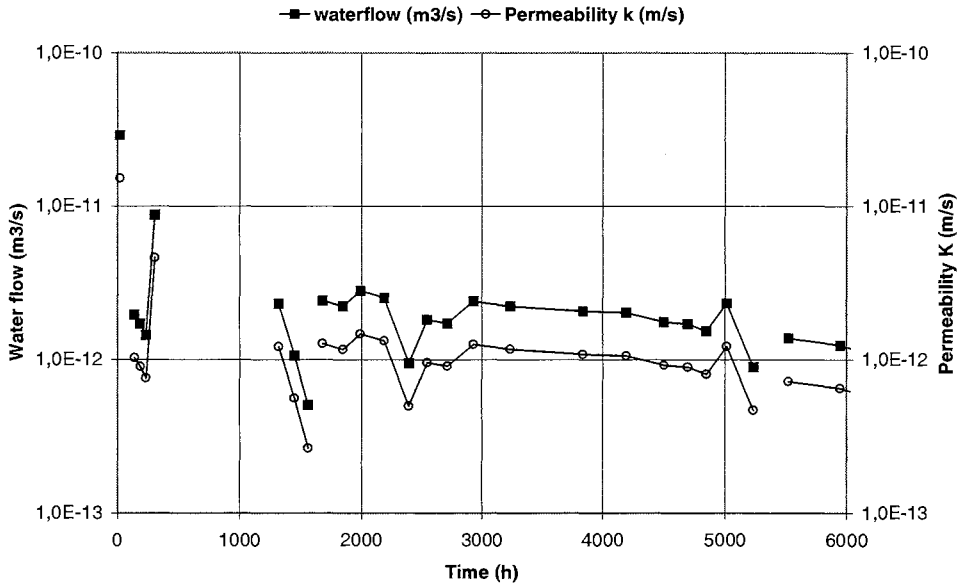

Figure 13 Measured water flow and permeability for concrete **specimen 25, exp. 3**. Early-heated w/c 0.6 concrete ϕ45x50mm. The water pressure was 6 bar.

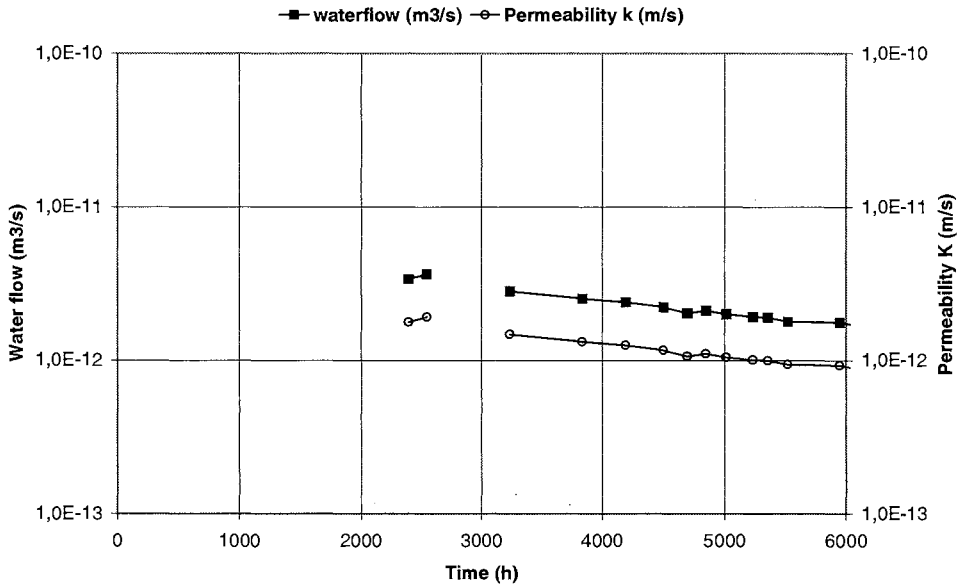

Figure 14 Measured water flow and permeability for concrete **specimen 26, exp. 3**. Early-heated w/c 0.6 concrete ϕ45x50mm. The water pressure was 6 bar.

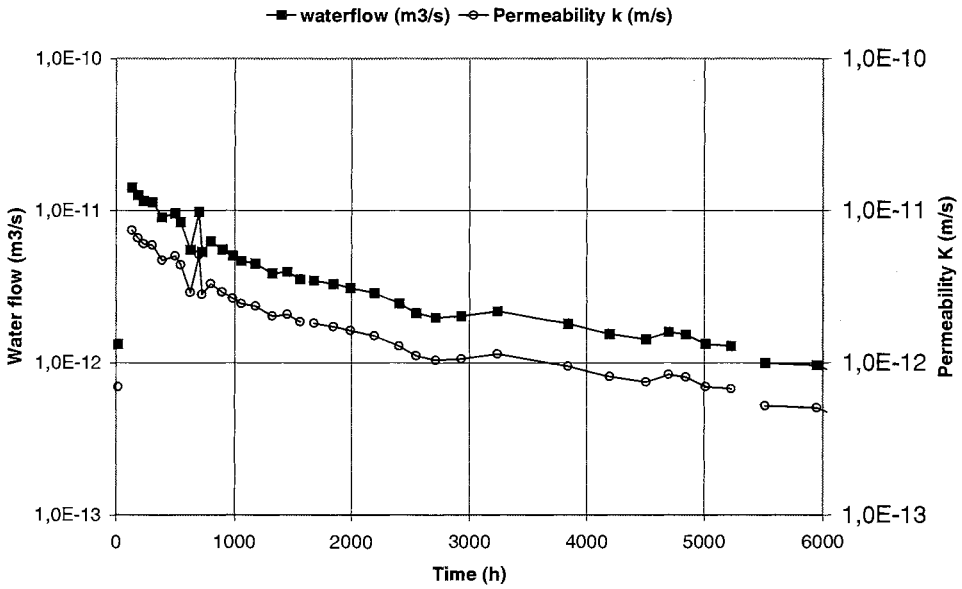

Figure 15 Measured water flow and permeability for concrete **specimen 27, exp. 3**. Early-heated w/c 0.6 concrete ϕ45x50mm. The water pressure was 6 bar.

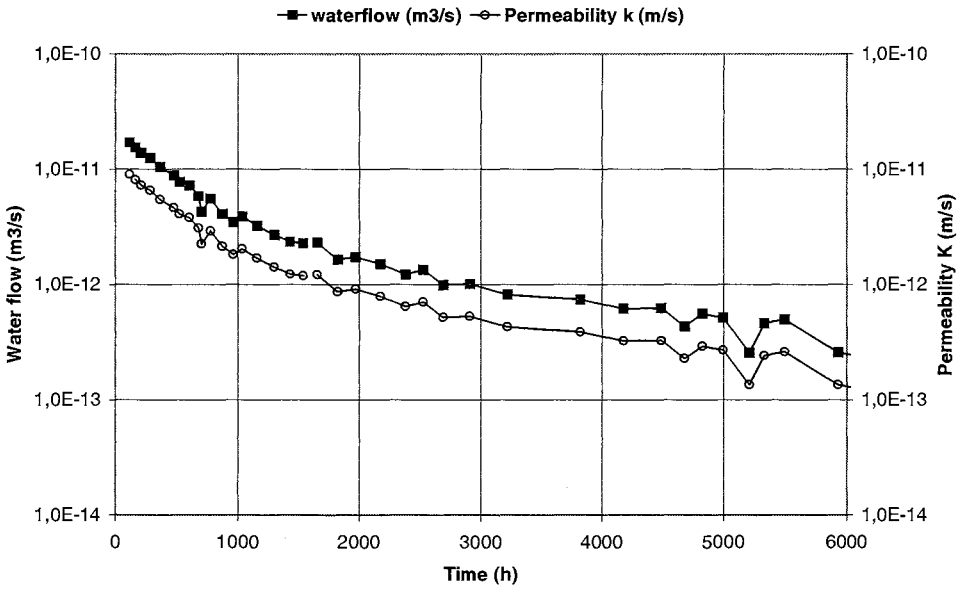

Figure 16 Measured water flow and permeability for concrete **specimen 28, exp. 3**. Early-heated w/c 0.6 concrete ϕ45x50mm. The water pressure was 6 bar.

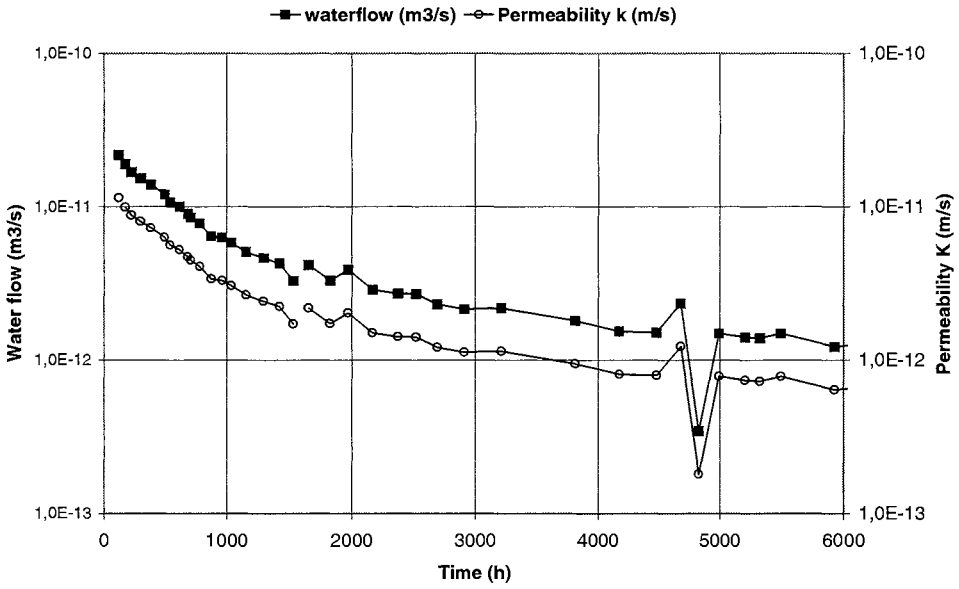

Figure 17 Measured water flow and permeability for concrete **specimen 29, exp. 3**. Early-heated w/c 0.6 concrete ϕ45x50mm. The water pressure was 6 bar.

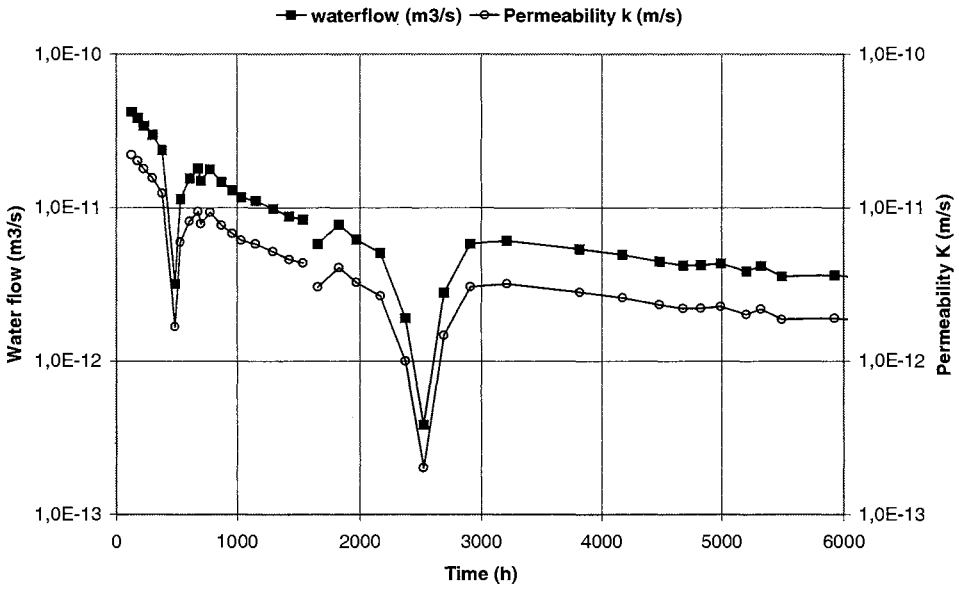

Figure 18 Measured water flow and permeability for concrete **specimen 30, exp. 3**. Early-heated w/c 0.6 concrete ϕ45x50mm. The water pressure was 6 bar. The drop at 500 and 2500 hours is due to possible evaporation from the measuring vessel.

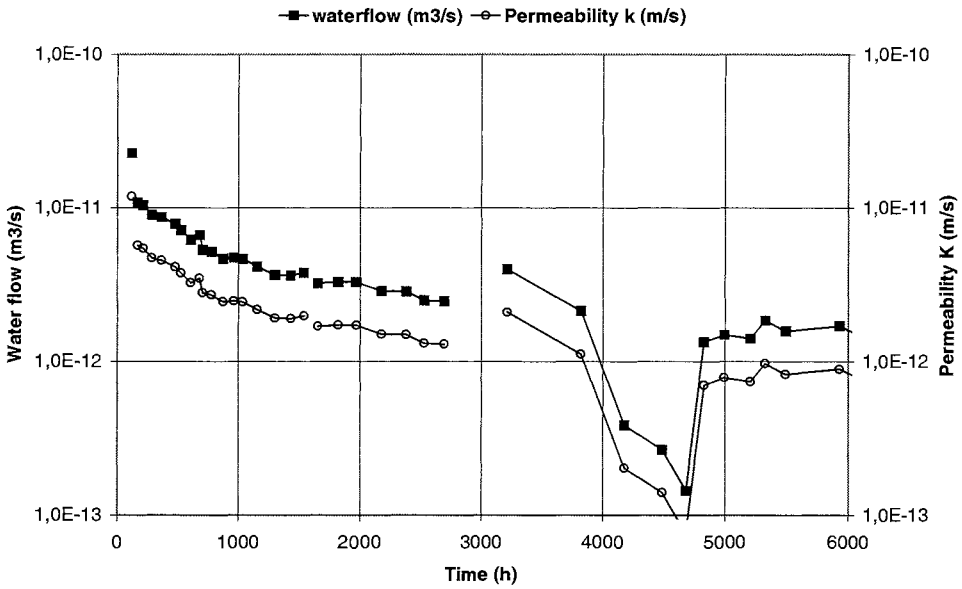

Figure 19 Measured water flow and permeability for concrete **specimen 31, exp. 3**. Early-heated w/c 0.8 concrete ϕ45x50mm. The water pressure was 6 bar.

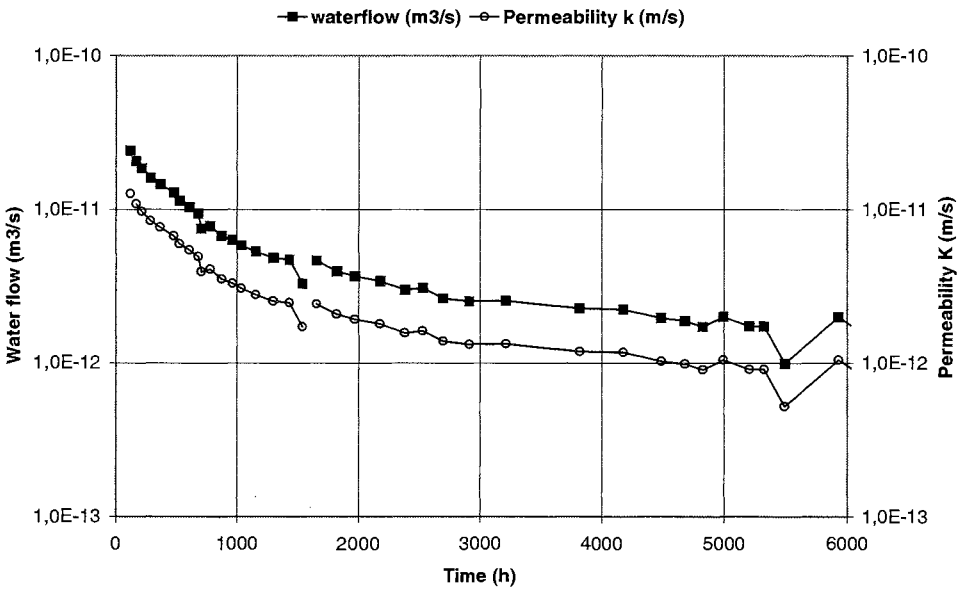

Figure 20 Measured water flow and permeability for concrete **specimen 32, exp. 3**. Early-heated w/c 0.8 concrete ϕ45x50mm. The water pressure was 6 bar.

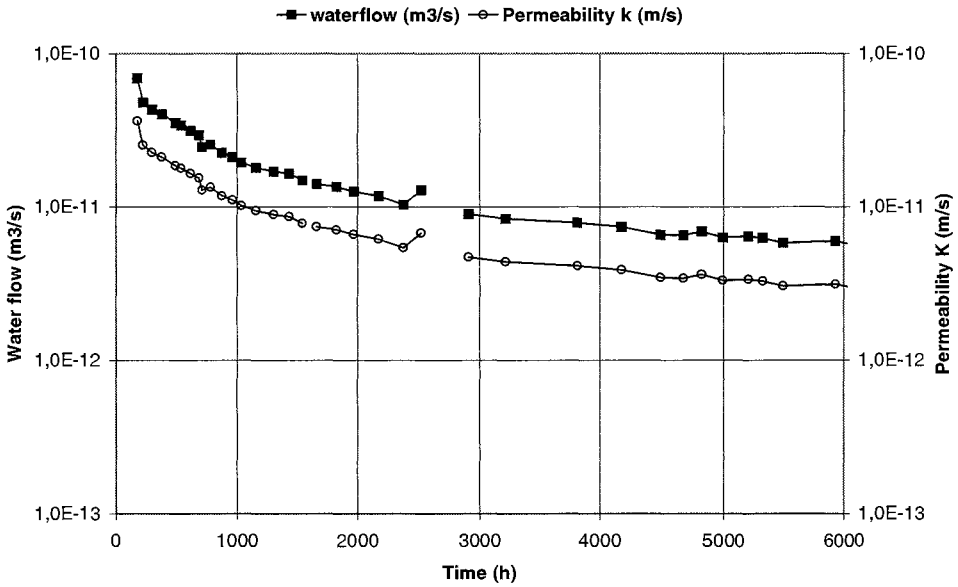

Figure 21 Measured water flow and permeability for concrete **specimen 33, exp. 3**. Early-heated w/c 0.8 concrete ϕ45x50mm. The water pressure was 6 bar.

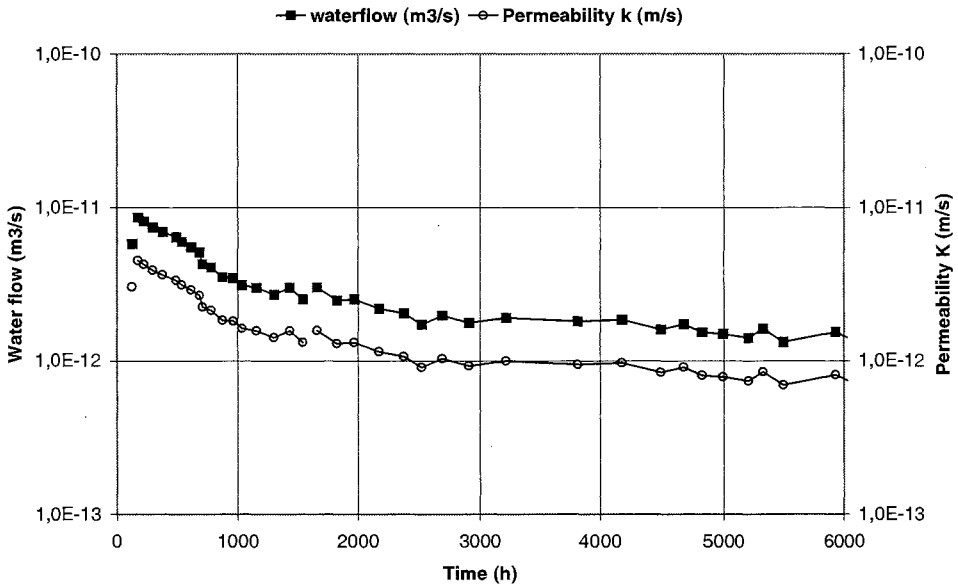

Figure 22 Measured water flow and permeability for concrete **specimen 34, exp. 3**. Early-heated w/c 0.8 concrete ϕ45x50mm. The water pressure was 6 bar.

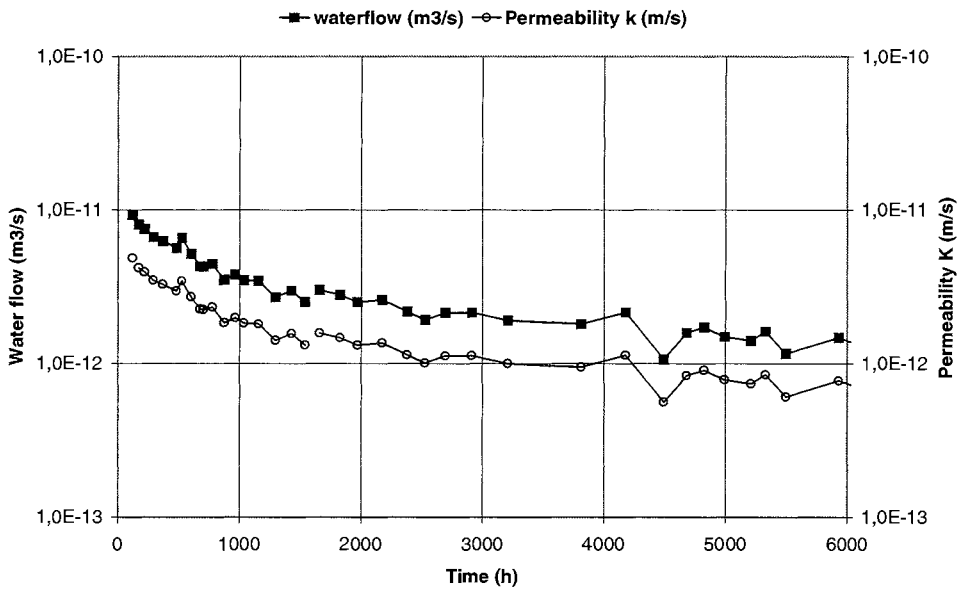

Figure 23 Measured water flow and permeability for concrete **specimen 35, exp. 3**. Early-heated w/c 0.8 concrete ϕ45x50mm. The water pressure was 6 bar.

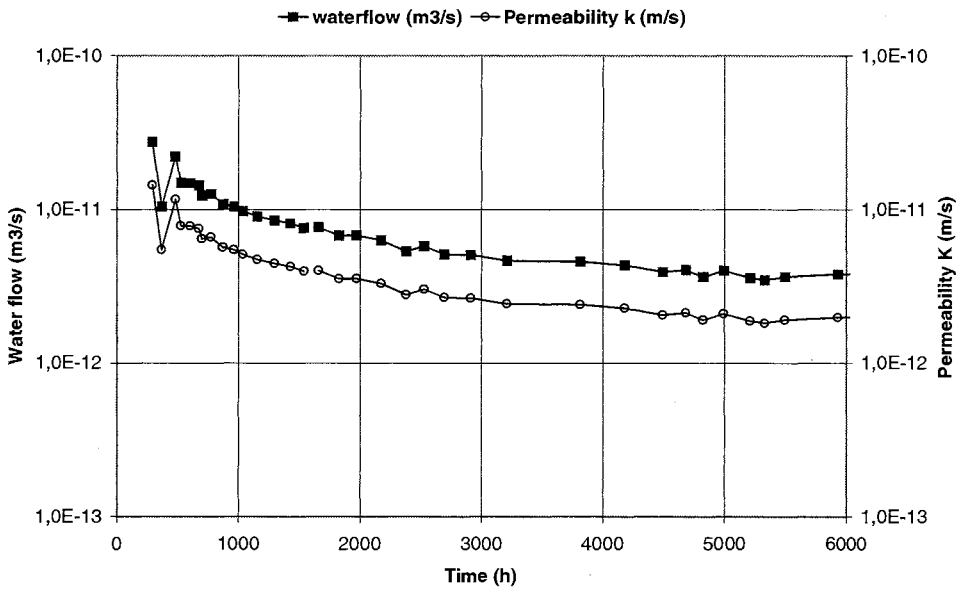

Figure 24 Measured water flow and permeability for concrete **specimen 36, exp. 3**. Early-heated w/c 0.8 concrete ϕ45x50mm. The water pressure was 6 bar.

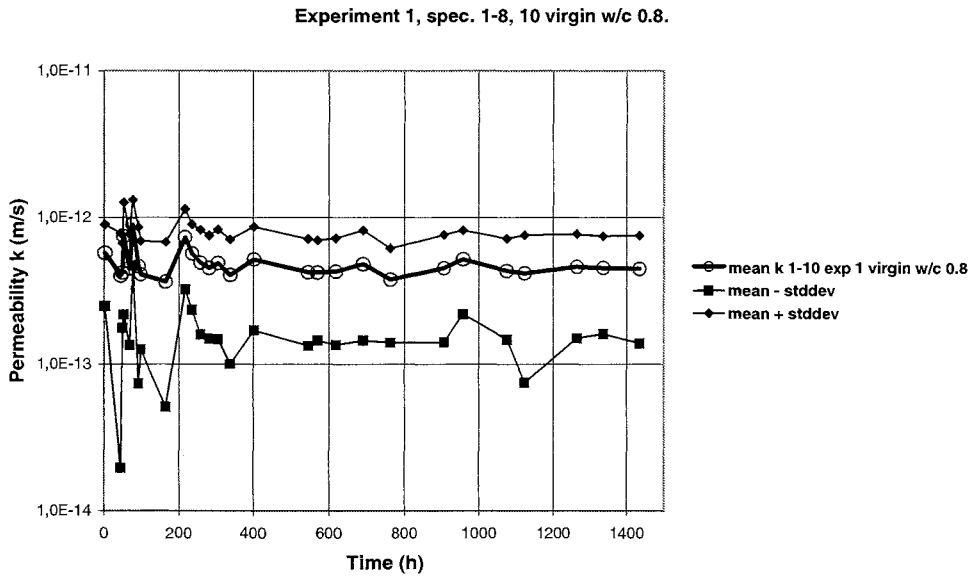

Figure 1 The mean permeability μ(k) (m/s) and standard deviation σ (m/s) for **specimens 1-8, 10, exp. 1** (virgin w/c 0.8). Observe the log scale. It is the same distance between + and – standard deviations in relation to the mean values.

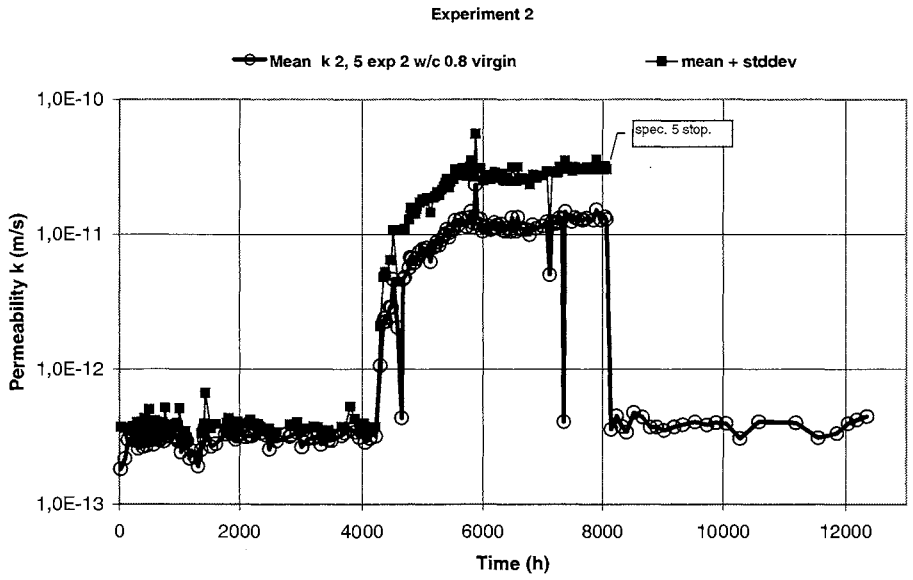

Figure 2 The mean permeability μ(k) (m/s) and standard deviation σ (m/s) for **specimens 2,5 exp. 2** (virgin w/c 0.8). The standard deviation is increased at 4000 hours due to a rapidly increased flow of water in specimen 5. After 8000 hours this specimen was stopped and after this occasion, the figure shows only one specimen.

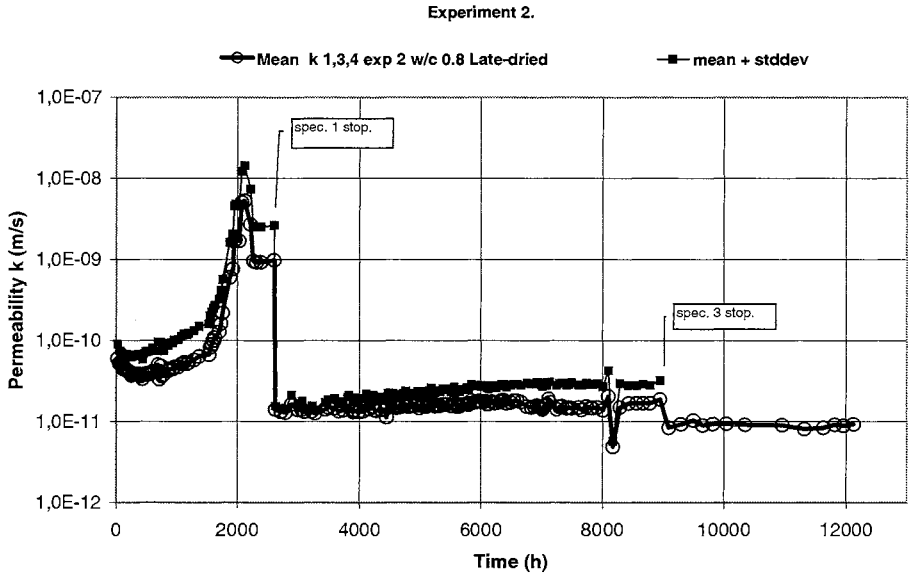

Figure 3 The mean permeability μ(k) (m/s) and standard deviation σ (m/s) for **specimens 1,3,4 exp. 2** (late-dried w/c 0.8).

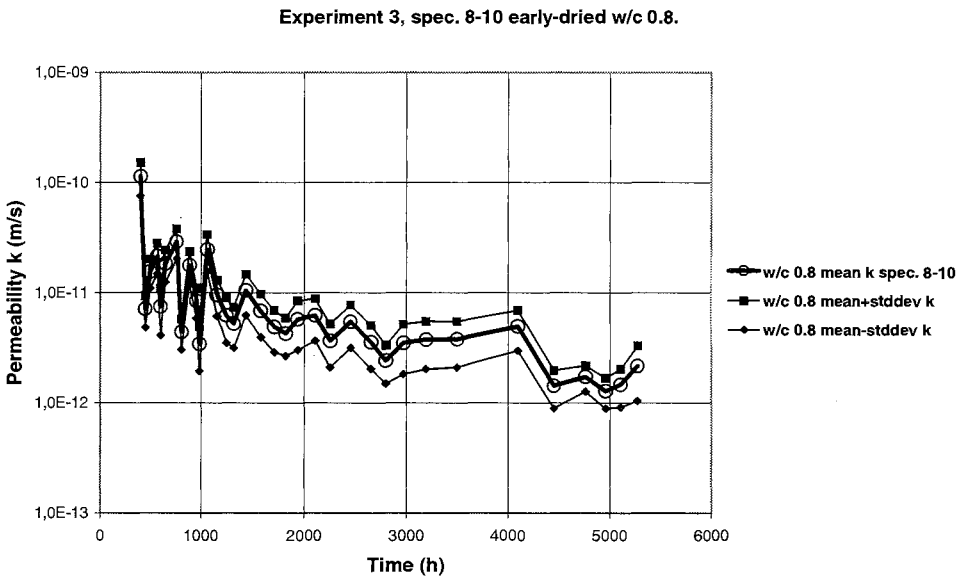

Figure 1 The mean permeability μ(k) (m/s) and standard deviation σ (m/s) for **specimens 8-10, exp. 3.**

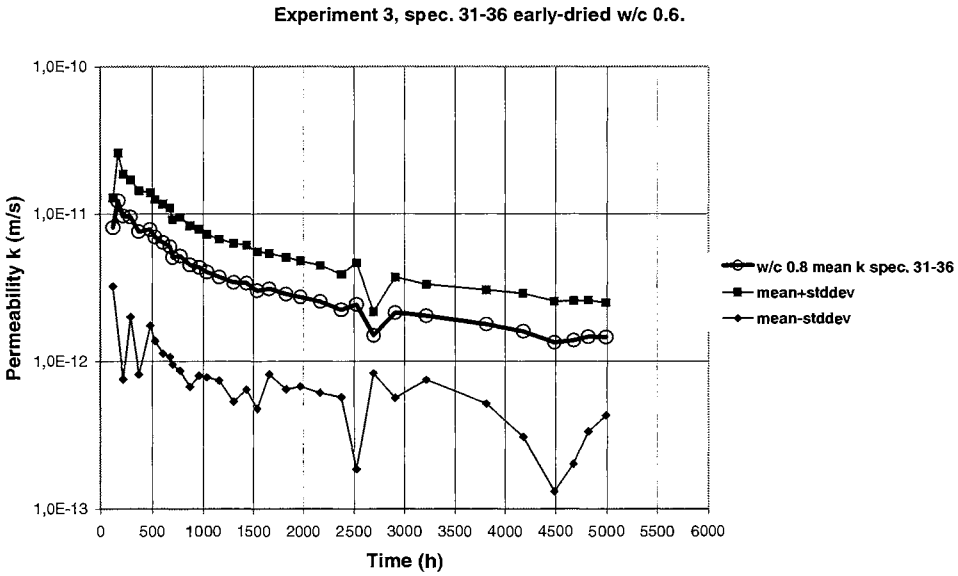

Figure 2 The mean permeability μ(k) (m/s) and standard deviation σ (m/s) for **specimens 31-36, exp. 3**.

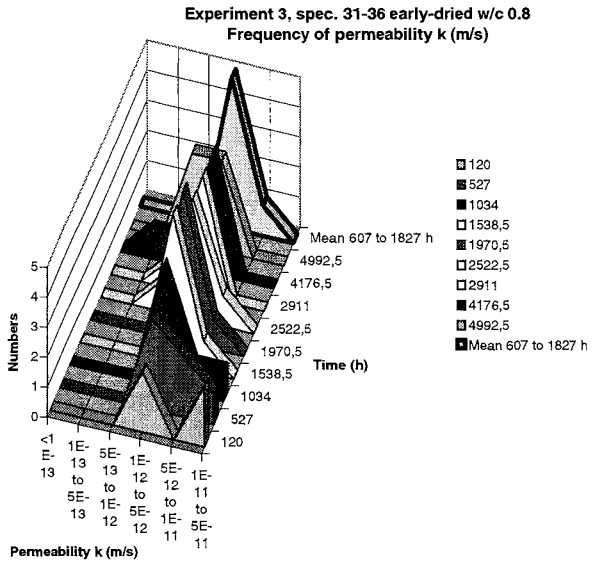

Figure 3 The frequency of the permeability k (m/s) for **specimens 31-36, exp. 3**. The flow was decreased with the time.

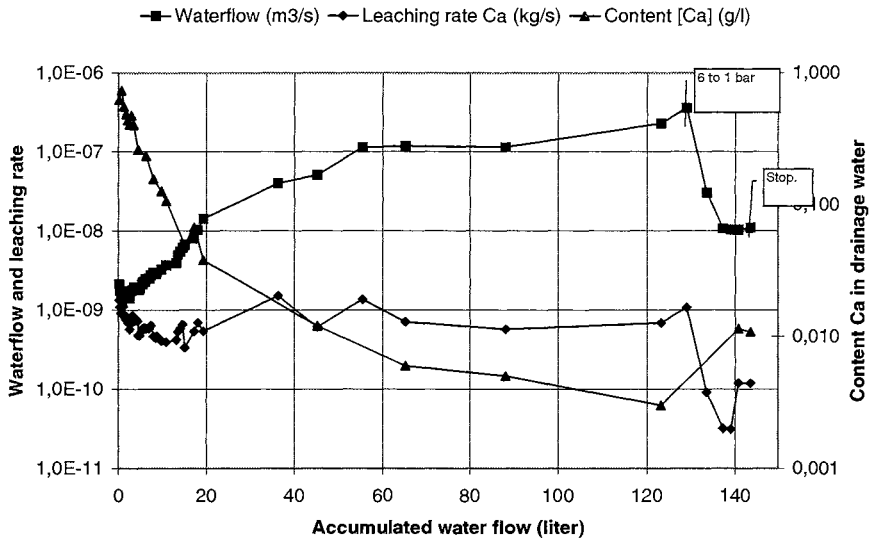

Figure 1 Measured drainage water flow and measured [Ca^{2+}] in the drainage water and calculated leaching rate kg Ca^{2+} /s for **specimen 1, exp. 2.**

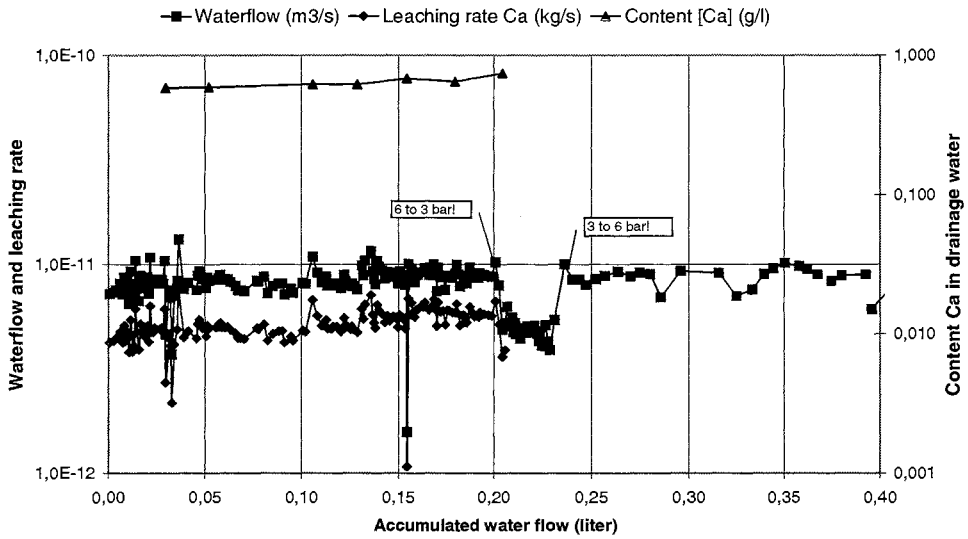

Figure 2 Measured drainage water flow and measured [Ca^{2+}] in the drainage water and calculated leaching rate kg Ca^{2+} /s for **specimen 2, exp. 2.**

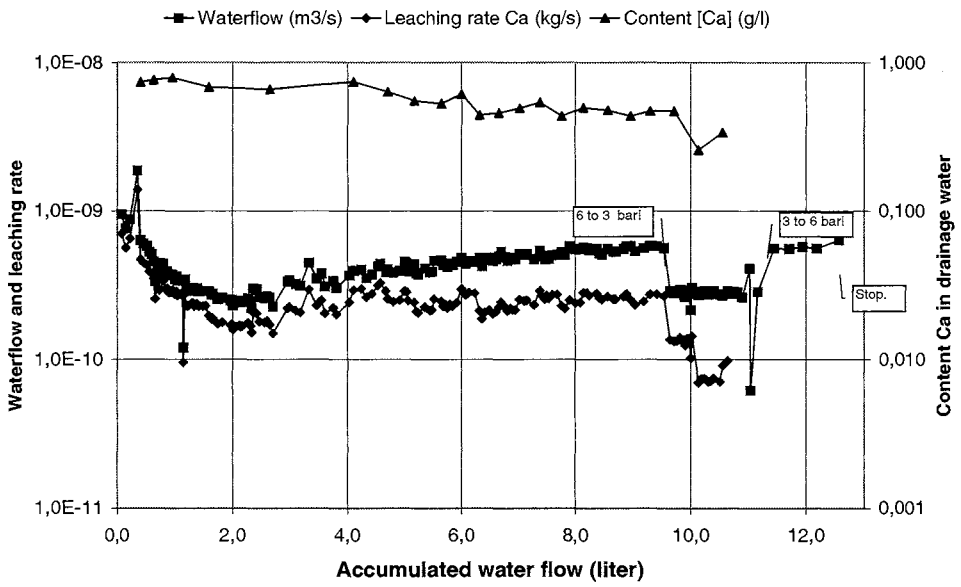

Figure 3 Measured drainage water flow and measured [Ca^{2+}] in the drainage water and calculated leaching rate kg Ca^{2+} /s for **specimen 3, exp. 2.**

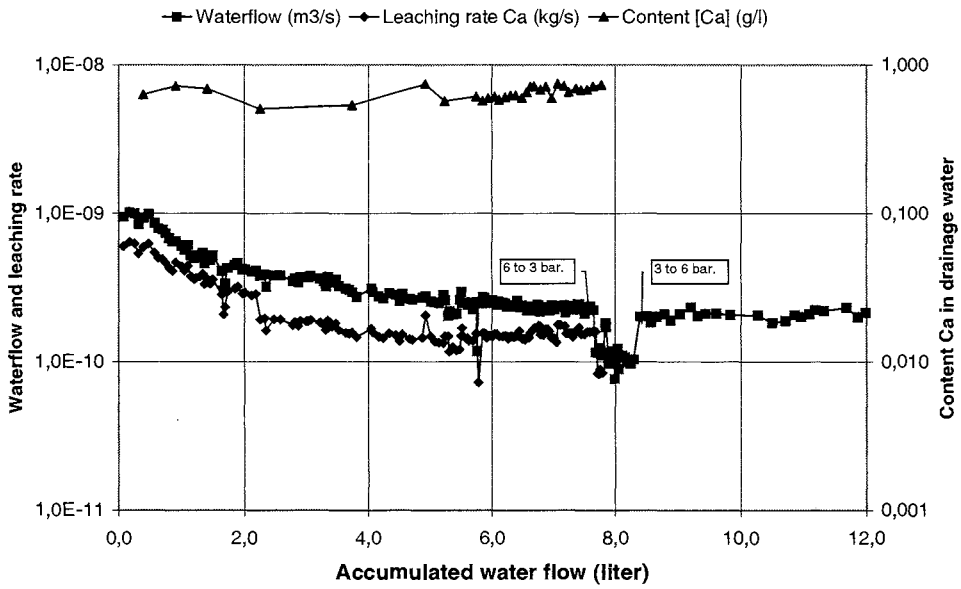

Figure 4 Measured drainage water flow and measured [Ca^{2+}] in the drainage water and calculated leaching rate kg Ca^{2+} /s for **specimen 4, exp. 2.**

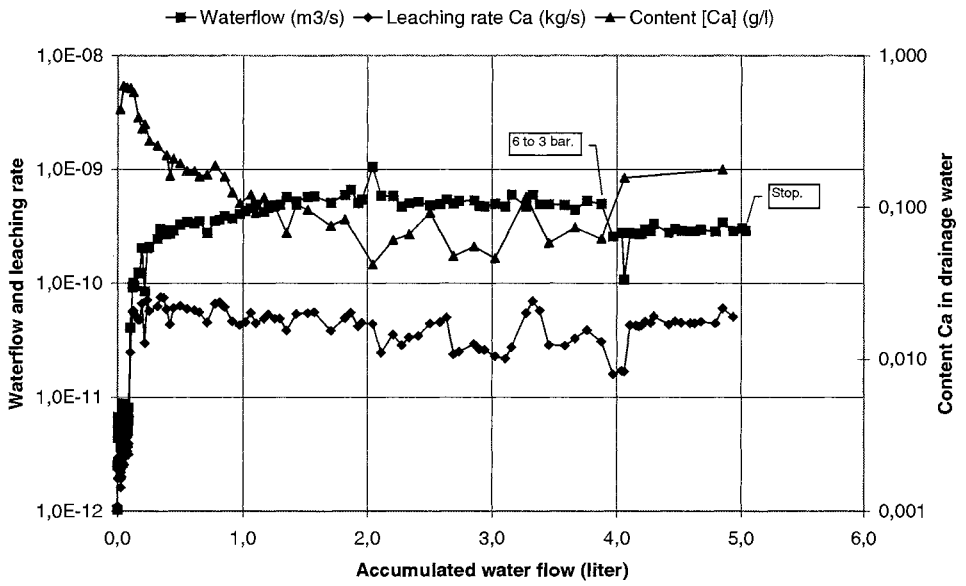

Figure 5 Measured drainage water flow and measured [Ca^{2+}] in the drainage water and calculated leaching rate kg Ca^{2+} /s for **specimen 5, exp. 2.**

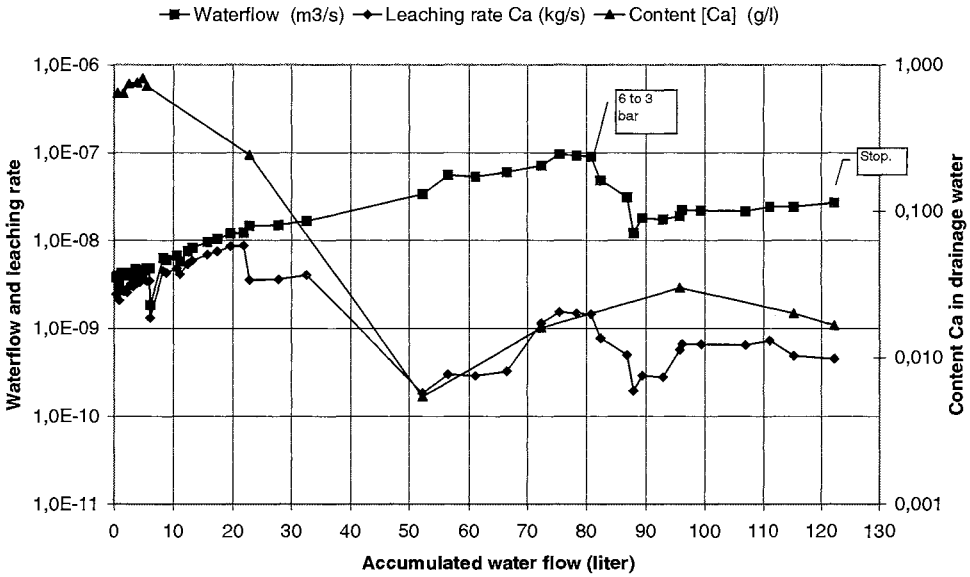

Figure 6 Measured drainage water flow and measured [Ca^{2+}] in the drainage water and calculated leaching rate kg Ca^{2+} /s for **specimen 6, exp. 2.**

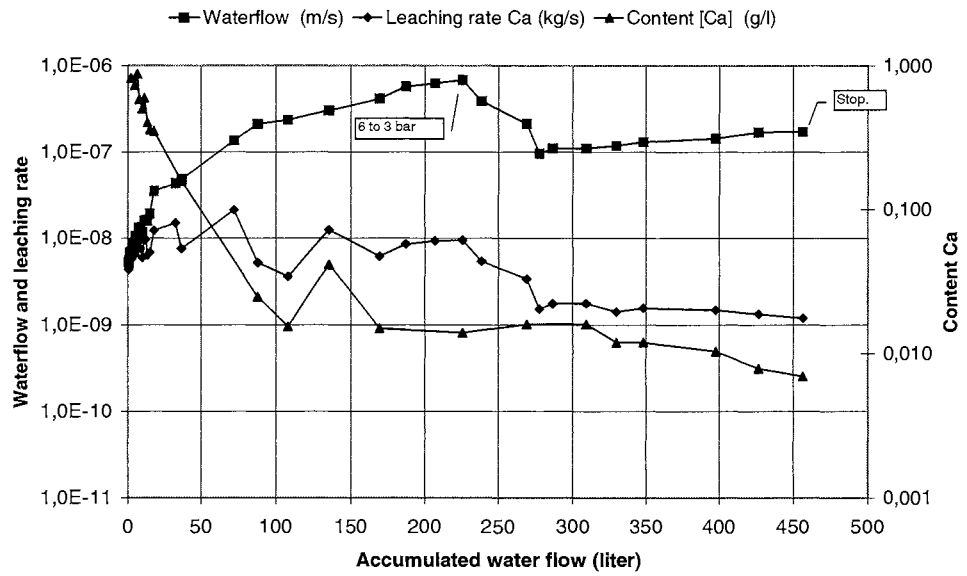

Figure 7 Measured drainage water flow and measured [Ca^{2+}] in the drainage water and calculated leaching rate kg Ca^{2+} /s for **specimen 7, exp. 2.**

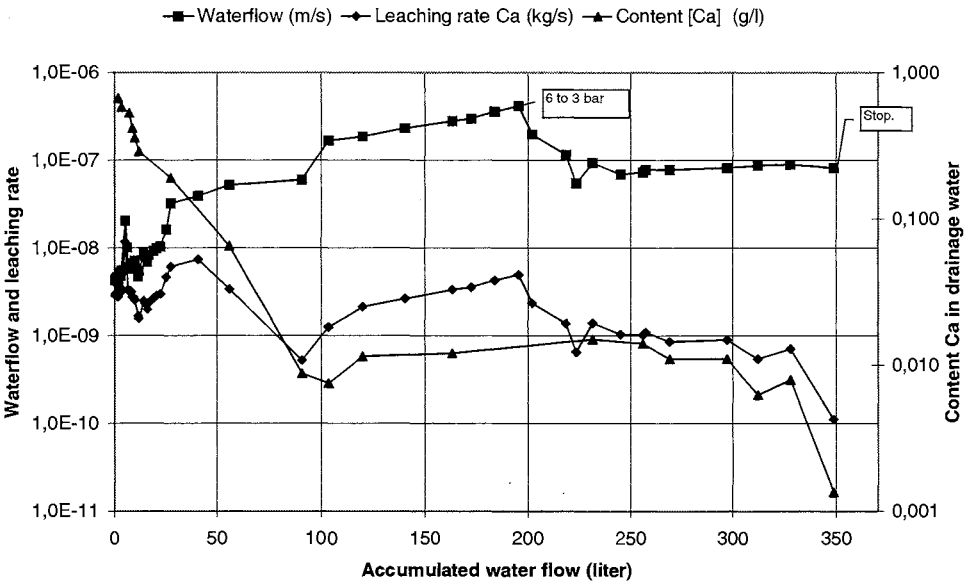

Figure 8 Measured drainage water flow and measured [Ca^{2+}] in the drainage water and calculated leaching rate kg Ca^{2+} /s for **specimen 8, exp. 2.**

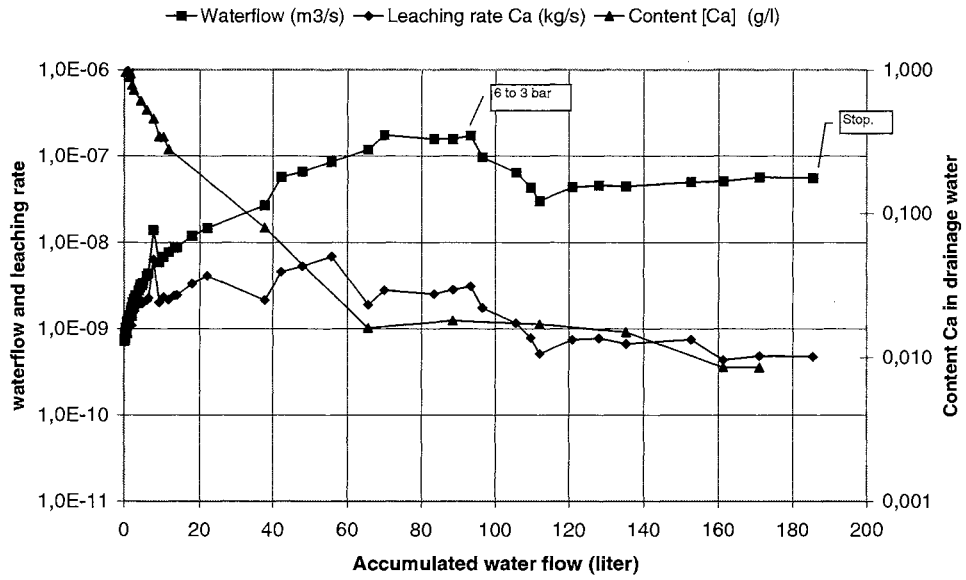

Figure 9 Measured drainage water flow and measured [Ca^{2+}] in the drainage water and calculated leaching rate kg Ca^{2+} /s for **specimen 10, exp. 2.**

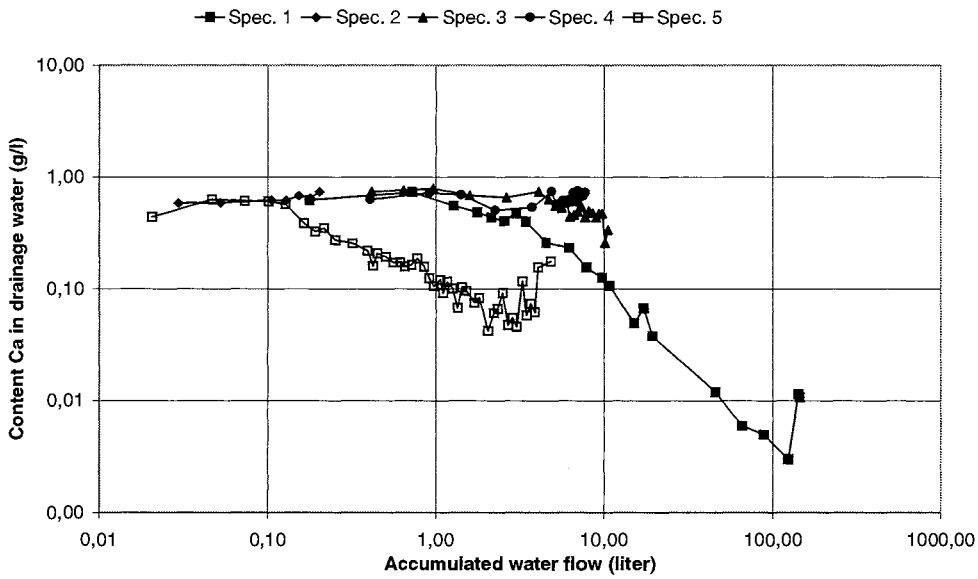

Figure 10 Measured [Ca^{2+}] in the drainage water for **specimen 1-5, exp. 2.**

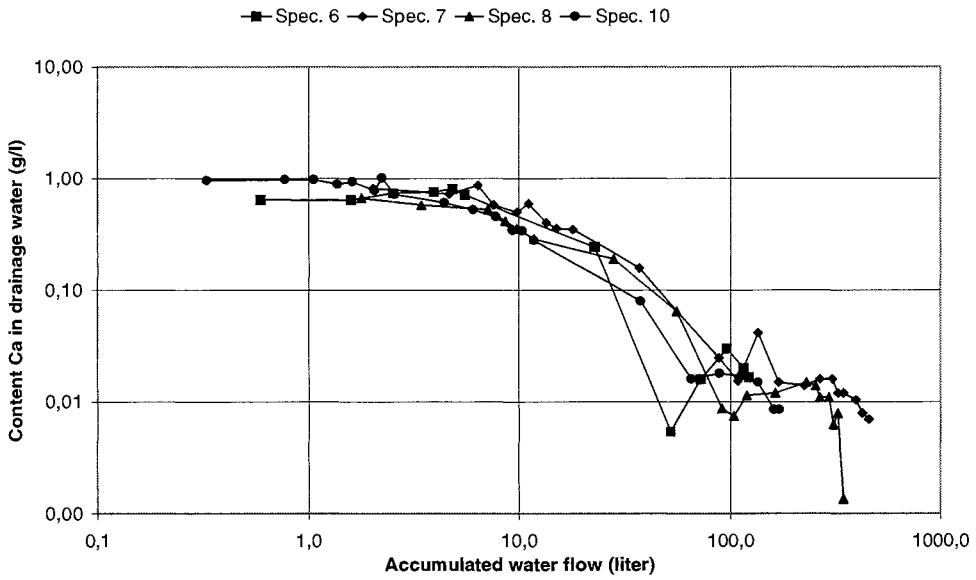

Figure 11 Measured [Ca^{2+}] in the drainage water for **specimen 6-8, 10, exp. 2.**

APPENDIX 7-4 Experiment 2: water flow and content of calcium in drainage water

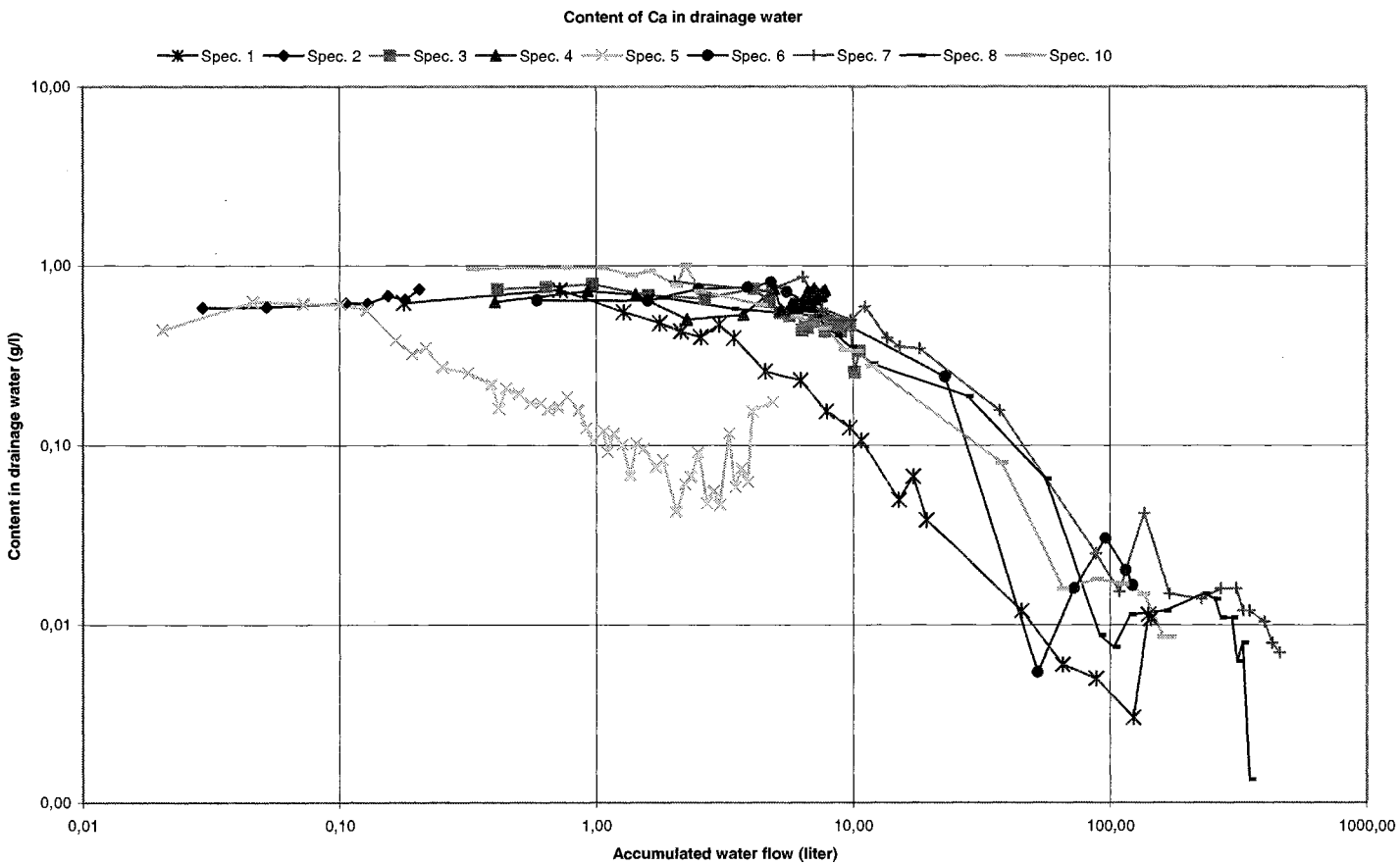

Figure 12 Measured [Ca^{2+}] in the drainage water for **specimen 1-8, 10, exp. 2**.

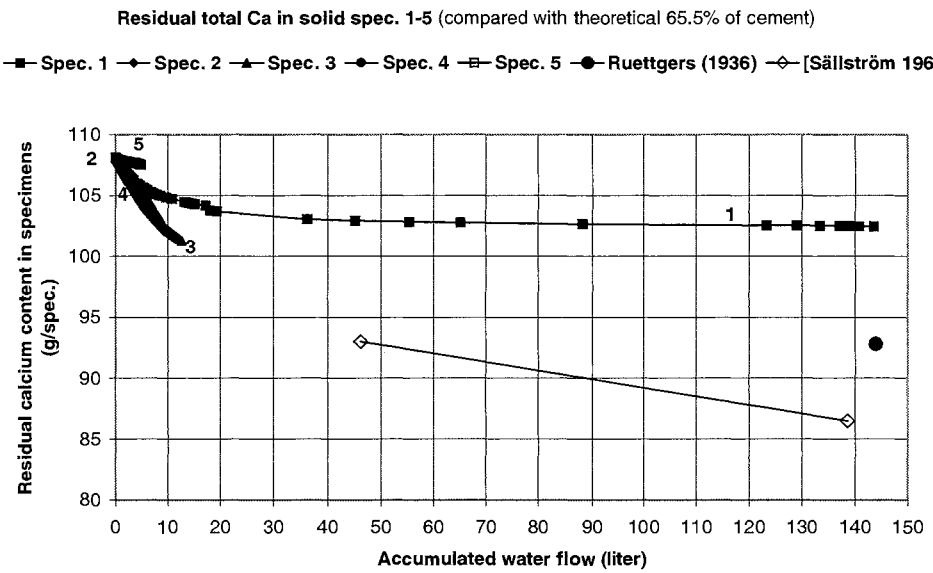

Figure 13 Estimated residual content of total Ca in the leached **specimen 1-5, exp. 2** at a accumulated flow of water of 0-150 (l). It is estimated as the assumed initial content of total Ca minus the measured, accumulated leaching of Ca in the drainage water.

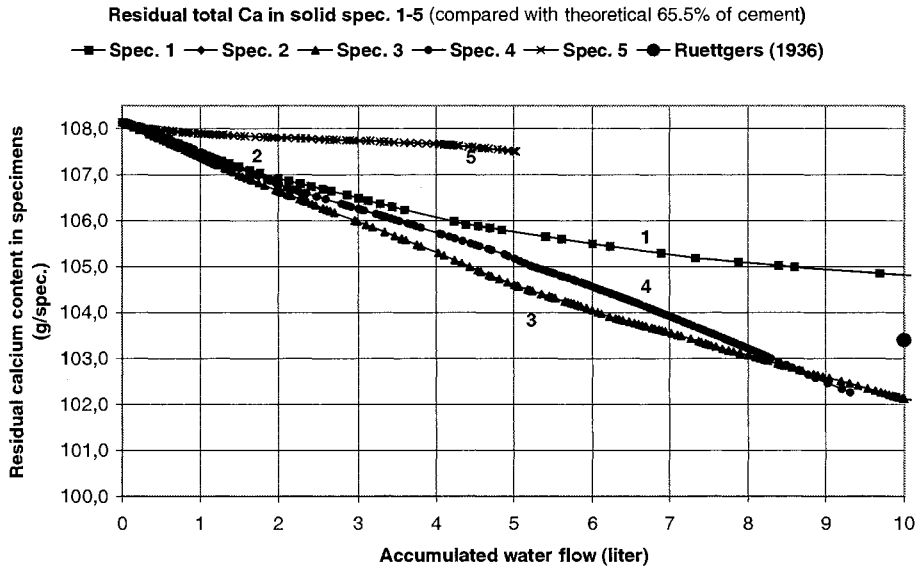

Figure 14 Estimated residual content of total Ca in the leached **specimen 1-5, exp. 2** at a accumulated flow of water of 0-10 (l). It is estimated as the assumed initial content of total Ca minus the measured, accumulated leaching of Ca in the drainage water.

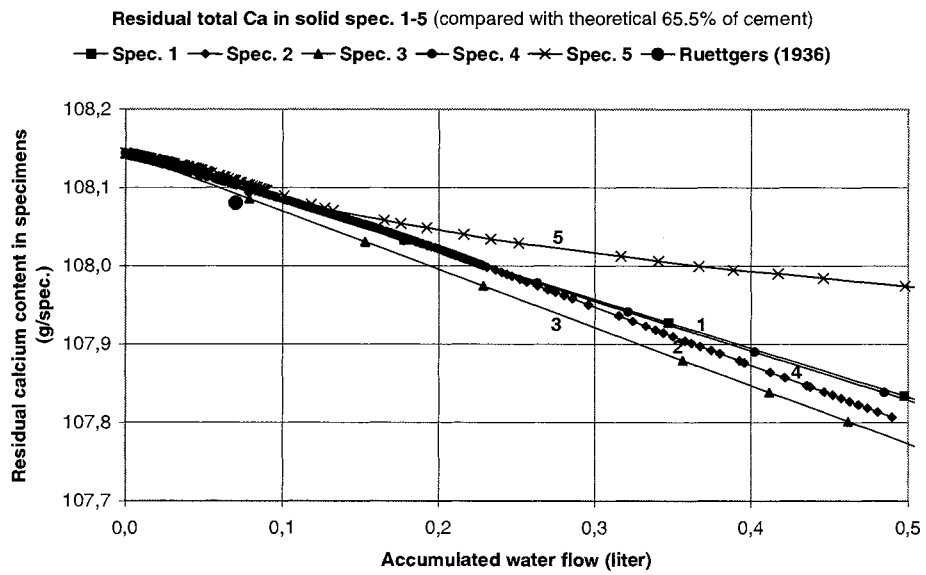

Figure 15 Estimated residual content of total Ca in the leached **specimen 1-5, exp. 2** at a accumulated flow of water of 0-0.5 (l). It is estimated as the assumed initial content of total Ca minus the measured, accumulated leaching of Ca in the drainage water.

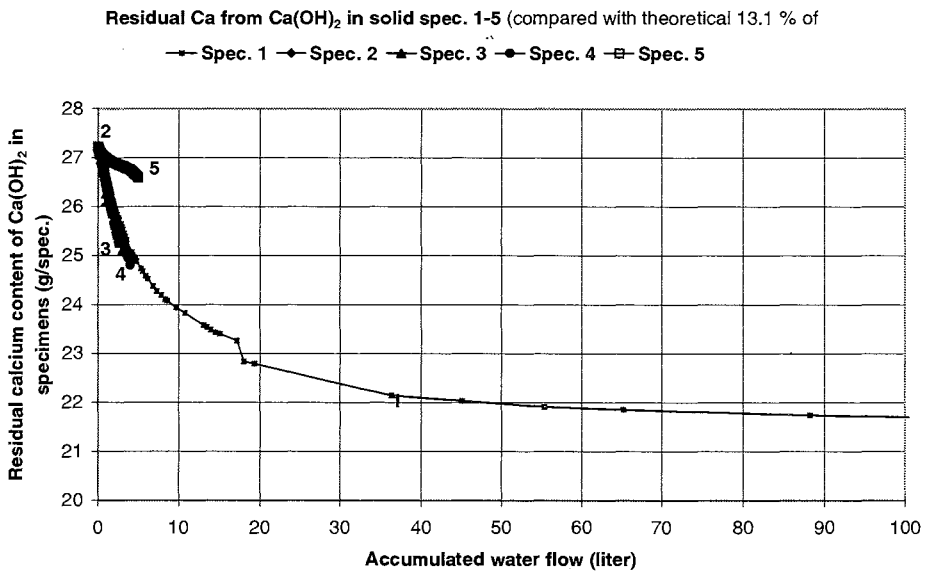

Figure 16 Estimated residual content of Ca in $Ca(OH)_2(s)$ in the leached **specimen 1-5, exp. 2** at a accumulated flow of water of 0-150 (l). It is estimated as the assumed initial content of Ca in $Ca(OH)_2(s)$ minus the measured, accumulated leaching of Ca in the drainage water.

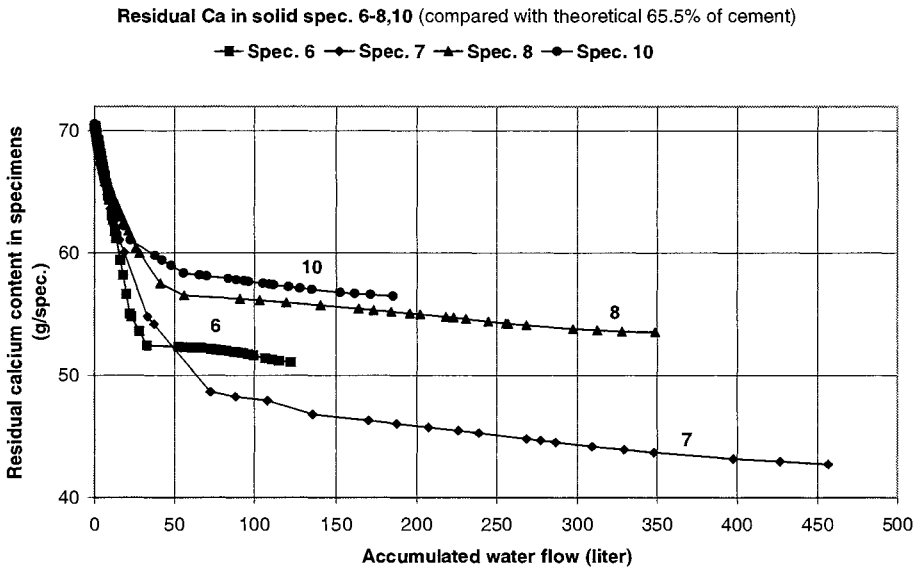

Figure 17 Estimated residual content of total Ca in the leached **specimen 6-8, 10, exp. 2** at a accumulated flow of water of 0-500 (l). It is estimated as the assumed initial content of total Ca minus the measured, accumulated leaching of Ca in the drainage water.

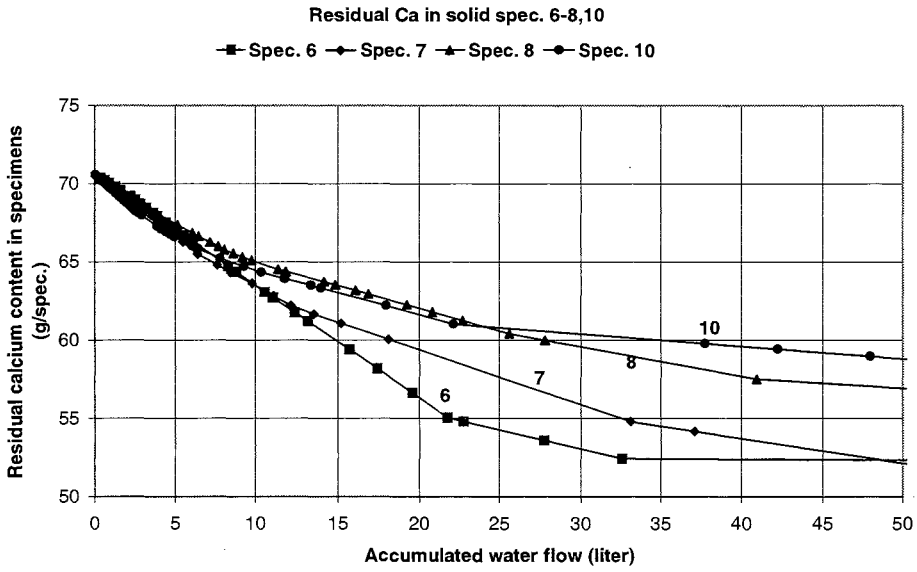

Figure 18 Estimated residual content of total Ca in the leached **specimen 6-8, 10, exp. 2** at a accumulated flow of water of 0-50 (l). It is estimated as the assumed initial content of total Ca minus the measured, accumulated leaching of Ca in the drainage water.

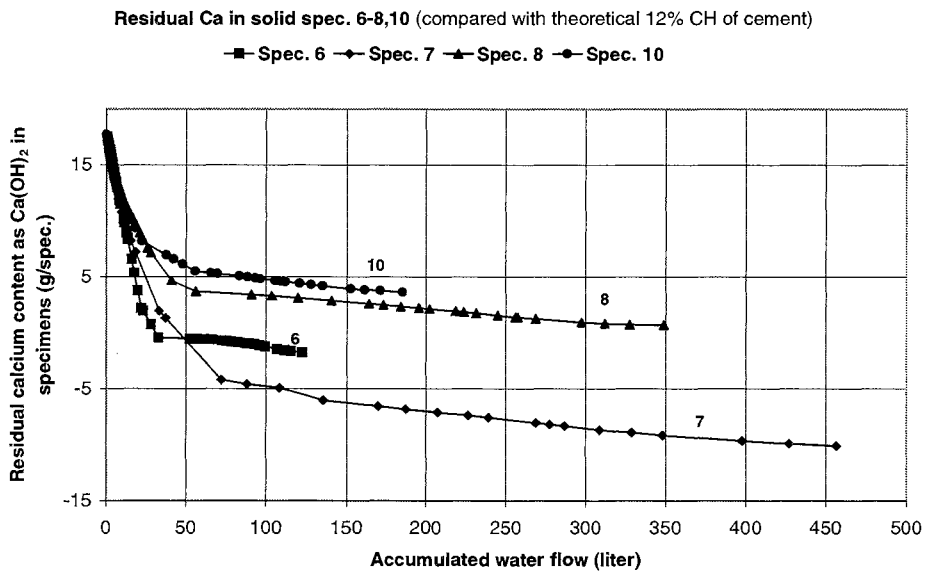

Figure 19 Estimated residual content of Ca in $Ca(OH)_2(s)$ in the leached **specimen 6-8, 10, exp. 2** at a accumulated flow of water of 0-500 (l). It is estimated as the assumed initial content of Ca in $Ca(OH)_2(s)$ minus the measured, accumulated leaching of Ca in the drainage water.

Leaching of K

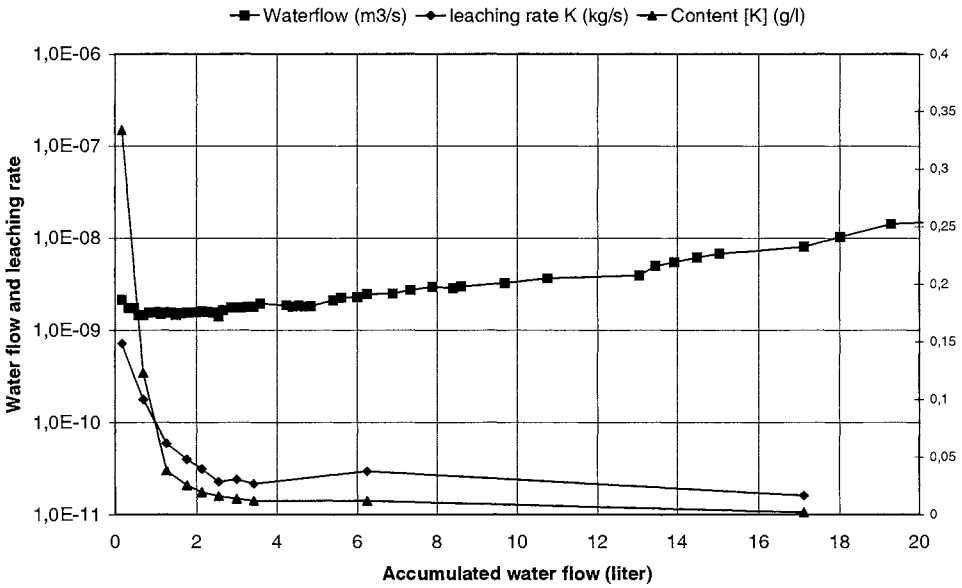

Figure 1 Measured drainage water flow and measured concentration of potassium in the drainage water and calculated leaching rate kg K^+ /s for **specimen 1, exp. 2.**

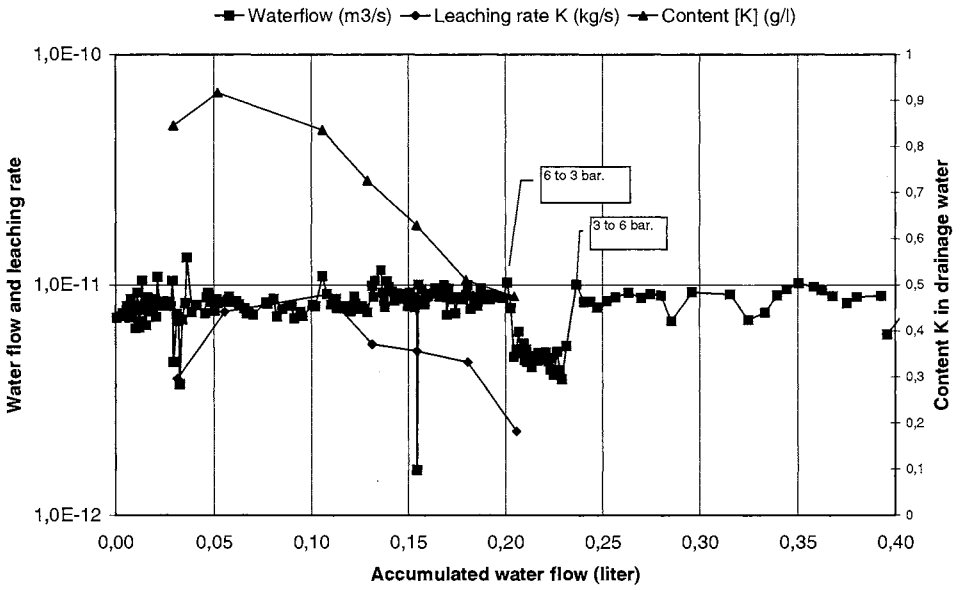

Figure 2 Measured drainage water flow and measured concentration of potassium in the drainage water and calculated leaching rate kg K^+ /s for **specimen 2, exp. 2.**

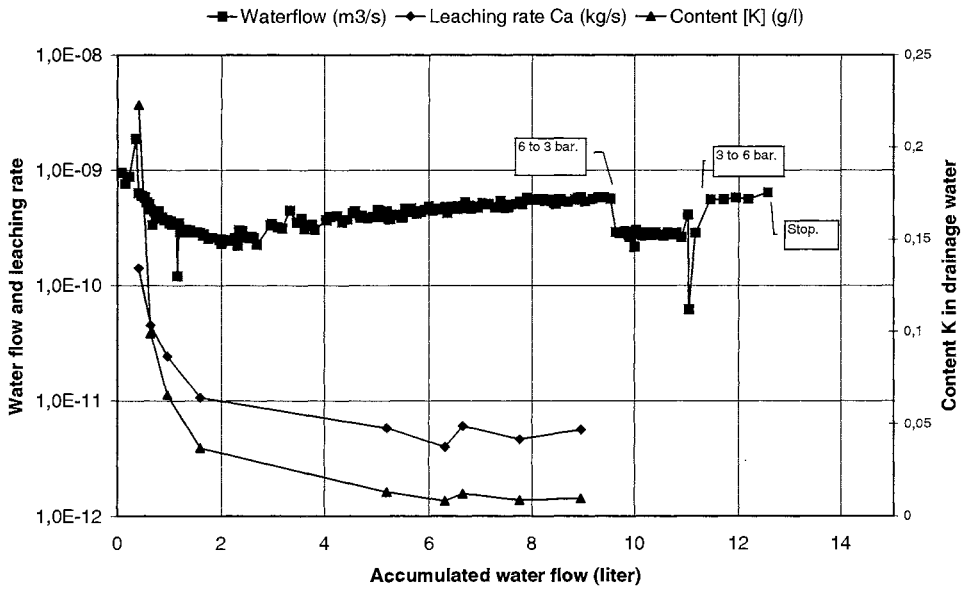

Figure 3 Measured drainage water flow and measured concentration of potassium in the drainage water and calculated leaching rate kg K^+ /s for **specimen 3, exp. 2.**

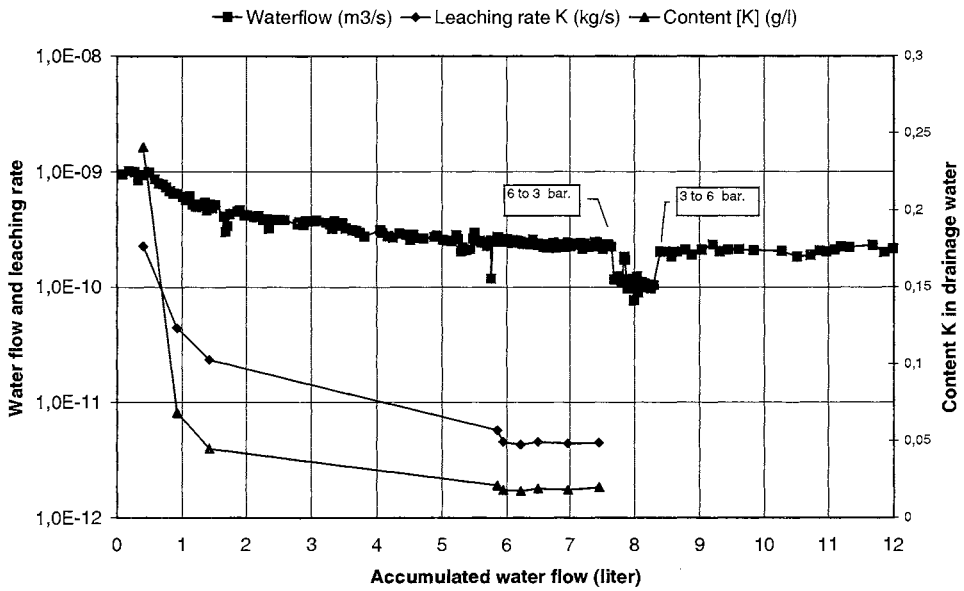

Figure 4 Measured drainage water flow and measured concentration of potassium in the drainage water and calculated leaching rate kg K^+ /s for **specimen 4, exp. 2.**

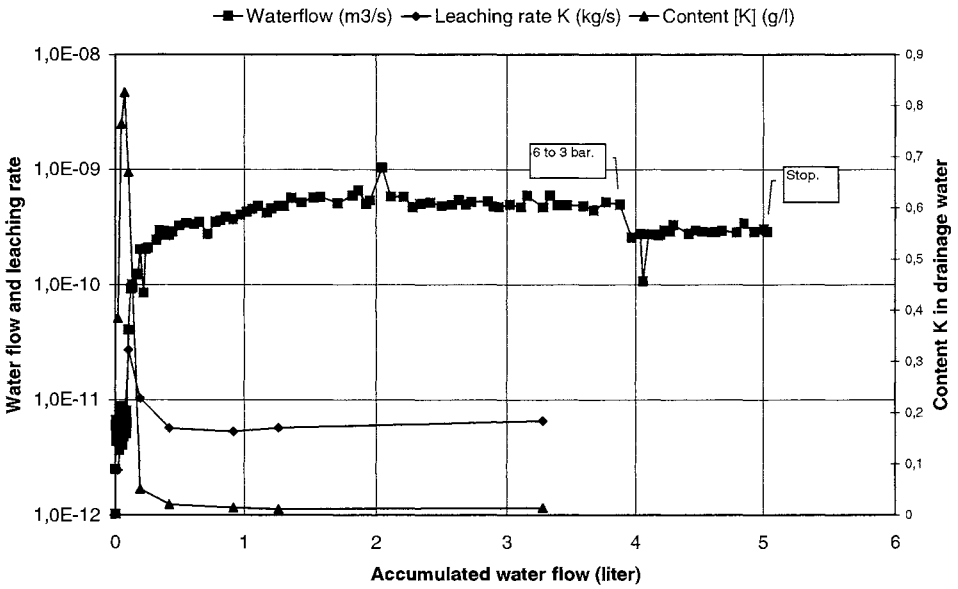

Figure 5 Measured drainage water flow and measured concentration of potassium in the drainage water and calculated leaching rate kg K^+ /s for **specimen 5, exp. 2.**

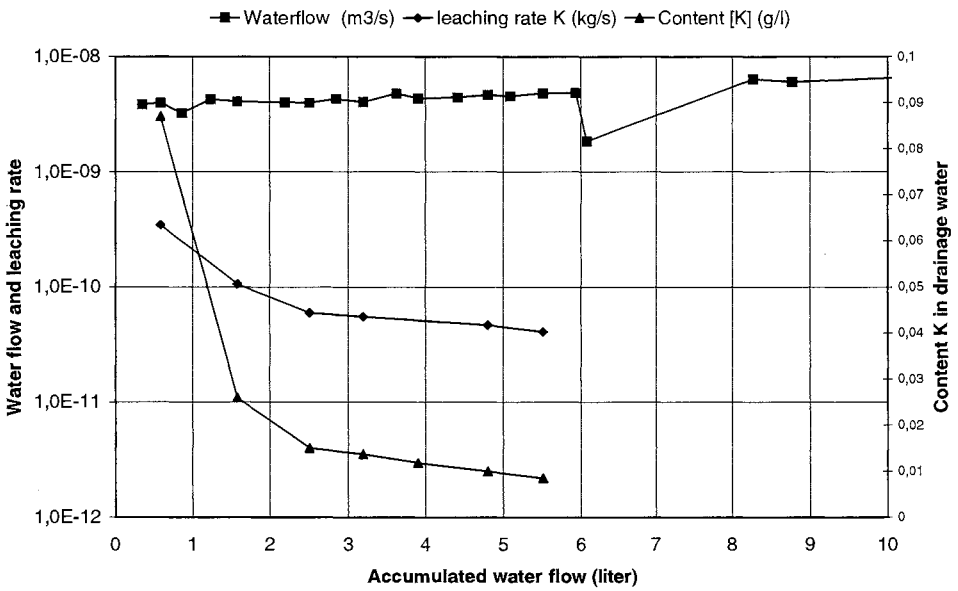

Figure 6 Measured drainage water flow and measured concentration of potassium in the drainage water and calculated leaching rate kg K^+ /s for **specimen 6, exp. 2.**

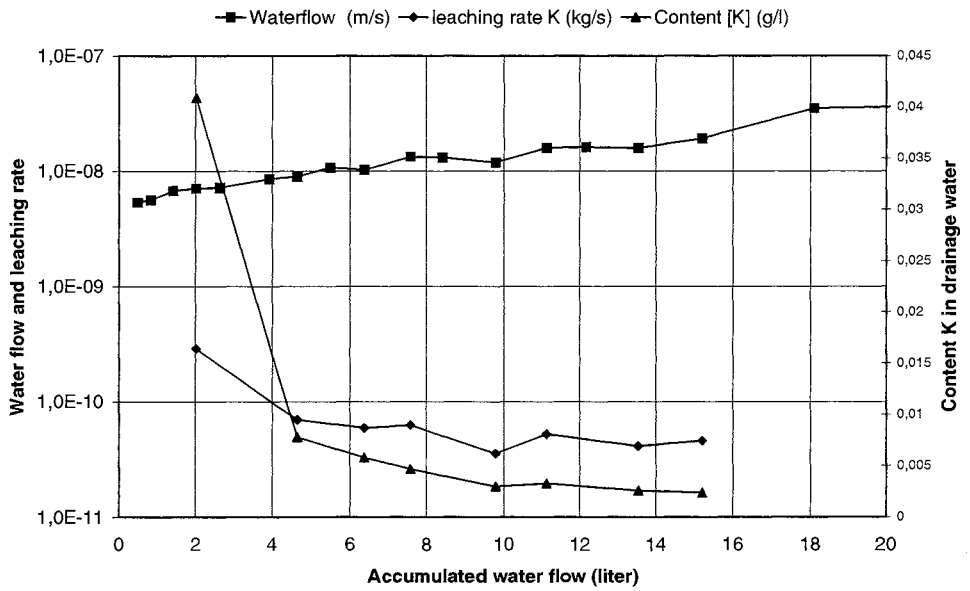

Figure 7 Measured drainage water flow and measured concentration of potassium in the drainage water and calculated leaching rate kg K^+ /s for **specimen 7, exp. 2.**

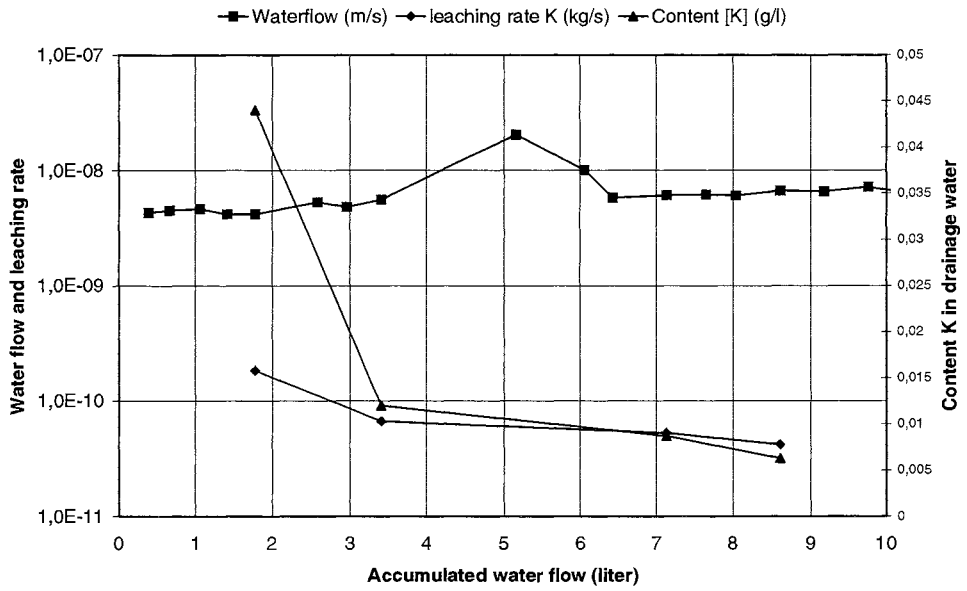

Figure 8 Measured drainage water flow and measured concentration of potassium in the drainage water and calculated leaching rate kg K^+ /s for **specimen 8, exp. 2.**

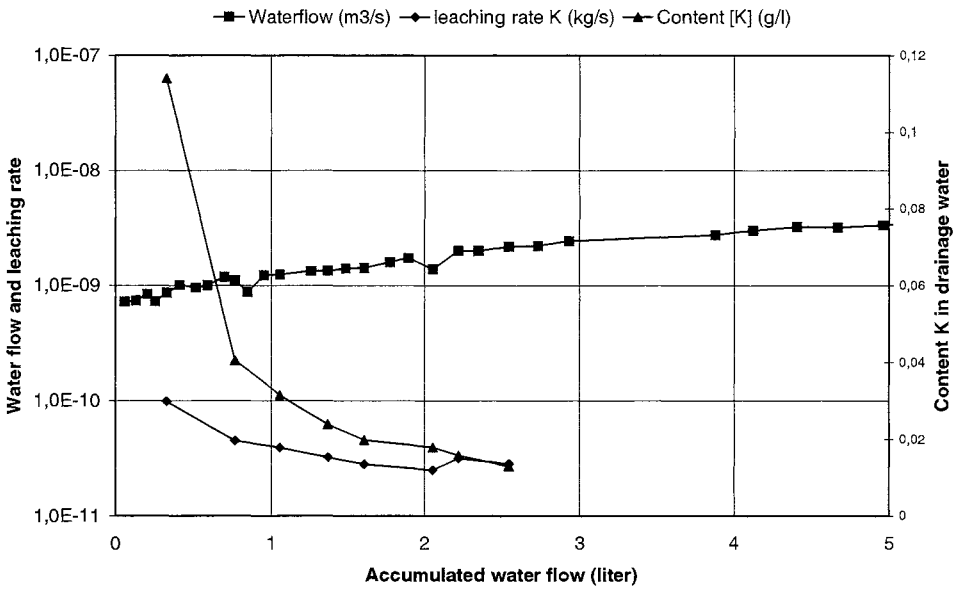

Figure 9 Measured drainage water flow and measured concentration of potassium in the drainage water and calculated leaching rate kg K^+ /s for **specimen 10, exp. 2.**

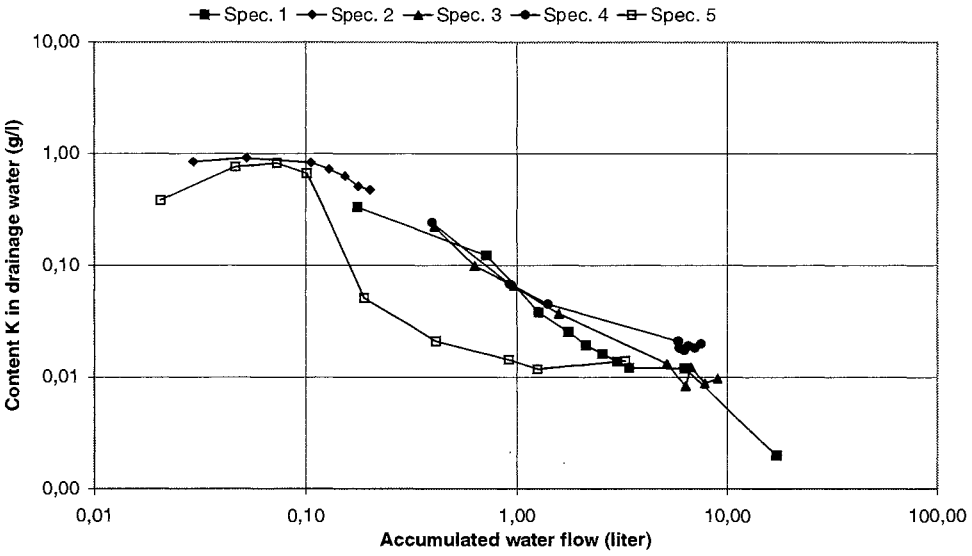

Figure 10 Measured concentration of potassium in the drainage water for **specimen 1-5, exp. 2.**

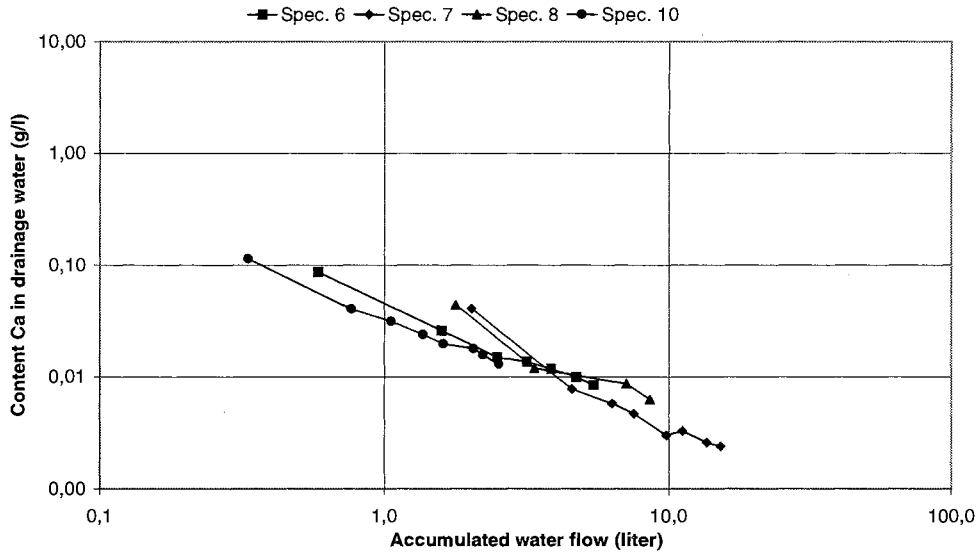

Figure 11 Measured concentration of potassium in the drainage water for **specimen 6-8, 10, exp. 2.**

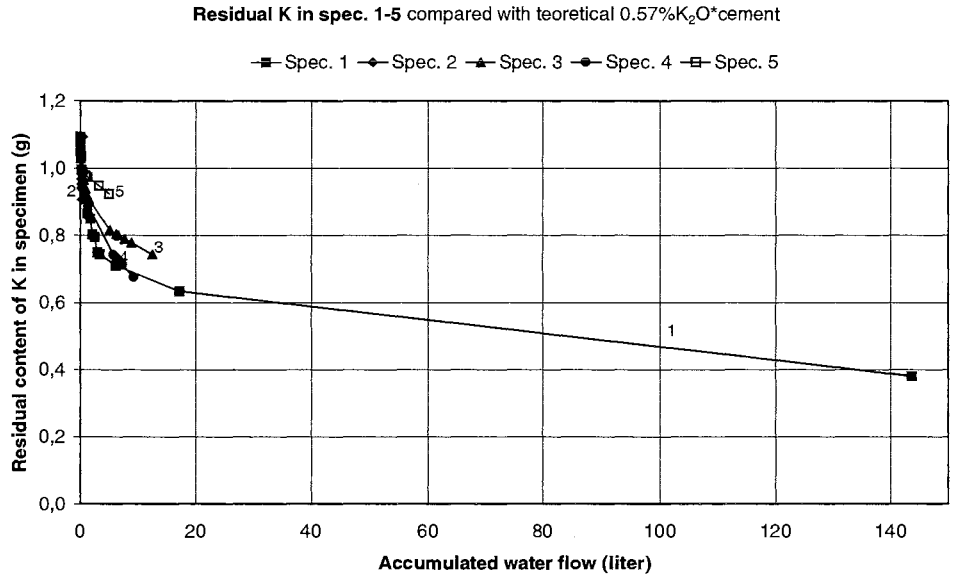

Figure 12 Residual content of K in specimens 1 to 5 in experiment 2. Spec. 2,5: virgin w/c 0.8. Spec. 1, 2-3: Late-dried w/c 0.8. The initial value is based on information from the cement supplier. The dots in the figure are measured values and the curve between is an interpolation. The last dot in each curve in the figure is extrapolated values. These last values can perhaps be overestimated especially when the drainage water flow was high.

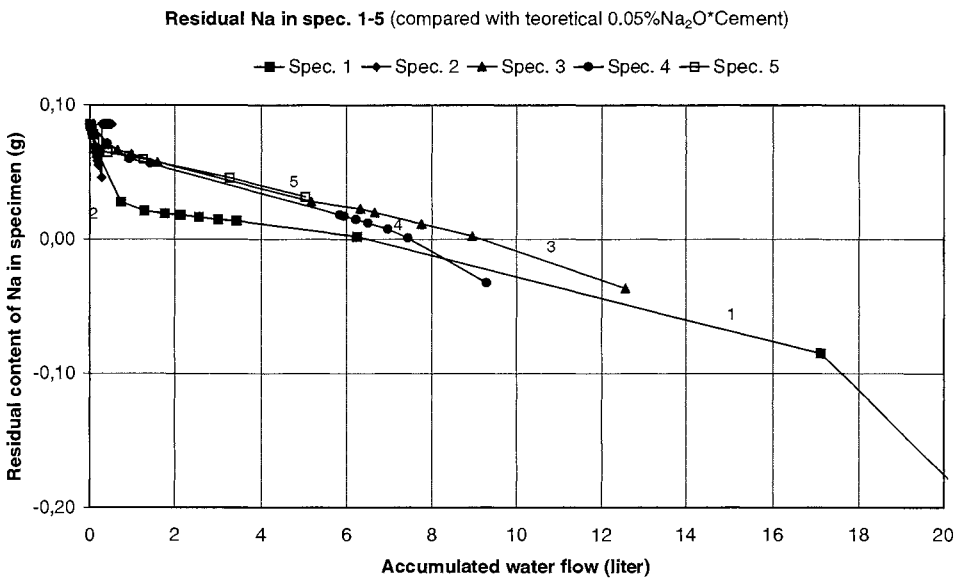

Figure 13 Residual content of K in specimens 6 to 8 and 10 in experiment 2. Spec. 10: virgin w/c 1.3. Spec. 6-8: Late-dried w/c 1.3. The initial value is due to the cement supplier. The dots in the figure are measured values and the curve between is an interpolation. The last dot in each curve in the figure is extrapolated values. These last values are probably overestimated especially when the drainage water flow was high. There can be no negative concentrations.

Leaching of Na

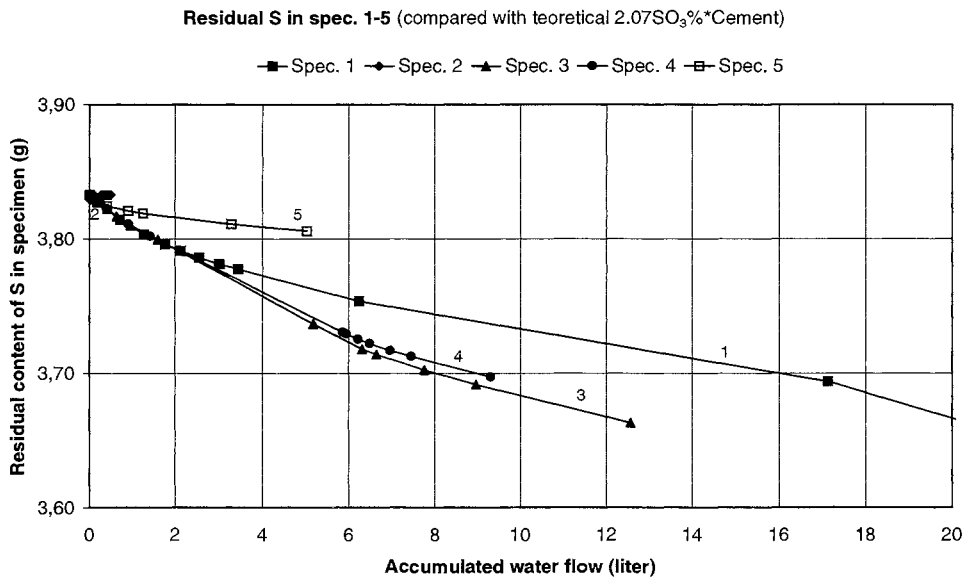

Figure 14 Residual content of Na in specimens 1 to 5 in experiment 2. Spec. 2,5: virgin w/c 0.8. Spec. 1, 2-3: Late-dried w/c 0.8. The initial value is due to the cement supplier. The dots in the figure are measured values and the curve between is an interpolation. The last dot in each curve in the figure is extrapolated values. These last values are probably overestimated, especially when the drainage water flow was high.

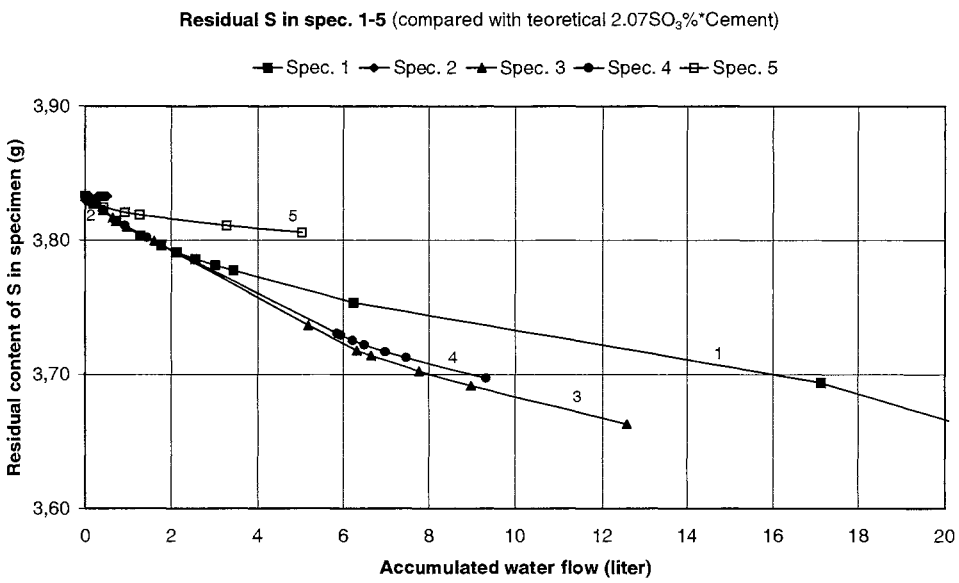

Figure 1 Residual content of S in specimens 1 to 5 in experiment 2. Spec. 2,5: virgin w/c 0.8. Spec. 1, 2-3: Late-dried w/c 0.8. The initial value is due to the cement supplier. The dots in the figure are measured values and the curve between is an interpolation. The last dot in each curve in the figure is extrapolated values. These last values can perhaps be overestimated especially when the drainage water flow was high.

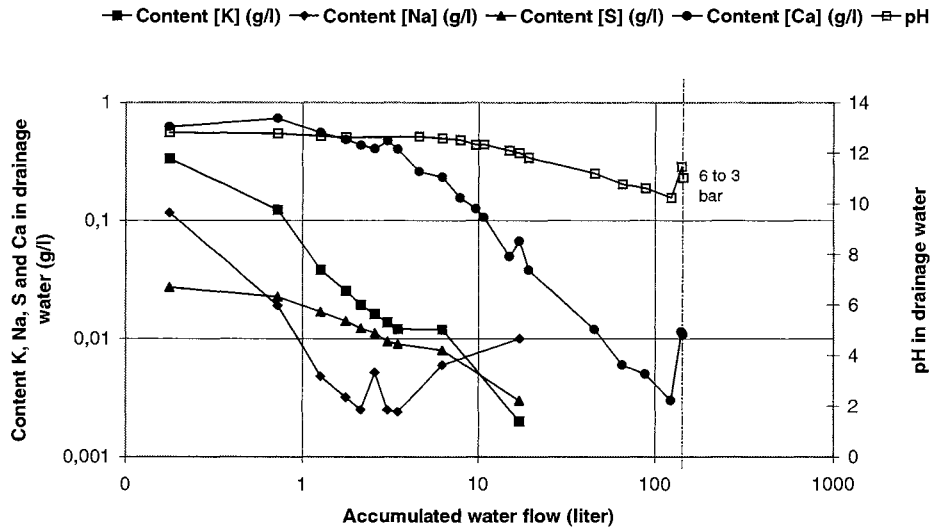

Figure 1 Content of K, Na, S, Ca and H^+ in the drainage water **for specimen 1, exp. 2.** The dots in the figure are measured values and the curves between are interpolations.

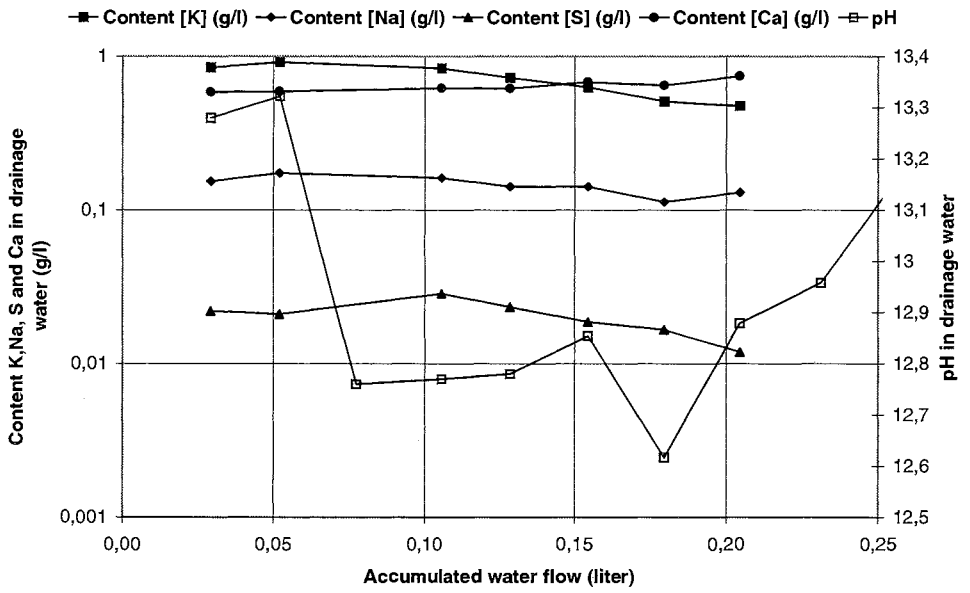

Figure 2 Content of K, Na, S, Ca and H^+ in the drainage water **for specimen 2, exp. 2.** The dots in the figure are measured values and the curves between are interpolations.

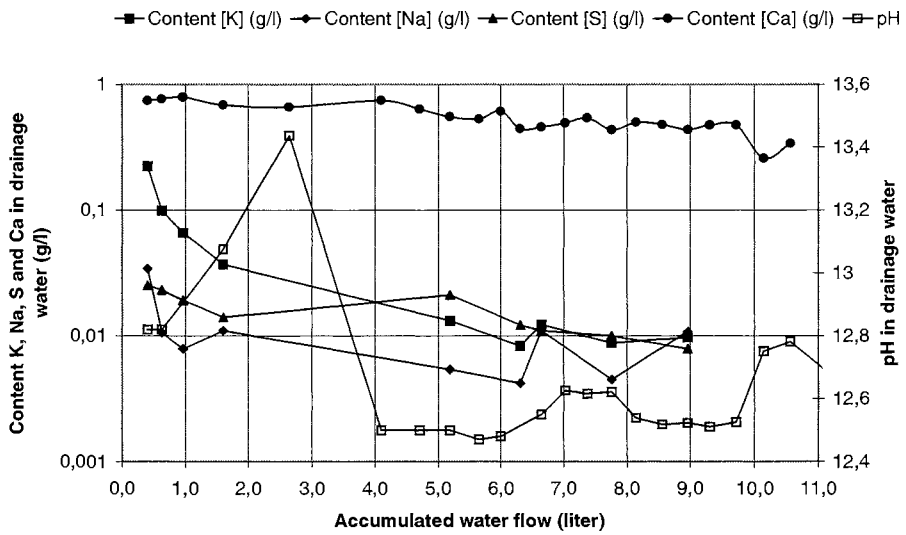

Figure 3 Content of K, Na, S, Ca and H^+ in the drainage water **for specimen 3, exp. 2.** The dots in the figure are measured values and the curves between are interpolations.

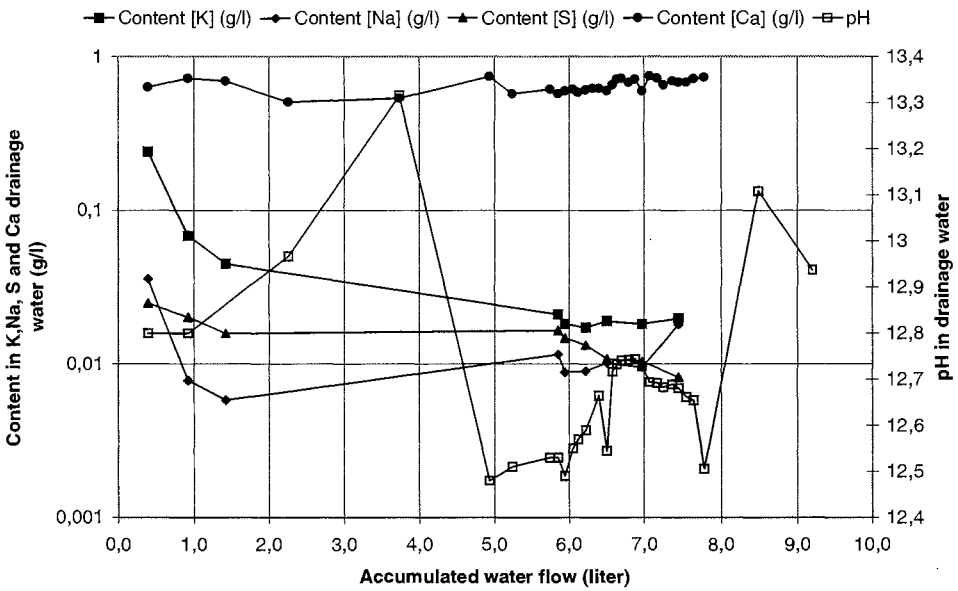

Figure 4 Content of K, Na, S, Ca and H^+ in the drainage water **for specimen 4, exp. 2.** The dots in the figure are measured values and the curves between are interpolations.

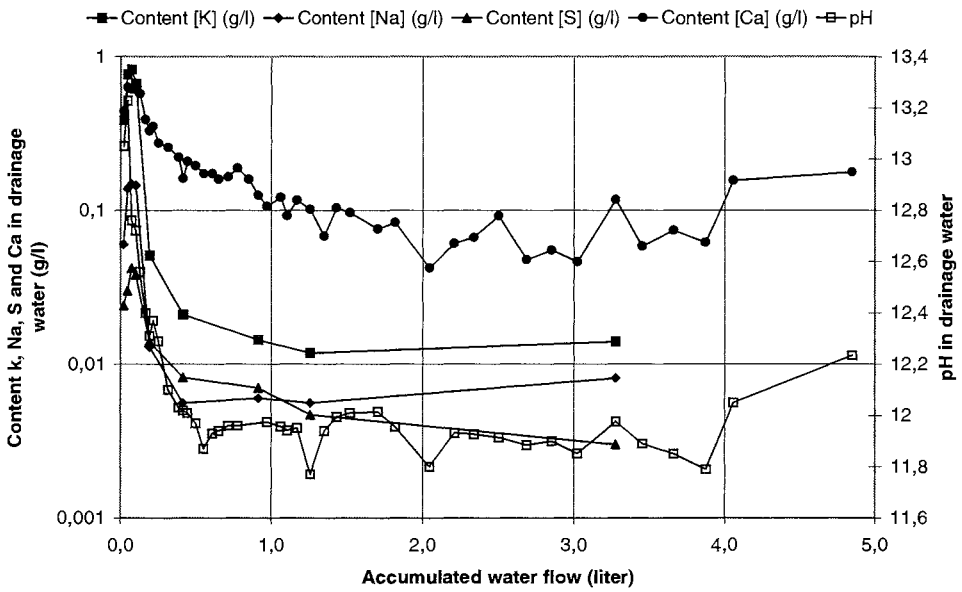

Figure 5 Content of K, Na, S, Ca and H^+ in the drainage water **for specimen 5, exp. 2.** The dots in the figure are measured values and the curves between are interpolations.

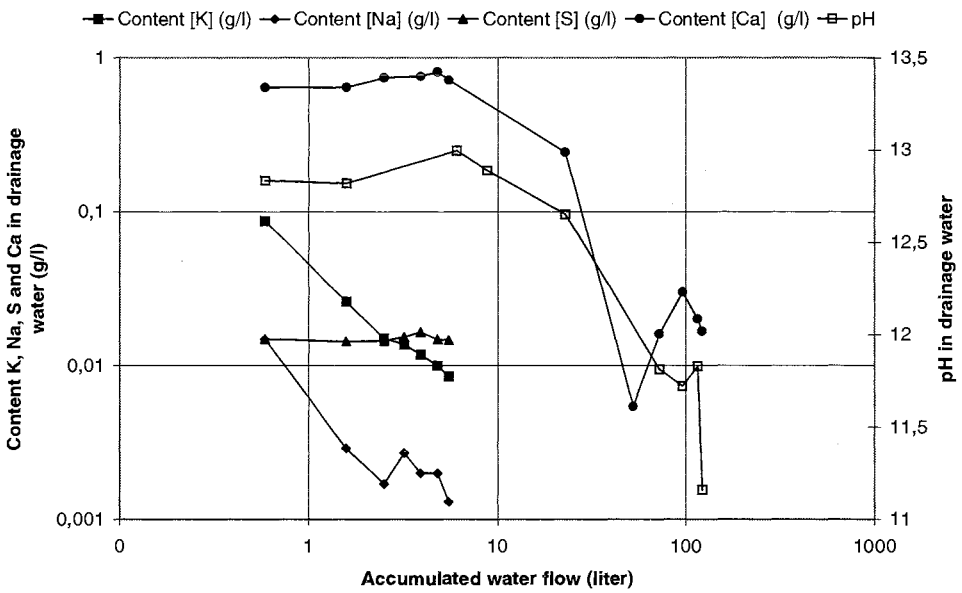

Figure 6 Content of K, Na, S, Ca and H^+ in the drainage water **for specimen 6, exp. 2.** The dots in the figure are measured values and the curves between are interpolations.

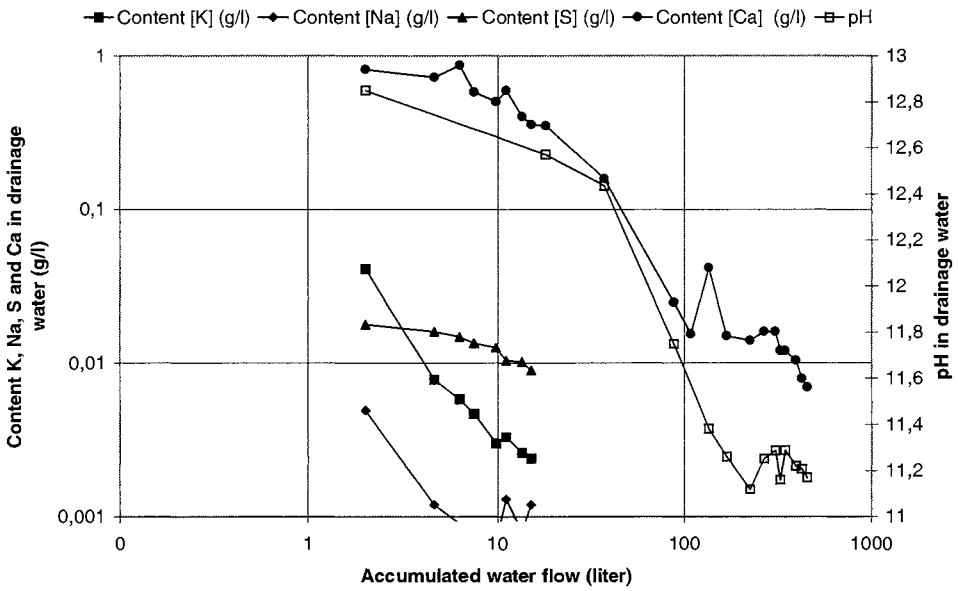

Figure 7 Content of K, Na, S, Ca and H^+ in the drainage water **for specimen 7, exp. 2.** The dots in the figure are measured values and the curves between are interpolations.

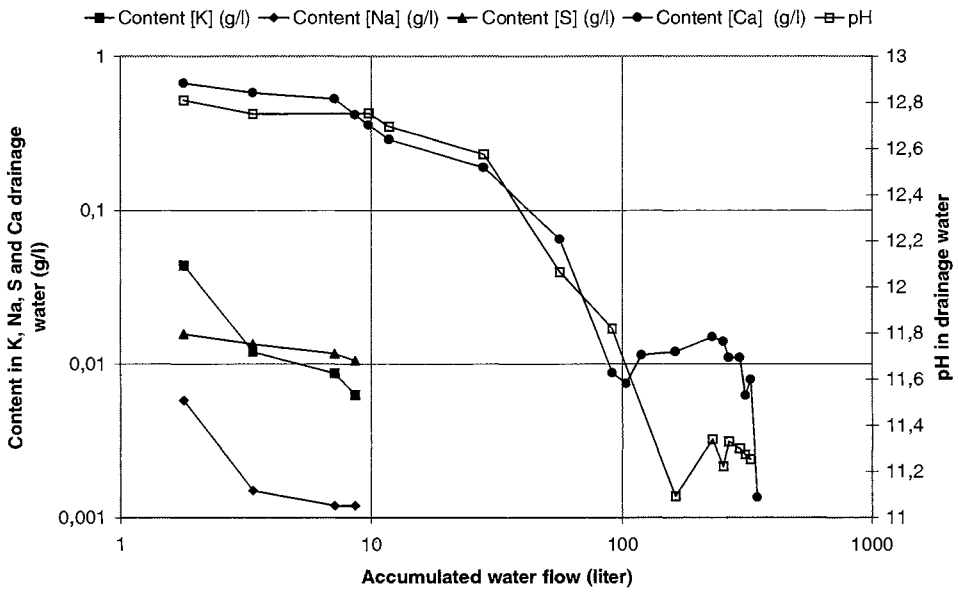

Figure 8 Content of K, Na, S, Ca and H^+ in the drainage water **for specimen 8, exp. 2.** The dots in the figure are measured values and the curves between are interpolations.

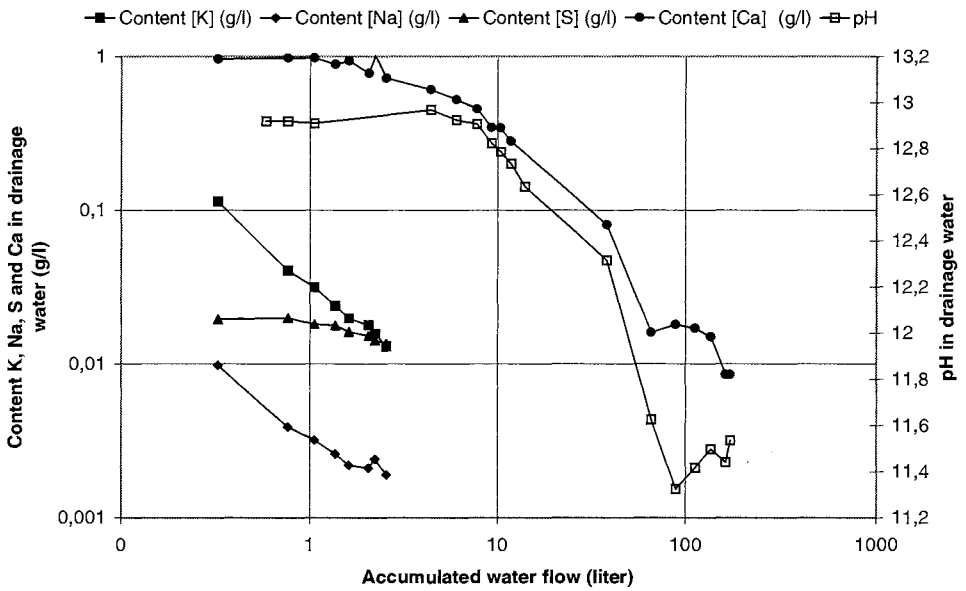

Figure 9 Content of K, Na, S, Ca and H^+ in the drainage water **for specimen 10, exp. 2.** The dots in the figure are measured values and the curves between are interpolations.

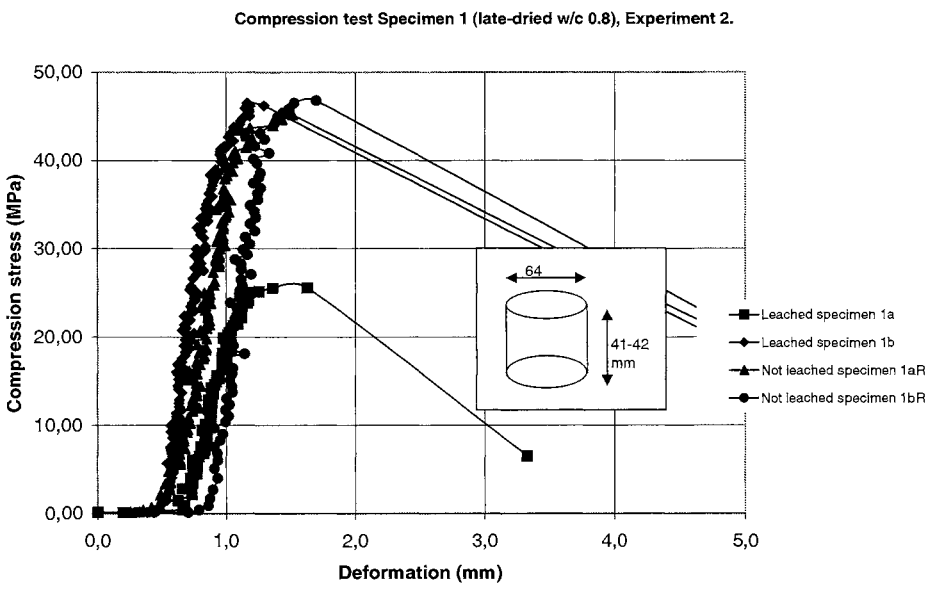
Compression test Specimen 1 (late-dried w/c 0.8), Experiment 2.
Compression stress (MPa)
50,00
40,00
30,00
20,00
10,00
0,00
0,0
1,0
2,0
3,0
4,0
5,0
Deformation (mm)
64
41-42 mm
Leached specimen 1a
Leached specimen 1b
Not leached specimen 1aR
Not leached specimen 1bR

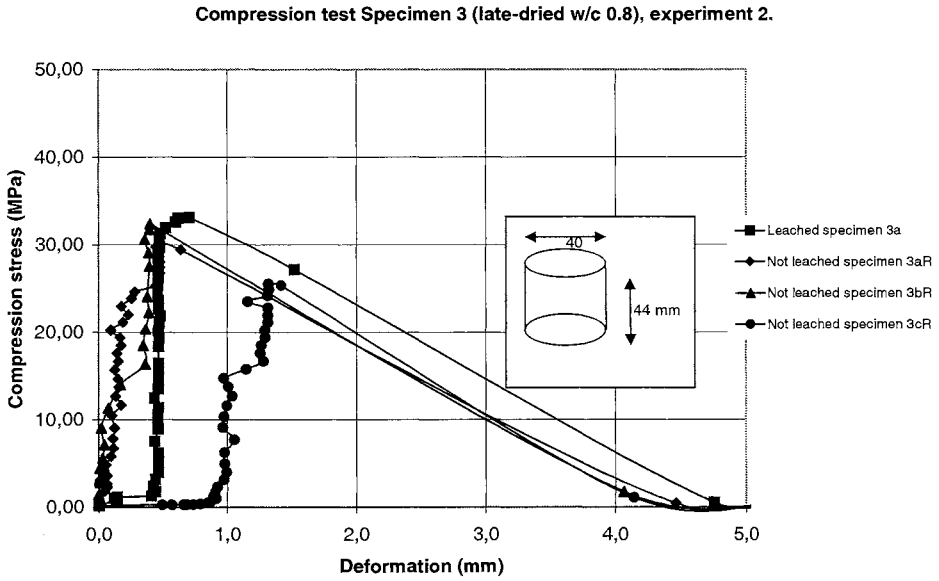
Compression test Specimen 3 (late-dried w/c 0.8), experiment 2.
Compression stress (MPa)
50,00
40,00
30,00
20,00
10,00
0,00
0,0
1,0
2,0
3,0
4,0
5,0
Deformation (mm)
40
44 mm
Leached specimen 3a
Not leached specimen 3aR
Not leached specimen 3bR
Not leached specimen 3cR

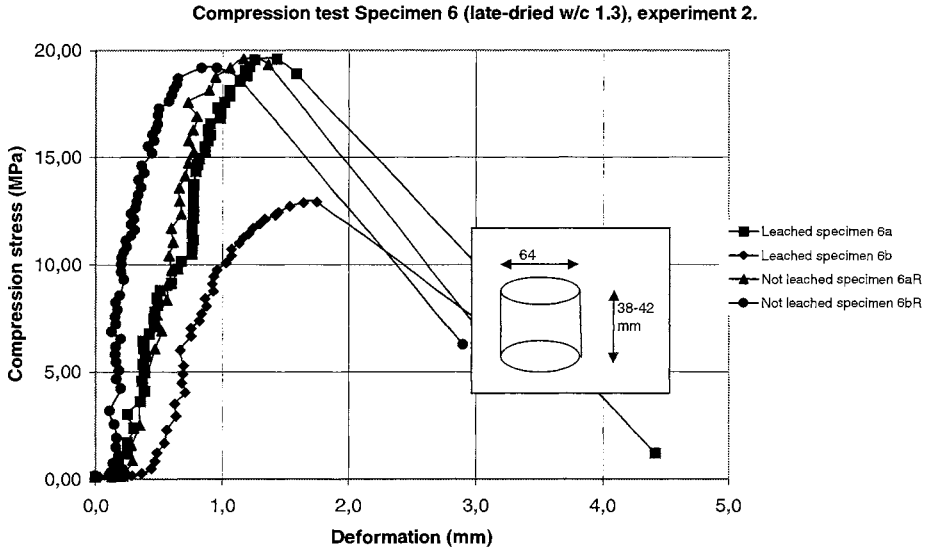
Compression test Specimen 6 (late-dried w/c 1.3), experiment 2.
Compression stress (MPa)
20,00
15,00
10,00
5,00
0,00
0,0
1,0
2,0
3,0
4,0
5,0
Deformation (mm)
64
38-42 mm
Leached specimen 6a
Leached specimen 6b
Not leached specimen 6aR
Not leached specimen 6bR

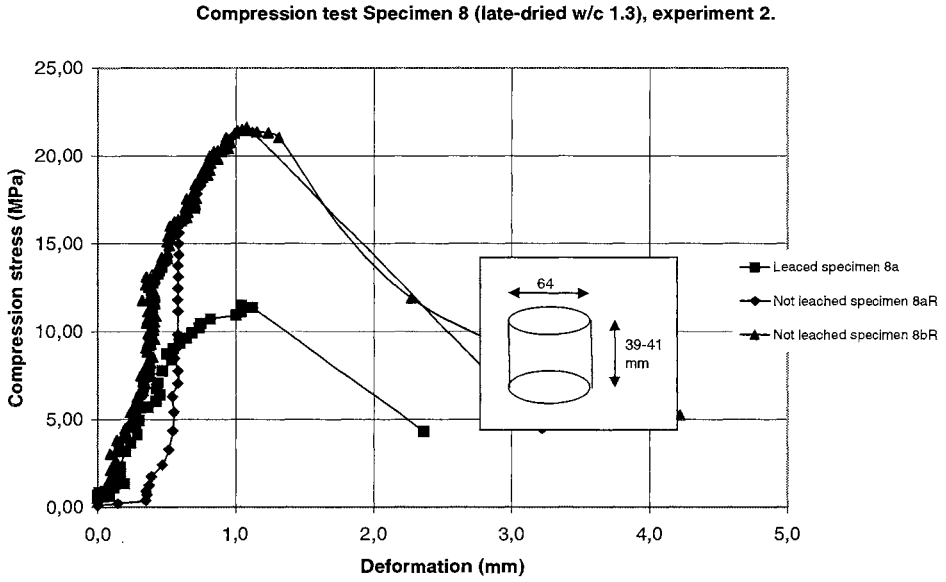
Compression test Specimen 8 (late-dried w/c 1.3), experiment 2.
Compression stress (MPa)
25,00
20,00
15,00
10,00
5,00
0,00
0,0
1,0
2,0
3,0
4,0
5,0
Deformation (mm)
64
39-41 mm
Leaced specimen 8a
Not leached specimen 8aR
Not leached specimen 8bR

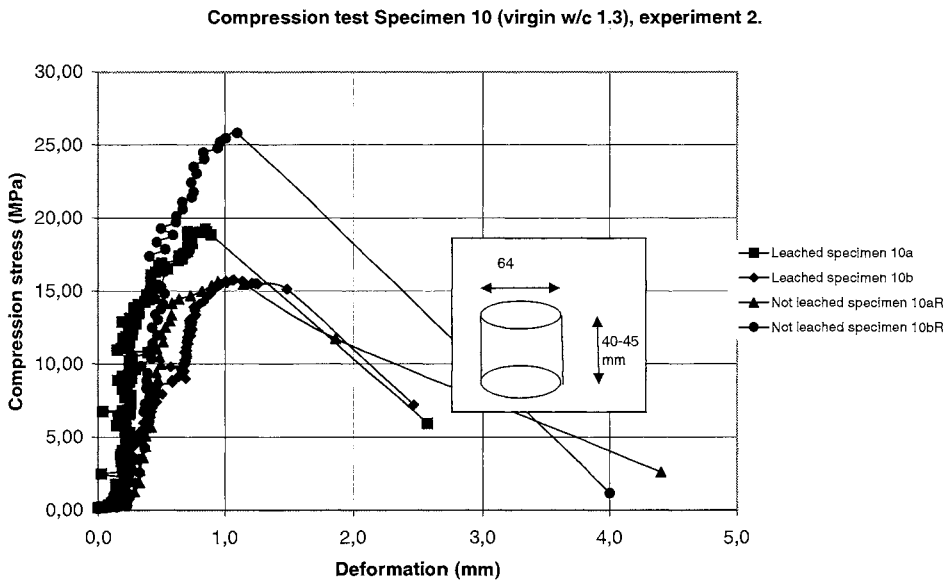
Compression test Specimen 10 (virgin w/c 1.3), experiment 2.
Compression stress (MPa)
30,00
25,00
20,00
15,00
10,00
5,00
0,00
0,0
1,0
2,0
3,0
4,0
5,0
Deformation (mm)
64
40-45 mm
Leached specimen 10a
Leached specimen 10b
Not leached specimen 10aR
Not leached specimen 10bR

APPENDIX TO CHAPTER 8

Leaching rate of calcium and potassium

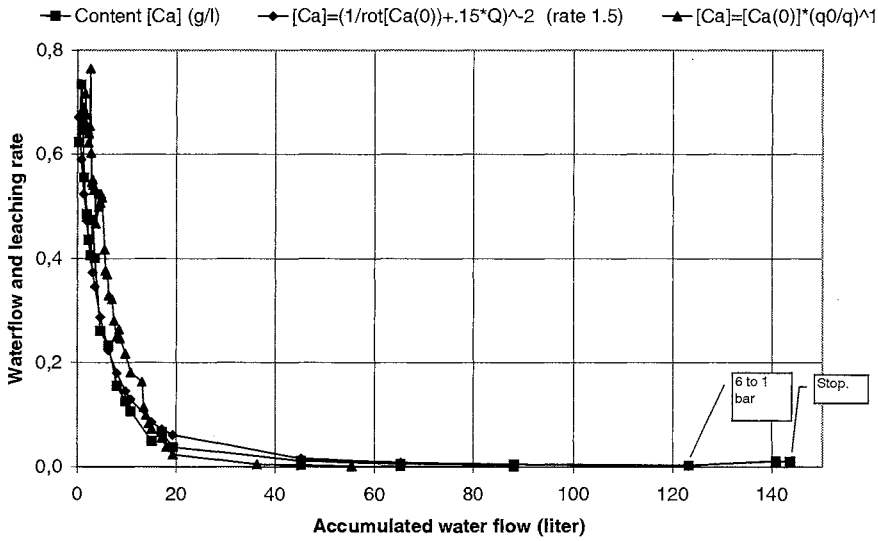

Figure 1 Assumed content of Ca in drainage water compared to measured content for **specimen 1, exp. 2.** The assumed content is calculated with 1); rate = -0.1473[Ca]$^{1.5}$ or expressed as $[Ca]_Q = \left(\frac{1}{\sqrt{[Ca]_0}} + k \cdot Q \right)^{-2}$, and 2); [Ca]=[Ca(0)]*(q0/q)^a, see chapter 8.3.3 for definitions.

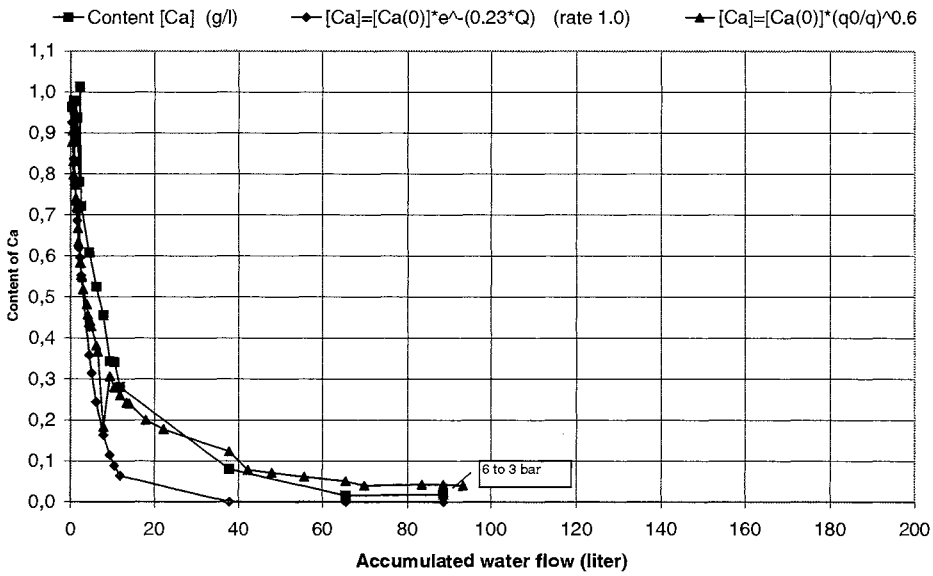

Figure 2 Assumed content of Ca in drainage water compared to measured content for **specimen 10, exp. 2.** The assumed content is calculated with 1); a rate = -0.2334[Ca]$^{1.0}$ and a rate = -0.9169[Ca]$^{1.5}$, and 2); [Ca]=[Ca(0)]*(q0/q)^a, see chapter 8.3.3 for definitions.

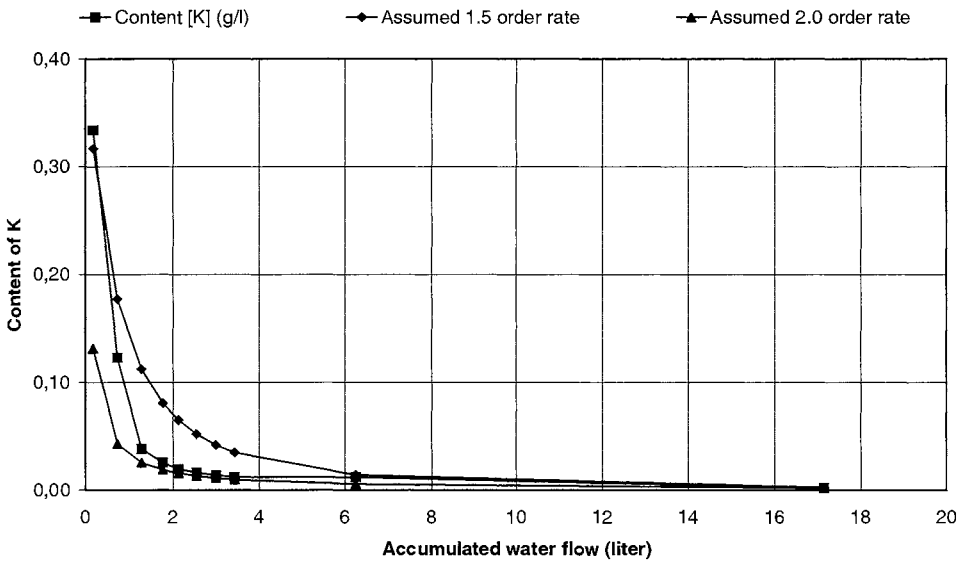

Figure 3 Assumed content of K in drainage water compared to measured content for **specimen 1, exp. 2.** The assumed content is calculated with 1); rate = $-1.1[K]^{1.5}$ and a rate = $28.8[K]^{2.0}$, and 2); $[K]=[K(0)]*(q0/q)^{a}$, see chapter 8.3.3 for definitions.

KFS AB, Lund 2001